STUDY ON BEHAVIOUR OF GEOPOLYMER CONCRETE

A thesis Submitted

in partial fulfilment of the requirements for the award of the degree of

DOCTOR OF PHILOSOPHY

In

CIVIL ENGINEERING

By

MANVENDRA VERMA

(En. No. - 2K16/PhD/CE/05)

Under the supervision of

Prof. Nirendra Dev

DEPARTMENT OF CIVIL ENGINEERING

DELHI TECHNOLOGICAL UNIVERSITY

SHAHBAD DAULATPUR, BAWANA ROAD, DELHI - 110042 (INDIA).

2021

DELHI TECHNOLOGICAL UNIVERSITY
(Formerly Delhi College of Engineering, Since 1941)
Shahbad Daulatpur, bawana road, Delhi- 110042

DECLARATION

I hereby declare that the research work presented in this thesis entitled "Study on behaviour of geopolymer concrete" is original and carried out by me under the supervision of Prof. Nirendra Dev, Professor, Department of Civil Engineering, Delhi Technological University, Delhi, and being submitted for the award of Ph.D. degree to Delhi Technological University, Delhi, India. The content of this thesis has not been submitted either in part or whole to any other university or institute for the award of any degree or diploma.

Date: / /2021 (Manvendra Verma)

Place: DTU, Delhi. En. No. – 2k16/PhD/CE/05

DELHI TECHNOLOGICAL UNIVERSITY

(Formerly Delhi College of Engineering, Since 1941)

Shahbad Daulatpur, bawana road, Delhi- 110042

Date: - / /2021

CERTIFICATE

This is to certify that the Ph.D thesis entitled, "Study on behaviour of geopolymer concrete", being submitted by Mr. Manvendra Verma for the fulfilment of the requirements for the award of the degree of Doctor of Philosophy in Civil Engineering, to the Department of Civil Engineering, Delhi Technological University, Delhi, India, is a bonafide record of original research work carried out by her under my guidance and supervision. The results embodied in this thesis have not been submitted to any other university or institution for the award of any degree or diploma.

Prof. Nirendra Dev
Supervisor & DRC Chairman
Department of Civil Engineering
Delhi Technological University
Delhi – 110042.

ACKNOWLEDGEMENTS

I would like to express my appreciations to the people who have helped me most during my research work. First and foremost, I am deeply grateful to my research supervisor, Prof. Nirendra Dev for his nonstop guidance, enduring patience, and nurturing support throughout this research without which successful completion would not have been possible. It has been an honor to be associated with such a great supervisor and learn from his experience.

I accord my heartfelt thanks to Mr. Mayank Nigam, assistant professor in the civil engineering department, GLA University, Mathura, Uttar Pradesh who was a source of inspiration for me to take up this research work. It would not have been possible without the support of central instrumentation facilities laboratories technicians, I am thankful to them.

I am grateful to my colleagues, Dr. Anju Agarawal, Dr. Ibadur Rehman, and Mr. Parvesh Kumar, Nisha Soni, Istuti Singh, Salila Bharti, Prashant Ramteke, Uzma Wani, Rahul Kumar, Sushant Kumar, Indrajeet Singh, Rahul Meena, Deepak Singh, Dinesh Reddy, Arti Raha, Suresh Kumar Nagar, Abhishek Paswan, Harshit Jayant, Prateek Roshan, and Vijay Kaushik for providing me with critical comments and suggestions and all those who interacted and exchanged ideas with me in completing the research.

I want to extend special thanks to the immense contribution made by my family especially my mother who not only encouraged and supported me but also stood by me like a pillar and gave me constant motivation. All my family member have shown enormous patience during this process and have cheerfully sacrificed the time that rightfully belonged to them. Finally, I extend a profound expression of respect to all elders in the family and especially my parents who have always showered me with their blessings and made me who I am today.

LIST OF PUBLICATIONS

- Manvendra Verma; Rahul Kumar; Nirendra Dev, "Investigation on the effect of seawater condition, sulfate attack, acid attack, Freeze-thaw condition, and wetting-drying on the Geopolymer concrete," *Iranian Journal of Science and Technology Trasactions of Civil Engineering*, 2021. (accepted)
- Manvendra Verma; Nirendra Dev, "Effect of Ground Granulated Blast Furnace Slag and FlyAsh ratio and the curing conditions on the Mechanical Properties of Geopolymer Concrete," *Structural Concrete*, February, pp. 1-15, 2021.
- Manvendra Verma; Nirendra Dev, "Effect of Liquid to Binder Ratio and Curing Temperature on the Engineering Properties of the Geopolymer Concrete" *Silicon.*, 6 February, pp. 1–15, 2021.
- Manvendra Verma; Nirendra Dev, "Effect of SNF-Based Superplasticizer on Physical, Mechanical and Thermal Properties of the Geopolymer Concrete" *Structural Concrete.*, 6 January, pp. 1–11, 2021.
- Manvendra Verma; Nirendra Dev, "Sodium hydroxide effect on the mechanical properties of flyash-slag based geopolymer concrete," *Structural Concrete*, 7 July, pp. 1–12, 2020.
- Manvendra Verma; Nirendra Dev (2020) "Effect of Superplasticiser on Physical, Chemical and Mechanical Properties of the Geopolymer Concrete" Challenges of Resilient and Sustainable Infrastructure Development in Emerging Economies, March 2–4, 2020, Kolkata, India.
- Manvendra Verma; Nirendra Dev, "Geopolymer concrete: A way of sustainable construction," International Journal of Recent Research Aspects, 2018
- Manvendra Verma; Nirendra Dev, "Review on effect of different parameters on the behavior of geopolymer Concrete" *Int. J. Innov. Res. Sci. Eng. Technology*, vol. 6, no. 6, pp. 11276–281, 2017.

ABSTRACT

Geopolymer concrete is an innovative, sustainable, cementless, and eco-friendly concrete that directly reduces carbon footprints due to the total replacement of the cement in the concrete. A very excessive amount of CO_2 is produced in the production of cement. In the experimental investigation, fresh, chemical, and mechanical properties of various parameters were tested to find the optimum point, in which the GGBFS to flyash ratio by weight ranged from 00/100 to 75/25, liquid-to-binder ratios ranged from 0.4 to 0.7, superplasticisers content percentage ranged from 0.5% to 2.0%, molarity of sodium hydroxide ranged from 8M to 16M, sodium silicate to sodium hydroxide ratios ranged from 0.5, tests for the durability studies, in which they compared the effect of elevated temperatures up to 800^0C, seawater condition, sulphate attack (both sodium sulphate and magnesium sulphate), acid attack, freeze-thaw condition, wetting-drying condition to the OPC concrete specimens

In the experimental investigation, the workability was tested using slump, density, compressive strength, splitting tensile strength, flexural strength, poisons ratio, elastic modulus, rebound hammer strength, and ultrasonic pulse velocity as various parameters. In durability tests, to check the density, mass loss, compressive strength, residual compressive strength, ultrasonic pulse velocity, and visual inspection.

The ambient-cured sample has less strength than the oven-cured samples, but in both cured samples, the 75/25 fly ash/GGBFS ratio gets the maximum engineering strength. The compressive strength, splitting tensile and flexural strength got the optimum point at the 0.60 liquid-to-binder ratios in the GPC mix design. The strength increases with the increment of the liquid-to-binder ratio, but it reduces randomly beyond the 0.60 ratios. 1% superplasticizer in the mix gets a higher strength compared to the other mixes with different percentages of superplasticiser. The compressive strength rises with the enlargement in molarity of NaOH in the mix design but beyond a point decreases the compressive strength in the oven-cured specimens. The highest compressive strength of oven cured 14M mix is 34.2N/mm^2 at 56 days. The engineering strength enlarges with the increment of alkaline ratio in the mix design, but it decreases beyond 2.5 alkaline ratio in both curing condition samples. The GPC design mix's mechanical strength increases with the increment of the curing temperature, but it reduces beyond the 100^0C

curing temperature. The higher curing temperature increases the gain rate of the GPC samples.

The GPC specimens have better stability against the elevated temperature compared to the OPC concrete specimens. The GPC specimens failed at an 800^0C temperature, whereas the OPC specimens failed at 600^0C. In seawater conditions, this initially increases the strength and density, but beyond 12 weeks, degradation occurs in both types of specimens. Both types of samples show a similar pattern in strength and mass loss. Both types of specimens show a similar pattern of strength and mass loss in the sulphate conditions, whereas the GPC specimens show better stability than OPC concrete specimens. In the freeze-thaw conditions, the OPC concrete specimens show better stability than the GPC specimens. The residual strength of GPC specimens was retained at 54% after 90 cycles, whereas the OPC concrete specimens retained 87% of the original. Both concrete specimens strengthen the mass continuously with an increment of wetting-drying cycles up to 60 cycles, and it decreases slightly after that. Mass loss occurs beyond 60 cycles, but conventional concrete specimens show no mass loss.

ABBREVIATIONS

GPC	Geopolymer Concrete
GGBFS	Ground Granulated Blast Furnace Slag
MK	Metakaolin
NaOH	Sodium hydroxide
Na_2SiO_3	Sodium silicate
XRD	X-ray diffraction
SEM	Scanning electronic microscope
EDS	Energy-dispersive X-ray spectroscopy
OPC	Ordinary Portland cement
PCE	Poly-carboxylate ester
SNF	Sulphonated naphthalene formaldehyde
CSH	Calcium silicate hydrate
UPV	Ultrasonic pulse velocity
ASTM	American standard testing materials
IS	Indian Standard
TGA	Thermogravimetric analysis
LBR	Liquid-to-binder ratio
FTIR	Fourier-transform infrared spectroscopy
FLGC	Flyash-based lightweight geopolymer concrete
UTM	Universal Testing Machine
CTM	Compression Testing Machine

TABLE OF CONTENTS

LIST OF FIGURES

LIST OF TABLES

CHAPTER 1 INTRODUCTION

1.1 Overview

Concrete is the second most abundant material used globally after water because conventional concrete uses Portland cement as a binding material in the concrete. India produced cement worth around 502 million tonnes in 2018. Cement is not eco-friendly, so many environmental issues are associated with cement production in the industry. Cement production contributes around 8% of carbon dioxide in greenhouse gas emissions. Cement production reduces natural resources and also pollutes the environment that is very hazardous for our future. There are limited natural resources available on the earth, so we must go for sustainable development.

On the other hand, an abundance of industrial solid waste like flyash, slag, and rice husk ash is available on the earth. In India, 200 million tonnes of flyash are produced annually in thermal power plants, and 20 million tonnes of slag are produced annually in steel manufacturing plants. Flyash and slag are wastes of that industry, so they dumped the industrial solid wastes in the ground using cultivated land and polluted the environment due to the limited use of industrial solid wastes like fly ash and slag.

Geopolymer was introduced by the Davidovits in 1978 and made by the alkaline solution's activation (consists of sodium or potassium silicate and sodium or potassium hydroxide) with the high alumina silica-rich materials. It is like ceramic composites that make the bonding between alumina and silica.

As it has similar structural properties, geopolymer-based concrete using Class-F fly ash has a high potential for use as a substitute for OPC-based concrete in the building industry (Albitar et al., 2015).

Sathonsaowaphak et al. (2009) stated that the flow and power of the geopolymer are increased by an improvement in the fineness of BA. The grinding increases the surface area and the reactivity, and in the as-received BA particles, the pores are also dissolved. Using field BA with 3% retained on sieve no. 325, comparatively good workability and strength are obtained.

Deb et al. (2014) stated that the workability of geopolymer concrete declined as the other mixture variables remained the same with the growth in GGBFS content and flyash in

the binder. That is largely due to the rapid reaction of calcium and the slag's angular form compared with the spherical shape of the fly ash particle. The addition of GGBFS has increased the ambient temperature setting of the concrete. With the reduction of the activator to binder ratio from 0.4 to 0.35, workability also deteriorated.

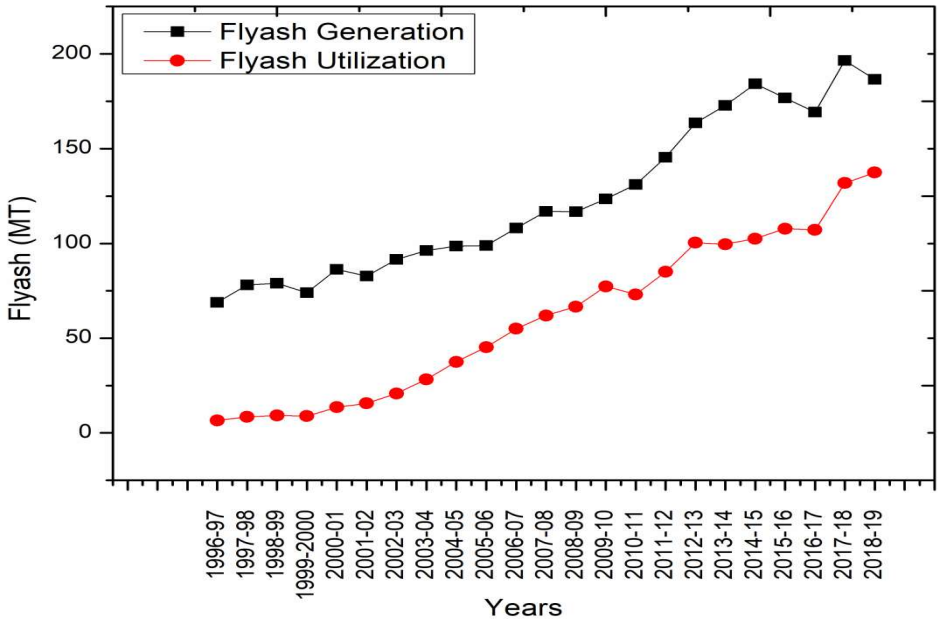

Fig. 1.1 Flyash generation and utilization in India 1996-2019

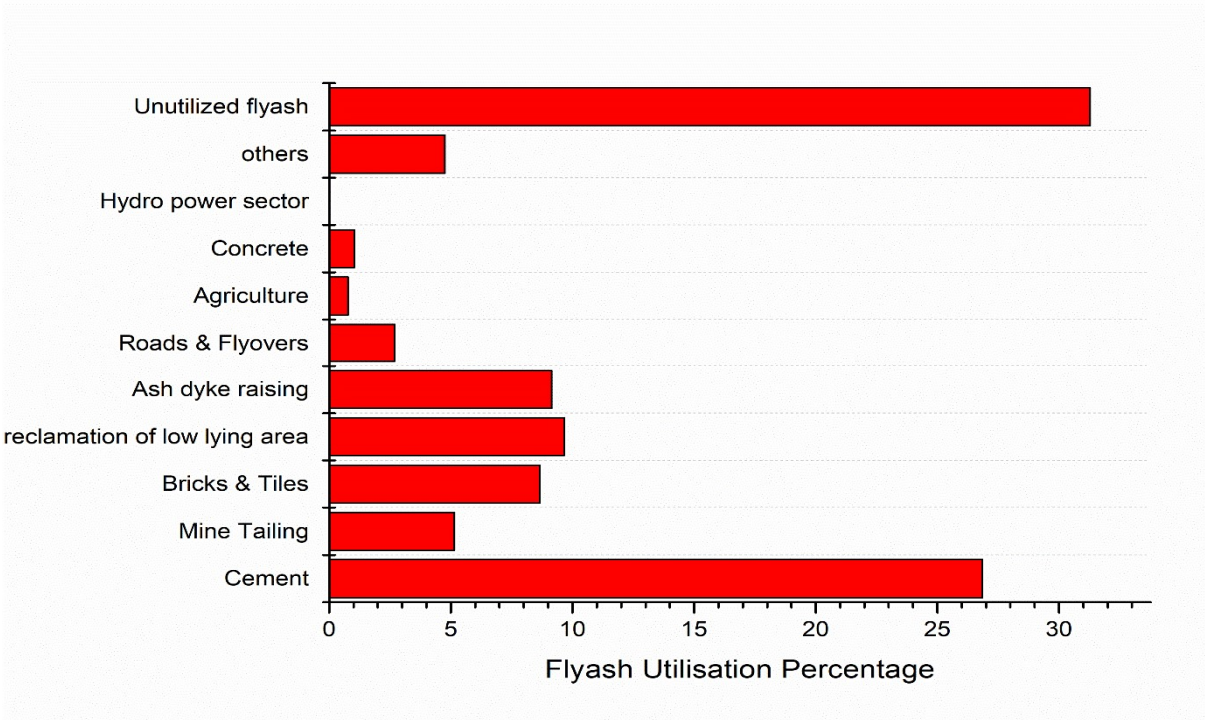

Fig. 1.2 Utilization of the flyash in various in India 2019

1.2 Mechanism of Geopolymerisation

Geopolymerisation is a reaction in which the formation of the alumino-silicate gel structure uses silica and alumina content from the pozzolan binding material like flyash and slag activated by the alkaline solution (containing NaOH and Na_2SiO_3). The microstructure of the geopolymer crosslinked shows higher stability against external environmental conditions. In the Geopolymerisation process, alkali metal plays an essential role in the reaction rate and reaction end products. It is an inorganic polymer that shows an amorphous nature at high temperatures. The heat-curing increases the geopolymerisation rate compared to the ambient-temperature curing. Eq.s (1.1) and (1.2) show the geopolymerisation reaction process from starting to the specimens hardening. The end products of the geopolymerisation show the three-dimensional structure.

$$n(Si_2O_5, Al_2O_3) + 2nSiO_2 + 4nH_2O + NaOH\ or\ KOH \rightarrow Na^+, K^+\, n(OH)_3 - Si - O - Al^-(OH)_2 - O - Si - (OH)_3 \quad (1.1)$$

$$n(OH)_3 - Si - O - Al^-(OH)_2 - O - Si - (OH)_3 \overrightarrow{NaOH\ or\ KOH}\ (Na^+, K^+)(-Si - O - Al^- - O - Si - O-) + nH_2O \quad (1.2)$$

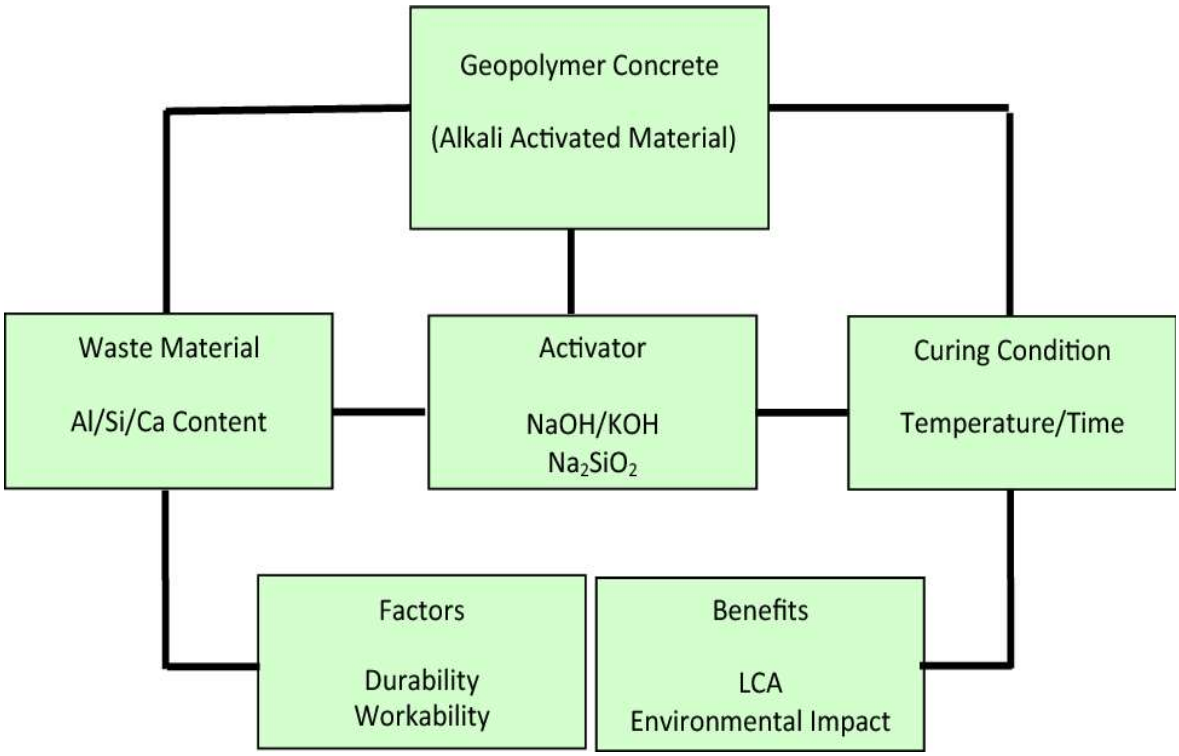

Fig. 1.3 Mechanism of Geopolymerisation

Like Na and K, the alkali metal is used in the activator solution to activate the pozzolanic binding material. They form the zeolitic structure during the geopolymerisation reaction. SiO_2/Al_2O_3 ratio content in the mix plays a vital role in forming the microstructure with curing temperature. Fig. 1.4 shows the effects of the curing temperature on the SiO_2/Al_2O_3 ratio in forming the zeolitic structure of the endproducts of the geopolymerisation. It also shows the amorphous nature of the gel product up to the elevated temperatures by forming the poly-sialate-siloxo $(Si\text{-}O\text{-}Al\text{-}O\text{-}Si\text{-}O\text{-})_n$. The content present in the mix design does not involve the end product of the geopolymerisation reaction.

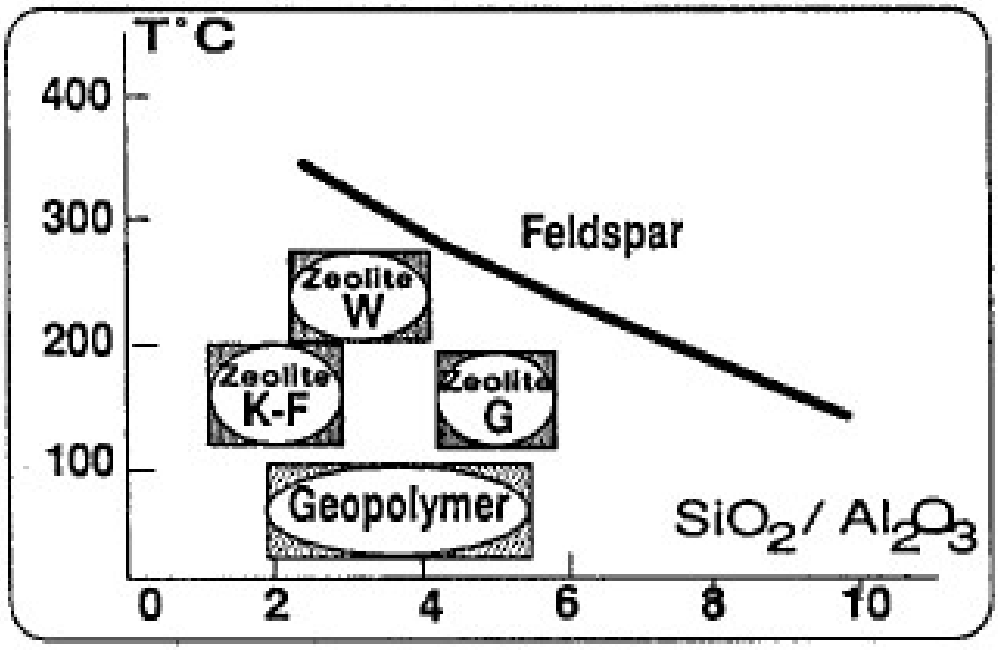

Fig. 1.4 Crystallization temperature ranges for K_20- Al_20_3- SiO_2 system[4]

Borges et al. (2014) have suggested that the quartz-made geopolymer concrete provided better properties than those made from glass aggregate and represented the technique of andreasen particle packing on geopolymer concrete growth. By studying the parameters such as andreasen packing factor, the solution to the rate of solids, and the aggregate form, they studied micro concrete.

Reddy et al. (2013) studied durability in the marine environment of flyash-based geopolymer structural concrete. For geopolymer concrete, the intensity increased by 15% (8M) and 7% (14M), respectively, 7 days and 28 days. For GPC compared to OPC steel, the fracturing tensile strength was also consistently higher. The marine environment did not greatly compromise geopolymer concrete's electrical resistivity.

Deb and Sarker (2016) studied ultrafine flyash on the setting time, power, and porosity of room temperature healed geopolymer concrete. The investigator stated after the test that the ultrafine flyash decreased the setting time, increased the compressive strength, and decreased the porosity of geopolymer concrete. And the highest compressive strength increase is only geopolymer concrete at 10% ultrafine flyash for flyash.

Chotetanorm et al. (2013) studied sorptivity, pore size, and resistance of high calcium bottom ash geopolymer mortar to sodium sulphate attack. After the test, the investigator stated that fine bottom ash presented high compressive power due to improved reactivity from a higher surface area than medium and coarse bottom ash. The fine bottom ash inclusion decreased the sorptivity and increased the resistance to the attack of sodium sulphateate.

Topark-Ngarm et al. (2015) studied The setting time, compressive power, elasticity modulus, and strong calcium flyash geopolymer concrete bond strength. The author stated after the test that high calcium flyash was sufficient for the development of high-strength geopolymer concrete with a high bond strength between concrete rebars. And the bond strength of geopolymer concrete with heavy calcium flyash was marginally higher than that of geopolymer concrete with calcium flyash.

Erdogan (2015) studied the properties of geopolymer mortar and ground perlite. The author stated after the test that the perlite could form a geopolymer mixture. By activation of ground unexpanded perlite, the compressive intensity of 30-40 MPa could be achieved. Analysis of XRD, FTIR, and NMR showed that NaOH solution activated mixtures undergo more geopolymerisation than water glass-activated mixtures when cured at 100^0C.

Chindaprasirt and Silva (2012) investigated fine high calcium flyash is used for high-strength geopolymer concrete. After the experimental investigation, the author concluded that while manufacturing ideal parameters of delay time, curing temperature, and curing length at high temperatures, geopolymer properties could be maximized. When kept in a normal atmospheric condition after the initial heat curing time, the high calcium flyash dependent geopolymer mortars begin to gain strength.

Nagalia et al. (2016) investigated the compressive power of flyash-based geopolymer concrete and its microstructural properties. The investigator concluded after the experimental investigation that the higher CaO content in flyash provided substantially

greater strength in finished geopolymer concrete. A large improvement in compressive strength was also obtained by a higher curing temperature and a long curing time. The analysis reveals that greater NaOH molarity increases kinetics with higher flyash-containing CaO.

Kupwade-patil and Allouche (2013) studied the effect on flyash-based geopolymer concrete of the alkali-silica reaction. The investigator concluded after the experimental investigation that the OPC concrete displayed higher average expansion by a factor of 6 compared to geopolymer concrete specimens after exposure to 1M NaOH solution at 80^0C for 90 days. The result shows the re-initiation of the geopolymerization process of unreacted flyash particles at elevated temperatures, leading to lower porosity and greater intensity.

Kupwade-patil et al. (2013) examined corrosion-induced by chloride in reinforcement concrete. The investigator concluded after the experimental analysis that the geopolymer concrete specimen was formed to exhibit lower average diffusion, coefficients, the content of chloride, and porosity than their equivalents of OPC. The resistance to chloride-induced corrosion of geopolymer concrete specimens made from class f flyash was considerably higher than that of OPC specimens and geopolymer concrete specimens made from class c flyash.

Liu et al. (2016) studied the properties of recycled aggregate concrete in geopolymeric. The investigator concluded after the experimental investigation that the compressive power, young module, and poissons ratio decreased for GRAC specimens with the rise in the w/c ratio. There was no well-developed interfacial transition zone between the old cement paste and the modern geopolymer cement paste revealed by SEM and nano-indentation technologies.

Ban et al. (2015) studied the effects of sodium silicate and the curing regime on the block properties of load-bearing geopolymer mortar. The investigator concluded after the experimental investigation that early intensity growth is triggered primarily by the formation of N-A-S-H and K-A-S-H geopolymeric gel. Meanwhile, the production of long-term intensity is caused by the formation of (Ca, K)-A-S-H geopolymeric gel and C-S-H secondary gels.

Zhao and Sanjayan (2011) analysed geopolymer and cement concrete from portland in the simulated blast. The investigator concluded after the experimental investigation that

geopolymer concrete had greater spalling resistance than portland cement concrete to increasingly increasing exposure to temperature. Portland cement concrete with high strength exhibited severe spalling, while portland cement concrete with normal strength exhibited mild spalling.

Ismail et al. (2013) studied the microstructural modifications in the sulphate-exposed alkali-activated flyash-slag geopolymer. The investigator concluded after the experimental investigation that magnesium sulfate is more offensive than sodium sulfate against geopolymer paste. The geopolymer paste densifies the binder at a low w/c ratio and decreases the attack rate on the binder system.

Kong et al. (2008) studied the influence of elevated temperatures on geopolymer paste, mortar, and asphalt. The investigator concluded after the experimental investigation that the smaller aggregate size (less than 10 mm) facilitates spalling and substantial cracking in geopolymer concrete while the larger aggregates of geopolymer concrete (more than 10 mm) are more durable with elevated temperature. In geopolymer concrete for elevated temperature efficiency, the use of superplasticizers is not advantageous.

Kong et al. (2007) studied the comparative output of the geopolymer generated with metakaolin and flyash after elevated temperature exposure. The investigator concluded after the experimental investigation that the geopolymer based on metakaolin had considerably higher moisture loss than the geopolymers based on flyash. The geopolymer pores of metakaolin were mainly composed of mesopores, while the pores of flyash contained larger micropores than the geopolymer of metakaolin.

Pan et al. (2009) investigated the geopolymer mortar's power gain or loss function after elevated temperature exposure. After the experimental investigation, the investigator concluded that at a higher temperature, the sintering or further geopolymerization has an impact on increasing the power, and the second is the harm due to thermal incompatibility.

Gluth et al. (2016) studied the acoustic emissions and microstructural shifts in simulated fire-exposed flyash geopolymer concrete. The author concluded that after the fire test, the degradation was usually less in GPC-EC than in GPC-Q and again attributed improved compatibility between paste and aggregate.

Pan et al. (2014) studied the stress-strain conduct and sudden loss of geopolymer rigidity at elevated temperatures. The author concluded after the experimental investigation that

the geopolymer exhibited glass transfer activity at 560^0C, and increased applied stress at elevated temperatures leads to high contraction.

Pan and Sanjayan (2010) studied the impact of transient creep on geopolymer concrete compressive strength for elevated exposure to temperature. The author concluded that the geopolymer temperature below 250^0C displayed a greater transient creep than OPC paste. The 250^0C-550^0C geopolymer range did not show any substantial increase in transient creep, although significant transient creep was generated by OPC paste. A strong increase in elastic modulus was shown by geopolymer, while OPC showed little improvement in elastic modulus.

Rickard et al. (2012) studied the thermal study of geopolymer pastes synthesised from fine flyash of variable composition. The author concluded that the fly ash with a high reactive Si: Al ratio greater than five was enabled by sodium aluminate and formed a geopolymer with a low to moderate compressive strength but excellent dimensional stability during heating and higher compressive strength after heating.

1.3 Gaps Found Through Literature Review

- There is much industrial solid waste like flyash generated without utilisation.
- There is no clear work on the ambient temperature curing conduction on geopolymer concrete.
- The durability test was not carried out on the geopolymer concrete based on flyash and slag.

1.4 The Objectives of The Research

After the literature survey on geopolymer concrete, we decided the following objectives for the PhD research work are as follows:

- To design the flyash-slag-based geopolymer concrete without using cement.
- To study the effect of salient parameters on the properties of geopolymer concrete.
- To recommend the mixed design of the flyash-slag-based geopolymer concrete for future applications.

1.5 Scope of Work

The research utilised flyash and GGBFs as binding materials in the mix design of geopolymer concrete. Flyash and GGBFs are industrial solid wastes activated by the alkaline solution for the concrete's binding property. It directly reduces cement consumption and indirectly reduces carbon footprints because it directly reduces cement production. Around one tonne of carbon dioxide is emitted into the environment during one cement production. The research work is to find the performance of geopolymer concrete and to project an alternative to ordinary concrete. After the experimental investigation, the author concluded that the geopolymer concrete would be used in the following applications:

- Retrofitting of structures/heritage structures and buildings
- Smart structures
- Bridges/overpasses
- Pavements/runways of airports
- Harbour structures
- In all applications of conventional and high-strength concrete
- In manufactured precast elements for residual and commercial buildings

1.6 Thesis Arrangement

Chapter 1 describes the general introduction of the research work area related to their aim of work and the research work scope in the field. At the start of the introduction, generalised information about the topic of research with respect to the usage of raw materials in production is presented.

Chapter 2 introduces a large, comprehensive survey of the literature about the geopolymer concrete research being done. The comprehensive survey is based on the factors that directly affect the performance of geopolymer concrete.

Chapter 3 describes the materials used in the mix design geopolymer concrete with their detailed properties. The tests carried out on the materials to find out the quality of the materials are also mentioned. The sample forming process for different mixes and

different tests performed on the same one is also defined. It also defined the complete experimental setup summary of the specimens with the equipment's working descriptions as per the standard codes.

Chapter 4 describes the results and discussion section of the various experimental tests conducted on the different specimens on all geopolymer concrete mix designs. In the experimental investigation, fresh, chemical, and mechanical properties of various parameters were tested to find the optimum point, in which the GGBFS to flyash ratio by weight ranged from 00/100 to 25/100, liquid-to-binder ratios ranged from 0.4 to 0.7, superplasticisers content percentage ranged from 0.5% to 2.0%, molarity of sodium hydroxide ranged from 8M to 16M, sodium silicate to sodium hydroxide ratios ranged from 0.5the optimum point of strength, the GPC specimens were subjected to tests for durability studies, in which they checked the effects of elevated temperatures up to 800^0C, seawater condition, sulphate attack (both sodium sulphate and magnesium sulphate), acid attack, freeze-thaw condition, wetting-drying condition, and freeze-thaw condition, and compared them with the OPC concrete specimens.

In the experimental investigation, the workability was tested using slump, density, compressive strength, splitting tensile strength, flexural strength, poisons ratio, elastic modulus, rebound hammer strength, and ultrasonic pulse velocity as various parameters. In durability tests, to check the density, mass loss, compressive strength, residual compressive strength, ultrasonic pulse velocity, and visual inspection.

Chapter 5 described the statistical analysis or regression analysis of the experimental data to generate the correlation eqs. among the mechanical properties and compared them to the other eqs. given by the various country's standard codes or other authors.

Chapter 6 described the sustainability and cost analysis of both mixed designs and compared them to find the best. The cost of the geopolymer concrete materials cost is comparably low to the OPC concrete materials at one metric cube.

Chapter 7 described the detailed conclusions of the experimental investigations, statistical analysis, and cost analysis of the geopolymer concrete mix designs. It also describes the effects of various parameters on the performance of the geopolymer concrete.

CHAPTER 2 LITERATURE REVIEW

2.1 Technical Aspects

2.1.1 Fly ash

The flyash is generated from the thermal power plant by the electrostatic precipitation of the coal combustion fume. Flyash rich in silica and alumina constituents shows the pozzolanic characteristics and demonstrates the binding properties. The flyash used in the GPC provides better workability and higher solids to liquid ratios than the other pozzolanic materials like slag, metakaolin, and rice husk ash due to their small particle size, spherical, and porous nature [20]. In the GPC, the bottom ash usage's fineness increases the strength and workability of the increasing surface for reactivity and collapses the pores in the matrix. Bottom ash increases the workability by the fine particle's porous structure in the GPC [2]. The dosage of the ultrafine flyash decreases the setting time, but up to the 15% dosage of ultrafine flyash, the setting time is longer than with the flyash-based GPC. The dosage of the ultrafine flyash increases the strength of up to 10% of the GPC by reducing the matrix's porosity [7]. The fineness of flyash is the deciding factor for the amount of flyash required for the mix design of GPC because of increasing the fineness of flyash, decreasing the quantity requirement for mix design [26]. The fineness of flyash plays a vital role by reducing the porosity and water absorption capacity of both concrete GPC and OPC concrete [27]. The fineness of the flyash increases the workability, density, and strength of the GPC. It slightly affects the alkalinity of the GPC but is similar to the OPC concrete [28].

2.1.2 GGBFS (Ground granulated blast furnace slag)

In the GPC, increasing the dosage of GGBFS decreases the mix's workability due to the angular particles of samples compared to the spherical particles of flyash, but it increases the setting in the ambient temperature by the reaction of calcium present in the slag. The slag's dosage with flyash in the GPC presents the compressive strength of ambient cured specimens similar to the water-cured OPC concrete. The specimens' strength gains slow down after 28 days but strengthen up to 180 days [3]. In the GPC, the strength increases with the dosage of GGBFS in the mix design and eliminates heating conditions for curing

[29]. The slag/flyash ratio increases in the mix design show less mass loss at the elevated temperatures [30].

2.1.3 Geopolymer Mortar

The geopolymer mortar required water and superplasticizer to increase the workability because of the increase of the sodium silicate and NaOH concentration degradation of the mortar's flowability or workability. The use of superplasticizer also shows the adverse effect on geopolymer mortar strength [31]. The GPC increases the dosage of slag, and sodium silicate in the mortar mix reduces the porosity and simultaneously reduces the mesopores volume and makes a denser matrix due to the more reaction products. The autogenous shrinkage of the geopolymer mortar develops due to the self-desiccation in the solid-state but the chemical shrinkage in the fresh state. The AFS mortar mortars show higher drying shrinkage than the OPC specimens due to the high capillary stress in the mix samples [32]. The AFS mortar has higher compressive strength, flexural strength, and lower water absorption than the OPC mortar samples. The hydration product of the AFS paste is mostly amorphous, and the higher flyash content shows the lesser length change [33].

The increase in the water to binder ratio in the AFS mortar increases the flow of mortar. When the fine-aggregate to binder ratio beyond 2.5 shows, the flow of mortar instantaneously decreases. The GGBFS-based mortar shows a higher strength than the flyash-based mortar, and the compressive strength of the mortar increases with the increment of the fine aggregate to binder ratio up to 2.5 and beyond 2.5, the ratio strength drastically degrades [34]. The geopolymer mortar strength increases with each increment of temperature, but strength reduces beyond the 800^0C temperature. The geopolymer mortar compressive strength depends on the bonding between the binder and aggregate, and increases in the proportion of the aggregate in mortar reduce the geopolymerisation [35]. The thickness of geopolymer paste is the main factor influencing the mortar's heat-resistant property and changes in aggregate, and the mass ratio of paste to fine aggregate affects the thickness of the paste. If it is too thick, the water vapour collapses the structure when released, and if it is too thin, the paste cannot bond aggregate together [36].

In the geopolymer matrix, high calcium flyash is added to the mix to gain a high-strength geopolymer mortar up to 86MPa at 28 days [37]. The heat evolution in the geopolymerisation is first due to sodium silicate and gelation and second to bulk

hydration of GGBFS responsible for strength development observed in the calorimeter. After the reaction, the products are amorphous and uniformly distributed throughout space in the matrix. In the hydration process, the IP regions containing Mg and Al were observed in the SEM analysis. The IP rims are highly responsible for slowing down the reaction rate [38].

2.1.4 Effect of Alkaline solution

The GPC used sodium hydroxide to increase the mechanical properties compared to the OPC concrete and got the higher strength and performance of the GPC [39]. Instead of the sodium silicate, KOH generates a much more heterogeneous structure, higher porosity, and lower strength developed after the hydration process [38]. Sodium hydroxide with sodium silicate is used as an alkaline activator of the binder in the 1:1 ratio in the mix design to produce the above 40MPa GPC in early time and verify the potential of flyash to replace cement [40]. The compressive strength of GPC increases with an increment in the molarity of sodium hydroxide, but the workability reduces [9,39,41–44]. The flyash/slag-based paste setting time reduces as the slag's dosage, sodium silicate, and sodium hydroxide molarity increase. The initial time is 55 minutes, and the final time is 160minutes of the flyash/slag-based paste at the room temperature of 17^0C [45]. The compressive strength of 30MPa was quickly achieved with the range of molarity of 9.5-14M of NaOH at room temperature in 28 days [46]. The geopolymer matrix developed in the GGBFS is similar to the matrix developed in the absence of the GGBFS. If the NaOH concentration is low, the calcium content of the GGBFs participates in the development of amorphous CSH gel and the formation of calcium-based geopolymer. If the NaOH concentration is high, the precipitation of calcium hydroxide develops [47].

The addition of sodium silicate extensively increases the hybrid geopolymer system's early strength development [16]. The interface between aggregate and geopolymeric paste is not apparent after the high soluble silicate dosage in the salt-free geopolymeric mortar. In the geopolymerisation process, soluble silicates are very useful in degrading alkali saturation in the GPC pore solution even after using a high-alkali-concentrated activating solution and promoting the higher inter-particle bonding binder as well as the aggregate surface. Geopolymerisation leads to reliable geopolymer results like binders, mortars, and concretes [48]. The ratio of sodium silicate to sodium hydroxide by mass

increases with the increasing compressive strength of GPC [44]. If the alkaline solution content increases in the mix, then the setting time and workability increase with the reduction of the compressive strength. The alkaline ratio increased from 1.5 to 2.5, and the alkaline solution increased from 35% to 45% by mass of binder and found the optimum point at 2.5 alkaline ratio and 40% alkaline solution in the mix [49]. In the GPC, the class C flyash used as binder activated by the alkaline activator with the higher alkaline ratio develops the high compressive strength in which the molar ratio of SiO_2/Na_2O is 1.5 [50]. The yield point of the compressive strength of mortar and paste found at the molar ratio of Na_2O/SiO_2 is 0.40 and shows the paste's denser morphology. If the Na_2O/SiO_2 molar ratio increases, then the consistency of the paste decreases. It forms the alumino-silicate gel with the flyash content and is responsible for the higher workability and the mechanical properties of the GPC samples in the hardened state [51]. If it increases the ratio of $Na_2SiO_3/NaOH$, it decreases the requirement of fine aggregate in the mix and increases the additional water requirement in the mix [26].

2.1.5 Effect of Aggregates

The GPC has better stability against elevated temperatures and better compatibility between the aggregates and pastes [22]. The aggregate size in GPC has a critical effect on the elevated temperature; the spalling of GPC decreases as the maximum aggregate size of the GPC mix design increases. The size of the fracture process zone increases with the aggregate size by shielding the crack tip. By improving stability, the maximum aggregate size increase in mix design became the higher resistance to fire [52]. Geopolymer aggregate was developed from the mine tailings of flyash and is used as lightweight aggregates in mortars and concrete. The geopolymer aggregate shows better mechanical properties than the LECAs in the solid-state of the mix design, whereas the rheological properties are the same. The geopolymer aggregate shows a better crushing value and excellent bonding due to the aggregate's rough surface [53]. Geopolymer sand dosage in the mix design shows better mechanical properties up to the 40% replacement with the natural sand, but beyond the 40%, the mechanical properties of the mix decrease with the increasing content of Geopolymer sand [54]. In the GPC, the strength of concrete increases with the increment of the m-sand in the design mix by replacing the natural sand up to 20%, but beyond that 20%, its strength slightly decreases compared to the nominal mix [55]. The GPC uses 100% m-sand to replace natural sand, which shows

adequate strength, and it is an economical, environment-friendly material that reduces carbon footprints by up to 80% [56]. In the GPC, the dosage of the RCA in the mix design shows an adverse effect on the compressive strength, splitting strength, sorptivity, chloride ion penetration, water absorption, and volume of voids, but the properties are better than in the OPC concrete [57].

2.1.6 Effect of Alkali Metal in Activator

Geopolymer concrete is made by the geopolymerisation reaction among the binding constituents of the concrete in which alkali metal cation plays a vital role in every stage of the reaction of geopolymerisation. The type of alkali metal cation is also an essential factor for the geopolymerisation reaction in all the reaction stages. It also affects the speed of the setting time of the paste and the condensation reaction of the GPC, and the alkali metal cation works as a template of the reaction's reaction in directing and controlling the molecules' reaction and final structure formation. The size of the alkali metal cation also plays a role in forming the structure of the geopolymer. The potassium cation (K) is responsible for a higher degree of condensation than the sodium (Na) cation in the same condition. Potassium cation shows a higher compressive strength due to the higher surface area, produces a higher amorphous structure, and is less resistant to HCl attack.

Alkali metal depends on the source material (Si and Al content) for the reaction because the different source materials directly affect the end products' physical and chemical properties [58]. The GGBFS-based geopolymer directly depends on the chemical composition of reactions. In the geopolymer reaction, K_2O content plays a vital role in the reaction; increasing the K_2O content in the composition increases the compressive strength, setting time, and fire-resistant characteristics of the end products [59]. The thermal stability of the geopolymer product made with the sodium-containing activators is less than the potassium activated due to functional changes in the microstructure. The sodium-activated geopolymer shows deterioration of strength sharply at 800^0C due to increases in the average pore size. The materials prepared with the potassium silicate and flyash show better thermal stability than the sodium-containing activator used. In the sodium activator, the amorphous structure was replaced by the crystalline Na-feldspar, but in the potassium activator used, the materials remain amorphous up to 1200^0C. The geopolymer material produced by using flyash and sodium or potassium silicate shows

very high shrinkage and effective changes in the compressive strength on increasing the temperature in the range 800^0C-1200^0C [60]. In the geopolymer materials, a sodium-containing activator shows thermal stability up to 500^0C, which is more stable than the regular concrete mix [61]. The geopolymer's thermal shrinkage mostly depends on the Si/Al ratio and alkali used in the activator. The low Si/Al ratio used in the mix shows better thermal stability than the higher Si/Al ratio and shows densification at elevated temperatures [62]. The alkali activator content also plays an effective role in finding the compressive strength of the GPC. Increasing the alkali content increases the compressive strength due to the solubility of the alumino-silicate with the increase in Na_2O concentration, but beyond 10% does not show an effective increase in strength. The content of Na_2O ranges between 6-15% by mass [50]. Suppose the sodium and silica content at a higher level shows higher autogenous shrinkage, but the mechanism of the geopolymer matrix's autogenous shrinkage is different from cement paste. In the geopolymer, the reorganisation and geopolymerisation of the structure generates a finer pore size distribution that generates autogenous shrinkage instead of self-desiccation in the cement matrix [63].

2.1.7 Effect of Activator liquid to binder ratio

f the activator to binder ratio decreases from 0.40 to 0.35, then the fresh mix's workability decreases, but extra water enhances the workability and strength reduced. The strength got up to 51MPa after 28 days of the GPC containing 20% slag and 80% flyash as the binder and cured at 20^0C [3]. In the flyash-slag based GPC, the slag/flyash plays an essential role in the mechanism of the geopolymerisation for strength development. If the slag content in the mix design is over 50% of the binder, then show the calcium silicate hydrate gel's primary reaction with the Na and Al and form the C–N–A–S–H bond. If increasing the flyash content in the binder, then the formation of N–C–A–S–H type gel as a primary reaction, bound the water tightly in the composition and got a higher degree of crosslinking compared to the composition formed of C–A–S–H type gel in the slag binder. This study provides critical evidence of the different mechanisms of the geopolymerisation based on the slag/flyash ratio content as a binder in the mix design. If the small dosage of the slag in the flyash is in the mix, the reactions slowdown information of C–A–S–H binding gel and the formation of the hybrid C–N–A–S–H gel due to the overtime release of the Si and Al in the reactions. Increasing the dosage of

class f flyash in the mix promotes the development of the zeolite in the hybrid gels after 28 days of higher temperature curing with a lower concentration of the activator. After the long curing age, the gels' microstructure formation predicted the mechanical capability and durability performance of the GPC samples [64]. If the 15% ACS replaces the GGBFS in GPC, it leads to the thermal stability of the GGBFS-based GPC up to 1000^0C and shows the amorphous nature to resist the heat treatments used in the formation of refractory bricks. If increasing the dosage of ACS by up to 25% decreases the thermal stability of the geopolymer, If the GGBFS replaces the silica fume by 10%, it increases the strength at a high level and shows thermal stability up to 500^0C, whereas the ACS dosage shows the thermal stability up to 800^0C [65]. If the dosage of slag and sodium silicate increases, the autogenous shrinkage and chemical shrinkage, and if the water binder ratio decreases, drying shrinkage becomes lesser and autogenous shrinkage becomes higher of the AFS mortar [32]. In the GPC, if the slag content above 70% in the mix reflects the rapid setting and cracks generated due to the autogenous shrinkage and shows the denser matrix of the hydration products. The Geopolymer matrix is not affected by using the superplasticizers in the mix design [66]. If increases, the inclusion of the GGBFS, OPC, and CH in the flyash increases the concrete's compressive strength, but it is applicable when no extra water is added with the alkaline solution [67]. With increasing GGBF dosage, GPC workability and setting time decrease. If the GGBFS dosage is up to 30% of the binder, it will have the strength of 55MPa of GPC and 63MPa of geopolymer mortar at 28 days [49]. In the GGBFS/flyash-based GPC, the formation of C-S-H gel at the 27^0C by activating GGBFS shows minimal interaction of the flyash and GGBFs due to different reaction processes. The strength of the mix design is developed by the C–S–H gel formation products [68]. The presence of the CSH gels and geopolymeric gels in the matrix enhances the strength of the system with the usual quantity of GGBFS. The CSH gel formation in the geopolymer matrix worked as the micro-aggregate and resulted in excellent mechanical strength [47].

In the GPC, the flyash to activator ratio plays an essential factor regarding strength and fire-resistant matrix, and silicate to hydroxide, binder age, and curing period show negligible effects on the early strength of the GPC. The optimum point of strength and fire-resistance is found at Na_2SiO_3/KOH = 2.5 and FA/activator = 3.0 [19,69]. In the GPC, water present in the fresh concrete mix and removed through evaporation makes a crack-free geopolymer [70]. The workability of the fresh concrete increases with the

increment of water dosage in the mortar mix. In the GPC, when the molarity of sodium hydroxide is above 10M, it shows an increment of workability with fewer effects on strength by increasing the water content in the mix [2]. The strength of the GPC decreases with the increment of the water to geopolymer solids ratio by mass. It made the loose microstructure of the geopolymer paste in the concrete [71].

2.1.8 ITZ (Interfacial Transition Zone)

The reaction mechanism of ITZ is slightly different from the matrix reaction. In the ITZ reaction, a tremendous number of voids with the water content of ITZ initially, but after the hydration process, the voids are filled by the hydration products. The difference between the microstructure of the matrix and ITZ is challenging to identify after the reaction. EDAX results describe K/Al and Si/Al content in the ITZ found at a higher level than the bulk matrix, and well-developed crystalline is not present in the ITZ and forms a sponge-like amorphous gel [72]. The ITZ properties of sodium silicate activated mortar are good with very low porosity at the interface, and thermal activation provides the early strength even when the reaction slows down to give a large age span before setting time [38]. A high concentration of the alkaline solution is required for the strong ITZ bond between the siliceous aggregate and class-f flyash [73]. There is no ITZ bond formation between the old cement paste and the geopolymer matrix, according to SEM and nanoindentation analysis [15]. The superplasticizer used in the mix design improved the microstructure of the ITZ of concrete. The ITZ thickness directly affects the compressive strength of the concrete, and it is affected by the superplasticizer dosage in the mix. If the ITZ thickness decreases, then the compressive strength of the mix increases. The lower dosage of the superplasticizer in the mix develops the loose and porous ITZ between the aggregate and binder and decreases the mix concrete's performance by reducing the compressive strength. When the superplasticiser dosage is high in the mix, it develops the dense ITZ and increases the performance of the concrete [74]. Soluble silicate in the mix as activator liquid plays an essential factor in developing the ITZ between the aggregate and paste in the GPC. If the soluble silicate quantity is meagre, the mix shows the weak compressive strength of the paste mortar and concrete compared to the high dosage of silicate soluble. The chloride present in the mix shows the debonding between the aggregate and paste by crystallising the paste at the ITZ [48]. Suppose the LWA used as aggregate in the GPC shows excellent bonding at the ITZ due

to the aggregate's porous and rough surface. The bonding zone deteriorates at the temperature of 800^0C due to the dehydration of microstructural water, and swelling the unreacted silicate content in the matrix creates microcracks between the paste and LWA [75].

2.1.9 Effect of curing conditions

The curing temperature plays a vital role in the setting and hardening of the GPC. If the curing temperature increases by 4 hours at ambient temperature, but if the ambient temperature is below the 10^0C setting, the fresh concrete setting takes up to 4 days without losing quality. The GPC specimens cured at the higher temperature got the mechanical strength within 1 day, but the hardening of the fresh concrete at ambient temperature got higher quality strength after 28 days compared to the strength gained in 1 day. The curing time also plays an essential role in gaining strength with temperature [76]. The compressive strength of the GPC increases with the increase in the curing temperature from 30°C to 90°C [39,44]. If the curing at the ambient temperature is impossible due to the delay in setting time of flyash-based GPC, the temperature for curing is favourable for gaining higher strength, and long curing time enhances the Geopolymerisation process. The higher temperature curing of the GPC samples for a long time leads to the development of microcavities in the microstructure, which creates cracks in the sample due to the water evaporation from the matrix [77]. The GPC flexural strength is higher than the OPC concrete of the same compressive strength samples [67]. In the natural pozzolanic-based GPC, the compressive strength increases with the increasing time and temperature. The application of curing in both conditions under atmospheric pressure up to 100^0C and autoclave curing above 100^0C enhances the compressive strength of mix samples by eliminating the micro-cracks in the samples [78]. If the curing time increases from 6hrs to 96hrs, it increases the compressive strength of the GPC, but beyond the 48hrs of curing, the compressive strength of the samples is not significant [44]. Pre-curing at ambient temperature with above 95% humidity at room temperature before the heat curing is beneficial for strength development [78]. Temperature curing is responsible for curing the specimens for 1 hr at an elevated temperature does not create remarkable strength development. The longer curing time is responsible for the strength development at early ages by accelerating the reaction rates [76]. The curing age enhances the polymerization process from 4 hours to 96 hours and

increases the compressive strength, but the strength development of the samples got at 24 hrs curing, so there is no need to cure beyond the 24 hrs [79].

The geopolymerisation reaction increases with the increase in curing temperature and develops the early strength of the GPC [1]. The GPC samples cured in the fog show the high absorption of the moisture. The fog cured samples develop the mostly open microstructure of the endproducts of GPC [71]. In the GPC, the oven-cured specimens got 90% strength in 3 days of 28 days of compressive strength, but the ambient-cured samples got up to 82% strength in 28 days. The ambient-cured specimens' ultimate strength got higher than the oven-cured samples because the rate of development of the strength beyond 7 days is not significant [80].

The elastic modulus of the GPC is directly affected by the curing temperature; the MOE of the specimens increases with the increasing temperature of curing up to a limit and is related to the water to binder ratio. The evaporation of the water from the matrix during the temperature curing reduces the elastic modulus of the GPC specimens [81].

2.1.10 Effect of calcium content

The calcium content present in the slag and OPC is used in the GPC to form the CSH gel with the geopolymeric gel at the low alkaline condition and improve the mix's compressive strength. The lower content of calcium content available to less CSH gel resulted in the mix's lower overall strength. In the high alkaline condition, the calcium content plays a negligible role in strength improvement and forms the precipitation at the CSH gels' place [82]. The high calcium BA's mechanical strength depends on the fineness of the raw sample of BA and the water content in the mix design [8]. The calcium content present in the mix's slag is essential for both early and more prolonged age. If the reaction rate is slow, low strength development confirmed the low calcium flyash used as a binder with the lower concentration of alkali activator used without heat curing. The C-S-H/C-A-S-H precipitation formation initiates the strength development of the GPC fresh concrete, but in the flyash GPC, the hardening of the concrete by forming aluminosilicate precipitation. The free calcium content from slag and flyash dissolution increases the formation of the gel and develops the later strength of the hardened concrete [83], and the higher amount of calcium in the mix emphasises the C-A-S-H type gels end product with a chain structure [30]. High calcium content is attributed to high-strength GPC [9,39].

2.1.11 Effect of superplasticizers addition

A superplasticizer is used to increase strength by reducing the water content of the mix design of concrete. The addition of a superplasticizer up to 2% of the binder mass enhances the workability of fresh GPC with little effect on the strength of the hardened GPC [44]. Superplasticiser usage is not beneficial for the high-temperature performance of the GPC [84]. The naphthalene-based superplasticizer is very useful by increasing the workability of a slump of around 136%, but in the PCE-based superplasticizer, it increases the workability larger than SNF based around 145%, but it affects the strength of the design mix specimens by reducing the strength around 29%. In some cases, SNF-based superplasticizer is not adverse to the concrete's strength [85]. The addition of citric acid and sucrose is the perfect alternative chemical admixture to flyash-based GPC to enhance paste's rheological properties with increasing strength. Sucrose works as a retarder in the GPC mix, while citric acid accelerates the mix for hardening. The compressive strength of the mix was controlled after the addition of the sucrose but affected the paste's porosity characteristics. Sucrose-added samples have created a relationship between the compressive strength and porosity, where porosity directly attaches to compressive strength. Sucrose works as a chemical admixture as a retarder in prospect for the GPC [86]. The polycarboxylate-based superplasticizer defines the retarding effect on the flyash-slag based GPC without affecting the heat of hydration of the paste and enhancing the workability larger than the SNF-based superplasticizer. Increasing the content of PCE-based superplasticizer beyond 2% affects the development of strength before the 7 days, but after it could be adverse effects on the strength of the GPC [66].

Superplasticiser enhanced the workability and mechanical strength of SCGC and increased the development of the microstructure of bonding between the paste and aggregate at ITZ of GPC. The ITZ's microstructure is different from the change in ITZ thickness due to the variation of superplasticiser content in the mix and affected the compressive strength of GPC. By decreasing ITZ thickness, increased superplasticiser utilisation improves the compressive strength of SCGC and the built-quality microstructure. Superplasticiser content over 2% was found insufficient to generate the desirable workability with the resistance to segregation. In comparison, the superplasticiser content of 6% and 7% gives the required workability properties within the EFNARC limits, and 7% superplasticiser dosage produced the most significant

strength at all ages and increased the microstructural properties [74]. Palacios et al. stated that the most significant drop in yield stress in alkali-activated slag cement was found when a naphthalene-derivative HRWRA was added to NaOH-activated slag pastes and mortars because of its inherent stability in alkaline media. However, the other admixtures incorporated in alkali-activated slag pastes and mortars do not significantly modify their rheological parameters [87]. The conventional superplasticizer is generally used in OPC concrete as an additive to the binder for increased strength, but in the GPC mixe deteriorates the strength of the hardened specimens. The use of superplasticiser at an elevated temperature has a negative effect on the GPC mixed specimens. The SNF-based superplasticiser had a negligible effect on the strength at the higher temperature. SNF-based superplasticiser is also useful for the high molar NaOH content used in the GPC mix design [1].

2.1.12 Effect of handling time

The fresh GPC is easily workable for up to 120 minutes without any strength deterioration [44]. The workability of the fresh GPC increases with increased hand mixing time up to 30 minutes [42]. If increasing the mixing time, it's drastically retarding the setting time of the fresh concrete so. It is beneficial for working conditions [88].

2.1.13 Effect of silicate and alumina

In the SEM analysis, if the Si/Al ratio ≤1.40 is present in the matrix shows the clustered dense microstructure with large interconnected pores, and if Si/Al ≥1.65, then the homogenous microstructure with the porosity is distributed in the small pores. The matrix gel's microstructure increases with the increase of the silicon content available when the ratio is 1.40≤Si/Al≤1.65. The geopolymer microstructure was affected by the absorption of nitrogen and resulted in the volume expansion of the matrix. The larger gel volume is responsible for the higher compressive load and increases the young modulus when the microstructure of the gel is homogenous at the ratio of Si/Al is 1.65. So, the young modulus depends on both compressive strength and homogeneity in the microstructures of the gel. The ultimate strength of the mixed specimens was reduced beyond Si/Al = 1.90 due to the unreacted silica present in the matrix [89]. The thermal shrinkage increases as the mixed content's Si/Al ratio increases due to dehydration, dehydroxylation, sintering, and resilience [62]. The silica and alumina content play a vital

role in the reaction of geopolymerisation. Silica content presents the amorphous end products in the reaction, contributing to the higher compressive strength of the mix design through the denser matrix development. The mechanical properties also increase with silica content and achieve the maximum strength of 65 MPa [90].

In the GPC, SiO_2/Al_2O_3 and SiO_2/Fe_2O_3 ratios increase with increments in the temperature of curing, and this increases the mechanical properties of the GPC. It also reduces the water absorption capacity compared to the OPC concrete. The CaO content present in the mix does not affect the reaction of the geopolymer matrix [91]. The molar ratio of SiO_2/Al_2O_3 increases up to 3.4-3.8, which is highly responsible for the high strength gain at a later age [92]. In the flyash-based GPC, the Si: Al ratio of less than 5 present in the flyash activated with the sodium silicate shows low to moderate strength at ambient curing, but after the heat, curing shows excellent dimensional stability and high compressive strength. When the Si: Al ratio is 2, it shows high compressive strength but poor dimensional stability and reduces the strength after heating [25]. In the Geopolymerisation reaction, increases in alumina and silica content accelerate the setting within 3.20–3.70. The alumina content increases in the mix neither show any zeolitic phase development nor show the strength development of the mix samples [11]. The alumina content present in the mix is highly responsible for the setting time of the mix; increasing the Si/Al ratio leads to a longer setting time, and increases in Al content decrease the strength of the concrete [92].

2.2 Durability Studies

In the durability studies, the long-term strength of the GPC against the various aggressive environment problems for the concrete deteriorates with time in the aggressive environmental conditions. Acid attack, seawater conditions, sulphate attack, carbonation of concrete, chloride penetration, alkali-aggregate reactions, and free-thaw conditions were included in the durability studies.

2.2.1 Effect of Sulphate Attack

The magnesium sulphate deteriorates the GPC at a very high level in the calcium-rich geopolymer formed in the end products, and it breaks the CSH bond and forms the Mg-SH by replacing the calcium present in the structure. The magnesium-formed structure expanded the volume that creates the crack formation in the GPC. At the same time, the

sodium sulphate is not deteriorating the GPC at a very high level. The magnesium sulphate reduces the mechanical properties of the GPC mix specimens [93]. The high-calcium BA Geopolymer mortar shows excellent resistant properties against sodium sulphate [8]. The flyash/GGBFS-based GPC shows a 33% deterioration in mechanical strength and a 0.04% expansion after immersion in magnesium sulphate for 360 days, but the OPC concrete deteriorates to 48% mechanical strength and 0.8 expansion in the same conditions. The Na_2SO_4 exposer to OPC concrete shows the deterioration of the strength and expansion are 30% and 0.412%, respectively, but in the GPC, the strength is increased in the same condition [94]. The clay-flyash-based GPC is less affected by the sulphate attack on the GPC than the OPC concrete because the clay-flyash-based GPC contains very little calcium in the mix [95]. BFA-based GPC is much less susceptible to sulphate exposure after 18 months. The OPC concrete reduces up to 20%, but the BFA-based GPC deteriorates up to 4% of strength in the same exposure condition as the sodium sulphate [96].

2.2.2 Effect of Acid Attack

The acid attack on the concrete decreases the concrete's performance and strength by reducing the mass loss of the specimens in the acidic conditions below the 6.5 PH of the concrete. The sulphuric acid immersion in the exposure condition for the 28 days shows the weakening of the concrete, and mass loss increased with the weakening of the GPC matrix. The loss reduction of concrete increases with the increase of acid content. The GPC shows better stability in acidic conditions than the OPC concrete due to less calcium content present in the GPC [97]. In the slag-based geopolymer mortar, sodium chloride effectively retards the strength and setting time of the mortar at the higher dosage, but a low dosage below 4% leads to accelerated setting of the mortar, which affects the mechanism of the geopolymerisation [98]. The pozzolanic content present in more than 50% shows the better durable properties against the conventional OPC concrete. It is less affected by acid attacks and chloride penetration in the concrete. So, HVFA cement and HVS cement are highly useful in acidic or seawater conditions [99].

2.2.3 Effect of Sea Water

The GPC concrete shows better properties against the seawater conditions by reducing the sulphate and chloride penetration of the concrete [6]. The flyash-based GPC shows

high compressive strength, tensile and flexural strength, low elasticity, water absorption, drying shrinkage, and sorptivity in seawater conditions. The flyash–based GPC had a strength of 55MPa after 28 days, which was higher than the OPC concrete and less susceptible to seawater conditions than the OPC concrete under the same conditions [100].

2.2.4 Effect on Carbonation

The carbonation reaction rate of the GPC depends on the mix design contents present in the concrete. Due to the activation of the pozzolanic binder by the sodium silicate in the mix, the flyash/GGBFS-based GPC exhibits weak resistance to the carbonation reaction.The carbonation reaction increases the permeability of the concrete, which is very hazardous for the durability of the concrete [101].

2.2.5 Effect of Alkali-Silica Reaction and Leaching

The RCA dosage increases in conventional concrete reduce the strength and mechanical properties of the concrete and lead to leaching in the concrete, but in the GPC, the RCA dosage does not affect the strength at a minimal level and reduces the strength the leaching in the concrete [102]. The flyash-based GPC is less susceptible to ASR compared to the OPC concrete [13,14]. The nonwood biomass ash-based GPC shows excellent properties against acidic conditions compared to the OPC concrete because the OPC concrete shows a 9% mass loss in 28 days of sulphuric acid conditions, but the nonwood biomass ash-based GPC shows less than 2% mass loss in the same conditions [103].

2.2.6 Effect of Elevated temperature

The aggregate size in the mix design of the concrete plays a vital role under high temperatures. If the maximum aggregate size is less than 10mm, the mix designs show the explosive spalling of the concrete specimens under high temperatures in both types of concrete, GPC and OPC concrete. The concrete's spalling was prevented by using a maximum aggregate size of more than and equal to 14mm in the design mix of the concrete. The spalling of the concrete is explained by the size of the fracture process zone (lp), and it varies with the size of the aggregate. The aggregate size is larger than the LP, which is also long and healthy because of the crack-tip shielding. GPC is chemically

stable under elevated temperatures, whereas the OPC concrete chemically decomposes and dehydrates under the same conditions and decreases the evaporation water content, decreasing the spalling probability of the concrete [52]. In the strength gain and loss mechanism at the elevated temperature, the GPC matrix sintering increases the concrete strength and after damage due to the incompatibility between the geopolymer matrix and aggregate [21]. The Si/Al ratio plays a vital role under the elevated temperature; the strength increases with the Si/Al ratio in the exposure of 800^0C of the mixed samples. The heat-cured specimens above 80^0C show higher stability against the elevated temperature, but the ambient-cured specimens show lower stability in the same conditions, and potassium-based geopolymer shows higher stability than sodium-based geopolymer in high-temperature conditions [19,69]. The GPC has better stability against elevated temperatures compared to the OPC concrete. The geopolymer specimens are more porous compared to the OPC concrete analysed by the sorptivity test. It reduces the risk of the spalling of concrete under high-temperature [17].

The FSGC shows similar trends to the Portland cement concrete weight loss under elevated temperatures up to 600^0C [104]. The geopolymer shows the glass transition behaviour at a temperature of 560^0C. Peak stress shows the transition changes beyond the peak. The strain rate rapidly increased and reached 0.64 at 680^0C, and also shows the changes in the material behaviour from solid-to-visco-elastic nature [105]. The GPC shows the greater degree of the transient creep; the OPC pastes below the 250^0C temperature. When the temperature ranged from 250^0C to 550^0C, the geopolymer did not increase the transient creep, while the OPC paste showed higher transient creep, and the geopolymer increased the elastic modulus, whereas OPC showed a negligible change in the elastic modulus [23]. At elevated temperatures, the geopolymer gets strengthened due to the sintering of the matrix, but the metakaolin shows plate-like structures that do not provide an escape for moisture, leading to the damage of the matrix [20]. The potassium-sialate formed in the geopolymerization reaction shows thermal stability up to the complete recrystallization of the feldspars leucite and kalsilite at 1000^0C. The silica-rich geopolymers showed amorphous heating up to 1400^0C and showed melting behaviour [106]. The dosage of the MPCM shows the vital effects on the thermal performance of the PCC and GPC. The number of microcapsules affects the thermal conductivity and latent heat of concrete. The dosage of the microcapsules responsible for the increase in porosity of the concrete shows stronger effects on the GPC than on the PCC [107]. The

geopolymer matrix's thermal conductivity is higher than the OPC pastes and shows that the geopolymer paste's specific heat is lesser than the PC pastes [108]. The pore size distribution plays a vital role in the FA/M-based GPC under elevated temperatures [109].

2.2.7 Effect on the Bond Strength

The GPC specimens explain a similar cracking pattern to the OPC concrete in the pull-out load test, and both fail in a brittle manner by the splitting of concrete along with the bond of concrete and bars. The bond strength increases with the increment of the concrete strength and concrete cover in both types of concrete. GPC shows higher bond strength than OPC concrete due to the higher splitting strength of GPC for the same compressive strength [110,111]. The GPC beams with lap spliced reinforcement show similar failure behaviour to the OPC concrete beams. For both types of concrete, the reinforcement from the Australian Standard and the ACI code [67]. The bond strengths of the beam-ends specimens have lower strength compared to the direct pull-out tests. Bond strength is affected by bar size; as bar size is reduced, bond strength increases [112]. The bond strength of the sand-coated GFRP-reinforced GPC compared to OPC concrete shows higher failure loads to the OPC concrete [113].

The ultimate strength and crack load increase with the increment of the fibre concentration in the mix designs, and it also reduces the cracking rate in the beam [114]. The sand-coated GFPR bars are a perfect alternative to the internal reinforcement of GPC structures [115]. The elastic behaviour of the GPC under reinforced beams is similar to the under-reinforced OPC concrete beams. GPC specimens show a more brittle nature in the flexural strength than OPC concrete specimens [110,116]. The compressive strength of the GPC increased by 5% with the 1% dosage of the 1% steel fibre in the mix [117]. The column load capacity increases with the increment of concrete strength, reduction in the eccentricity of the loading, and increasing the longitudinal-reinforcement ratio in the design. The column-designed specimens show a similar failure to the design code AS 3600 and ACI 318–02 [118]. The flexural strength of the composites shows a minimum temperature of 600°C to 800°C due to the loss of hydration water of the geopolymer matrix [119].

2.3 Applications

Geopolymer is cost-effective due to its stable performance against elevated temperatures and is used as an alternative to epoxy resins in structural retrofitting with FRP. It is also used as a cost-efficient lining for the trenches during rehabilitation of sewage pipelines [120]. Geopolymer is used in the form of the aggregate, as fine as coarse, in any concrete type. It also shows better strength and stability compared to the natural aggregates [121].

Table 2.1 Geopolymer materials applications

Si/Al ratio	Applications
1	➢ Bricks ➢ Ceramics ➢ Fire protection
2	➢ Low CO_2 Cements and Concretes ➢ Radioactive and toxic waste encapsulation
3	➢ Fire protection fibreglass composites ➢ Foundry equipment ➢ Heat resistant composites, 200-1000^{0}C ➢ Tooling for aeronautics SPF aluminium
>3	➢ Sealant for industry, 200-600^{0}C ➢ Tooling for aeronautics SPF aluminium
20-35	➢ Fire-resistant and heat resistant fibre composites

CHAPTER 3 EXPERIMENTAL PROGRAM

3.1 Materials

All the constituents that were used in forming the GPC and OPC concrete are explained separately in the paragraphs.

3.1.1. Cement

The OPC 43 grade of cement was purchased from JK Cement for the test. Preliminary cement quality testing includes consistency, initial and final setting time, specific gravity, particle fineness, and soundness. The cement passes all preliminary tests as per the Indian standard codes [122–128]. The cement sample shows excellent properties as per the Indian standard codes. Fig. 3.1 shows the picture of sample cement bags used in the laboratory's experimental analysis. The cement is manufactured by JK Super Cement Pvt. Ltd. Table 3.1 illustrates the preliminary test results conducted on the sample cement content.

Table 3.1 Cement Properties

Test	Result
Consistency	30%
Initial setting time	40 min
Final setting time	1 hr 20 min
Specific gravity	3.15
Fineness	2.9%
Soundness	2mm

Fig. 3.1 Cement sample used in the controlled mix design

3.1.2. Flyash

Flyash is an industrial solid waste product from a thermal power plant by the electrostatic precipitation of coal ash fumes. The particle size of the flyash is somewhat lower or similar to the OPC particle size and contains high silica and alumina in the composition. Flyash was brought from the national thermal power plant, Dadri, Gautam Budh Nagar, Uttar Pradesh. The flyash used for the test is a class-c type flyash in the mix design. The particles of the flyash are spherical and porous, confirmed by the SEM image. Fig. 3.2 shows the amorphous nature of the flyash sample, whereas Fig. 3.4 shows the porous spherical particles of the flyash. Table 3.2 depicts the composition of the chemical constituents present in the flyash and GGBFS. Fig. 3.5 shows the EDS graph describing the element content present in the flyash [129,130]. Fig. 3.7 describes the particle size analysis of the flyash and GGBFS, which shows that the GGBFS is well graded.

Table 3.2 Composition of Flyash and GGBFS

Characteristics	SiO_2	Al_2O_3	CaO	Fe_2O_3	MgO	SO_3	LOI
Flyash (%)	45.8	21.4	13.7	12.6	1.3	1.9	.1
GGBFS (%)	34.52	20.66	32.43	.57	10.09	.77	.3

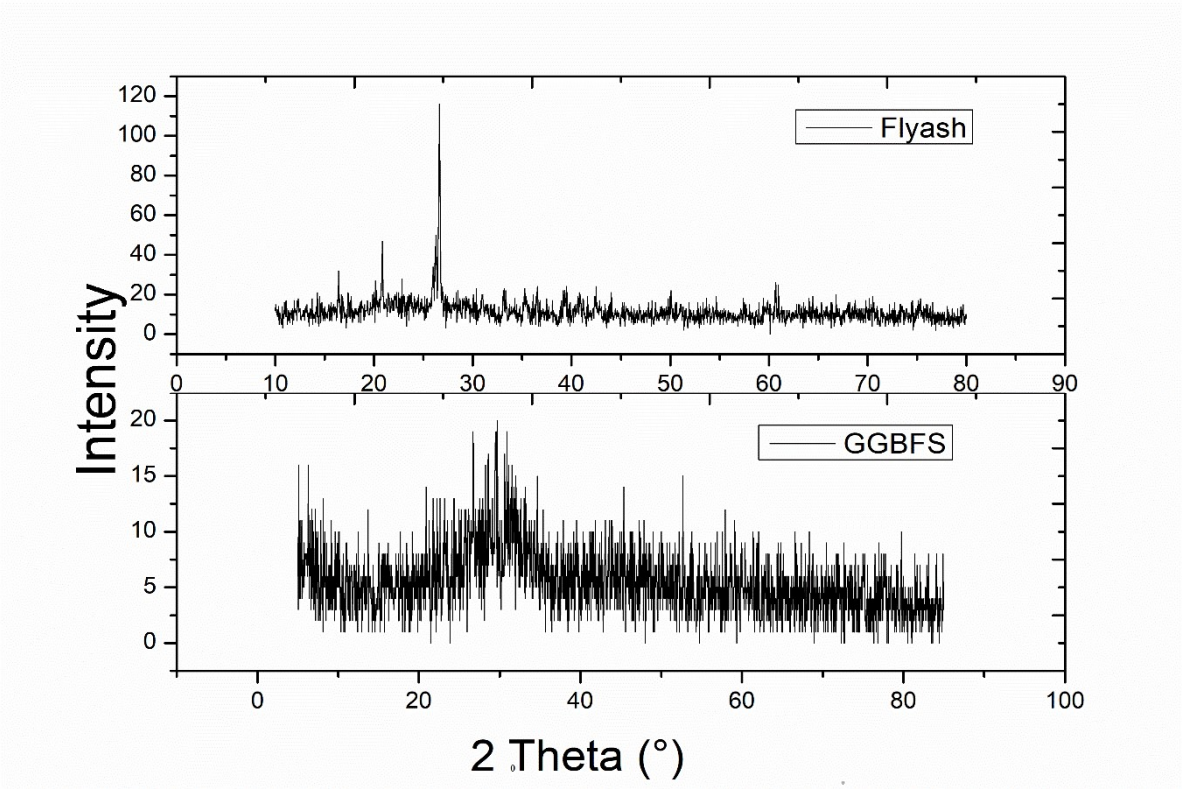

Fig. 3.2 XRD Pattern of Flyash and GGBFS

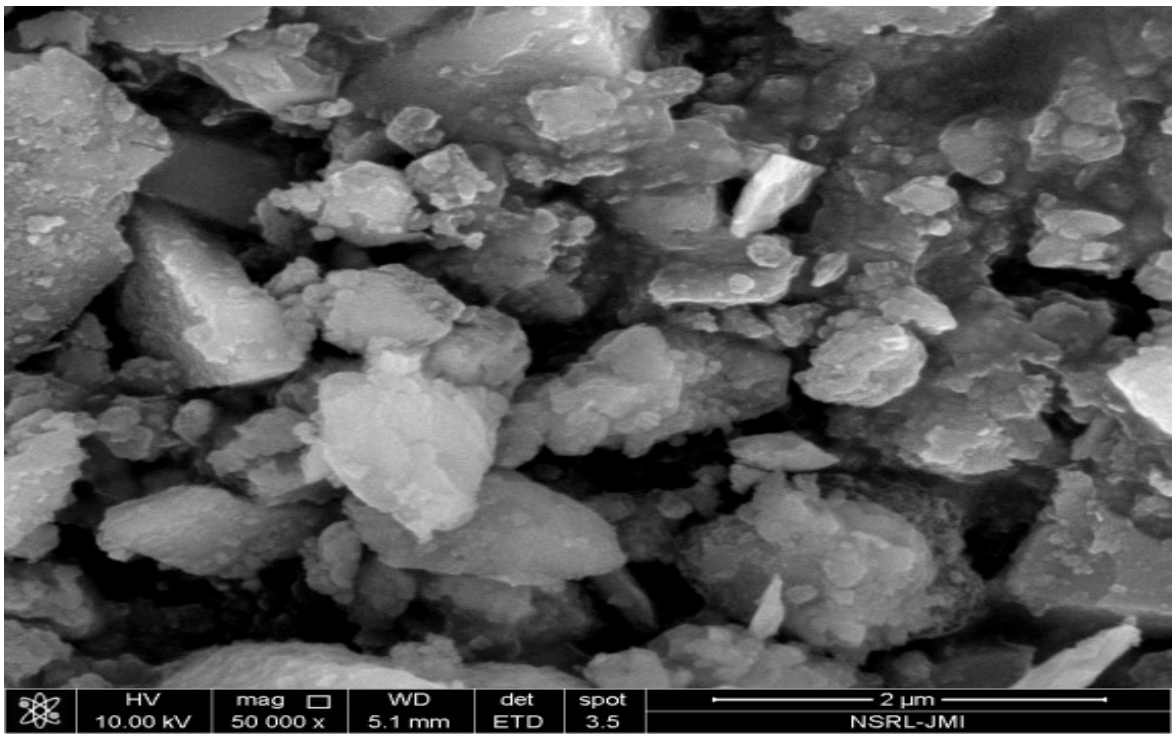

Fig. 3.3 SEM Image of GGBFS(Ground Granulated Blast Furnace Slag)

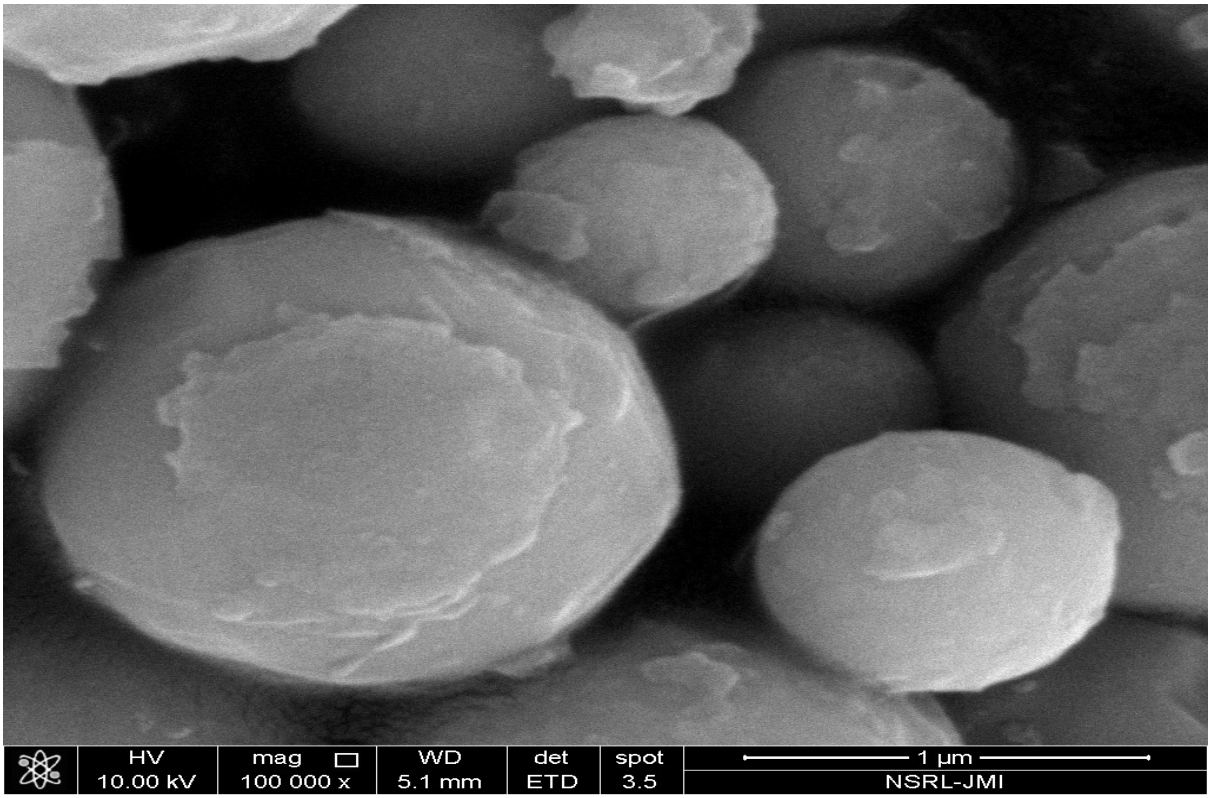

Fig. 3.4 SEM Image of Flyash

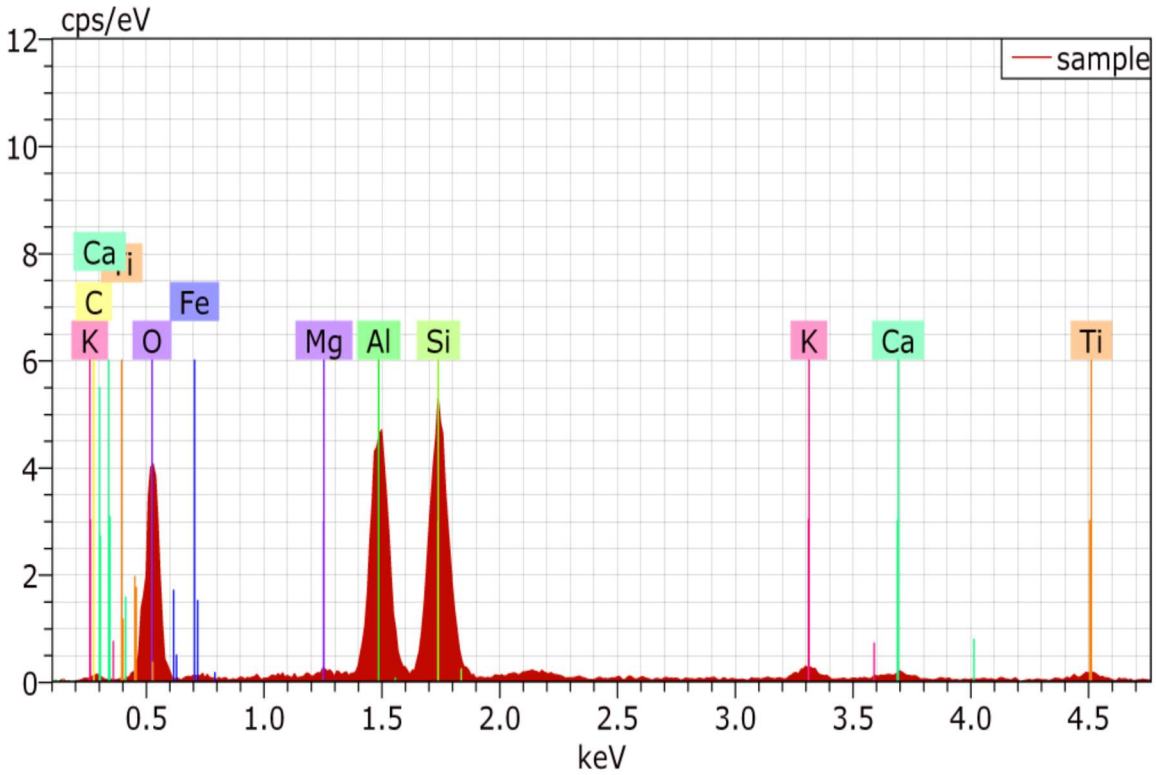

Fig. 3.5 EDS Graph of Flyash

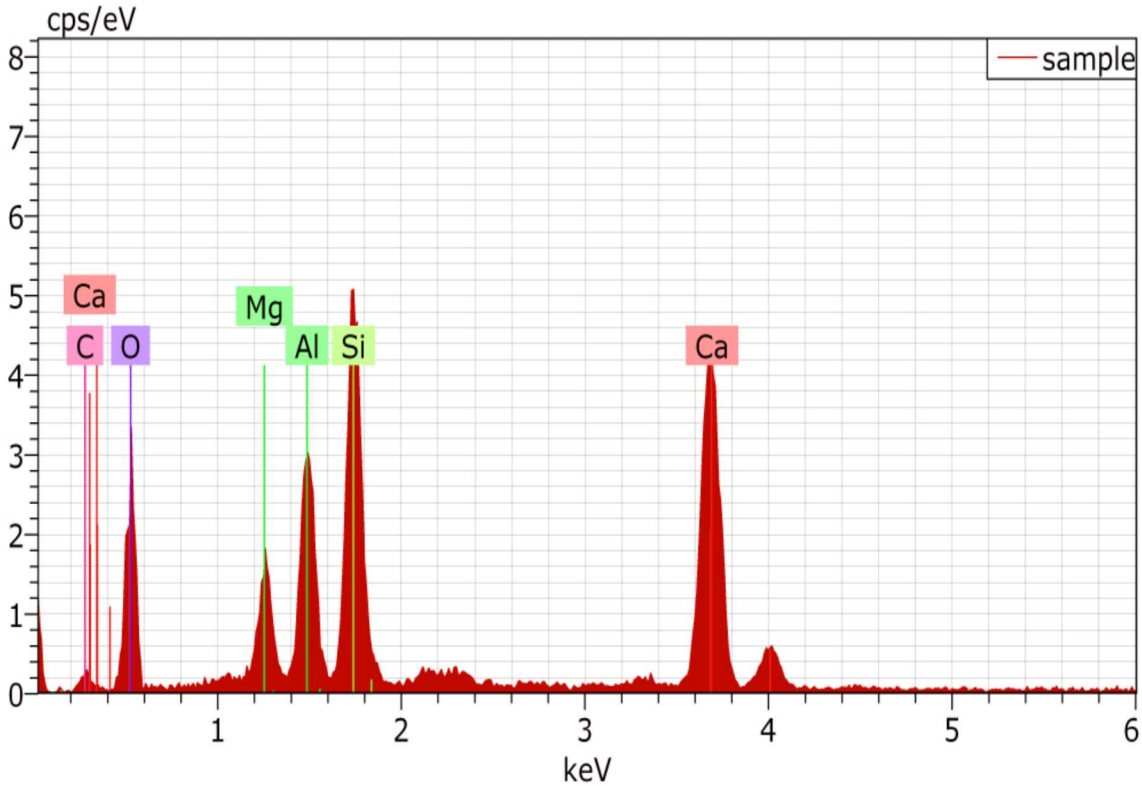

Fig. 3.6 EDS Graph of GGBFS(Ground Granulated Blast Furnace Slag)

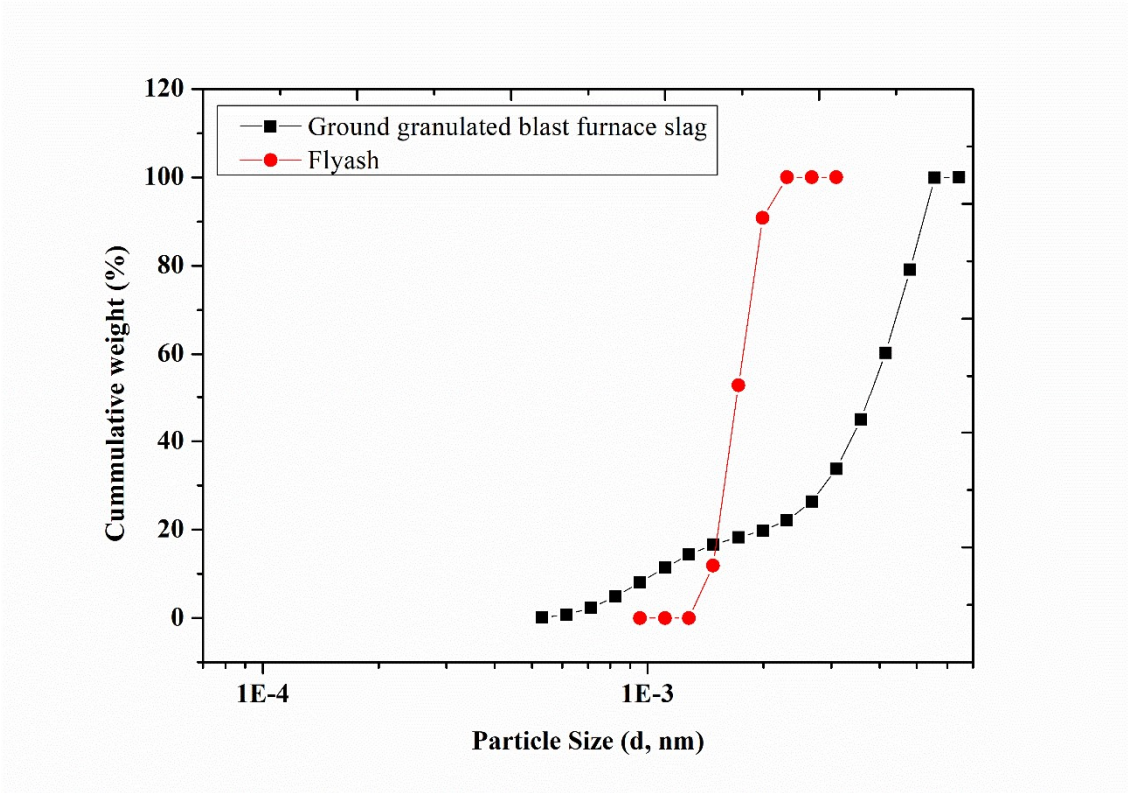

Fig. 3.7 Particle size of flyash and GGBFS

3.1.3. GGBFS(Ground Granulated Blast Furnace Slag)

GGBFS is produced at the steel manufacturing plant by quenching the slag from the molten iron-steel material. The waste material present in the iron or steel ores is called slag after separating the waste from the manufacturing of steel. GGBFS also contains high amounts of silica and alumina content in the composition. GGBFS was brought from the Bhilai steel plant, Bhilai, Chattishgarh, India, to test and produce the GPC specimens. Fig. 3.2 shows the XRD graph of the GGBFS, showing the amorphous nature of the sample, whereas Table 3.2 shows the chemical composition present in the GGBFS sample. Fig. 3.3 describes the SEM image of the GGBFS sample and shows the irregular shape of the particles, whereas Fig. 3.6 shows the EDS graph, which describes the elements present in the samples.

3.1.4. Sodium Hydroxide

The alkaline solution is used to activate the pozzolanic binding materials in the geopolymer for the Geopolymerisation reaction. The alkaline solution contains sodium hydroxide and sodium silicate solution, and it is mixed before the 20-24 hours for sampling. Sodium hydroxide was purchased from Fisher Scientific in the business park, Powai, Mumbai, Maharashtra, India.

Fig. 3.8 Sodium hydroxide flakes

3.1.5. Sodium Silicate Solution

Sodium silicate is a part of the alkaline solution to activate pozzolan materials for the binding properties. The solution is alkaline and contains a higher amount of Na_2O. Sodium silicate solution (water glass) was purchased from Central Drug House (P) Ltd. in New Delhi-110002 (India). Sodium silicate is present in compact, Tacky/Slightly cloudy liquid form with the minimum assay of Na_2O titrimetric is 10.0% and SiO2, gravimetric is 25.5-28.5% in the solution of the sample.

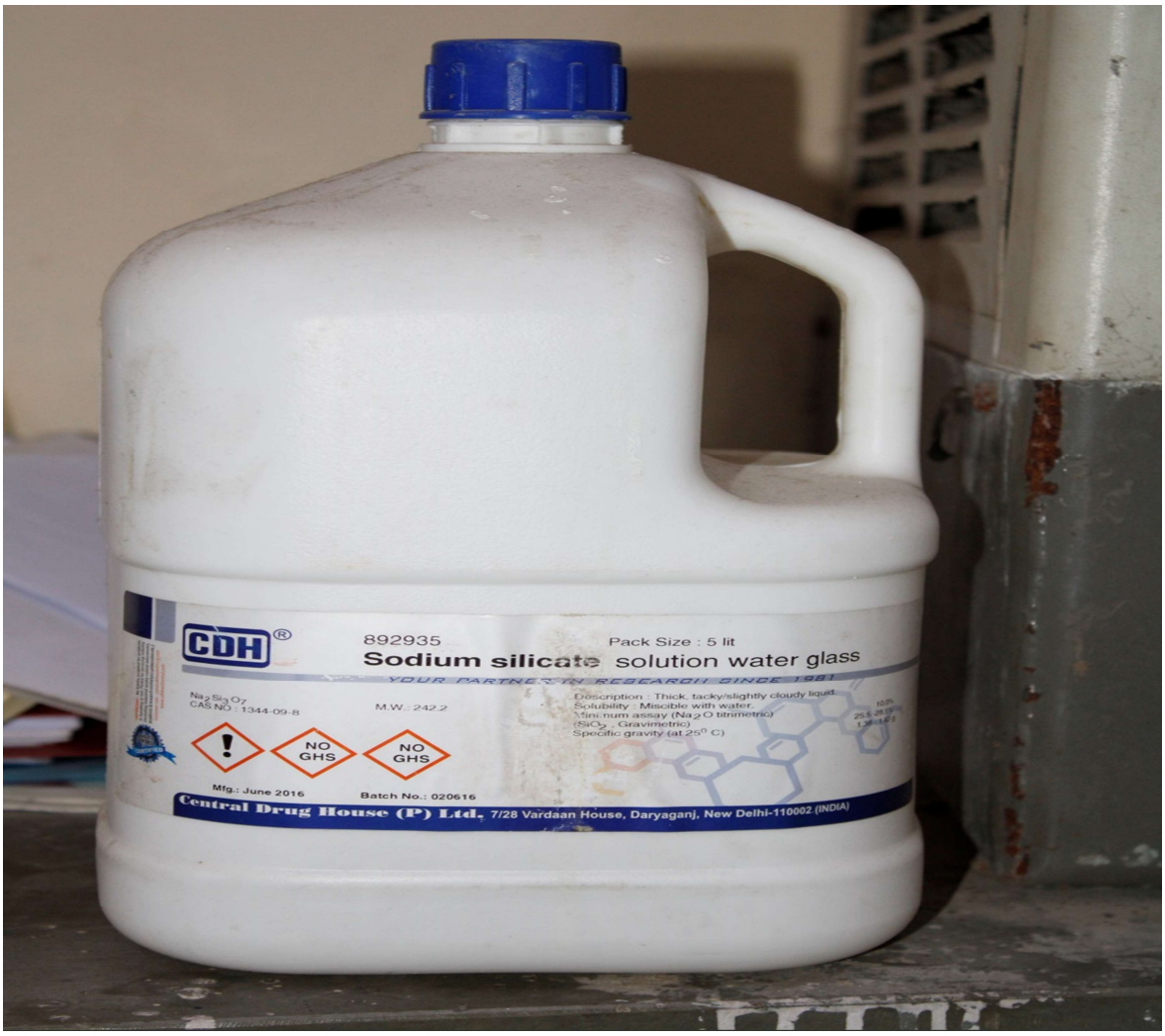

Fig. 3.9 Sodium Silicate Solution

3.1.6. Fine Aggregates

Aggregate is used as the concrete skeleton because it occupies up to 85% of the volume of the concrete. The aggregate used in the mix is mostly classified into two categories: fine aggregates and coarse aggregates. The aggregate size below 4.75mm is called fine

aggregates, and above 4.75mm is called coarse. In the coarse aggregate, two types of aggregate used are 10mm and 20mm in the design mix, whereas fine aggregate uses the crushed stone dust in the mix of both concretes. Before using aggregate in the mix design, check the aggregate quality as per the Indian standard codes. In the preliminary test, check the gradation of the aggregates, zone, fineness modulus, specific gravity, water absorption, silt content, and bulk density of the stone dust/fine aggregates samples [131–137]. Fig. 3.10 shows the picture of the stone dust sample used for the test in the different mix designs. Table 3.3 describes the particle size retained on the seize size and passing sieve number with percentage and found different particles in the samples. Fig. 3.11 shows the dust samples' grain size distribution and accurately describes them in the logarithmic graph. The dust sample was found in zone II, medium, and well-graded form of the particle sizes, and Table 3.4 describes all properties of the dust samples found after testing the sample materials.

Fig. 3.10 Stone-Dust or Fine Aggregate

Table 3.3 Sieve Analysis of Sand/Stone Dust

Sieve Size	Weight Retained (g)	Cumulated Weight Retained	Cumulated % Weight Retained	Cumulated % passing	Remarks
4.75mm	0	0	0	100	Sand falls in zone II
2.36mm	107	10.7	10.7	89.3	
1.18mm	298	29.8	40.5	59.5	
600µ	214	21.4	61.9	38.1	
300µ	130	13	74.9	25.1	
150µ	127	12.7	87.6	12.4	
75 µ	38	3.8	91.4	8.6	
pan	86	8.6	100	0	

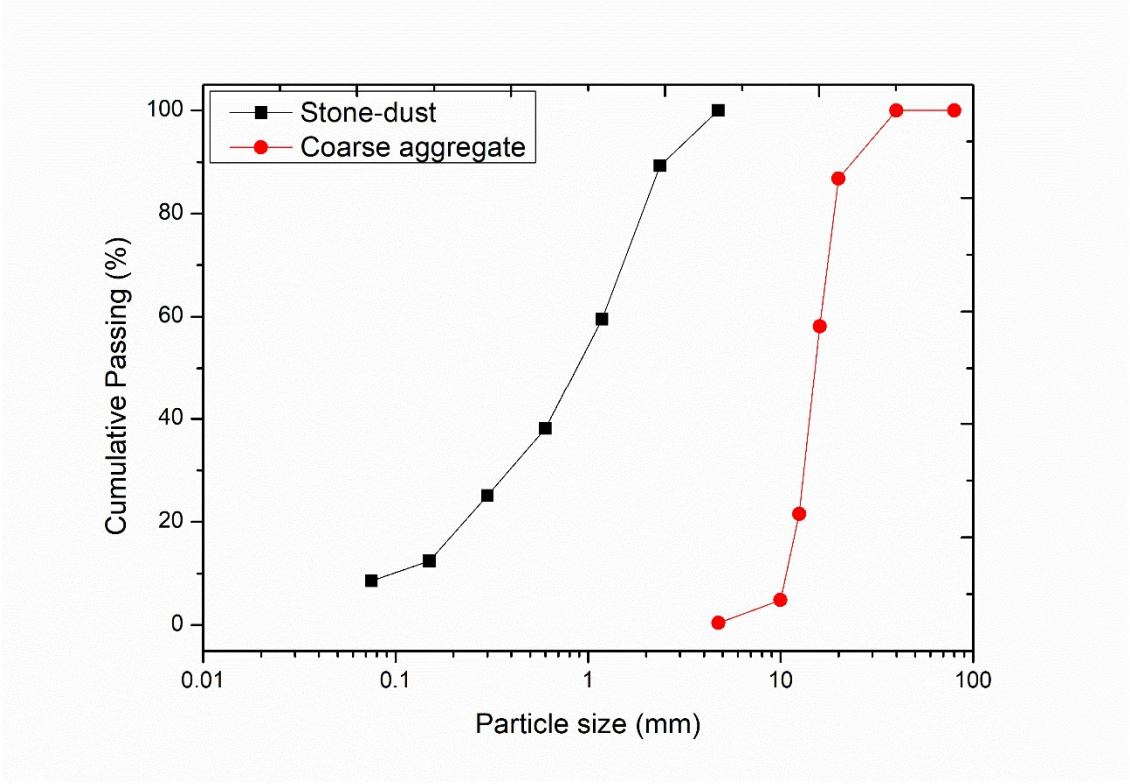

Fig. 3.11 Grain size distribution curve

As the percentage passing 600µ sieve is between 35 and 59, the sand belongs to gradation II. From the gradation curve, we find D_{10}=0.1 D_{30}=0.4 D_{60}=1.2

$C_u = D_{60}/ D_{10} = 1.2/0.1 = 12 > 6$

$C_c = D_{30}^2/ (D_{10} \times D_{60}) = 0.4^2/ (0.1 \times 1.2) = 1.33$

Thus, the sand is well graded sand.

Table 3.4 Properties of fine aggregate/stone dust (m-sand)

S.No.	Test	Results
1.	Zone	Zone II
2.	Grade	well graded
3.	Fineness modulus	2.756 (medium sand)
4.	Specific gravity	2.62
5.	Water absorption	1.21 %
6.	Silt content	6 %
7.	Bulk density	1610 kg/m^3

3.1.7. Coarse Aggregate

Locally available coarse aggregate sample material is used in the various mix designs. Table 3.5 described all the particle size aggregates present in the sample with their percentages and found the fineness modulus of the coarse aggregate. Fig. 3.12 shows the coarse aggregate samples pic, whereas Table 3.6 describes the properties of the coarse aggregates [138–142]. All the preliminary tests were conducted to check the quality of the raw materials before being used in the research project.

Fig. 3.12 Coarse Aggregate samples

Table 3.5 Sieve analysis of coarse aggregate

Sieve size	Weight retained(g)	Cumulative wt. retained	Cumulative % wt. retained	% Cumulative passing	% Passing of nominal size IS-383
80mm	0	0	0	100	85-100
40mm	0	0	0	100	-
20mm	264	264	13.2	86.8	-
16mm	573	837	41.85	58.15	-
12.5mm	732	1569	78.45	21.55	-
10mm	334	1903	95.15	4.85	0-20
4.75mm	89	1992	99.6	0.4	0-5
PAN	8	2000	100	0	-

Fineness modulus: (13.2+41.85+78.45+95.15+99.6+5X100)/100 =7.29

Table 3.6 Properties of coarse aggregate

S. No.	Test	Results
1.	Fineness modulus	7.29
2.	Specific gravity	2.79
3.	Water absorption	0.2%
4.	Crushing value	23%
5.	Impact value	22%
6.	Flakiness index	24%
7.	Elongation index	30%
8.	Abrasion value	8%

3.1.8. Superplasticiser

Superplasticiser is used to enhance the performance of the concrete by reducing the water content in the mix design and increasing the workability of the fresh mix. SNF-based superplasticizer is used in the mix design of concrete made by the fosroc industry named SP conplast-430 in the market [143]. Table 3.7 describes the properties of the superplasticizer sample. **Fig. 3.13** shows the picture of the superplasticizer used in the mix designs.

Table 3.7 Superplasticiser properties

S. No.	Test	Results
1.	Appearance	Brown liquid
2.	Specific gravity	1.18 @ 25°C
3.	Chloride content	Nil to BS 5075 / BS: EN934
4.	Air entrainment	Less than 2% additional air entrained at usual dosages.

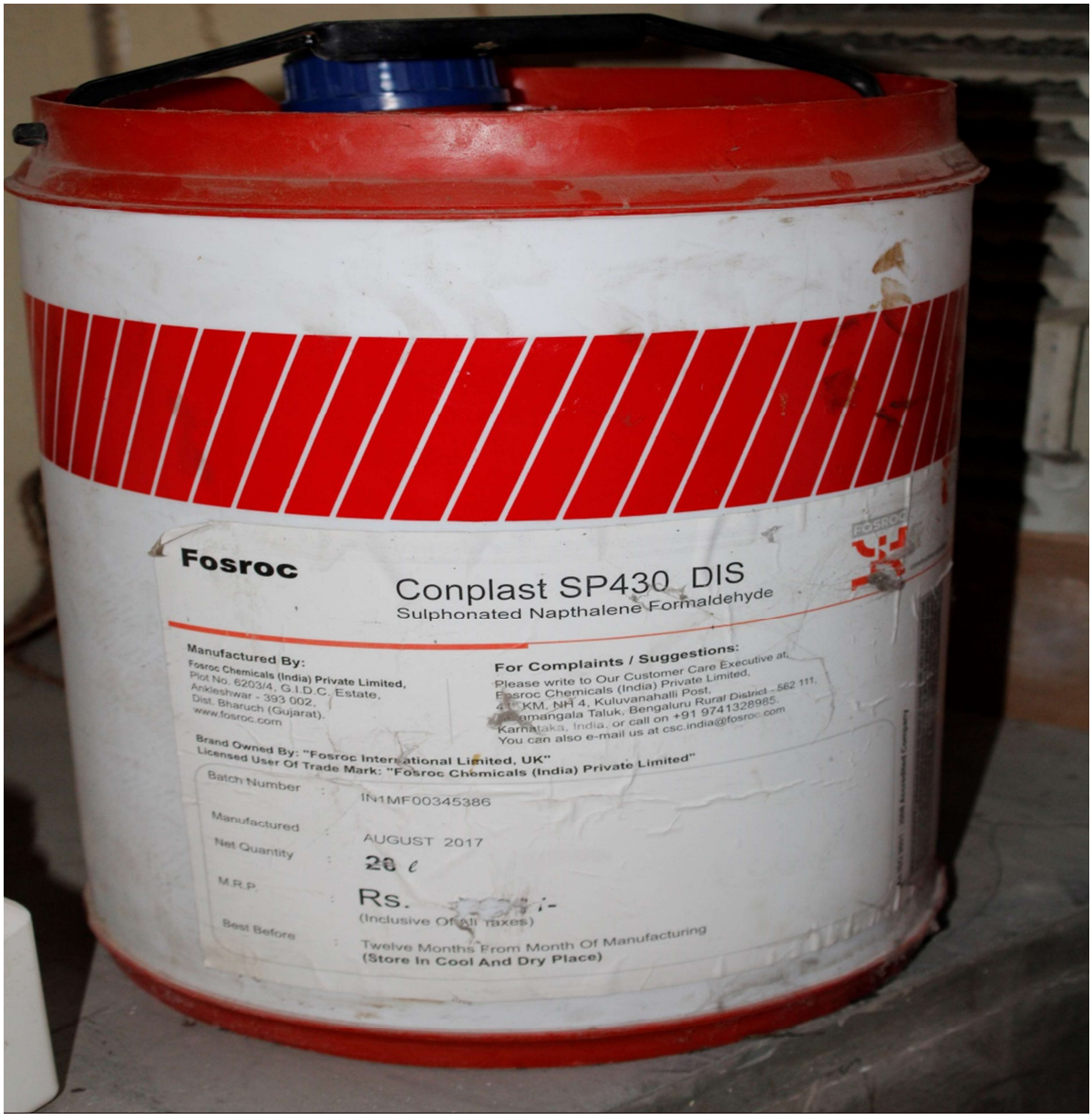

Fig. 3.13 Superplasticiser sample picture

3.2. Mix Proportion

The mix design calculation was done after testing the material samples for both geopolymer concrete and OPC concrete control. **Table** 3.8 describes the various mix designs used for the tests. OPC concrete mix design was done as per IS 10262:2008 and GPC mix design as empirical relations or reference journals.

Table 3.8 Mix designs of various mixes

Mix Designs	Cement (kg/m^3)	Fly ash (kg/m^3)	GGBFS (kg/m^3)	Coarse Aggregate (kg/m^3)	Fine Aggregate (kg/m^3)	NaOH Solution (kg/m^3)	Sodium Silicate (kg/m^3)	Super Plasticizer (kg/m^3)	Extra Water (kg/m^3)
M1	330	-	-	1300	797	-	-	3.7	148
M2	370	-	-	1289	683	-	-	3.7	148
M3	-	405	-	1269	683	81.0 (13M)	81.0	-	81
M4	-	303.75	101.25	1269	683	81.0 (13M)	81.0	-	81
M5	-	202.5	202.5	1269	683	81.0 (13M)	81.0	-	81
M6	-	101.25	303.75	1269	683	81.0 (13M)	81.0	-	81
M7		303.75	101.25	1269	683	81.0 (13M)	81.0	-	0
M8		303.75	101.25	1269	683	81.0 (13M)	81.0	-	20.25
M9		303.75	101.25	1269	683	81.0 (13M)	81.0	-	40.5
M10		303.75	101.25	1269	683	81.0 (13M)	81.0	-	60.75
M11		303.75	101.25	1269	683	81.0 (13M)	81.0	-	101.25
M12		303.75	101.25	1269	683	81.0 (13M)	81.0	-	121.5
M13	-	303.75	101.25	1269	683	81.0 (13M)	81.0	2.025	20.25
M14	-	303.75	101.25	1269	683	81.0 (13M)	81.0	4.05	20.25

M15	-	303.75	101.25	1269	683	81.0 (13M)	81.0	6.075	20.25
M16	-	303.75	101.25	1269	683	81.0 (13M)	81.0	8.10	20.25
M17	-	303.75	101.25	1269	683	81.0 (8M)	81.0	4.05	20.25
M18	-	303.75	101.25	1269	683	81.0 (10M)	81.0	4.05	20.25
M19	-	303.75	101.25	1269	683	81.0 (12M)	81.0	4.05	20.25
M20	-	303.75	101.25	1269	683	81.0 (14M)	81.0	4.05	20.25
M21	-	303.75	101.25	1269	683	81.0 (16M)	81.0	4.05	20.25
M22	-	303.75	101.25	1269	683	108.0 (14M)	54.0	4.05	20.25
M23	-	303.75	101.25	1269	683	64.8 (14M)	97.2	4.05	20.25
M24	-	303.75	101.25	1269	683	54.0 (14M)	108.0	4.05	20.25
M25	-	303.75	101.25	1269	683	46.28 (14M)	115.72	4.05	20.25
M26	-	303.75	101.25	1269	683	40.5 (14M)	121.5	4.05	20.25

3.3. Mixing, Casting and Curing

The mix designs of the controlled OPC concrete and GPC were implemented by mixing all constituents in their proportion in the pan mixture. The mixing procedure was as per the Indian standard [144]. Specimens made of the controlled OPC concrete mix usually mix all constituents in the pan mixture for around 2 to 5 minutes and cast in the mould of the specimens for 24 hours. In the case of GPC, the alkaline solution is mixed before 20-24 hours, mixing the concrete constituents in the pan mixture and casting them in the mould of the specimens with the proper compaction of the cast samples. The OPC concrete specimens were cured in the water tank, but the GPC specimens were cured in the oven at 60^0C for 24 hours. The cubical, cylindrical, and beam-shaped specimens were cast from both types of concrete for the testing. Physical and mechanical properties were tested for both types of concrete.

Fig. 3.14 Pan Mixture in the laboratory

3.4. Test Setup

3.4.1. Slump and Compaction factor

Slump and compaction factor tests are used to analyse the fresh concrete's workability (physical property). Slump is most common for testing the workability of concrete on site or in the laboratory, but the compaction factor is usually used in the laboratory only. The slump is a conical-shaped instrument, but the compaction factor instrument is made of two conical-shaped buckets fitted in vertical alignment with a standard gap, and the surface of the buckets is openable. The compaction factor checks the self-compaction ability of the concrete with the gravity force [145].

Fig. 3.15 Compaction factor and slump apparatus

3.4.2. Curing of Specimens

There are two types of curing conditions that were used to strengthen the GPC specimens. Fig. 3.16 shows specimens during ambient curing, whereas Fig. 3.17 shows the picture of specimens during oven curing.

Fig. 3.16 Specimens during ambient curing

Fig. 3.17 Specimens during oven-curing

Fig. 3.18 Digital weight machine for finding density by weight of the cube

3.4.3. Density

The weight of the specimens identifies the density of the mixed specimens before the destructive tests. The density of the mixes is primarily determined by the cubed weight 28 days after casting.The mass calculates the density to volume ratio of the cube specimens. Fig. 3.18 shows the picture of a specimen during weight on the digital weight machine.

3.4.4. Compressive strength

The compressive strength of both types of concrete mixes was tested by the cube sample test under the CTM machine at a 5.25kN/sec loading rate statically applied to the specimens. The 150mm*150mm*150 mm cube sizes are as per the IS code. The mixes samples were tested at 3, 7, 14, 28 days after the casting of the specimens. Fig. 3.19 shows the picture of a cube specimen during the compressive strength test on the UTM.

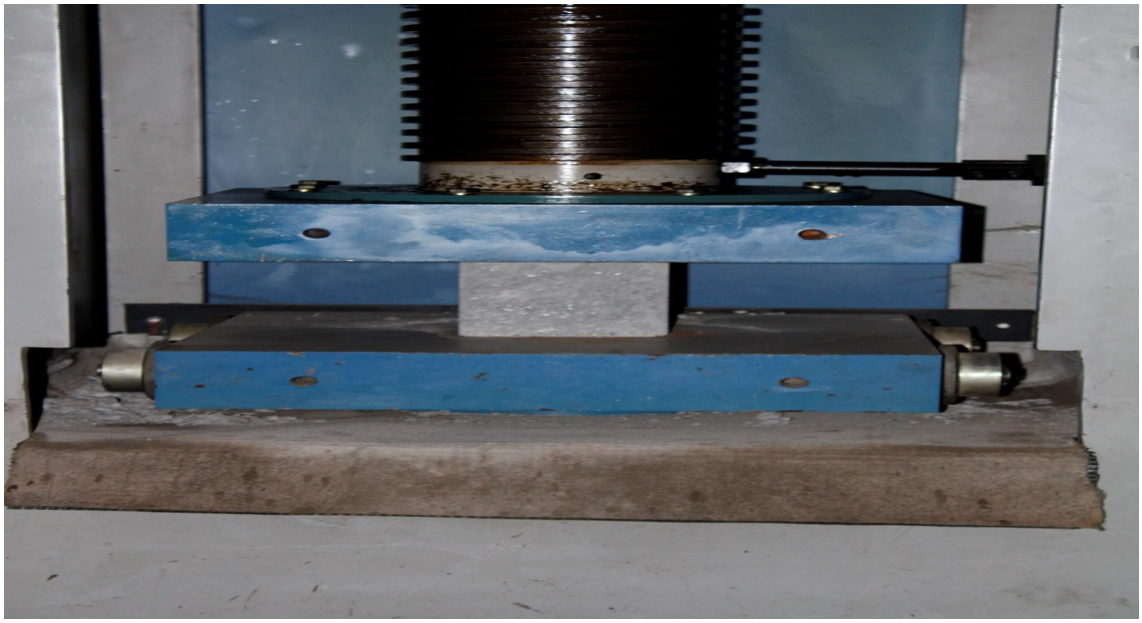

Fig. 3.19 Compressive strength test in the CTM

3.4.5. Splitting Tensile Strength

The splitting tensile is used to find the indirect tensile strength of the concrete. The cylindrical shape of size dia*length is 150mm*300mm as per the Indian Standard codes used to find the splitting tensile of the concrete mix specimens. The 4.5kN/sec rate of loading was applied in the transverse direction of the cylindrical specimens to test the concrete's splitting tensile. The splitting tensile is higher than the direct tensile but lower

than the flexural strength of the same concrete mix design. Fig. 3.20 shows the picture of the cylinder specimen after failure due to the splitting tensile test.

Fig. 3.20 Picture of splitting tensile failure of the specimen

Fig. 3.21 Picture of the flexural strength test setup during testing

3.4.6. Flexural Strength

Flexural strength is also called a rupture of the concrete used to find the bending capability of the concrete specimens. If the maximum aggregate size is less than equal to 20mm, then the beam of standard size 100mm*100mm*500mm is used for the cast specimens to analyse the flexural strength. A two-point load was applied along the transverse direction of the specimens for the test on the flexural testing machine. Fig. 3.21 shows the picture of a prism or beam specimen during the flexural strength test.

3.4.7. Elastic Modulus and Poisson Ratio

The elastic modulus and Poisson ratio of the concrete mix are determined by testing cylindrical specimens.The uniaxial statical load was applied along the verticle direction to the cylindrical specimens and found the cylinder's vertical and horizontal displacement and strength. From the displacements, the Poisson ratio is calculated through the ratio of horizontal strain to vertical strain. The elastic modulus finds through the load applied to the cylindrical specimens about one-third of their strength and release and going continuously for the same procedure many times, then draw the stress-strain graph and find the elastic modulus through the chord modulus as per the ASTM. Fig. 3.22 shows the setup of the elastic modulus and Poisson's ratio tests on the CTM.

3.4.8. Rebound Strength

A rebound hammer is the name of the apparatus that examines the strength of the geopolymer concrete hardened sample without destroying the specimens of a mix of geopolymer concrete. Both types of sample cube and cylinder test for the strength of the mix samples [146,147]. A rebound hammer identifies the strength through the surface indentation of the concrete samples. Fig. 3.23 shows the picture during the rebound hammer strength test.

3.4.9. UPVT (Ultrasonic pulse velocity test) Strength

The ultrasonic pulse velocity test is a non-destructive test for concrete strength analysis through the speed of passing ultrasonic pulse waves through the concrete. The higher the velocity shows the higher strength of the concrete. UPVT also analyses the dynamic Poisson ratio and dynamic modulus of elasticity of the concrete mix design by testing beam specimens of that mix [148]. Fig. 3.24 shows the picture during the UPVT.

Fig. 3.22 Elastic modulus and poisons ratio test setup

Fig. 3.23 Picture during rebound hammer strength test

Fig. 3.24 Picture during UPVT conduction

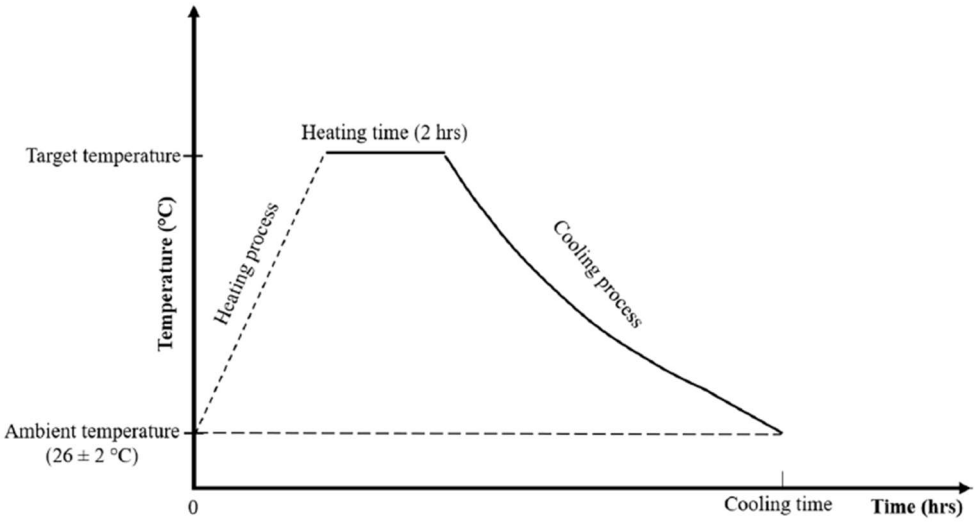

Fig. 3.25 Picture of heating process

Fig. 3.26 Picture of muffle furnace

3.1.10 Elevated temperature exposure condition

Both concrete cube specimens were tested at an elevated temperature ranging from 100^0C to 800^0C. The cube specimens were put in the muffle furnace for 2 hours of elevated temperature, whereas the increment of temperature from room to specific elevated temperature with the rate of 10^0C/minutes, and cooling randomly in the surrounding ambient temperature. Fig. 3.25 depicts the heating process for the elevated temperature exposure to the concrete cube specimens, whereas Fig. 3.26 shows the picture of the muffle furnace used in this elevated temperature research. After cooling specimens, exposure to elevated temperatures was tested for mass loss, UPVT, and compressive strength.

Fig. 3.27 Picture of seawater solution with the cube specimens

3.1.11 Seawater condition

The seawater condition is made using salt to make a saline condition as per the ASTM. The 5% concentration of salt dissolved in the tap water is stored in a tub of 40 litres. After making the saline solution, they put the GPC and conventional concrete cube specimens in the saline solution for durability testing. The specimens' weight checks,

UPVT, and compressive strength analysis after 6 weeks, 12 weeks, 18 weeks, and 24 weeks were put into the saline solution [149]. Fig. 3.27 shows the seawater condition created in a water tub with concrete specimens.

Fig. 3.28 Picture of sulphate solutions with the cube specimens

3.1.12 Sulphate attack

There are two types of sulphate solution made in the laboratory by using sodium sulphate and magnesium sulphate. In both conditions, 5% sulphate chemicals dissolve in the tap water stored in a 40-litre tub. The sulphate attack test was conducted on the GPC and conventional concrete cube specimens to put the cube specimens in the sulphate solution for 24 weeks. Fig. 3.28 shows the sulphate attack condition created in water tubs with concrete cube specimens. The specimens for both GPC and conventional concrete tests were put through weight check, UPVT, and compressive strength analysis after 6 weeks, 12 weeks, 18 weeks, and 24 weeks, respectively. The sulphate solutions were made as per the ASTM for durability analysis [150].

4.3.12. Acid attack

The acid attack resistance quality of the concrete specimens was tested by putting them in the acidic solution for 28 days. The acidic solution is made as per the ASTM by using sulphuric acid, in which 5% acid is dissolved with the tap water in the tub. The specimens for both GPC and conventional concrete tests were put through weight check, UPVT,

and compressive strength analysis after 28 days in the solution. A visual inspection was also conducted on the specimens after the acid attack [151].

4.3.13. Freeze-thaw condition

The freeze-thaw condition was tested on both GPC and conventional concrete specimens. The specimens are put in the deep freezer up to-28^0C and continuously cycled after a normal or room temperature. The specimens of both GPC and conventional concrete tests for weight check, UPVT, and compressive strength analysis after the 30cycles, 45cycles, 60cycles, 75cycles, and 90cycles of freeze-thaw [152]. Fig. 3.29 depicts the picture of a deep-freezer with a minimum temperature used in the freeze-thaw condition.

Fig. 3.29 Picture of deep-freezer with temperature meter

4.3.14. Wetting-drying condition

The wetting-drying condition was tested on both GPC and conventional concrete specimens. The specimens were put in the water for 24 hours at a normal or room temperature, and after a continuous cycle was conducted. Both GPC and conventional concrete specimens were tested for weight check, UPVT, and compressive strength analysis after 30 cycles, 45 cycles, 60 cycles, 75 cycles, and 90 cycles of wetting-drying. [153].

CHAPTER 4 RESULTS AND DISCUSSION

This chapter describes all the experimental results from the mixed design specimens and shows them in the graphs. All the mix designs of the GPC cured under the two curing conditions are ambient-curing and oven-curing. All the result data came from the tests of the specimens given in the tables. The experimental investigation tests the specimens of their mixed designs for the results of workability, density, compressive strength, splitting tensile, flexural strength, Poisson ratio, elastic modulus, and non-destructive tests such as rebound strength and UPVT (ultrasonic pulse velocity test). The various parameters used to analyse the behaviour of the mix design of the GPC are as follows:

- The effect of the GGBFS/flyash ratio
- The effect of liquid on the binder ratio
- The effect of the percentage of superplasticizer in the mix design of GPC
- The effect of the molarity of sodium hydroxide on the mix design of GPC
- The effect of the ratio of sodium silicate to sodium hydroxide
- The effect of the different temperatures of curing
- The effect of elevated temperatures
- The effect of seawater conditions
- The effects of sulphate attack
- The effect of acid attack
- The effect of freeze-thaw conditions
- The effect of wetting-drying conditions

4.1 Effect of GGBFS/Flyash Ratio

4.1.1 Slump and Compaction Factor

The slump and compaction factors decrease with the increment of GGBFS replacement in the mix design, consecutively. Fig. 4.1 describes the graph of the slump and compaction factor in the GPC mix.

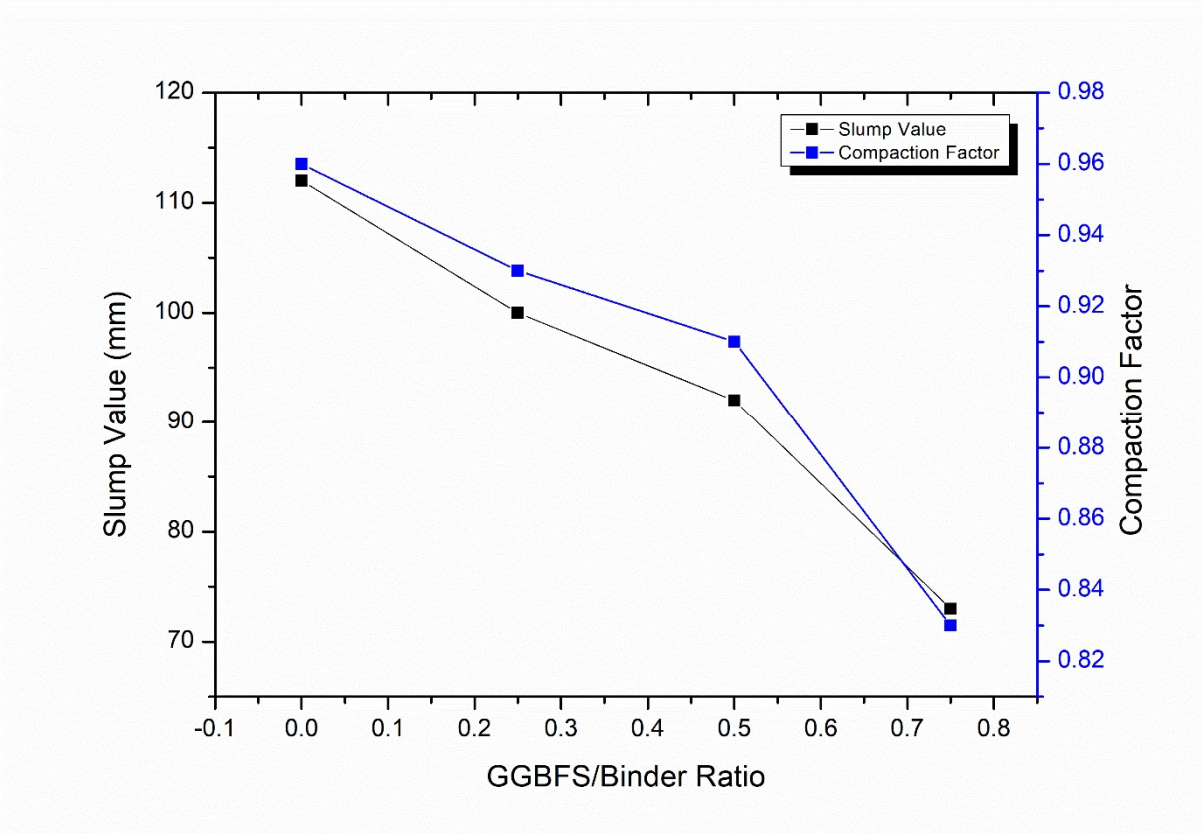

Fig. 4.1 Slump and Compaction factor vs GGBFS/Binder ratio

4.1.2 Density

Fig. 4.2 presents the mixed specimens' density and the effect of GGBFS in the mix designs of GPC specimens. The results of all four mix designs in which the fly ash and GGBFS ratio vary from 100/0, 75/25, 50/50, and 25/75, respectively by weight percentage, specimens cured by ambient-curing and oven-curing at a temperature of 60^0C for 24 hours, and the sample tests at 28 days by weight of the specimens and compression of the cylindrical specimen with the vertical and transverse extensometer fit the specimens perfectly. The ambient-cured sample has a higher density than the oven-cured GPC specimens of different mix designs. Still, 75/25 fly ash/GGBFS ratio mix design

samples got the average maximum density in both cured samples. A mix of GGBFS with fly ash at 25% by weight instantly increases the design mix specimen density. Still, after the increase, the replacement of GGBFS with fly ash slightly decreases the density of the mixed-design specimens. At 28 days of ambient curing, the 75/25 fly ash/GGBFS ratio mix designs samples had the highest average density of 2491 kg/m^3, while the oven-cured samples had an average density of 2473 kg/m^3.

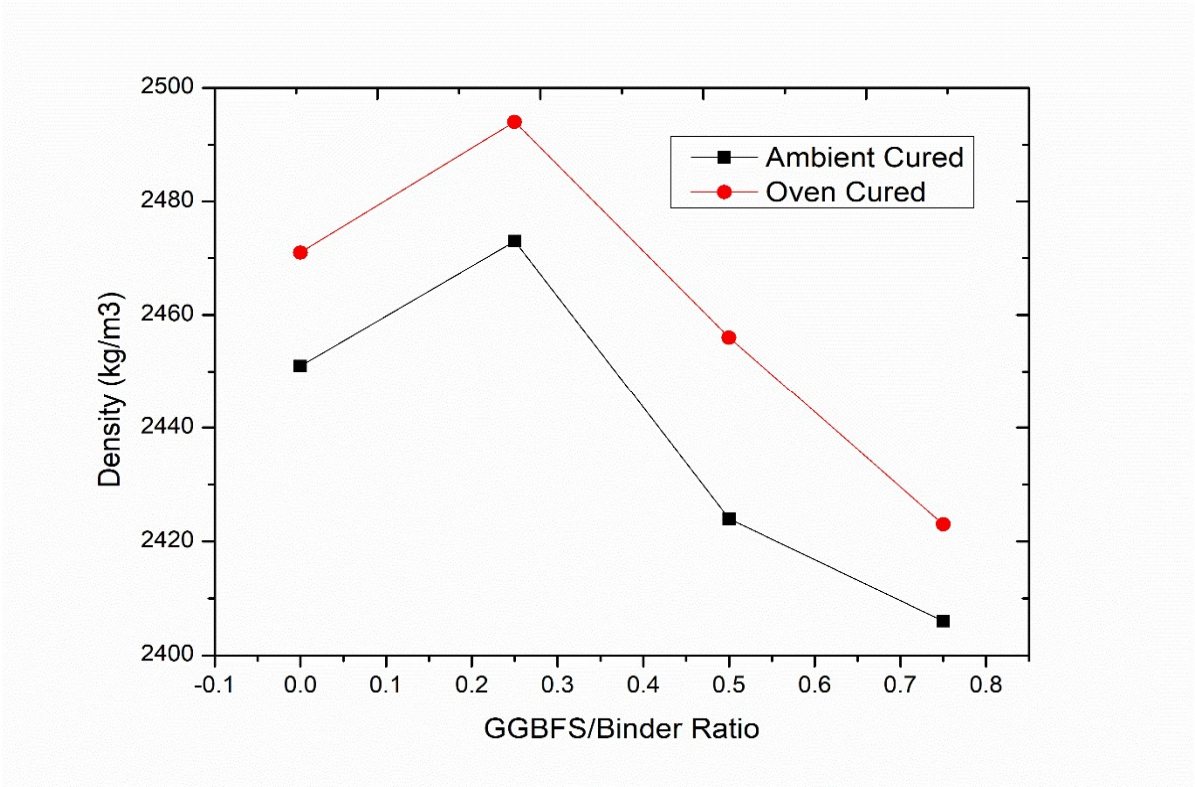

Fig. 4.2 Graph b/w the density and GGBFS/binder ratio of mix designs

4.1.3 Compressive Strength

Fig. 4.3 and Fig. 4.4 presented the results of all four mix designs in which the fly ash to GGBFS ratio varied from 100/0, 75/25, 50/50, and 25/75, respectively, by weight percentage. The ambient-curing and oven-curing cured all the mix design samples at the temperature of 60^{0}C for 24 hours and the sample tests at seven days, 14 days, 28days, 42 days, and 56 days in UTM for compressive strength. The ambient-cured sample has less compressive strength than the oven-cured samples, but the 75/25 flyash/GGBFS ratio mix got the maximum compressive strength in both cured samples. The dosage of GGBFS is approximately 25% of the fly ash replacement, which instantly increases the strength of the mix design. But beyond that, the 25% dosage of the GGBFS slightly

decreases the strength of the mix designs. Fig. 4.3 shows the compressive strength of ambient-cured GPC specimens in which the 75/25 binding ratio mix got the highest average compressive strength of 24.3 N/mm^2 at 56 days, whereas the 100/0, 50/50, and 25/75 binding ratio mixes got the lowest average compressive strength of 18.2 N/mm^2, 21.8 N/mm^2, and 20.3 N/mm^2 at 56 days, respectively. The compressive strength of the oven-cured samples of GPC in which the 75/25 binding ratio mix got the highest average compressive strength is 32.9 N/mm^2 at 56 days, whereas 100/0, 50/50, and 25/75 binding ratio mixes get the lowest average compressive strength of 29.0 N/mm^2, 30.2 N/mm^2, and 29.3 N/mm^2 at 56 days, respectively. Around 95% of the strength of the GPC specimens was lost after that; they gained significantly less strength in that ambient-cured samples gained more strength than the oven-cured samples after 28 days. Table 4.1 contains the whole ambient-cured GPC compressive strength, whereas Table 4.2 contains the oven-cured compressive strength of the GPC specimens.

Table 4.1 Compressive strength of ambient-cured

Flyash/Slag ratio	7 days	14 days	28 days	42 days	56 days
100/0	9.3	12.8	16.0	17.4	18.2
75/25	15.4	18.9	22.1	23.9	24.3
50/50	13.6	16.1	19.8	21.0	21.8
25/75	12.1	14.8	17.4	19.1	20.3

Table 4.2 Compressive strength of oven-cured

Flyash/Slag ratio	7 days	14 days	28 days	42 days	56 days
100/0	21.5	25.4	28.3	28.7	29.0
75/25	24.4	29.1	32.1	32.6	32.9
50/50	22.9	26.4	29.6	30	30.2
25/75	21.7	25.1	28.4	29.0	29.3

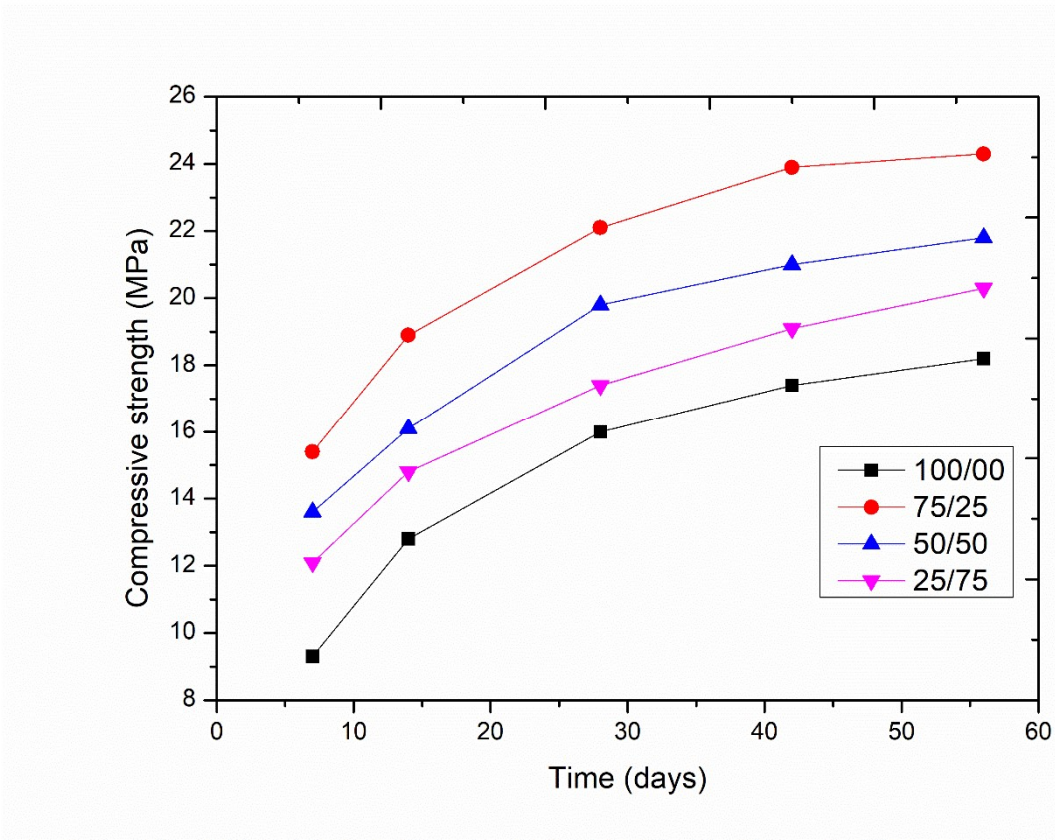

Fig. 4.3 Compressive strength of ambient-cured GPC

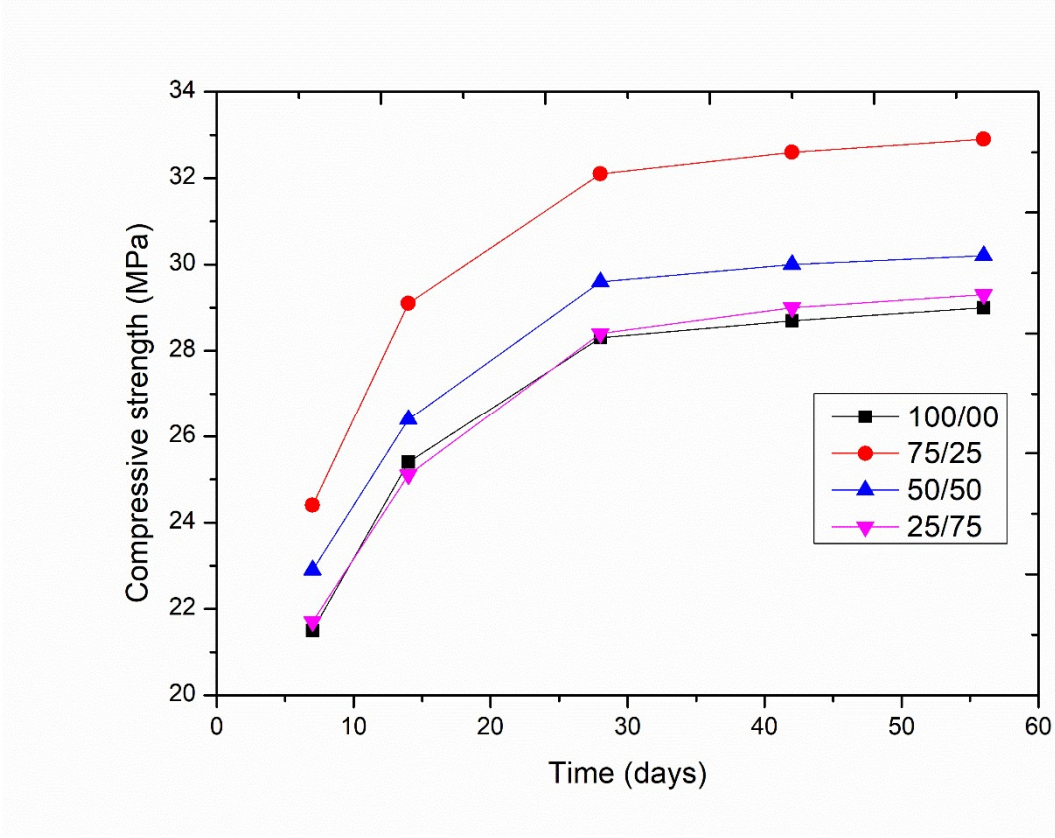

Fig. 4.4 Compressive strength of oven-cured GPC

4.1.4 Splitting Tensile Strength

Fig. 4.5 and Fig. 4.6 presented the splitting tensile strength results of all four mix designs in which the fly ash to GGBFS ratio varied from 100/0, 75/25, 50/50, and 25/75, respectively, by weight percentage. The ambient-curing and oven-curing cured all the mix design samples at the temperature of 60^0C for 24 hours and the sample tests at seven days, 14 days, 28days, 42 days, and 56 days in UTM for splitting tensile strength. The ambient-cured sample has less splitting tensile strength than the oven-cured samples, but in both cured samples, 75/25 fly ash/GGBFS ratio mix design samples got the maximum splitting tensile strength. A 25% by weight mix of GGBFS and fly ash increases the splitting tensile strength immediately, but after the increase, the replacement of GGBFS with fly ash slightly decreases the splitting tensile strength of the mix designs samples. Fig. 4.5 shows the splitting tensile strength of ambient-cured GPC specimens in which the 75/25 fly ash/GGBFS ratio mix got the highest average splitting tensile strength of 3.4 N/mm^2 at 56 days, whereas the 100/0, 50/50, and 25/75 fly ash/GGBFS ratio mixes got the lowest average splitting tensile strength of 2.4 MPa, 3.3 MPa, and 2.7 MPa at 56 days, respectively. Fig. 4.6 shows the splitting tensile strength of the oven-cured samples of GPC in which the 75/25 fly ash/GGBFS ratio mix got the highest average splitting tensile strength of 4.8 N/mm^2 at 56 days, whereas 100/0, 50/50, and 25/75 fly ash/GGBFS ratio mixes got the lowest average splitting tensile strength of 3.2 N/mm^2, 4.6 N/mm^2, and 4.2 N/mm^2 at 56 days, respectively. Around 95% of the strength of the GPC specimens was gained at day 28. After that, they gained very little strength, in which ambient-cured samples gained more strength comparable to the oven-cured samples after 28 days. Table 4.3 contains the whole ambient-cured GPC splitting tensile, whereas Table 4.4 contains the oven-cured splitting tensile of the GPC specimens.

Table 4.3 Splitting tensile of ambient-cured

Flyash/Slag ratio	7 days	14 days	28 days	42 days	56 days
100/0	1.1	1.5	2.1	2.3	2.4
75/25	1.8	2.4	3.1	3.2	3.4
50/50	1.7	2.4	2.8	3.0	3.3
25/75	1.3	2.0	2.4	2.6	2.7

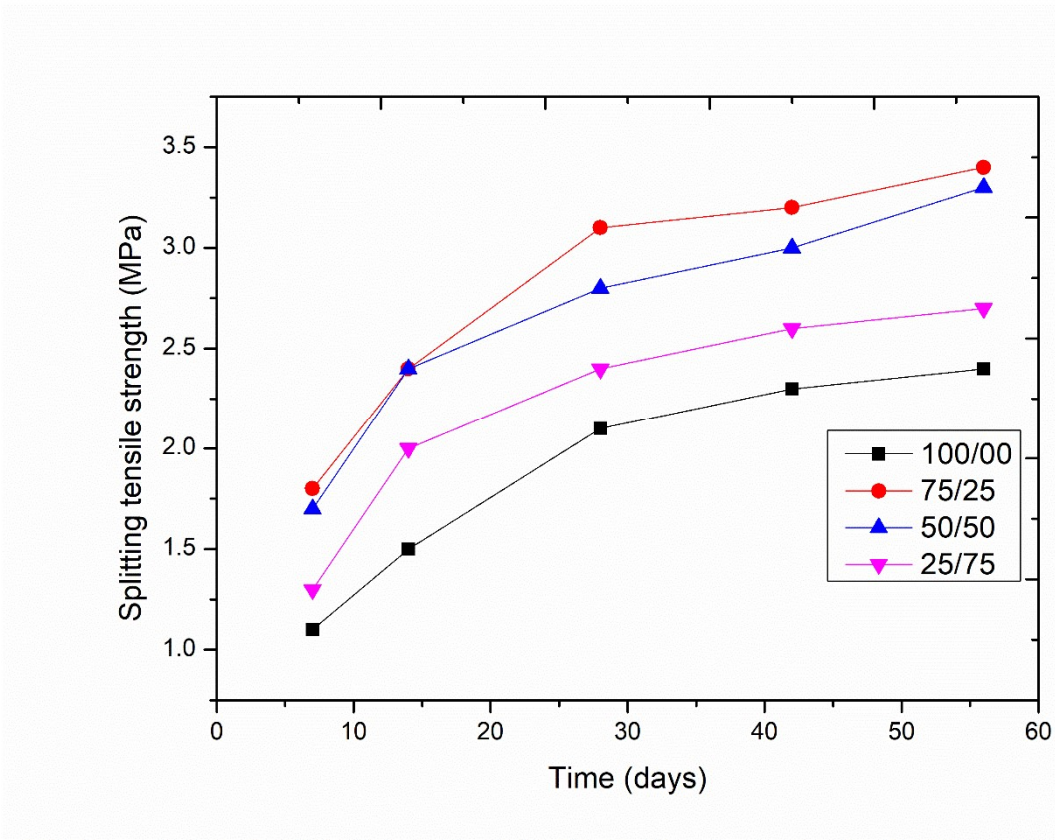

Fig. 4.5 Splitting Tensile Strength of ambient-cured GPC

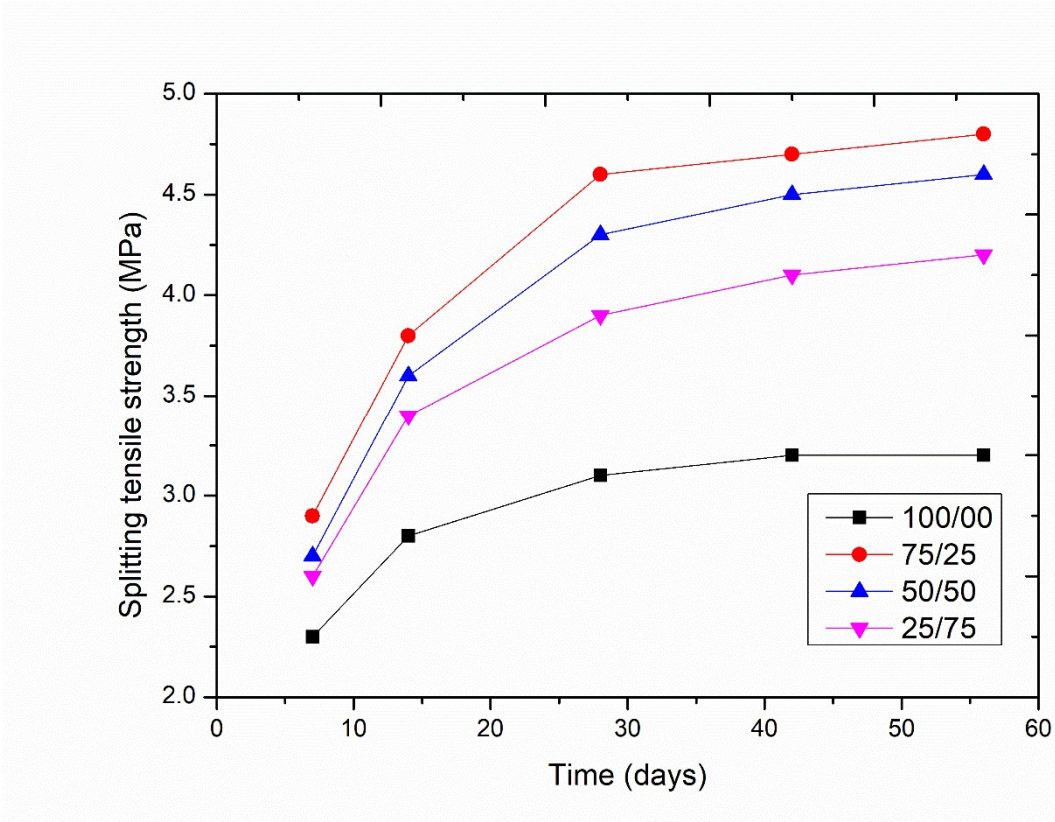

Fig. 4.6 Splitting tensile strength of oven-cured GPC

Table 4.4 Splitting tensile of oven-cured

Flyash/Slag ratio	7 days	14 days	28 days	42 days	56 days
100/0	2.3	2.8	3.1	3.2	3.2
75/25	2.9	3.8	4.6	4.7	4.8
50/50	2.7	3.6	4.3	4.5	4.6
25/75	2.6	3.4	3.9	4.1	4.2

4.1.5 Flexural Tensile Strength

Fig. 4.7 and Fig. 4.8 presented the flexural tensile strength of all four mix designs in which the fly ash to GGBFS ratio varies 100/0, 75/25, 50/50, 25/75, respectively, by weight percentage. The ambient-curing and oven-curing cured all the mix design samples at a temperature of 60^0C for 24 hours and the samples were tested at seven days, 14 days, 28 days, 42 days, and 56 days on the flexural testing machine for flexural strength. The ambient-cured sample has less flexural tensile strength than the oven-cured samples, but the 75/25 fly ash/GGBFS ratio mix design samples got the maximum average flexural tensile strength in both cured samples. Mixes of GGBFS with the fly ash at 25% by weight instantly raise the sample's flexural tensile strength. Still, after the increase, the replacement of GGBFS with fly ash slightly decreases the flexural tensile strength of the mix design samples. Fig. 4.7 shows the flexural tensile strength of ambient-cured GPC specimens in which the 75/25 fly ash/GGBFS ratio mix got the highest average flexural tensile strength of 3.6 N/mm^2 at 56 days, whereas 100/0, 50/50, and 25/75 fly ash/GGBFS ratio mixes got the lowest average flexural tensile strength of 2.5 N/mm^2, 3.4 N/mm^2, and 2.9 N/mm^2 at 56 days respectively. Fig. 4.8 shows the flexural tensile strength of the oven-cured samples of GPC in which the 75/25 fly ash/GGBFS ratio mix got the highest average flexural tensile strength of 5.3 N/mm^2 at 56 days, whereas 100/0, 50/50, and 25/75 fly ash/GGBFS ratio mixes got the lowest average flexural tensile strength of 3.6 MPa, 4.9 MPa, and 4.6 MPa, respectively. Around 95% strength of the GPC samples got 28 days after they gained significantly less strength in which ambient-cured samples gained more strength than the oven-cured samples after the 28 days. Table 4.5 contains the whole ambient-cured GPC flexural strength, whereas Table 4.6 contains the oven-cured flexural strength of the GPC specimens.

Table 4.5 Flexural strength of ambient-cured

Flyash/Slag ratio	7 days	14 days	28 days	42 days	56 days
100/0	1.2	1.6	2.2	2.4	2.5
75/25	2.0	2.6	3.3	3.5	3.6
50/50	1.9	2.5	3.0	3.2	3.4
25/75	1.5	2.2	2.6	2.8	2.9

Table 4.6 Flexural strength of oven-cured

Flyash/Slag ratio	7 days	14 days	28 days	42 days	56 days
100/0	2.5	3.0	3.5	3.6	3.6
75/25	3.1	4.0	5.0	5.2	5.3
50/50	2.9	3.7	4.5	4.7	4.9
25/75	2.7	3.6	4.2	4.4	4.6

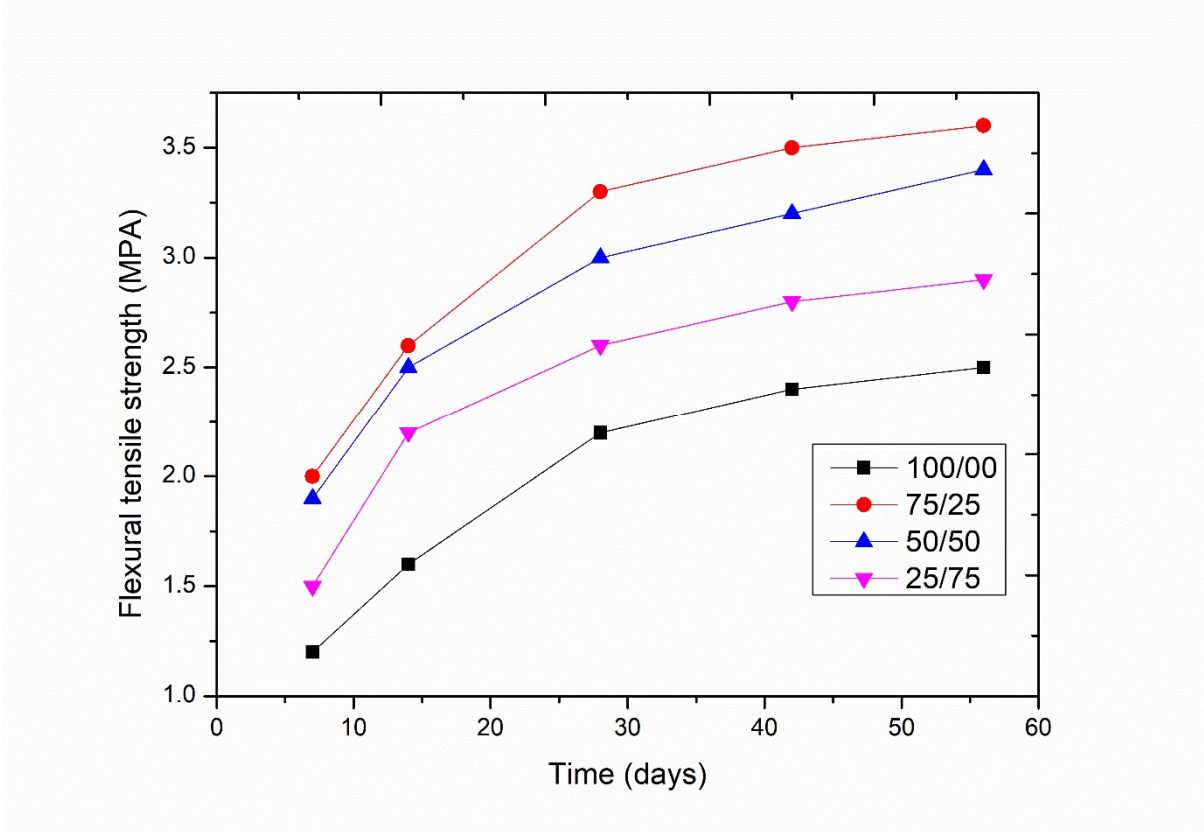

Fig. 4.7 Flexural tensile strength of ambient-cured GPC

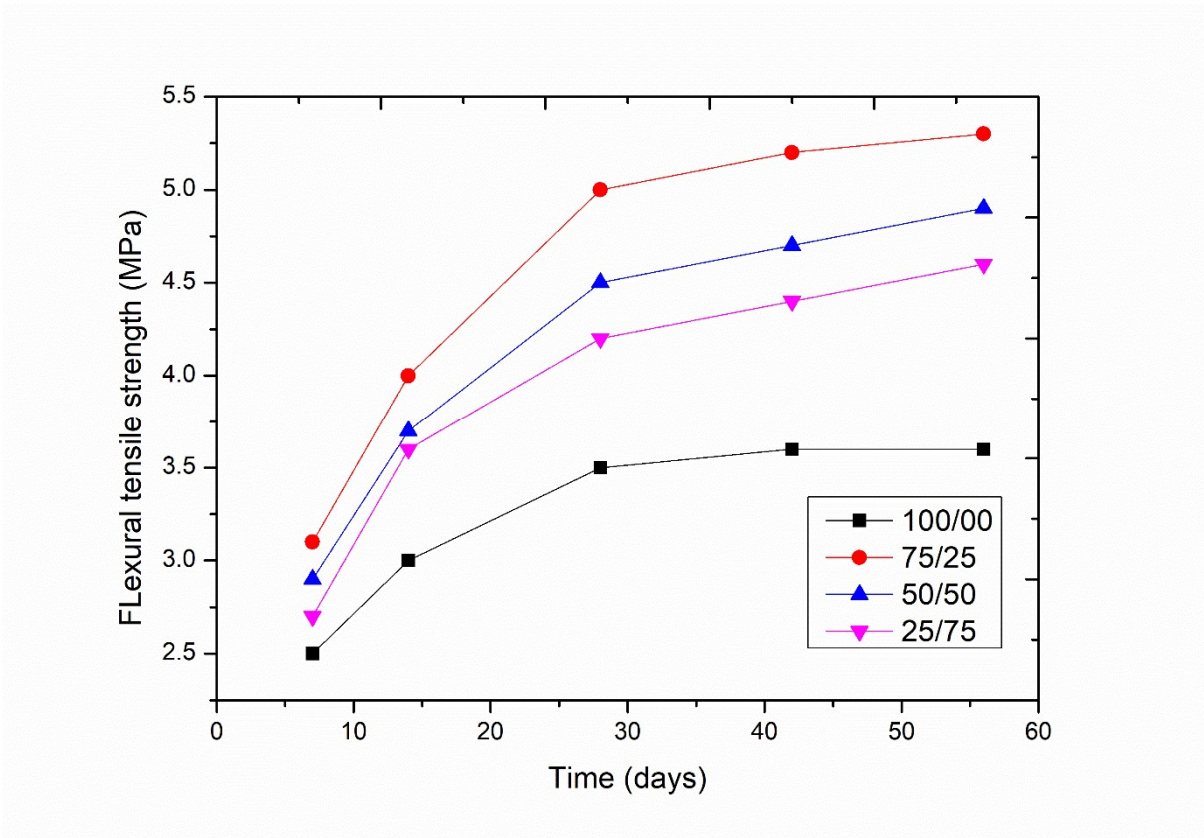

Fig. 4.8 Flexural tensile strength of oven-cured GPC

4.1.6 Rebound Hammer Strength

Fig. 4.9 and Fig. 4.10 presented the rebound hammer strength of all four mix designs in which the fly ash to GGBFS ratio varies 100/0, 75/25, 50/50, 25/75, respectively by weight percentage. All the mixed design samples were cured by ambient curing and oven curing at a temperature of 60^0C for 24 hours, and the samples were tested at seven days, 14 days, 28 days, 42 days, and 56 days by rebound hammer test under the non-destructive test of concrete specimens. The ambient-cured sample has less compressive strength than the oven-cured samples, but in both cured samples, 75/25 fly ash/GGBFS ratio mix design samples got the maximum average rebound hammer strength. A mix of GGBFS with fly ash at 25% by weight instantly increases the rebound strength of the design mix samples, but after the increase, the replacement of GGBFS with fly ash slightly decreases the rebound strength of the mixed specimens. Fig. 4.9 shows the rebound hammer strength of ambient-cured GPC specimens in which the 75/25 fly ash/GGBFS ratio mix got the highest average rebound hammer strength of 28.1 N/mm^2 at 56 days, whereas 100/0, 50/50, and 25/75 fly ash/GGBFS ratio mixes got the lowest average rebound hammer strength of 20.8 N/mm^2, 25.7 N/mm^2, and 24.4 N/mm^2 at 56 days, respectively.

Fig. 4.10 shows the rebound hammer strength of the oven-cured samples of GPC in which the 75/25 fly ash/GGBFS ratio mix got the highest average rebound hammer strength of 35 N/mm^2 at 56 days, whereas 100/0, 50/50, and 25/75 fly ash/GGBFS ratio mixes got the lowest average rebound hammer strength of 28.9 N/mm^2, 33.8 N/mm^2, and 32.7 N/mm^2 at 56 days, respectively. Around 95% of the strength of the GPC specimens was gained at day 28. After that, they gained significantly less strength in that ambient-cured samples gained more strength comparable to the oven-cured samples after 28 days. Rebound hammer test strength was slightly more excessive than the destructive compressive strength of the same mix designs specimens. Table 4.7 contains the whole ambient-cured GPC rebound strength, whereas Table 4.8 contains the oven-cured rebound strength of the GPC specimens.

Table 4.7 Rebound strength of ambient-cured

Flyash/Slag ratio	7 days	14 days	28 days	42 days	56 days
100/0	14.2	16.4	18.9	20.0	20.8
75/25	16.9	20.1	24.2	26.4	28.1
50/50	16.1	18.9	21.8	24.1	25.7
25/75	14.7	16.9	20.4	23.0	24.4

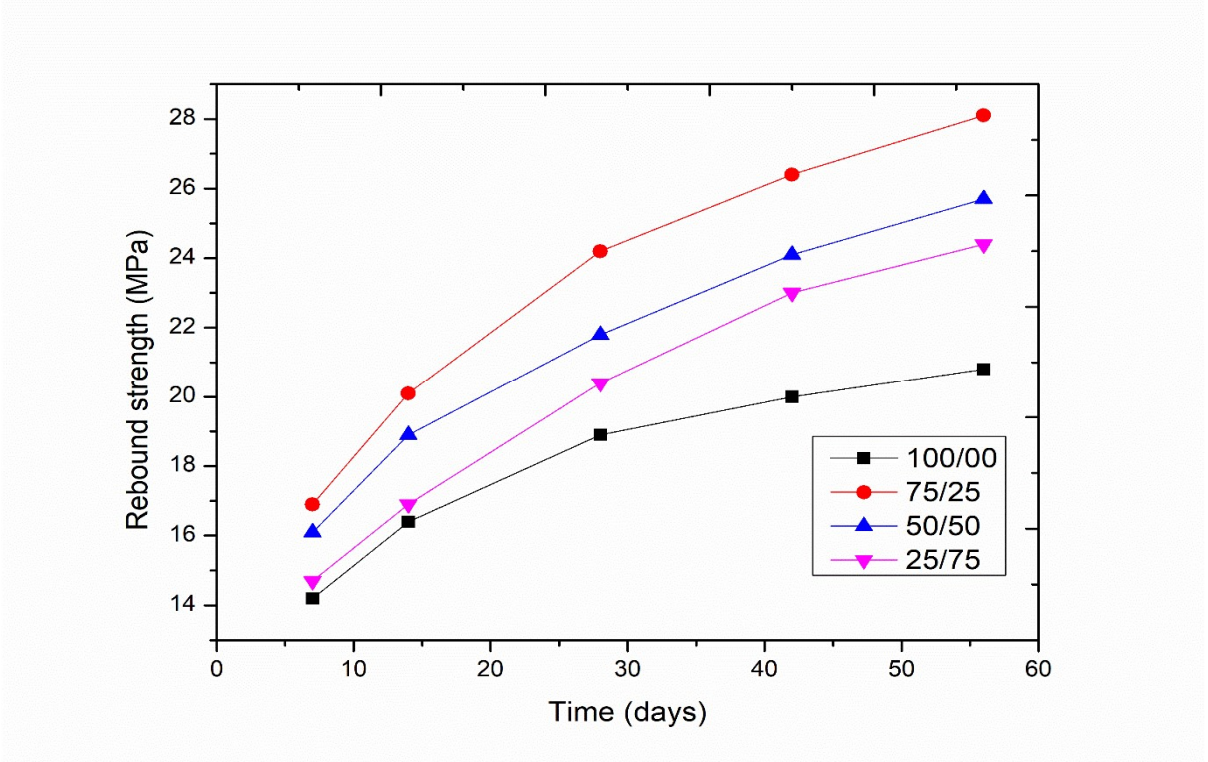

Fig. 4.9 Rebound hammer strength of ambient-cured GPC

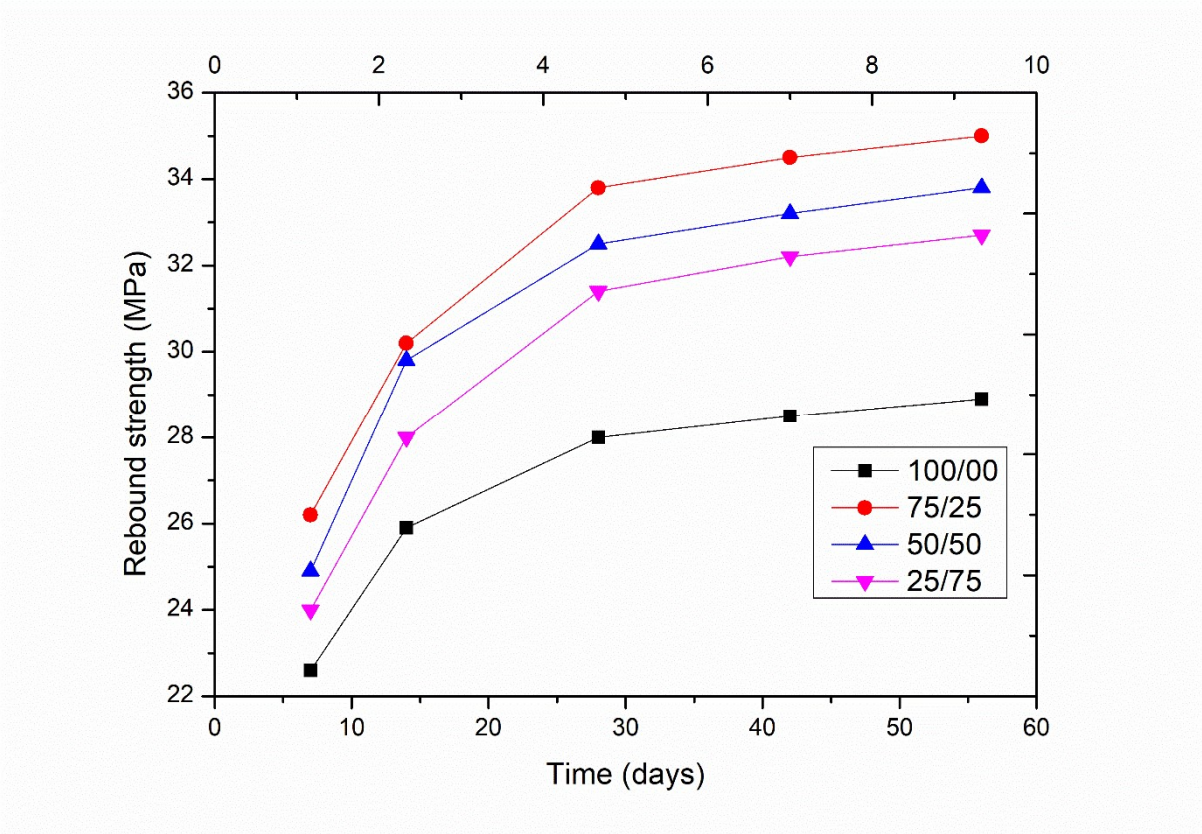

Fig. 4.10 Rebound hammer strength of oven-cured GPC

Table 4.8 Rebound strength of oven-cured

Flyash/Slag ratio	7 days	14days	28 days	42 days	56 days
100/0	22.6	25.9	28.0	28.5	28.9
75/25	26.2	30.2	33.8	34.5	35.0
50/50	24.9	29.8	32.5	33.2	33.8
25/75	24.0	28.0	31.4	32.2	32.7

4.1.7 UPVT(Ultrasonic Pulse Velocity Test)

The ultrasonic pulse velocity test is a non-destructive test of the material. The UPV test apparatus has a transducer used to emit the ultrasonic pulse wave in the material, and another one is used to receive the wave transmitted through the material. The UPV wave passes through the 150mm GPC sample cube and measures the velocity. The 55kHz natural frequency is used for transmitting through cube samples. For the smallest displacement between the transducers, keep both transducers at the opposite ends of the cube.The surface of the cube should be clean to transmit the UPV wave efficiently. The

sample UPV tests were done at 7 days, 14 days, 28 days, 42 days, and 56 days after specimen casting. Fig. 4.11 shows the ambient-cured samples UPV of the various mix designs at several days of testing, whereas Fig. 4.12 describes the oven-cured specimens UPV of the same mix designs at several days of testing. The ratio of 75/25 fly ash/GGBFS got higher UPV among the all mix design in both curing conditions. UPV graphs also show similar trends to another non-destructive rebound hammer test. The ratio of 100/00 of fly ash/GGBFS got the minimum UPV among all the mix designs in both-cured conditions.

The UPV of the GPC specimens increases with the days of testing after the casting. It directly affects the strength of the GPC specimens. The oven-cured specimens got a higher UPV compared to the ambient-cured conditions. The UPV in the mix designs varies with the different dosages of the fly ash-GGBFS content. The UPV increases instantaneously when the GGBFS dosage increases up to 25% from 0% of the binder. When the dosage of GGBFS increases beyond 25%, then the UPV slightly reduces. The maximum UPV of the ambient-cured and oven cured specimens is 3.624 km/sec and 4.226 km/sec. The UPV of the GPC specimens increases by a significantly smaller amount after the 28-day tests. Table 4.9 contains the whole ambient-cured GPC UPVT results, whereas Table 4.10 contains the oven-cured UPVT results of the GPC specimens.

Table 4.9 UPV of ambient-cured

Flyash/Slag ratio	7 days	14 days	28 days	42 days	56 days
100/0	3.125	3.267	3.326	3.362	3.389
75/25	3.456	3.582	3.604	3.612	3.624
50/50	3.345	3.402	3.489	3.497	3.503
25/75	3.287	3.312	3.398	3.406	3.412

Table 4.10 UPV of oven-cured

Flyash/Slag ratio	7 days	14 days	28 days	42 days	56 days
100/0	3.384	3.486	3.603	3.613	3.626
75/25	3.621	3.862	4.126	4.198	4.226
50/50	3.526	3.689	3.826	3.845	3.858
25/75	3.487	3.606	3.721	3.748	3.764

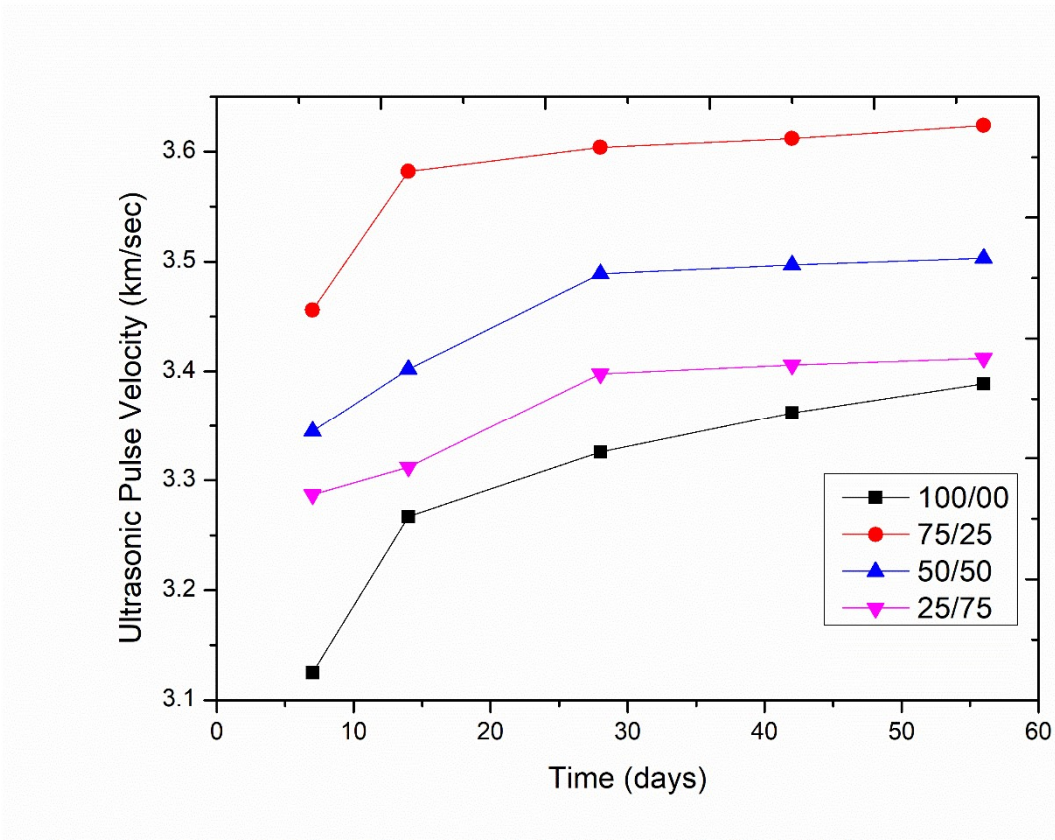

Fig. 4.11 UPVT results of ambient-cured GPC

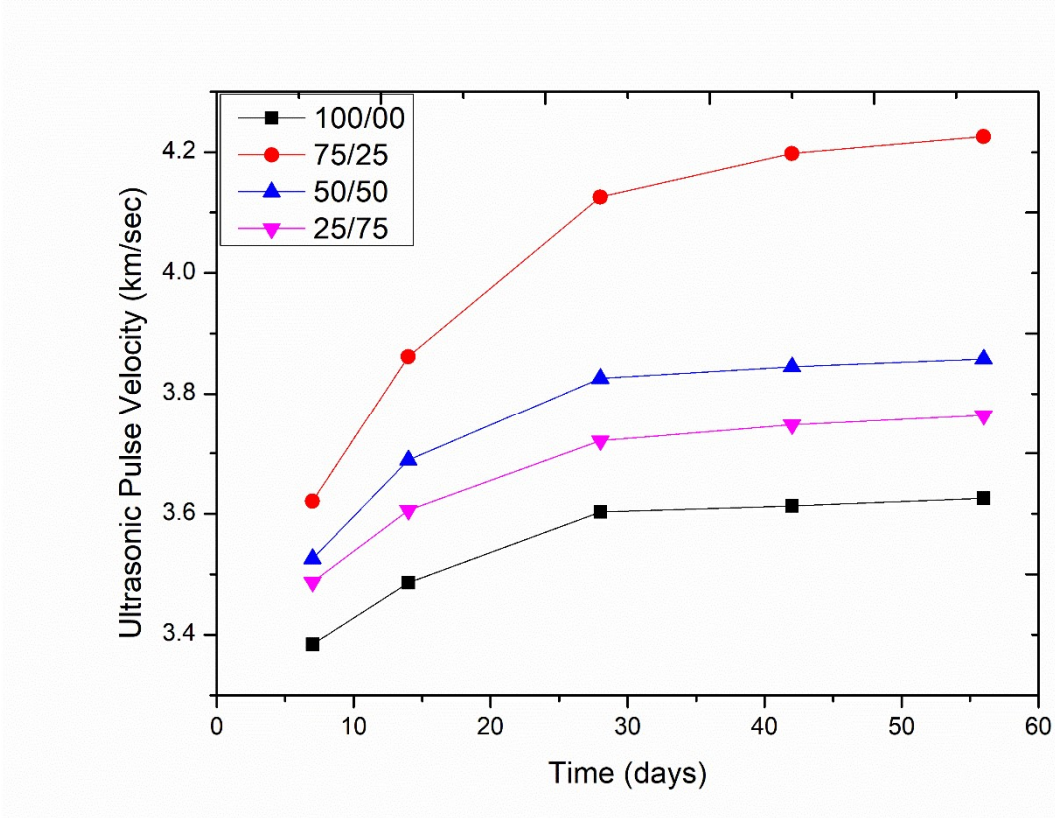

Fig. 4.12 UPVT results of oven-cured GPC

4.1.8 Poisson Ratio and Modulus of Elasticity

The Poisson ratio of the ambient-cured GPC samples is slightly higher than that of the oven-cured samples. Still, the modulus of elasticity of the GPC mix designs more top for the oven-cured samples. The maximum modulus of elasticity of the 75/25 fly ash/GGBFS ratio mix design of oven-cured specimens is 23.2 GPa, whereas the ambient-cured specimens modulus of elasticity is 20.8 GPa of the same mix design. Fig. 4.13 describes the MOE of both-cured GPC samples. Table 4.11 contains the MOE, poisons ratio, density, slump value, and compaction factor value of GPC samples.

Table 4.11 Poissons ratio, density, and MOE of GPC

Mix Design	Slump Value (mm)	Compaction factor	Density (Kg/m^3)		Poisson Ratio		Modulus of Elasticity (GPa)	
			Ambient Cured	Oven Cured	Ambient Cured	Oven Cured	Ambient Cured	Oven Cured
100/0	112	.96	2471	2451	.14	.14	19.8	21.4
75/25	100	.93	2494	2473	.16	.15	20.8	23.2
50/50	92	.91	2456	2434	.15	.15	20.5	22.9
25/75	73	.83	2423	2406	.14	.13	20.1	22.0

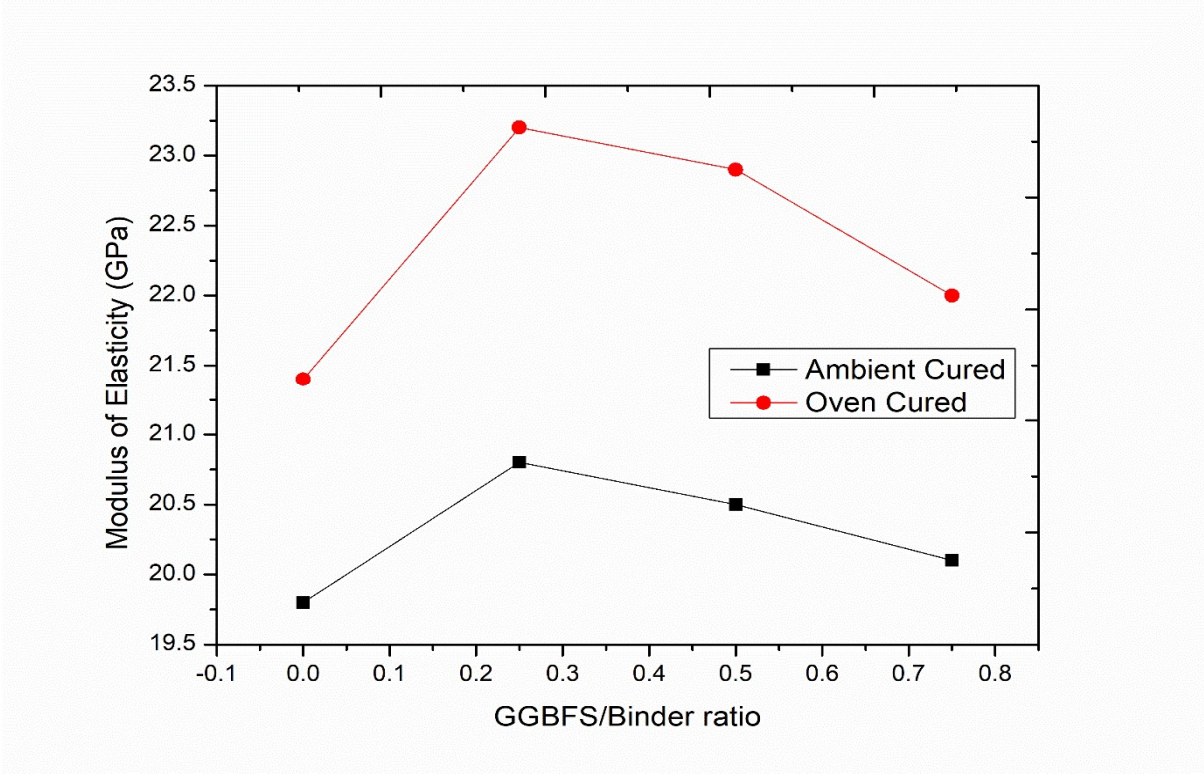

Fig. 4.13 Elastic modulus vs GGBFS/binder ratio

4.2 Effect of Liquid to Binder Ratio

4.2.1 Slump and Compaction Factor

In the experimental investigation, workability was examined by the slump test and the compaction factor in the laboratory. The slump value increases with the increment of water content in the mix design, so the slump value increases consecutively with the increase of the liquid-to-binder ratio in mixes of GPC. Similarly, the compaction factor value also increases with the increment of the liquid-to-binder ratio. Fig. 4.14 describes the effect of the liquid-to-binder ratio on both slump value and compaction factor on the fresh mix of GPC. The workability of GPC increases with the increment of the alkaline solution/flyash ratio [154].

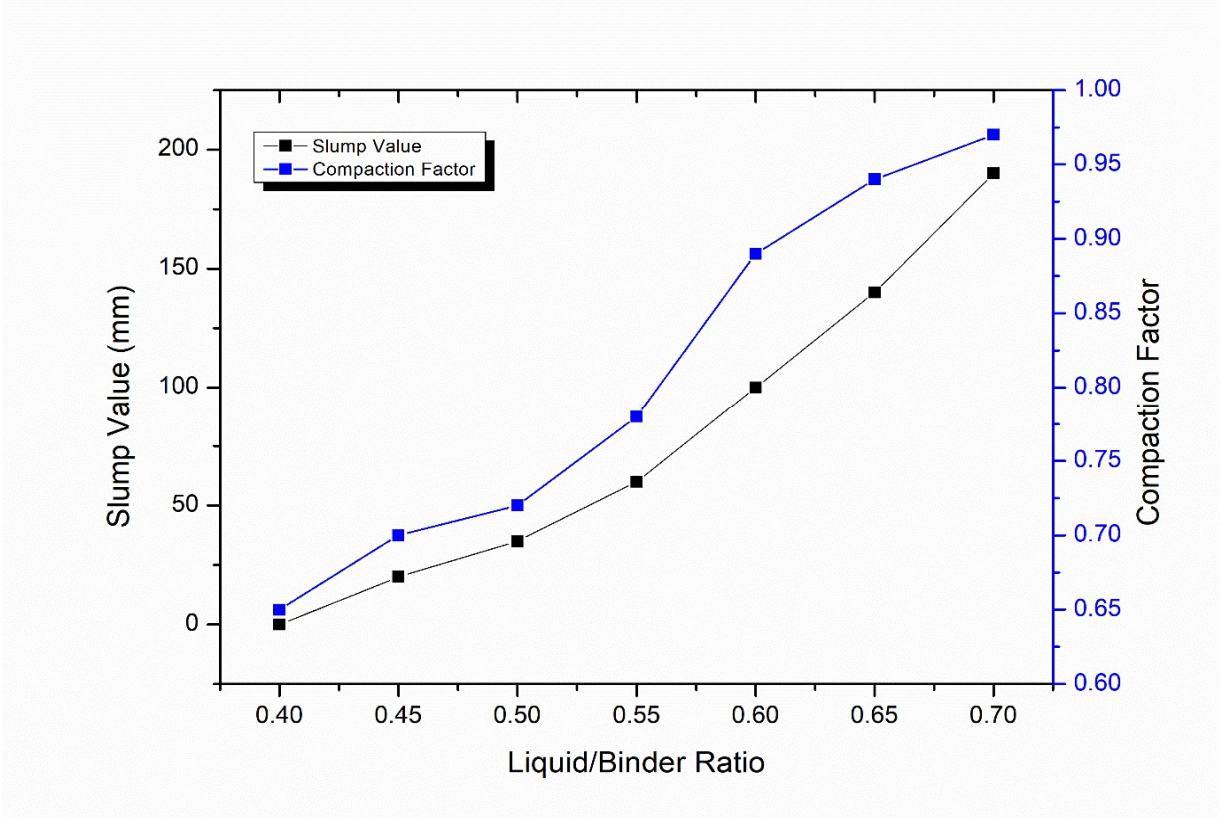

Fig. 4.14 The graph between the slump and compaction factor vs liquid/binder ratio

4.2.2 Density

The density and drying shrinkage of the concrete mix design shows the chemical properties of the GPC. The chemical reaction decides the density or unit weight and

drying shrinkage of the GPC mix design. The density of ambient-cured GPC mix design specimens is higher than oven-cured specimens of the same mix designs. The density of GPC mix specimens decreases with the increment of the liquid-to-binder ratio. Fig. 4.15 describes the variation of density with the variation of the curing conditions, liquid-to-binder ratio.

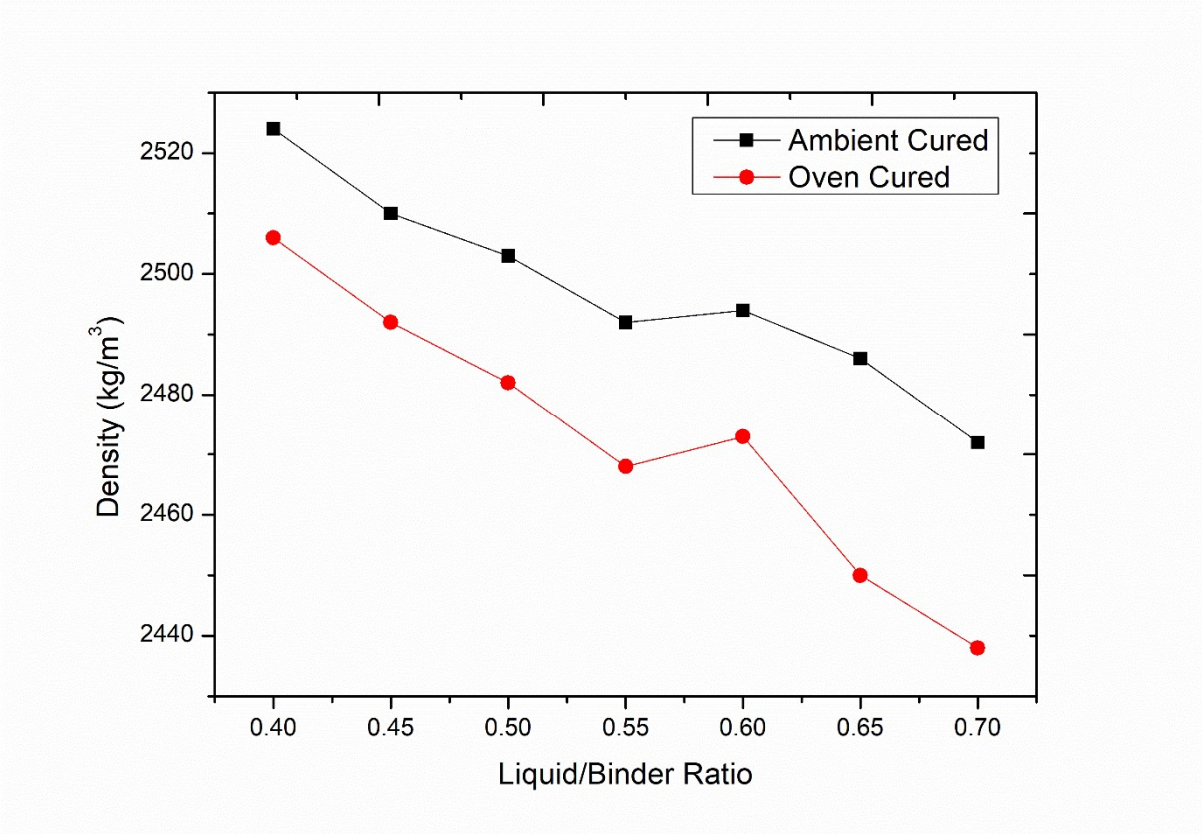

Fig. 4.15 Graph between the density and liquid/binder ratio

4.2.3 Compressive Strength

In the GPC mix design, the liquid-to-binder ratio plays a vital role in mechanical and durability properties. In the experimental investigation analysis, the liquid-to-binder ratio varies from 0.40 to 0.70 in the GGBFS flyash-based GPC. The compressive strength increases with the ratio's increment but beyond the 0.60 liquid-to-binder ratio decreases randomly in the mix samples. The oven-cured specimens got higher strength than the ambient-cured specimens of the same design mix, but in both conditions, 0.60 liquid-to-binder ratios got the optimum compressive strength. Fig. 4.16 and Fig. 4.17 describe the graph of compressive strength of different mixes of both curing conditions, in which Fig. 4.16 shows the ambient-cured GPC specimens, and Fig. 4.17 shows the oven-cured GPC specimens. The compressive strength of specimens was around 85-90% and 95-98% in

ambient-cured and oven-cured conditions, respectively. Table 4.12 contains the whole ambient-cured GPC compressive strength, whereas Table 4.13 contains the oven-cured compressive strength of the GPC specimens.

Table 4.12 Compressive strength of ambient-cured

Liquid/Binder Ratio	7 days	14 days	28 days	42 days	56 days
0.4	8.9	10.4	12.6	13.2	13.9
0.45	12.4	14.9	18.2	19.9	20.4
0.50	14.8	17.8	20.9	22.0	22.8
0.55	15.2	18.6	21.8	23.7	24.0
0.60	15.4	18.9	22.1	23.9	24.3
0.65	15.0	18.2	21.4	23.4	23.8
0.70	14.8	18.0	21.0	22.9	23.1

Table 4.13 Compressive strength of oven-cured

Liquid/Binder Ratio	7 days	14 days	28 days	42 days	56 days
0.4	16.2	18.1	19.9	20.3	20.8
0.45	21.3	23.8	26.9	27.3	27.7
0.50	23.6	27.6	30.8	31.2	31.6
0.55	24.1	28.9	31.9	32.4	32.6
0.60	24.4	29.1	32.1	32.6	32.9
0.65	24.0	28.4	31.6	32.0	32.4
0.70	23.4	27.6	30.2	30.8	31.1

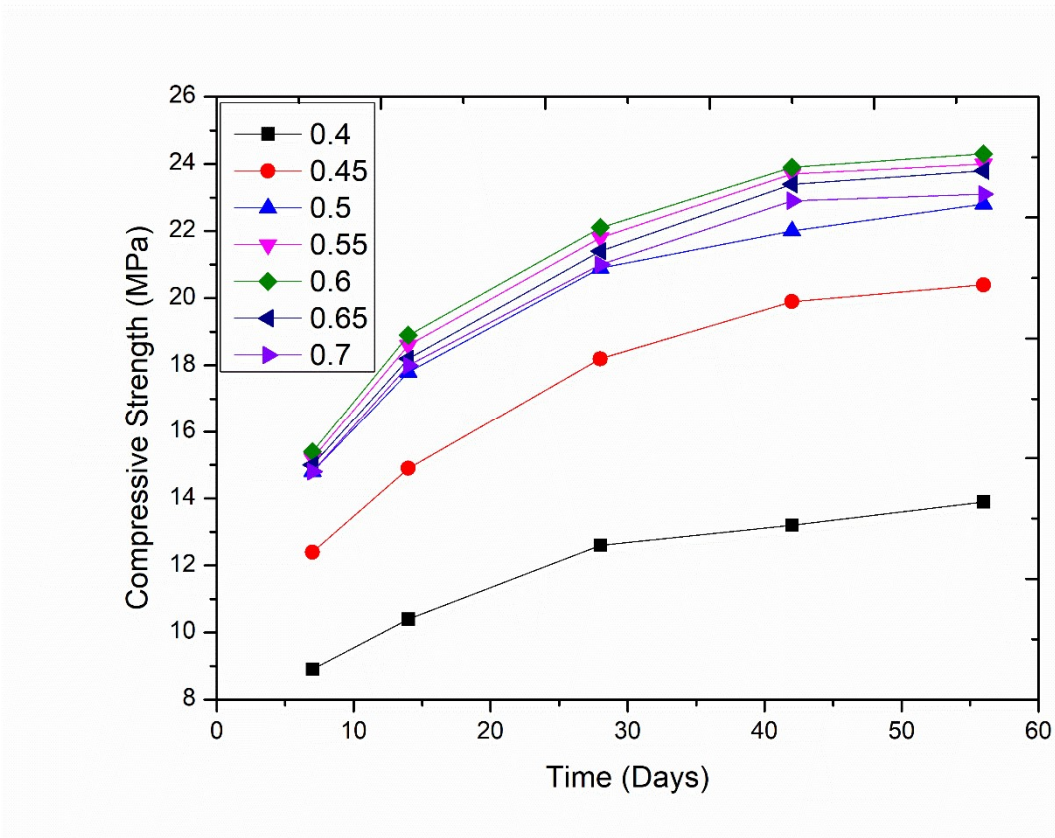

Fig. 4.16 Compressive strength of ambient-cured GPC

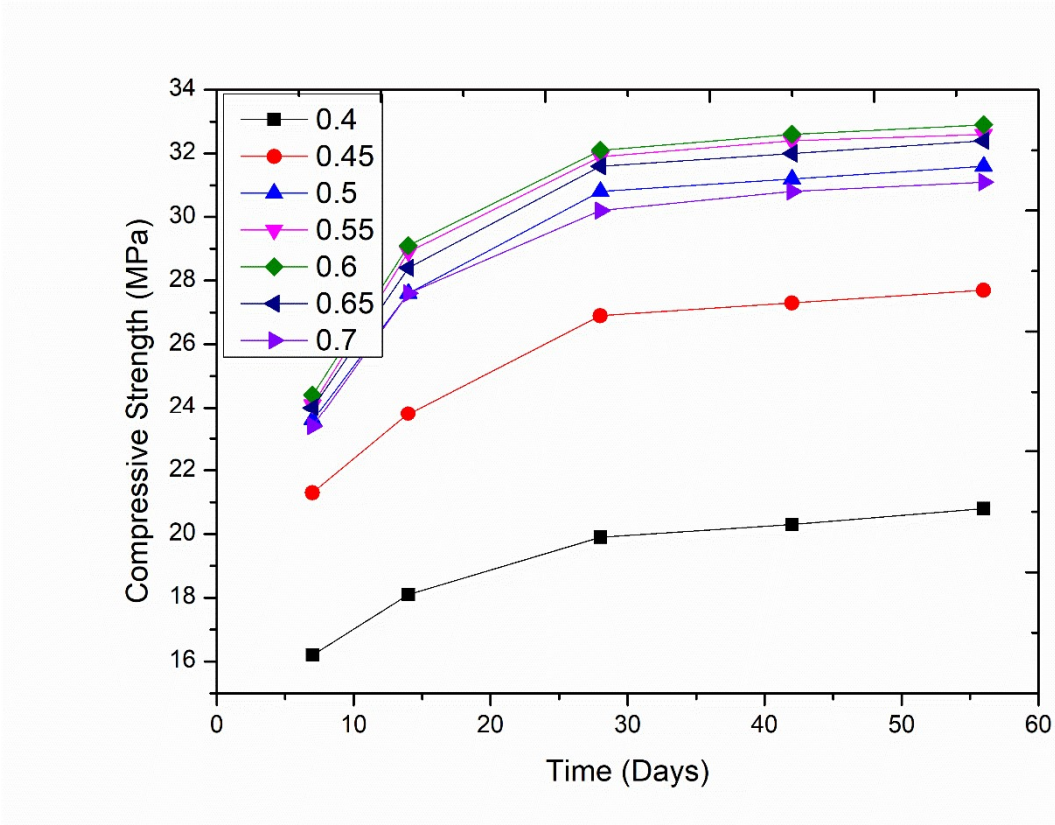

Fig. 4.17 Compressive strength of oven-cured GPC

4.2.4 Splitting Tensile

The splitting tensile measured by the statically applied load on the cylindrical sample along the UTM lateral dimension is an indirect tensile strength. The splitting tensile shows a similar strength compared to the mixed compressive strength in both curing conditions. The oven-cured specimens got higher strength compared to the ambient-cured specimens of the same design mixes. Among all design mixes, the 0.60 liquid-to-binder ratio produced the best splitting tensile in both curing conditions. Fig. 4.18 and Fig. 4.19 describe the graph of splitting tensile of different design mixes in both curing conditions, in which Fig. 4.18 shows the ambient-cured splitting tensile; and Fig. 4.19 shows the oven-cured splitting tensile of the different GPC mix designs. Table 4.14 contains the whole ambient-cured GPC splitting tensile, whereas Table 4.15 contains the oven-cured splitting tensile of the GPC specimens.

Table 4.14 Splitting tensile of ambient-cured

Liquid/Binder Ratio	7 days	14 days	28 days	42 days	56 days
0.4	1.1	1.3	1.6	1.8	2.0
0.45	1.4	1.8	2.1	2.4	2.6
0.50	1.6	2.0	2.6	2.8	2.9
0.55	1.8	2.3	3.0	3.1	3.3
0.60	1.8	2.4	3.1	3.2	3.4
0.65	1.7	2.3	2.9	3.0	3.2
0.70	1.5	2.0	2.6	2.6	2.8

Table 4.15 Splitting tensile of oven-cured

Liquid/Binder Ratio	7 days	14 days	28 days	42 days	56 days
0.4	1.9	2.2	2.8	2.9	3.0
0.45	2.2	2.9	3.6	3.8	3.9
0.50	2.6	3.4	4.0	4.2	4.3
0.55	2.8	3.8	4.4	4.6	4.7
0.60	2.9	3.8	4.6	4.7	4.8
0.65	2.7	3.6	4.3	4.5	4.6
0.70	2.5	3.2	3.9	4.2	4.3

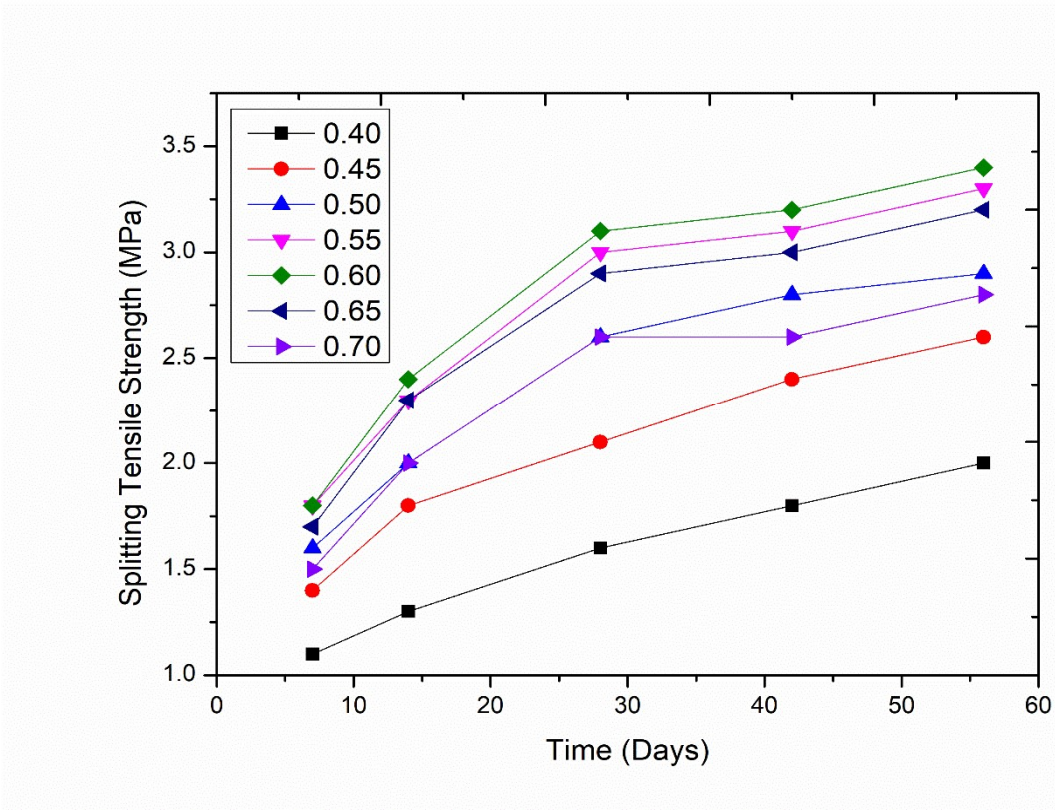

Fig. 4.18 Splitting tensile of ambient-cured GPC

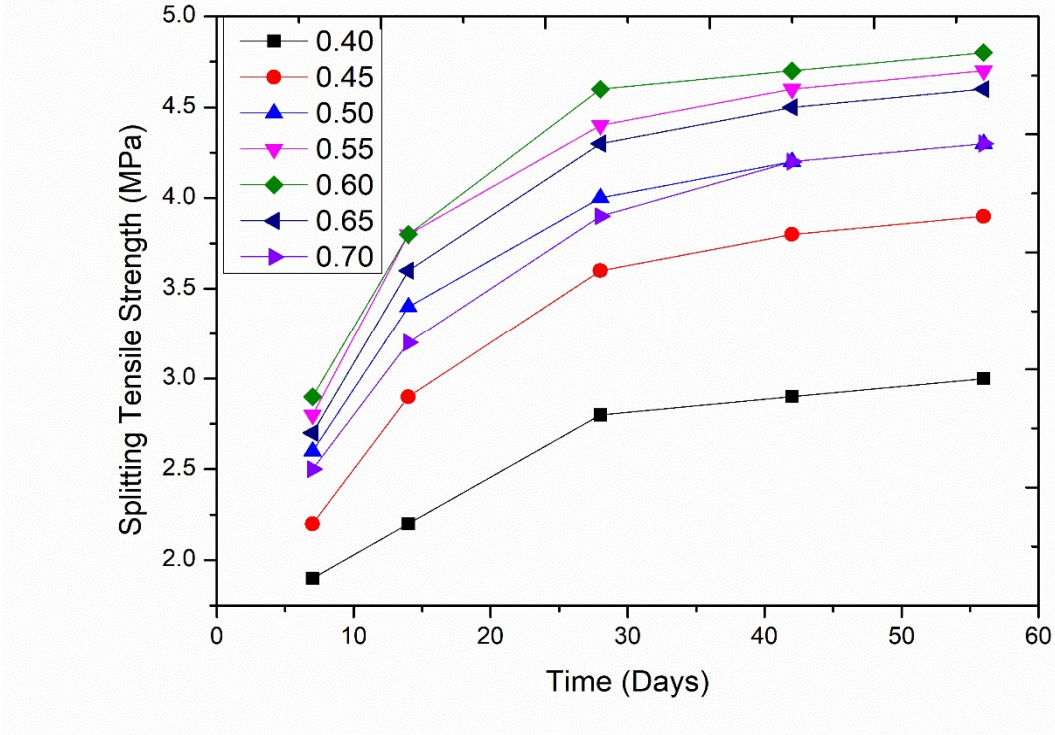

Fig. 4.19 Splitting tensile of oven-cured GPC

4.2.5 Flexural Strength

The flexural strength is used to examine the bending strength or property of the concrete. The flexural strength of GPC also has the same pattern as compressive strength, and it is around 12-18% of the compressive strength in all design mixes of GPC. The oven-cured specimens got higher flexural strength than ambient-cured for the same mix designs, and the mix design with 0.60 liquid-to-binder ratios got the optimum point of the strength. Fig. 4.20 and Fig. 4.21 describe the flexural strength of the different mix designs of both curing conditions, whereas Fig. 4.20 shows the ambient-cured strength and Fig. 4.21 oven-cured strength GPC specimens. Table 4.16 contains the whole ambient-cured GPC flexural strength, whereas Table 4.17 contains the oven-cured flexural strength of the GPC specimens.

Table 4.16 Flexural strength of ambient-cured

Liquid/Binder Ratio	7 days	14 days	28 days	42 days	56 days
0.4	1.0	1.4	1.7	1.9	2.1
0.45	1.4	2.0	2.3	2.5	2.6
0.50	1.7	2.4	2.7	3.0	3.2
0.55	1.9	2.6	3.1	3.3	3.5
0.60	2.0	2.6	3.3	3.5	3.6
0.65	1.8	2.4	2.9	3.1	3.3
0.70	1.6	2.2	2.6	2.8	3.0

Table 4.17 Flexural strength of oven-cured

Liquid/Binder Ratio	7 days	14 days	28 days	42 days	56 days
0.4	2.1	2.4	3.0	3.2	3.3
0.45	2.5	3.1	3.7	3.9	4.0
0.50	2.8	3.5	4.2	4.4	4.5
0.55	3.0	3.8	4.6	4.7	4.8
0.60	3.1	4.0	5.0	5.2	5.3
0.65	2.9	3.6	4.4	4.6	4.7
0.70	2.7	3.2	4.0	4.2	4.3

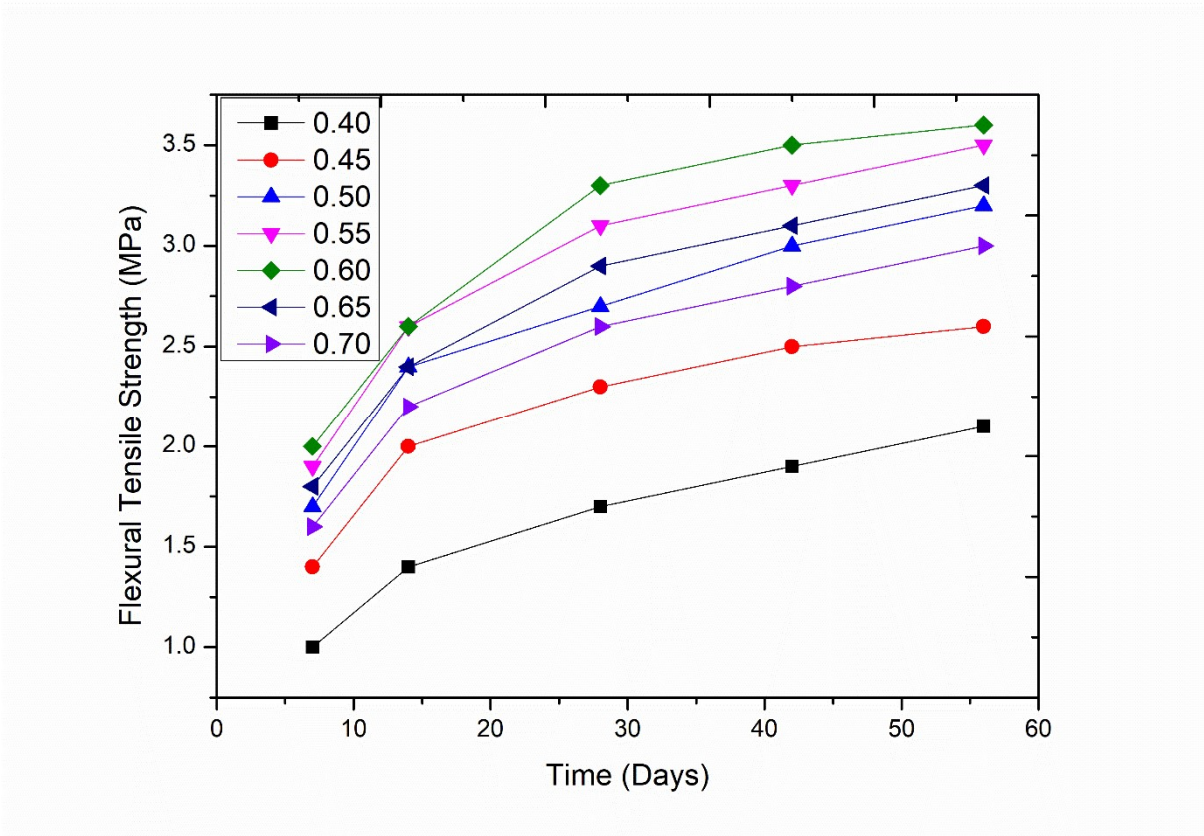

Fig. 4.20 Flexural strength of ambient-cured GPC

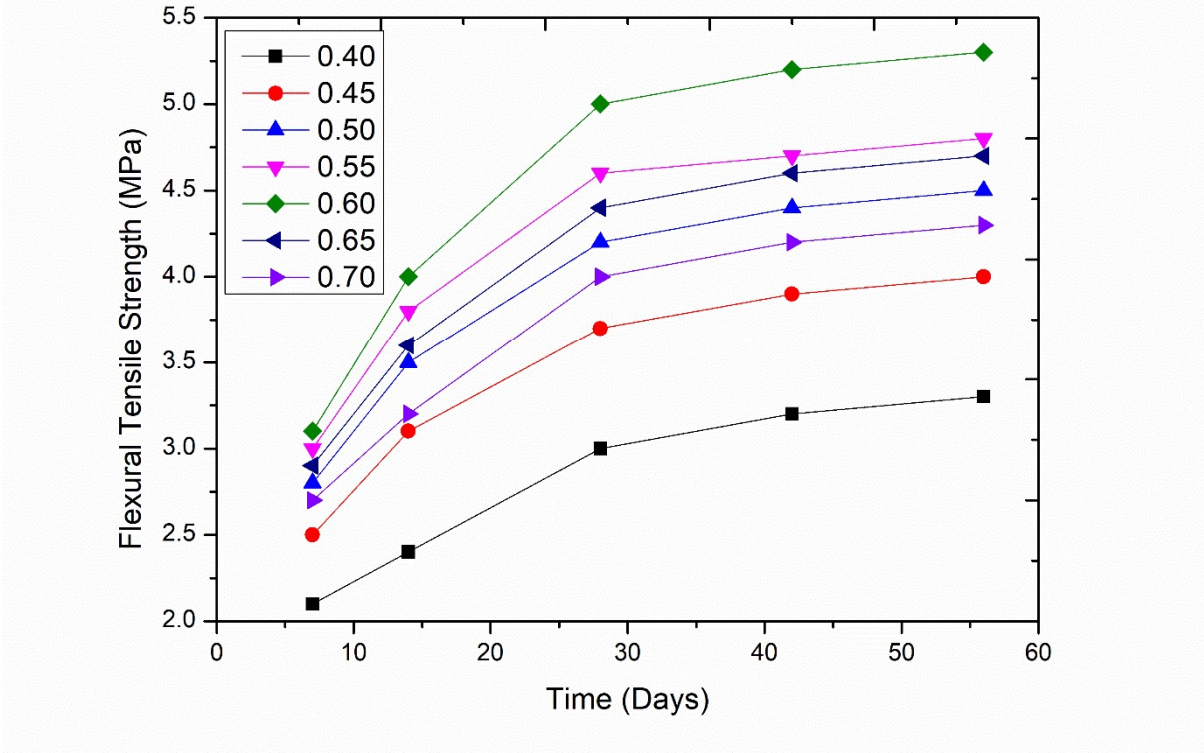

Fig. 4.21 Flexural strength of oven-cured GPC

4.2.6 Rebound strength

The non-destructive test is used to check the strength or quality of the concrete specimen without destruction. It includes the rebound hammer test and UPV test. The rebound strength shows the similar compressive strength of the concrete specimens with a precision of 20% as per the IS code. It is based on the specimen's surface hardness gives the specimen strength, whereas the UPV test is used to find the strength or quality by measuring the time passage of the ultrasonic pulse wave. The time would increase with the reduction in quality or strength of the specimens. The crack develops inside the specimen, also checked by the UPV test. Fig. 4.22 and Fig. 4.23 describe the rebound strength graph of different mixes of both cured samples, whereas Fig. 4.22 shows the ambient-cured specimens' rebound strength, and Fig. 4.23 shows the oven-cured specimens' rebound strength. Table 4.18 contains the whole ambient-cured GPC rebound strength, whereas Table 4.19 contains the oven-cured rebound strength of the GPC specimens.

Table 4.18 Rebound strength of ambient-cured

Liquid/Binder Ratio	7 days	14 days	28 days	42 days	56 days
0.4	12.8	14.7	18.9	20.6	21.1
0.45	14.9	17.9	21.9	23.0	23.8
0.50	16.0	19.2	23.0	23.8	24.5
0.55	16.5	19.8	23.9	26.0	27.3
0.60	16.9	20.1	24.2	26.4	28.1
0.65	16.2	19.4	23.4	25.4	26.8
0.70	15.6	18.6	22.7	24.2	25.0

Table 4.19 Rebound strength of oven-cured

Liquid/Binder Ratio	7 days	14 days	28 days	42 days	56 days
0.4	20.4	24.8	26.9	27.4	27.8
0.45	23.0	27.1	30.2	30.6	30.9
0.50	25.6	29.2	32.5	32.8	33.2
0.55	26.0	29.9	33.4	34.0	34.4

0.60	26.2	30.2	33.8	34.5	35.0
0.65	25.8	29.6	33.0	33.4	33.8
0.70	24.9	28.7	31.6	32.0	32.4

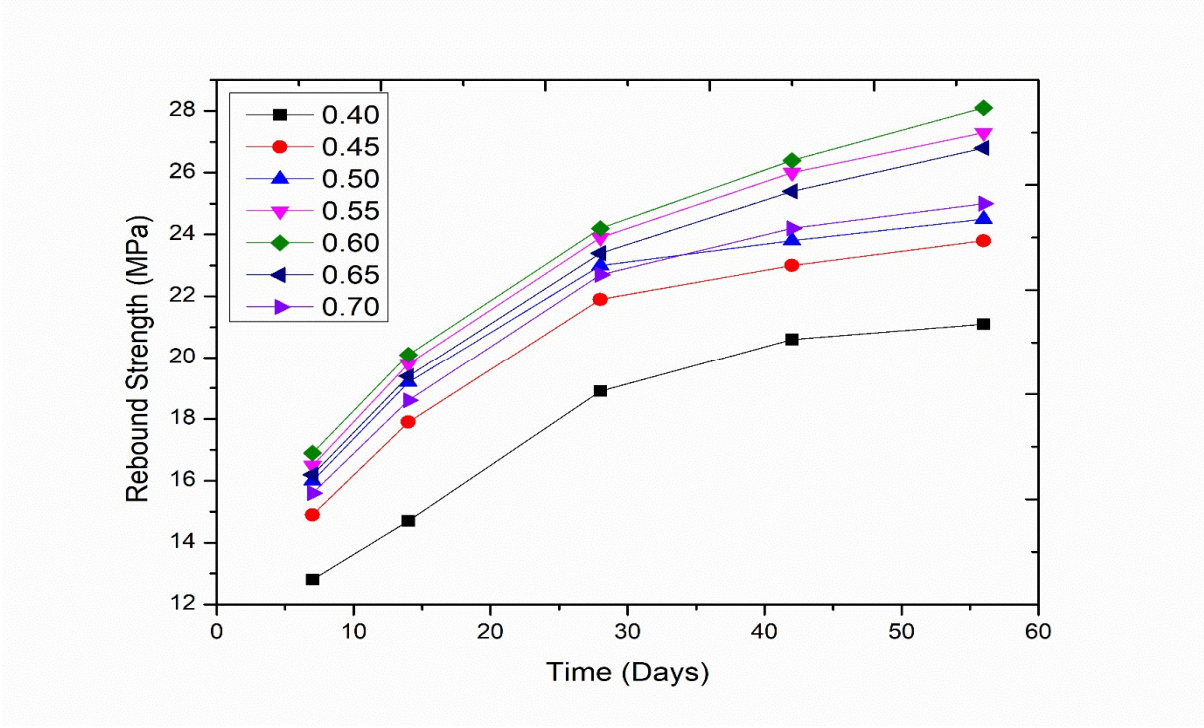

Fig. 4.22 Rebound strength of ambient-cured GPC

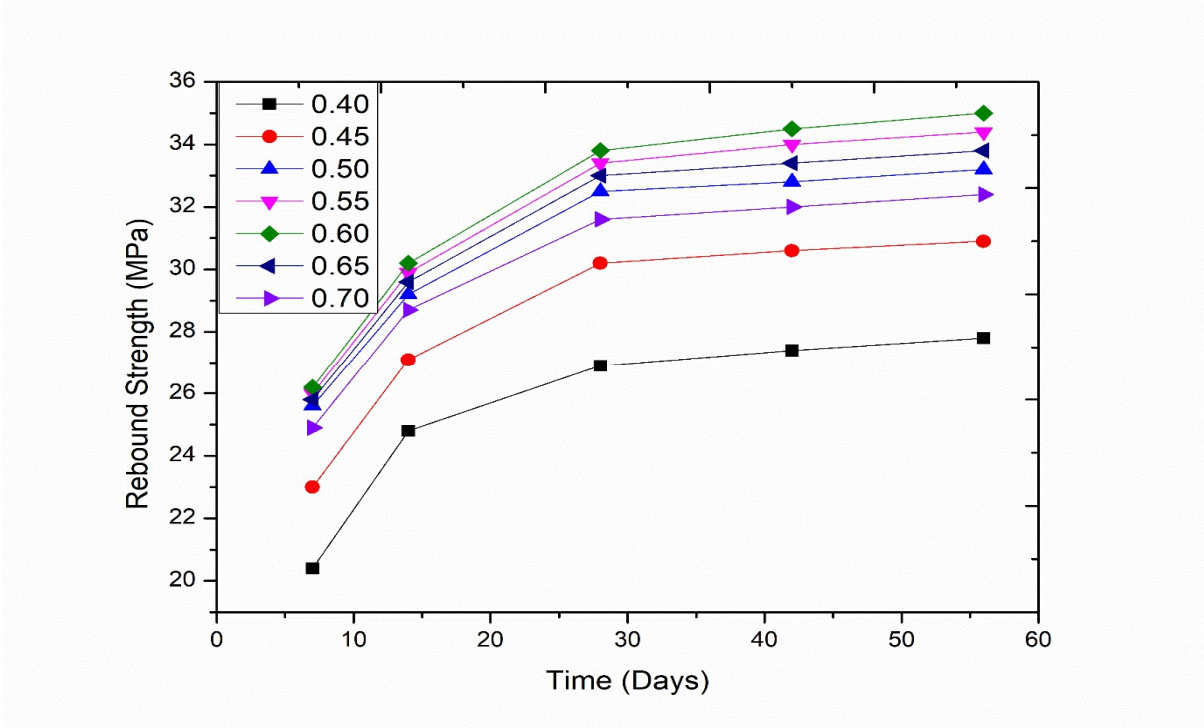

Fig. 4.23 Rebound strength of oven-cured GPC

4.2.7 UPVT(Ultrasonic Pulse Velocity Test)

Fig. 4.24 and Fig. 4.25 describe the UPV of the different mixes in both cured samples, whereas Fig. 4.24 shows the ambient-cured specimens and Fig. 4.25 shows the oven-cured specimens the GPC. The graph shows a similar pattern of the UPV to the rebound strength in both cured conditions. The optimum point of non-destructive strength was achieved at the 0.60 liquid-to-binder ratio in the GPC mix design. Table 4.20 contains the whole ambient-cured GPC UPVT results, whereas Table 4.21 contains the oven-cured UPVT results of the GPC specimens.

Table 4.20 UPV of ambient-cured

Liquid/Binder Ratio	7 days	14 days	28 days	42 days	56 days
0.4	1.82	1.97	2.13	2.17	2.18
0.45	2.16	2.27	2.39	2.43	2.45
0.50	2.26	2.43	2.63	2.74	2.82
0.55	2.32	2.44	2.68	2.71	2.82
0.60	3.345	3.402	3.489	3.497	3.503
0.65	2.31	2.42	2.64	2.69	2.75
0.70	1.82	1.98	2.23	2.41	2.46

Table 4.21 UPV of oven-cured

Liquid/Binder Ratio	7 days	14 days	28 days	42 days	56 days
0.4	2.23	2.36	2.42	2.44	2.45
0.45	2.45	2.73	3.23	3.34	3.62
0.50	2.81	3.23	4.02	4.12	4.15
0.55	2.92	3.67	4.13	4.21	4.23
0.60	3.526	3.689	3.826	3.845	3.858
0.65	2.89	3.56	4.01	4.13	4.17
0.70	2.81	3.43	4.01	4.09	4.12

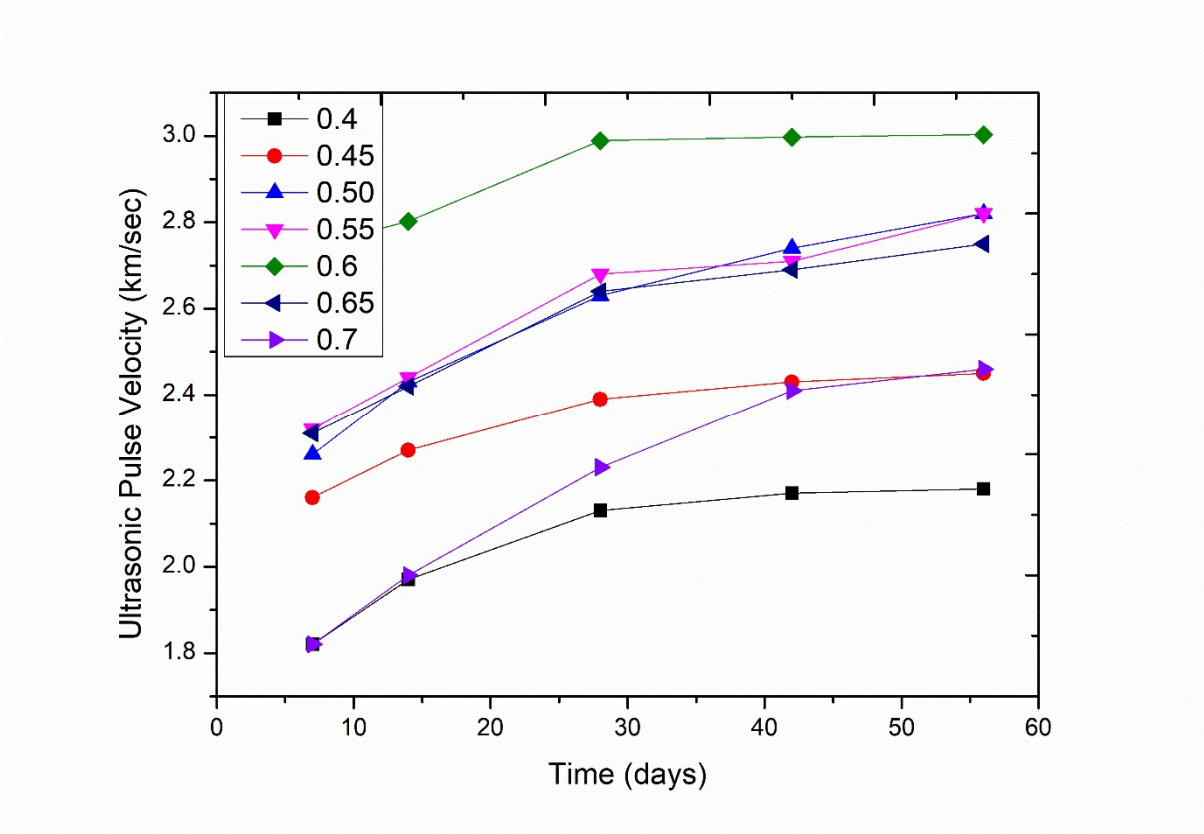

Fig. 4.24 UPVT results of ambient-cured GPC

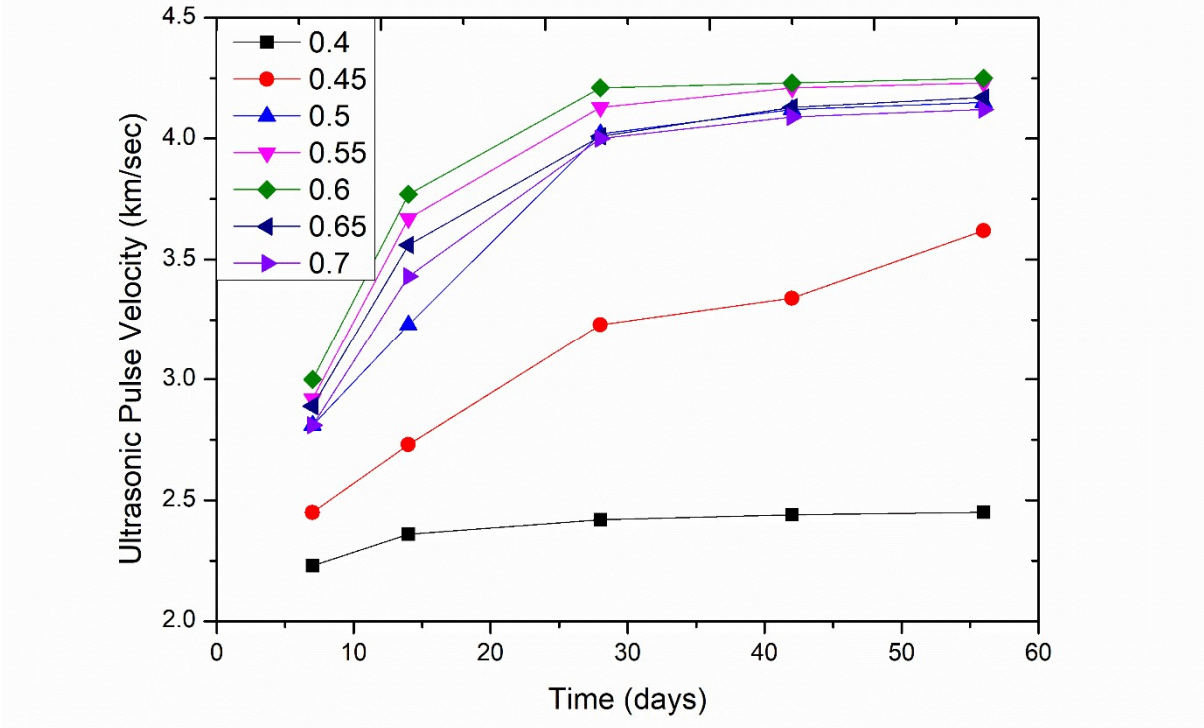

Fig. 4.25 UPVT results of oven-cured GPC

4.2.8 Poisson Ratio and Elastic Modulus

The Poisson's ratio and modulus of elasticity of the mix design measured by testing the cylinder specimens of size length and diameter are 300mm and 150mm, respectively. The static load applies to the specimens along the vertical direction and measures the horizontal and vertical deformation for Poisson's ratio calculation. The modulus of elasticity of the mix design is calculated by the repetition load applying the cylindrical specimen of one-third crushing load statically and measures the elastic modulus by the secant modulus method. Fig. 4.26 describes the graph of modulus of elasticity of both curing conditions at the different liquid-to-binder ratios in the mix designs.

Table 4.22 Poissons ratio, density, and MOE of GPC

	Slump Value (mm)	Compaction factor	Density in Kg/m^3		Poisson Ratio		Modulus of Elasticity (GPa)	
			Ambient Cured	Oven Cured	Ambient Cured	Oven Cured	Ambient Cured	Oven Cured
0.4	00	0.65	2524	2506	.14	.13	17.0	18.8
0.45	20	0.7	2510	2492	.14	.14	20.0	22.0
0.50	35	0.72	2503	2482	.15	.14	20.3	22.7
0.55	60	0.78	2492	2468	.16	.15	20.6	23.0
0.60	100	0.89	2494	2473	.16	.15	20.8	23.2
0.65	140	0.94	2486	2450	.17	.16	20.4	22.8
0.70	190	0.97	2472	2438	.18	.17	20.1	22.4

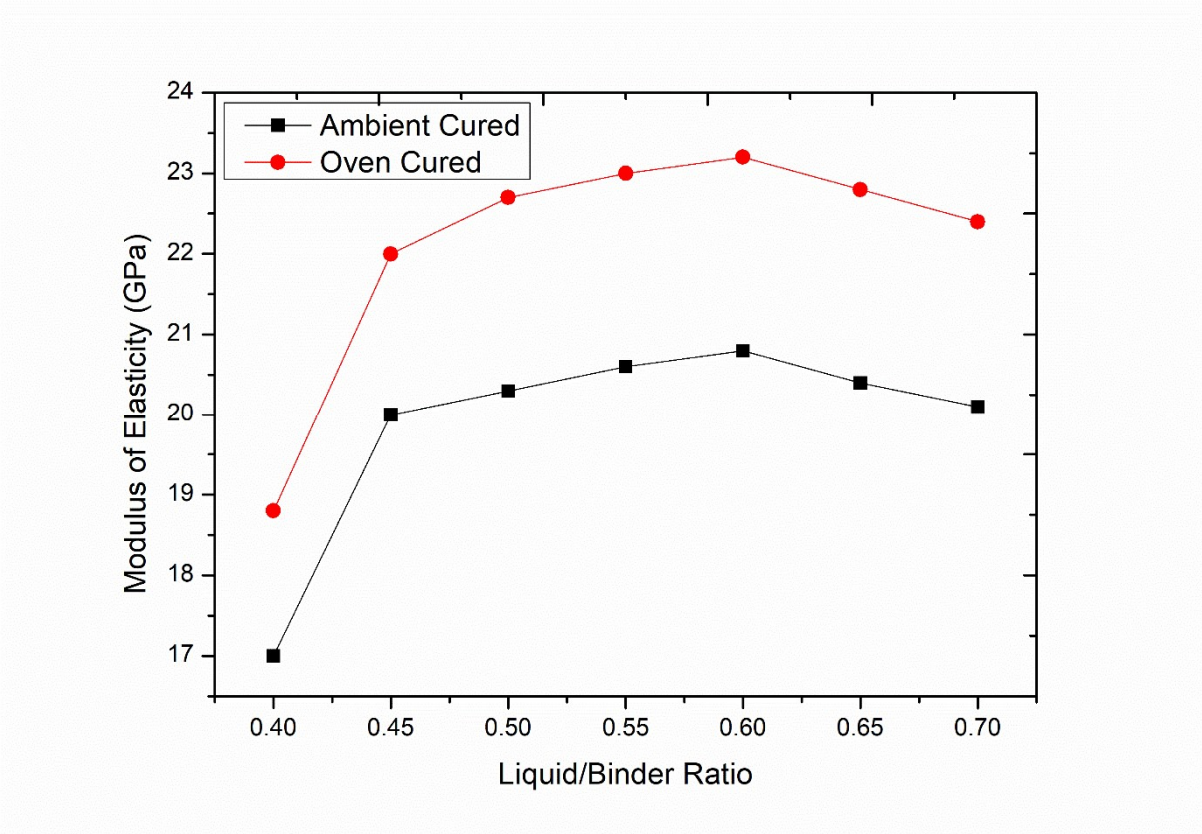

Fig. 4.26 Graph between the MOE and liquid/binder ratio

4.3 Effect of Superplasticiser Dosage Percentage

4.3.1 Slump and Compaction factor

In the experimental investigation, workability was examined by the slump test and the compaction factor in the laboratory. The slump value increases with the increment of superplasticiser content in the mix design, so the slump value increases consecutively with the increase of the superplasticiser content in mixes of GPC. Similarly, the compaction factor value also increases with the increment of the superplasticiser content. Fig. 4.27 describes the effect of the liquid-to-binder ratio on both slump value and compaction factor on the fresh mix of GPC.

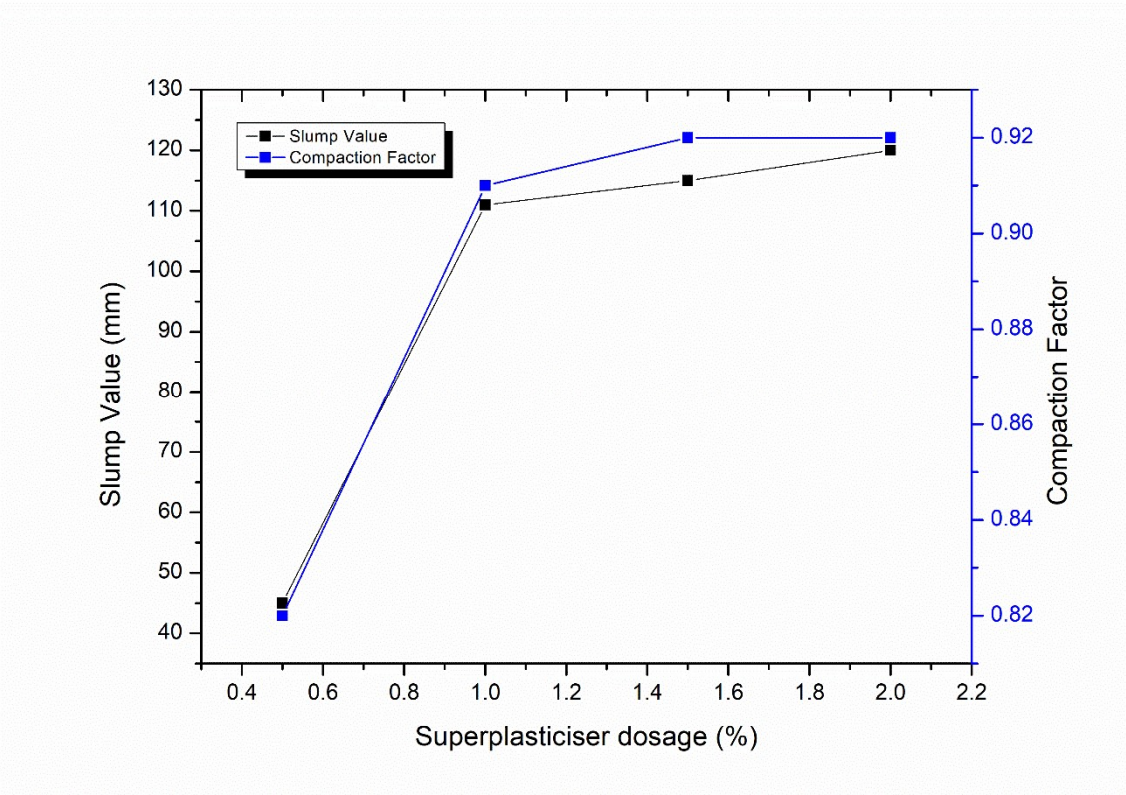

Fig. 4.27 Graph between the slump, compaction factor, and superplasticizer dosage of GPC

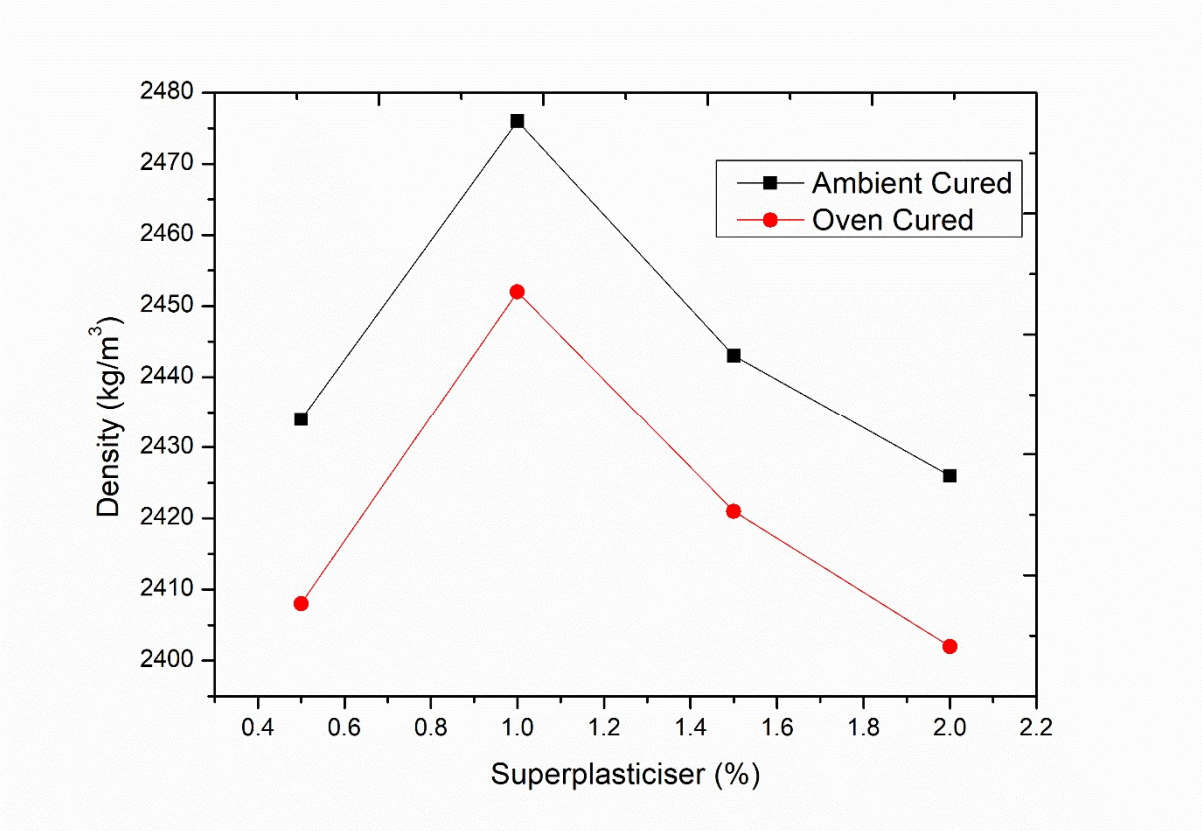

Fig. 4.28 Graph between density and superplasticizer dosage of GPC

4.3.1 Density

The mix's density is measured through the weight of specimens before the destructive test of cube samples. The ambient-cured specimens had higher density compared to the oven-cured samples. The specimens' density increases from 0.5% to 1%, then decreases gradually with increases in the superplasticizer content in the GPC mix design. The 1% superplasticiser content mix design got the optimum point of density in both cured samples. The superplasticiser content mix of ambient cured got the highest, at 2476kg/m3 of all mixes of GPC. Fig. 4.28 describes the relationship between the density of the mix and superplasticizer dosage in the mixes for both curing conditions.

4.3.2 Compressive strength

The compressive strength of the mix results is determined through the testing of cube samples in the UTM machine at 7, 14, 28, 42, and 56 days after the casting. The oven-cured samples' compressive strength is higher than the ambient-cured samples of the same mix of GPC. In the GPC mixes, Superplasticisers 1% dosage got a higher strength than the other mixes with different percentage dosages. The superplasticiser dosage varies from 0.5%-2.0% in the GPC mix design to check the effect of dosage variation in the compressive strength of the mix. The compressive strength increases with the increment of superplasticiser dosage from 0.5% to 2.0%, but after the increment of dosage reduces the compressive strength of GPC mix specimens in both curing conditions. The maximum compressive strength of ambient-cured and oven-cured specimens is 24.4 MPa and 33.2 MPa, respectively, 56 days after the casting. The compressive strength of mixes got 95% strength at 28 days in both curing conditions, but the oven-cured specimens' initial seven days is higher than ambient-cured specimens of the same mix.

Table 4.23 Compressive strength of ambient-cured

Superplasticiser (%)	7 days	14 days	28 days	42 days	56 days
0.5	14.1	17.8	21.0	23.0	23.2
1.0	14.6	18.2	22.0	24.0	24.4
1.5	14.2	17.9	21.2	23.4	23.5
2.0	13.0	16.4	19.5	20.1	20.3

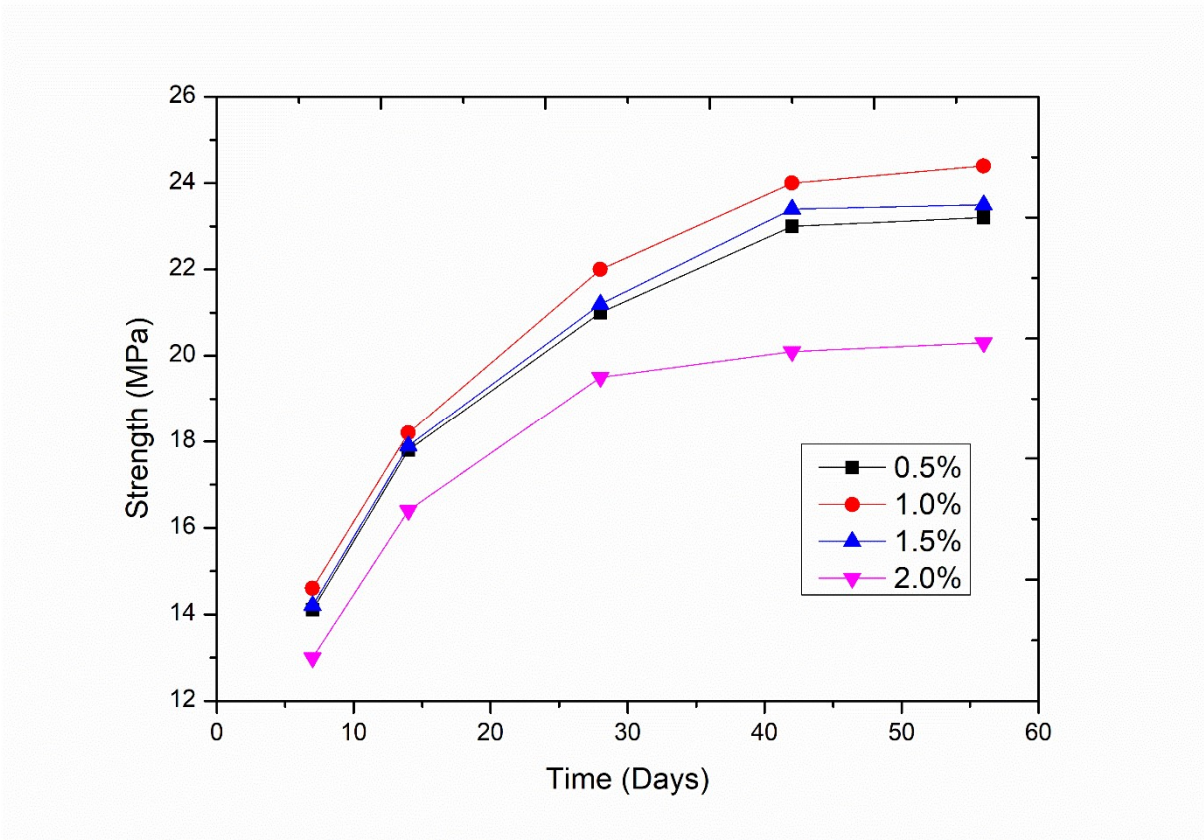

Fig. 4.29 Compressive strength of ambient-cured GPC

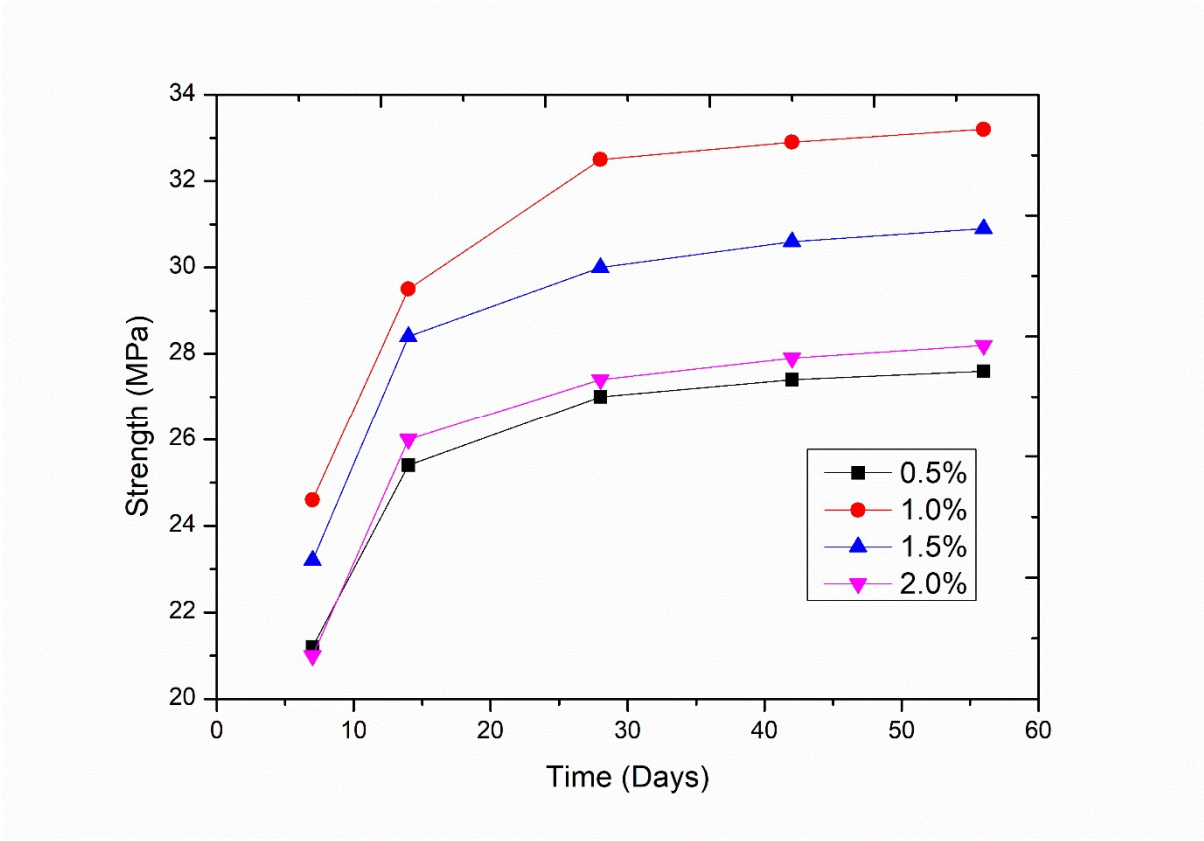

Fig. 4.30 Compressive strength of oven-cured GPC

Table 4.24 Compressive strength of oven-cured GPC

Superplasticiser (%)	7 days	14 days	28 days	42 days	56 days
0.5	21.2	25.4	27.0	27.4	27.6
1.0	24.6	29.5	32.5	32.9	33.2
1.5	23.2	28.4	30.0	30.6	30.9
2.0	21.0	26.0	27.4	27.9	28.2

4.3.3 Splitting Tensile Strength

The splitting tensile strength is measured through the destructive test of the cylinder specimens in the UTM machine by giving static load along the transverse direction on the samples. The oven-cured samples' splitting strength is higher than the ambient-cured samples of the same mix of GPC. In the GPC mixes, Superplasticisers 1% dosage got a higher strength than the other mixes with different dosages. Fig. 4.31 and Fig. 4.32 show the splitting strength of the various design mixes. Fig. 4.31 shows the ambient cured specimens strength, and Fig. 4.32 shows the oven-cured specimens of GPC. In both curing conditions, the 1% superplasticiser content mix got optimum strength. The variation in the splitting strength is similar to the compressive strength of the mix. The maximum splitting tensile of ambient-cured and oven-cured specimens is 3.5MPa and 5.0MPa, respectively, at 56 days after casting. The splitting tensile of ambient-cured specimens is 2.4MPa, 3.5MPa, 3.1MPa, and 2.6MPa, respectively, at 56 days after the test, whereas oven-cured specimens are 3.5MPa, 5.0MPa, 4.5MPa, and 3.9MPa, respectively, at 56 days after the casting.

Table 4.25 Splitting tensile of ambient-cured GPC

Superplasticiser (%)	7 days	14 days	28 days	42 days	56 days
0.5	1.2	1.7	2.2	2.3	2.4
1.0	1.7	2.3	3.1	3.3	3.5
1.5	1.6	2.1	2.8	3.0	3.1
2.0	1.2	1.8	2.4	2.5	2.6

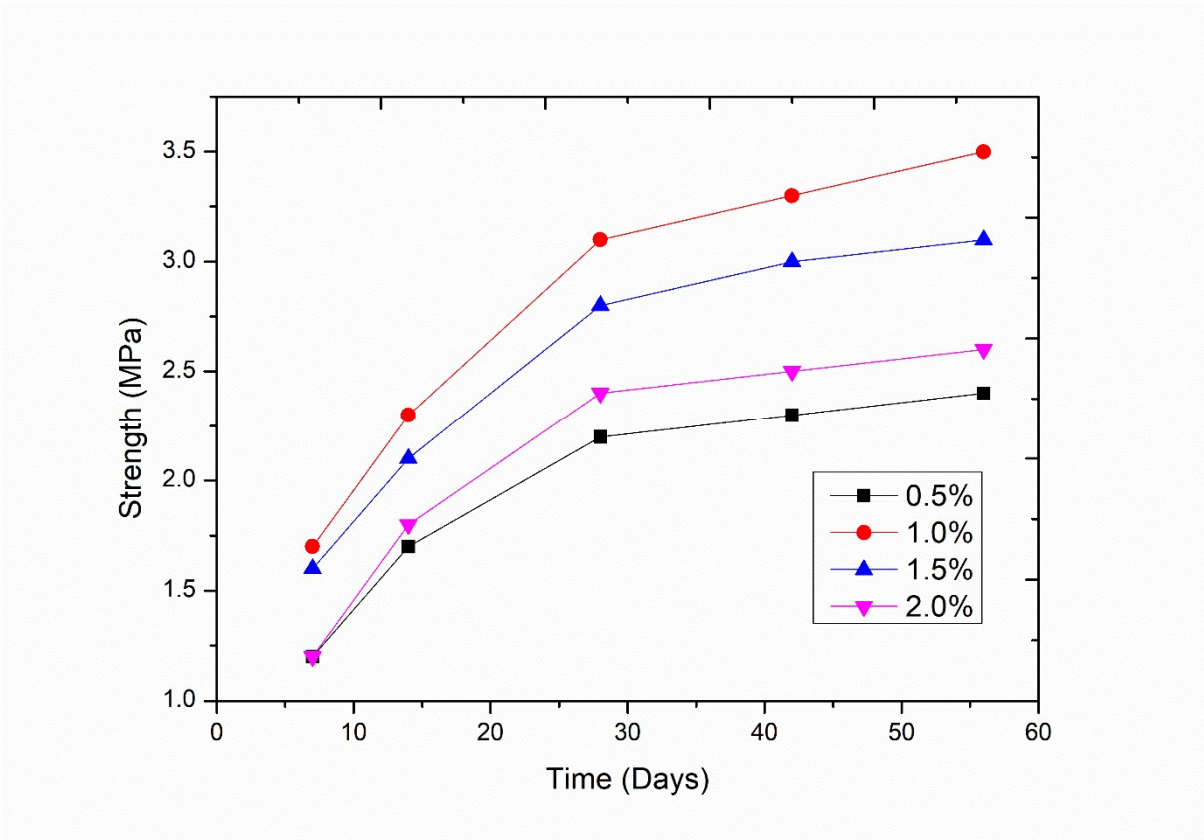

Fig. 4.31 Splitting tensile of ambient-cured GPC

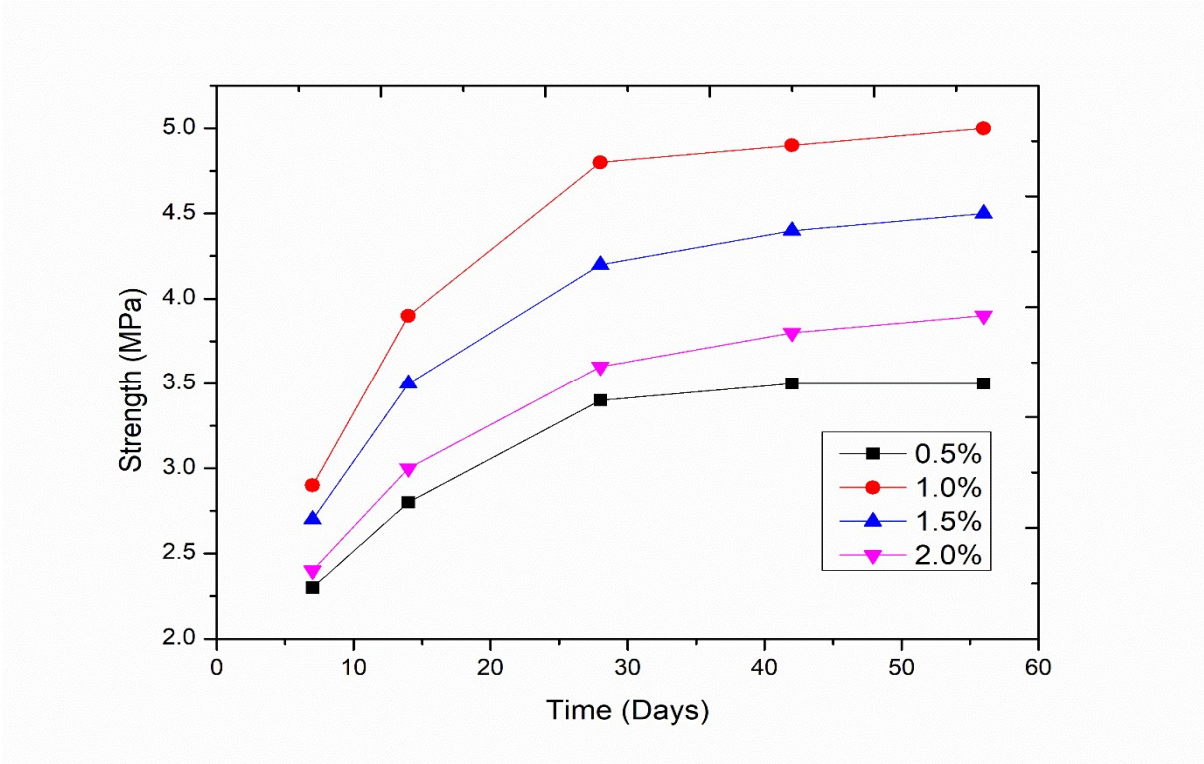

Fig. 4.32 Splitting tensile of oven-cured GPC

Table 4.26 Splitting tensile of oven-cured

Superplasticiser (%)	7 days	14 days	28 days	42 days	56 days
0.5	2.3	2.8	3.4	3.5	3.5
1.0	2.9	3.9	4.8	4.9	5.0
1.5	2.7	3.5	4.2	4.4	4.5
2.0	2.4	3.0	3.6	3.8	3.9

4.3.4 Flexural Strength

The flexural strength is measured through the destructive test of the beam specimens in the flexure testing machine by giving statical load and the two-point load on the samples. The oven-cured samples' flexural strength is higher than the ambient-cured samples of the same mix of GPC. In the GPC mixes, Superplasticiser 1% dosage got a higher strength than the other mixes with various dosages. Fig. 4.33 and Fig. 4.34 show the flexural strength of the various design mixes. Fig. 4.33 shows the ambient-cured specimen strength, and Fig. 4.34 shows the oven-cured specimens of the GPC. In both curing conditions, the 1% superplasticiser content mix got the optimum strength. The flexural strength shows the bending properties or indirect tensile strength of the concrete mix samples. It's about 15%-20% of the compressive strength of the mix. The maximum flexural strength of mixes with superplasticiser dosage of 0.5%, 1.0%, 1.5% and 2.0% is 2.7MPa, 3.7MPa, 3.4MPa, and 3.0MPa, respectively, of ambient-cured specimens, whereas 4.3MPa, 5.4MPa, 5.0MPa, and 4.6MPa, respectively, of oven-cured specimens at 56 days after casting.

Table 4.27 Flexural strength of ambient-cured

Superplasticiser (%)	7 days	14 days	28 days	42 days	56 days
0.5	1.4	1.8	2.5	2.6	2.7
1.0	1.9	2.6	3.4	3.6	3.7
1.5	1.8	2.4	3.1	3.3	3.4
2.0	1.4	1.9	2.7	2.9	3.0

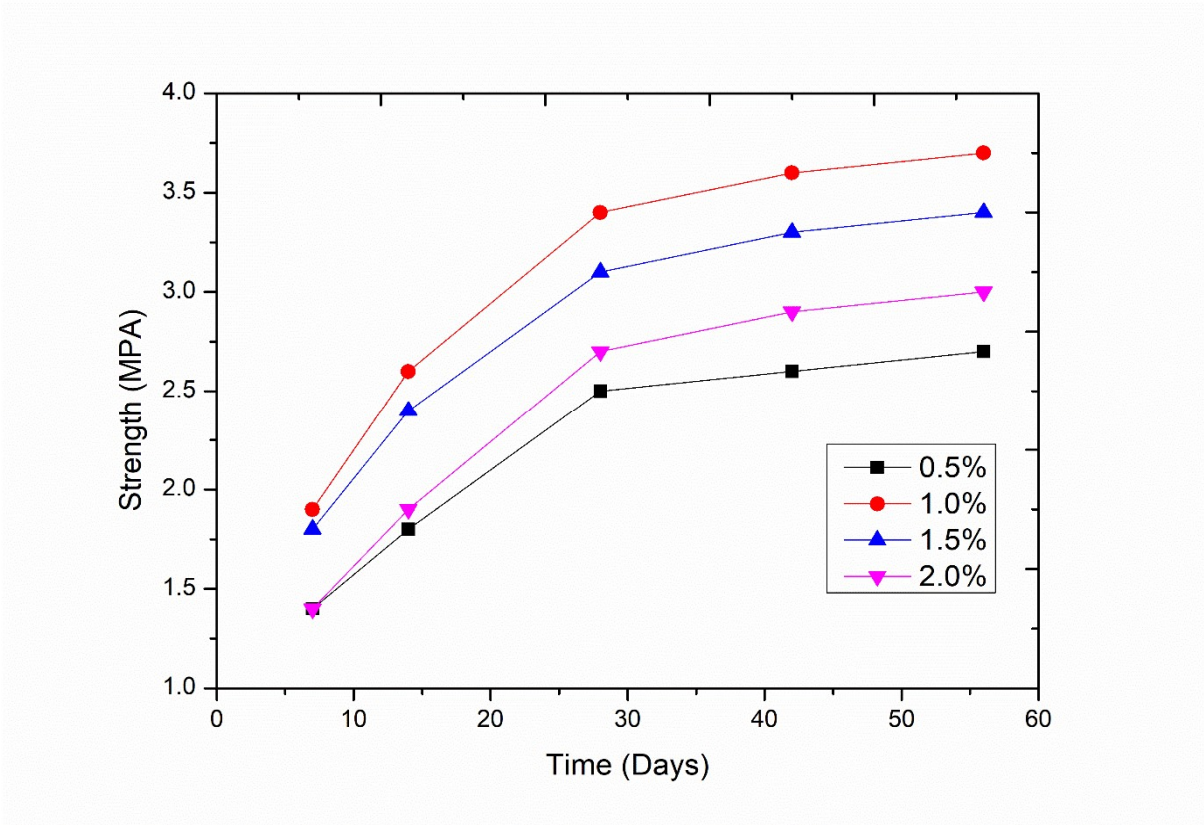

Fig. 4.33 Flexural strength variations with superplasticizer dosage of ambient-cured GPC

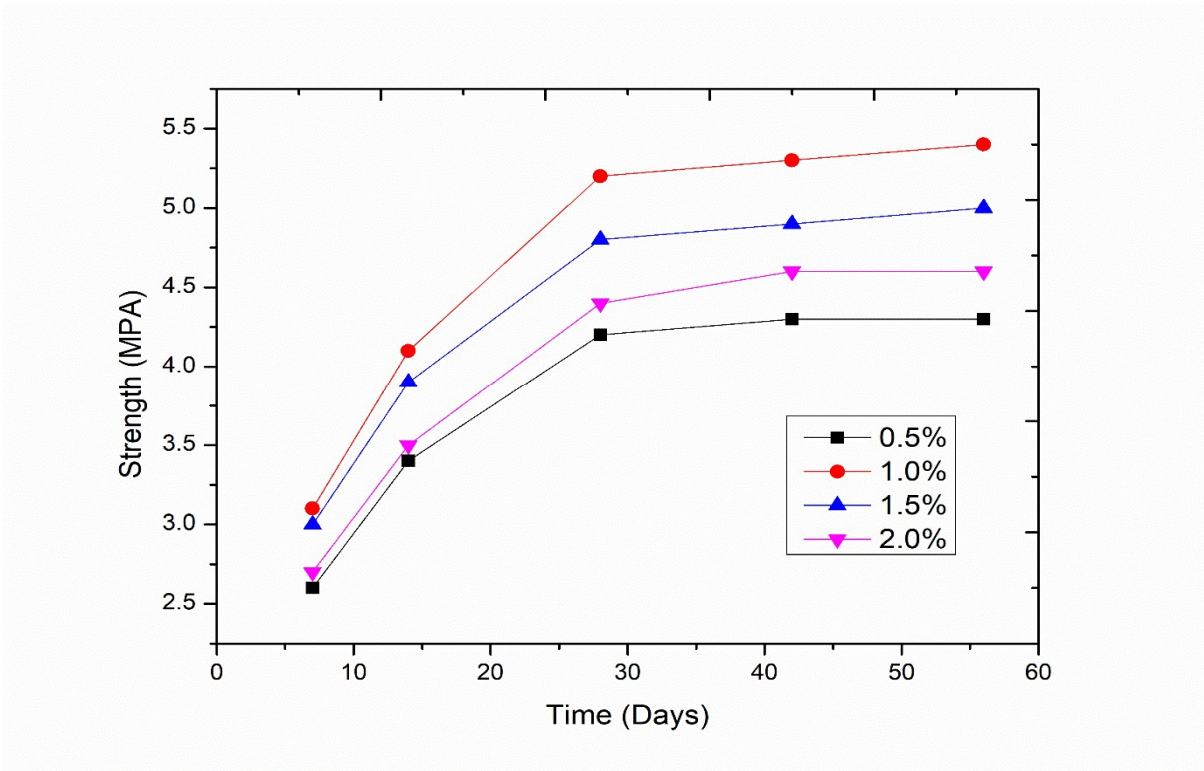

Fig. 4.34 Flexural strength variations with superplasticizer dosage of oven-cured GPC

Table 4.28 Flexural strength of oven-cured

Superplasticiser (%)	7 days	14 days	28 days	42 days	56 days
0.5	2.6	3.4	4.2	4.3	4.3
1.0	3.1	4.1	5.2	5.3	5.4
1.5	3.0	3.9	4.8	4.9	5.0
2.0	2.7	3.5	4.4	4.6	4.6

4.3.5 Rebound strength

The rebound test is a non-destructive experiment for the specimens. All mixed specimens of both cured conditions were tested for rebound strength at 7, 14, 28, 42, and 56 days after casting and before the destructive test on the samples. The oven-cured samples' rebound strength is higher than the ambient-cured samples of the same mix of GPC. In the GPC mixes, Superplasticizer 1% dosage got a higher strength than the other mixes with various dosages. Fig. 4.35 and Fig. 4.36 show the rebound strength graph with the time variation of both curing conditions. Fig. 4.35 shows the ambient-cured specimens strength, and Fig. 4.36 shows the oven-cured specimens of the GPC. The 1% superplasticiser content mix got the optimum strength in both curing conditions. The rebound strength is slightly higher than the destructive compressive strength but does not exceed the IS code's limit. The rebound strength is based on the surface hardness of the specimens.

Table 4.29 Rebound strength of ambient-cured

Superplasticiser (%)	7 days	14 days	28 days	42 days	56 days
0.5	14.8	17.2	19.5	21.0	21.4
1.0	16.7	20.0	24.4	26.9	28.5
1.5	16.0	18.7	21.6	24.4	25.4
2.0	15.0	17.4	19.7	21.2	22.0

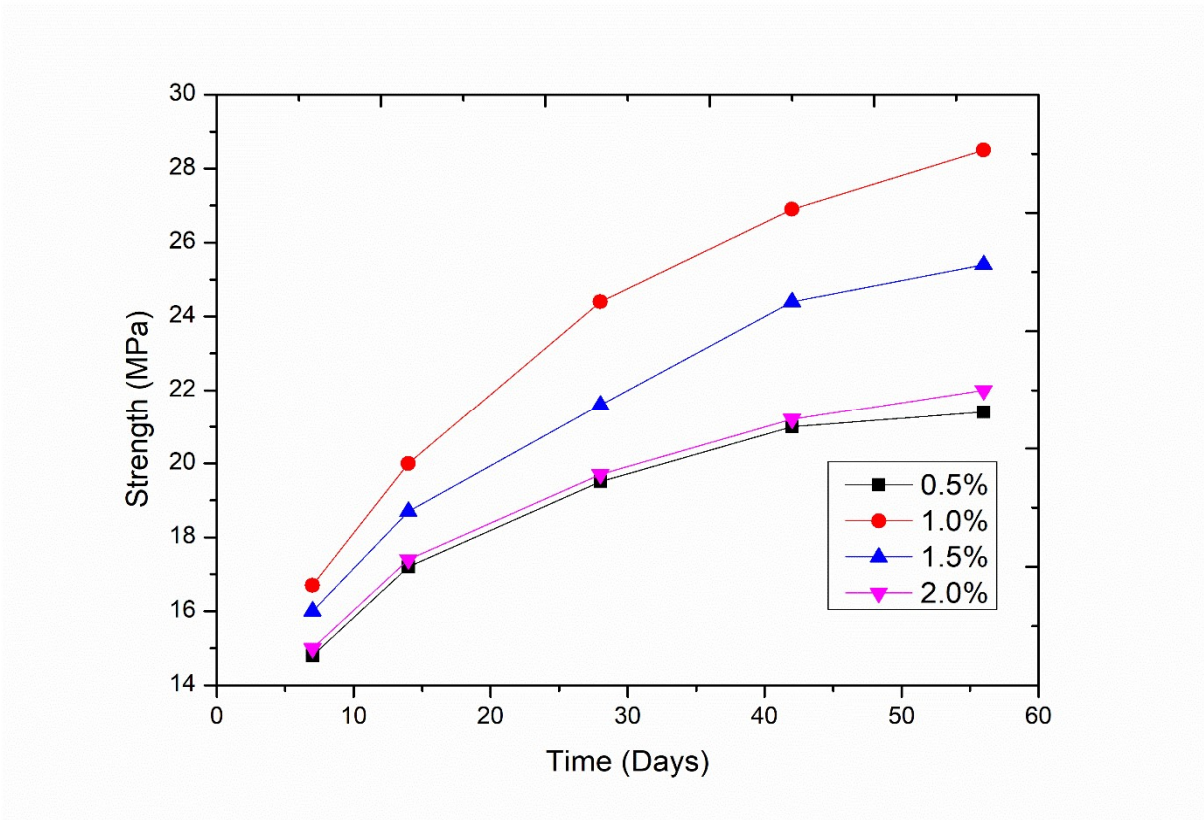

Fig. 4.35 Rebund strength variations with superplasticizer dosage of ambient-cured GPC

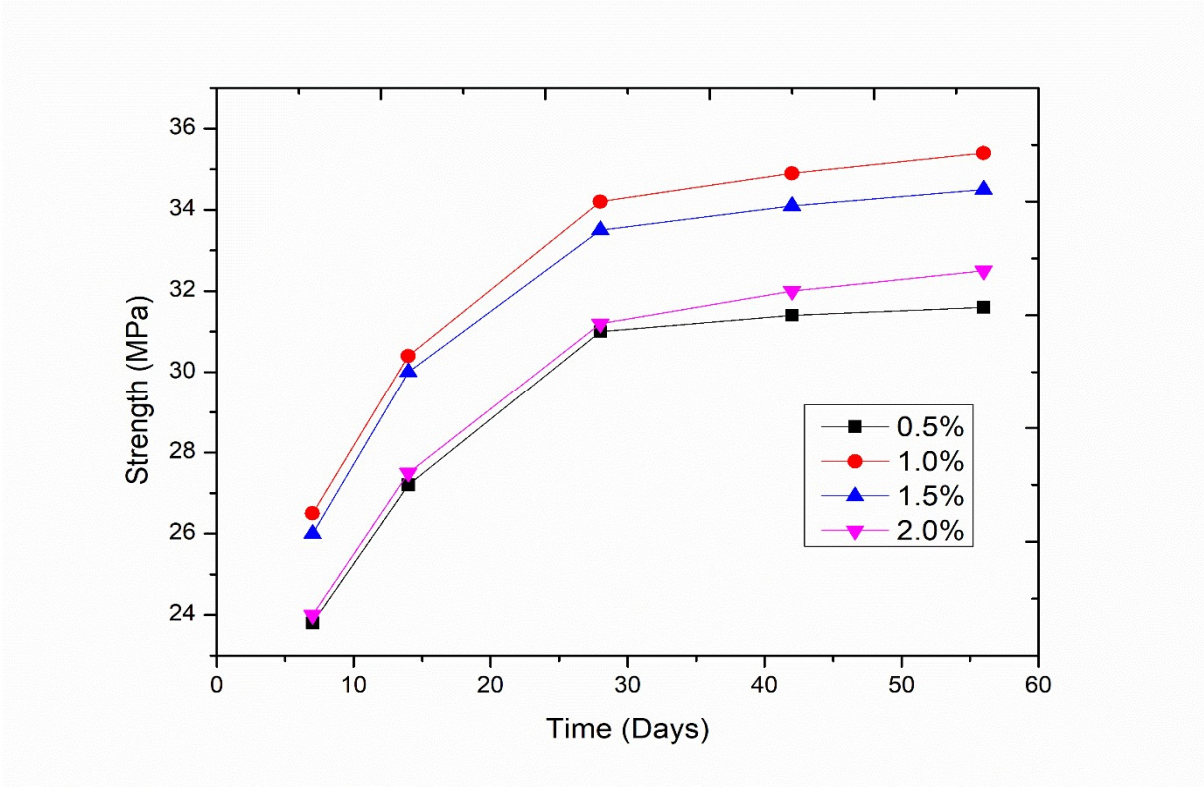

Fig. 4.36 Rebound strength variations with superplasticizer dosage of oven-cured GPC

Table 4.30 Rebound strength of oven-cured

Superplasticiser (%)	7 days	14days	28 days	42 days	56 days
0.5	23.8	27.2	31.0	31.4	31.6
1.0	26.5	30.4	34.2	34.9	35.4
1.5	26.0	30.0	33.5	34.1	34.5
2.0	24.0	27.5	31.2	32.0	32.5

4.3.6 UPVT(Ultrasonic Pulse Velocity Test)

The UPV test uses the quality of the hard material by quantifying the time passage from the specimens. It is a non-destructive test to evaluate concrete strength without destruction. The UPV tests are conducted on cube samples at 7 days, 14 days, 28 days, 42 days, and 56 days after the casting and before the destructive tests conducted on the samples. The apparatus records the time duration of the UPV wave and calculates the velocity that defines the quality of GPC samples. When the time passage of the UPV wave is high, it shows less strength and vice-versa [155]. The 1% superplasticiser content mix shows a higher velocity than the other mixes, and it shows the superplasticiser dosage of 1% of binder gives the optimum point strength in both curing conditions. Fig. 37 and Fig. 4.38 describe the graph of UPV of various mixes in the same graph, in which Fig. 4.37 shows the ambient-cured results and Fig. 4.38 shows the oven-cured GPC samples. The maximum velocity of oven-cured specimens and ambient-cured specimens is 4.27km/sec and 2.41km/sec, respectively, at 56 days of testing.

Table 4.31 UPV of ambient-cured

Superplasticiser (%)	7 days	14 days	28 days	42 days	56 days
0.5	1.8	1.96	2.19	2.35	2.38
1.0	1.86	1.97	2.24	2.36	2.41
1.5	1.82	1.94	2.18	2.26	2.32
2.0	1.79	1.91	2.01	2.12	2.14

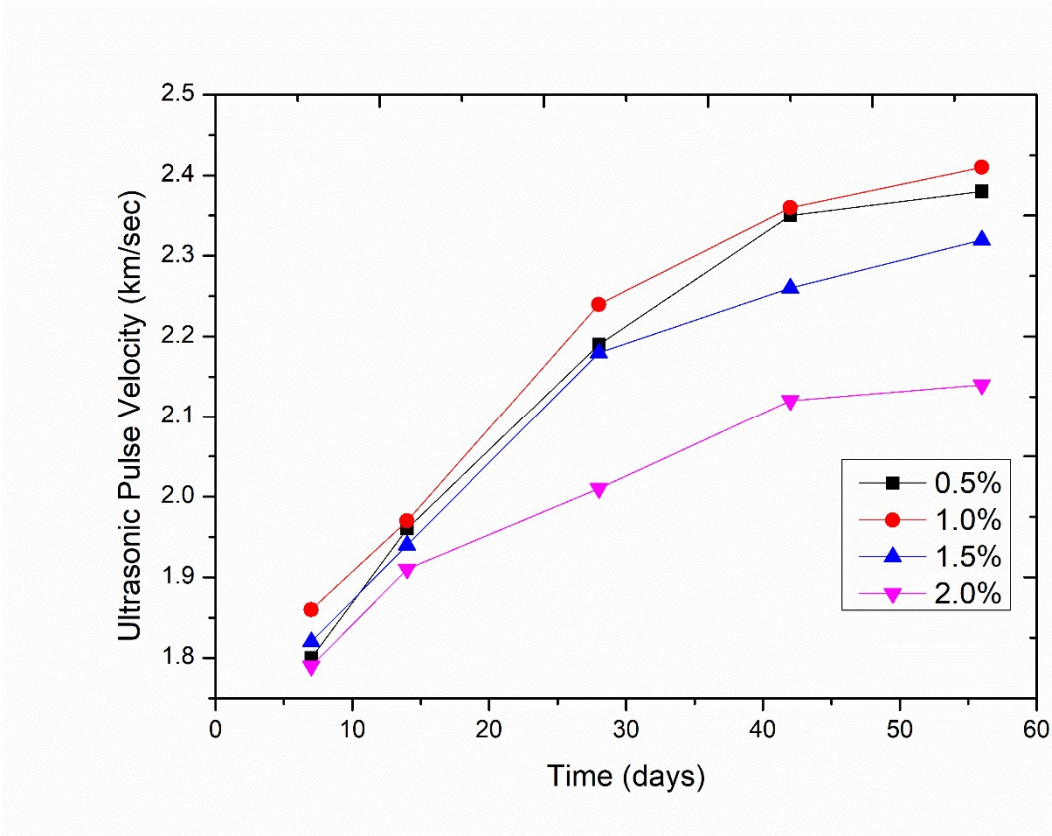

Fig. 4.37 UPV varaitions with superplasticiser dosage of ambient-cured GPC

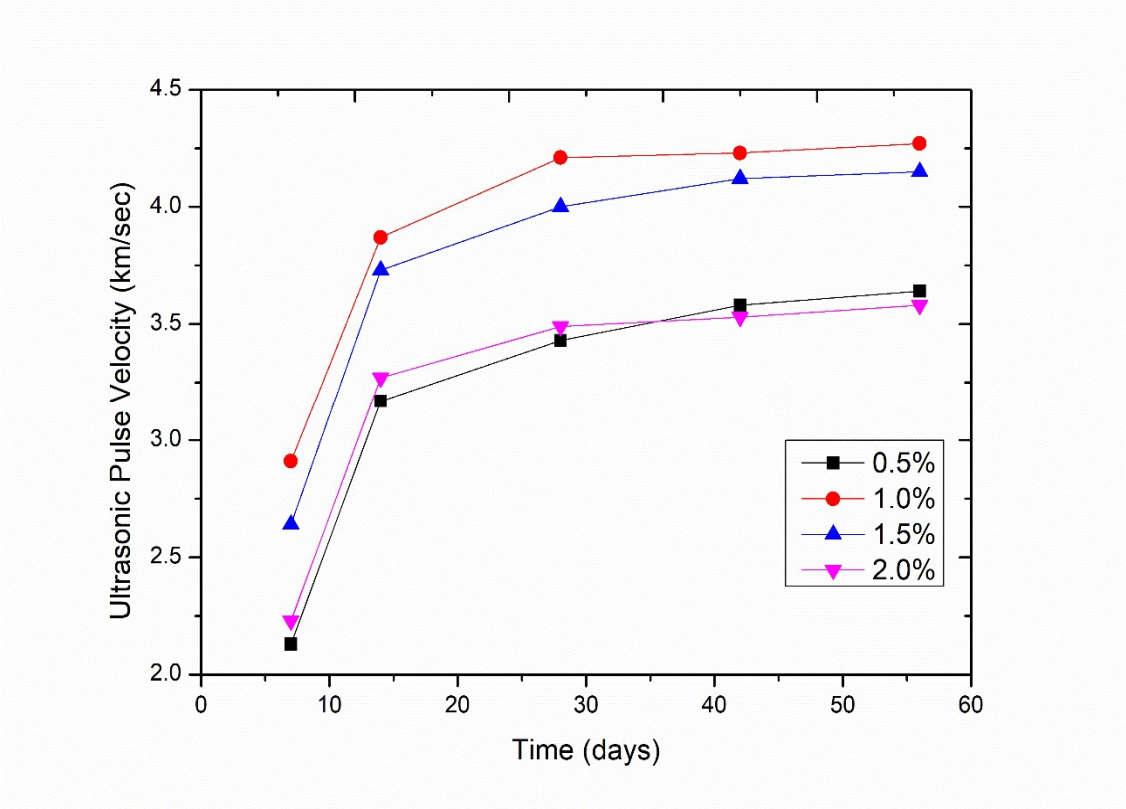

Fig. 4.38 UPV variations with superplasticizer dosage of oven-cured GPC

Table 4.32 UPV of oven-cured

Superplasticiser (%)	7 days	14 days	28 days	42 days	56 days
0.5	2.13	3.17	3.43	3.58	3.64
1.0	2.91	3.87	4.21	4.23	4.27
1.5	2.64	3.73	4	4.12	4.15
2.0	2.23	3.27	3.49	3.53	3.58

4.3.7 Poisson Ratio and Modulus of Elasticity

The modulus of elasticity of the mix design samples was obtained by the static load applied on the cylinder specimen along the longitudinal axis and measured the sample's deflection in vertical and horizontal directions. Stress is concluded by the load applied to the specimen to the surface area of the specimen. Poisson ratio was also measured through this test by the ratio of lateral strain to the linear strain of the samples. The 1% superplasticiser content mix specimens had a higher modulus of elasticity than the other mix designs. The oven-cured specimens got a higher MOE compared to the ambient-cured specimens. The optimum point of the MOE of the ambient-cured and oven-cured specimens is 21.4MPa and 21.9MPa, respectively. Table 4.33 describes the relationship between the MOE and superplasticizer dosage percentage in both curing conditions.

Table 4.33 Poissons ratio, density, and MOE of GPC

Superplasticiser (%)	Slump Value (mm)	Compaction factor	Density in Kg/m^3		Poissons Ratio		Modulus of Elasticity (GPa)	
			Ambient Cured	Oven Cured	Ambient Cured	Oven Cured	Ambient Cured	Oven Cured
0.5	45	0.82	2434	2408	.16	.15	20.5	20.9
1.0	111	0.91	2476	2452	.14	.14	21.4	21.9
1.5	115	0.92	2443	2421	.15	.15	21.0	21.6
2.0	120	0.92	2426	2402	.15	.15	20.7	21.0

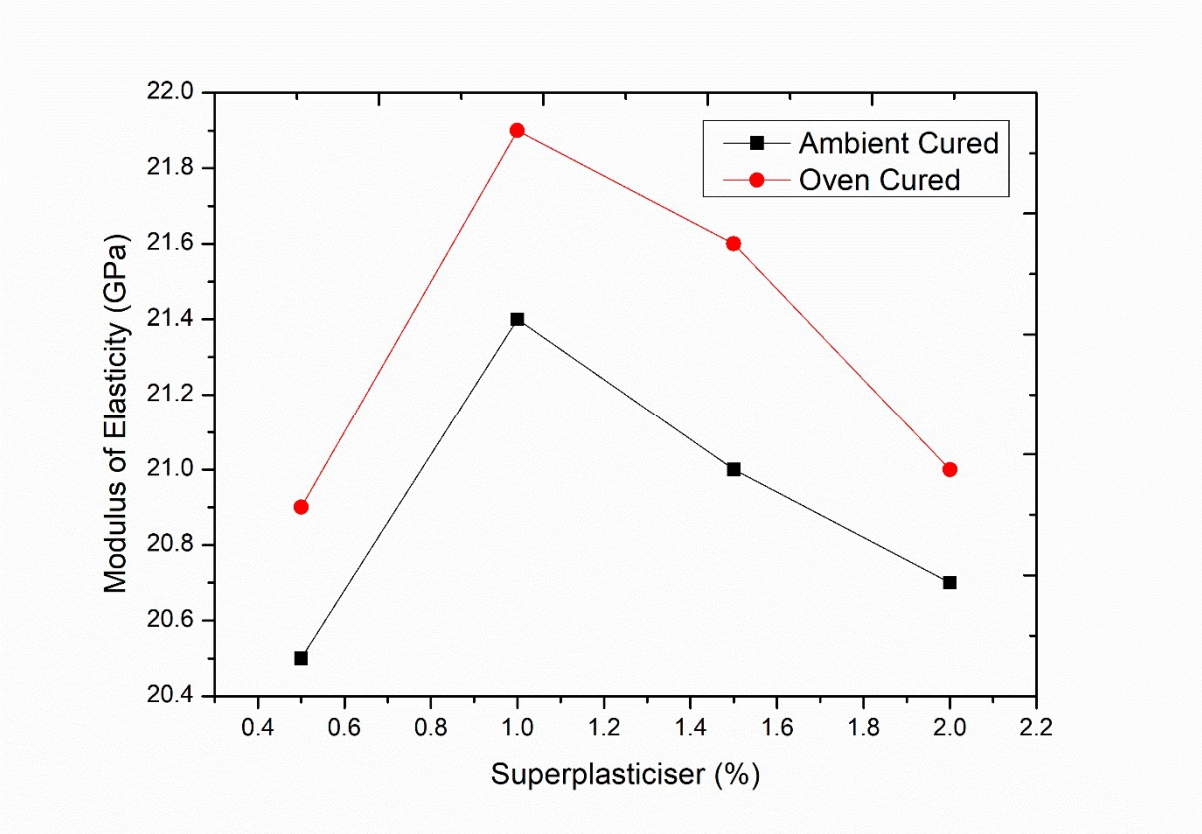

Fig. 4.39 MOE variations with superplasticiser dosage of both cured GPC

4.4 Effect of Molarity of Sodium Hydroxide

Sodium hydroxide works as a binder (Flyash and GGBFS) activator in the mix designs of geopolymer concrete. The changes in the molar concentration of NaOH directly affect the mix design of the GPC. Analysis of the molarity of NaOH's Mix designs of the GPC by varying 8M-16M and examining the specimens' test results of all design mixes by the destructive strength test and non-destructive rebound strength test.

4.4.1 Slump and Compaction

The slump value decreases with the increment of molarity in the mix design, so the slump value decreases consecutively with the increase of the molarity of NaOH in mixes of GPC. Similarly, the compaction factor value also decreases with the increment of the molarity. Fig. 4.40 describes the effect of the molarity of NaOH on both slump value and compaction factor on the fresh mix of GPC.

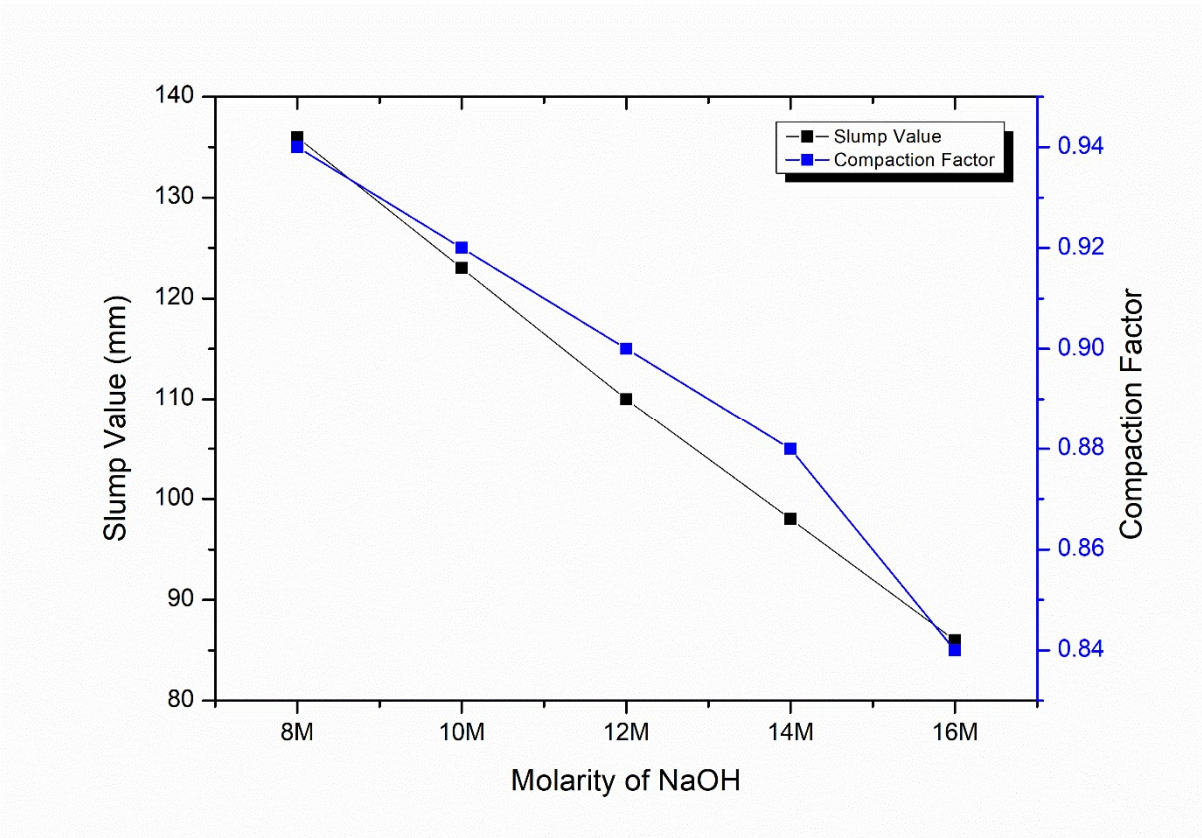

Fig. 4.40 Slump and compaction factor variation with a molarity of sodium hydroxide of GPC

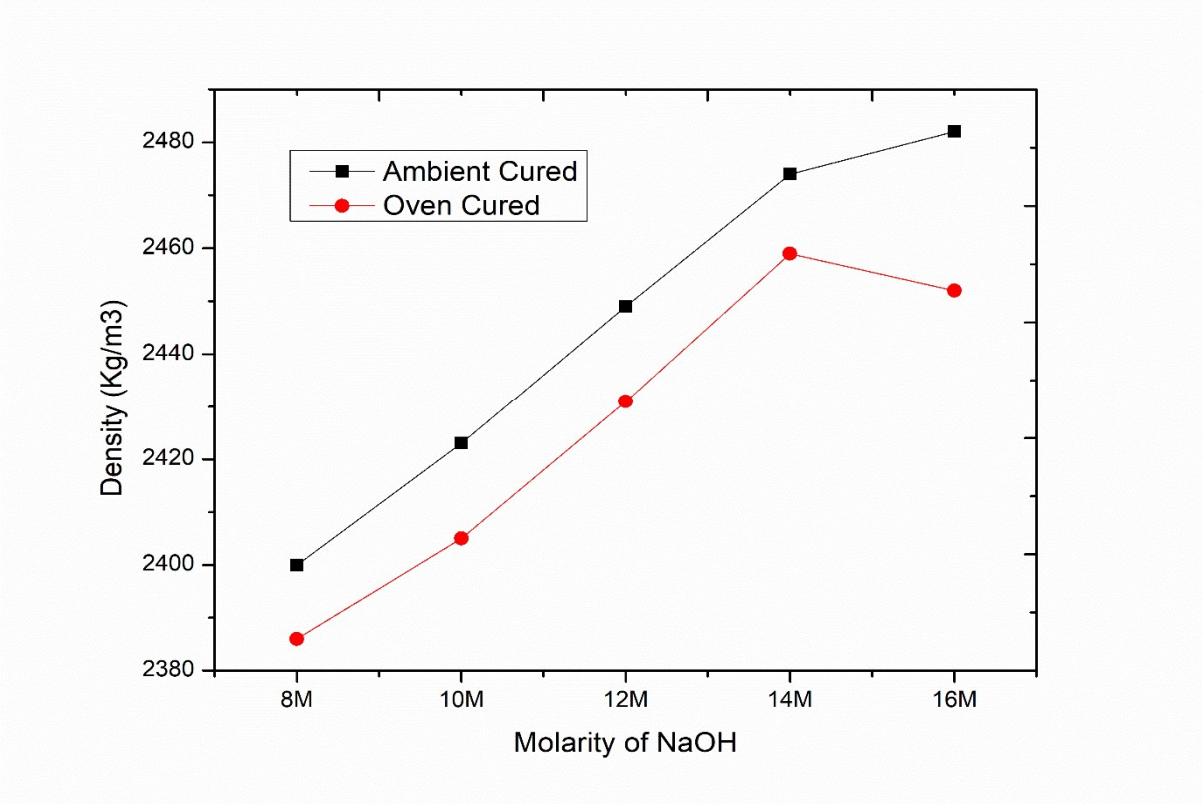

Fig. 4.41 Density variations with the molarity of sodium hydroxide of both cured GPC

4.4.1 Density

The mix's density is measured through the weight of specimens before the destructive test of cube samples. The ambient-cured specimens got higher density than the oven-cured samples, and the specimens' density increases continuously from 8M to 16M in the GPC mix design. The 14M mix design got the optimum density point in oven-cured samples, whereas 16M got the optimum point in ambient-cured specimens. The 16M mix of ambient cured got the highest weight of 2482kg/m^3 of all the mixes of GPC. Fig. 4.41 describes the relationship between the density of the mix and NaOH molarity in the mixes for both curing conditions.

4.4.2 Compressive Strength

The compressive strength of the GPC varies with the varying molarity of the NaOH and curing conditions. The compressive strength rises with the increment in the molarity of NaOH in the mix design but beyond an optimum point decreases the compressive strength in the oven-cured specimens. The highest compressive strength of the oven cured 14M mix is 34.2N/mm^2 at 56 days, but in the ambient cured specimen at 16M mix it is 25N/mm^2 at 56 days. Fig. 4.42 shows the compressive strength of ambient cured specimens, and Fig. 4.43 shows the compressive strength of oven cured specimens with the variation of the molarity of NaOH in the design mix of GPC. The highest compressive strength of design mixes of 8M, 10M, 12M, 14M and 16M are 13.9N/mm^2, 15.5N/mm^2, 21.8N/mm^2, 24.0N/mm^2 and 25.0N/mm^2 respectively at 56 days after ambient-curing but after oven-curing compressive strength of 8M, 10M, 12M, 14M and 16M are 23.2N/mm^2, 25.0N/mm^2, 27.9N/mm^2, 34.2N/mm^2 and 31.0N/mm^2 respectively at 56 days.

Table 4.34 Compressive strength of ambient-cured

Molar Concentration	7 days	14 days	28 days	42 days	56 days
8M	5.6	7.6	11.0	12.3	13.9
10M	6.4	10.6	13.6	14.9	15.5
12M	7.6	14.6	19.1	20.9	21.8
14M	12.4	18.4	22.6	23.4	24.0
16M	13.2	20.8	24.4	24.8	25.0

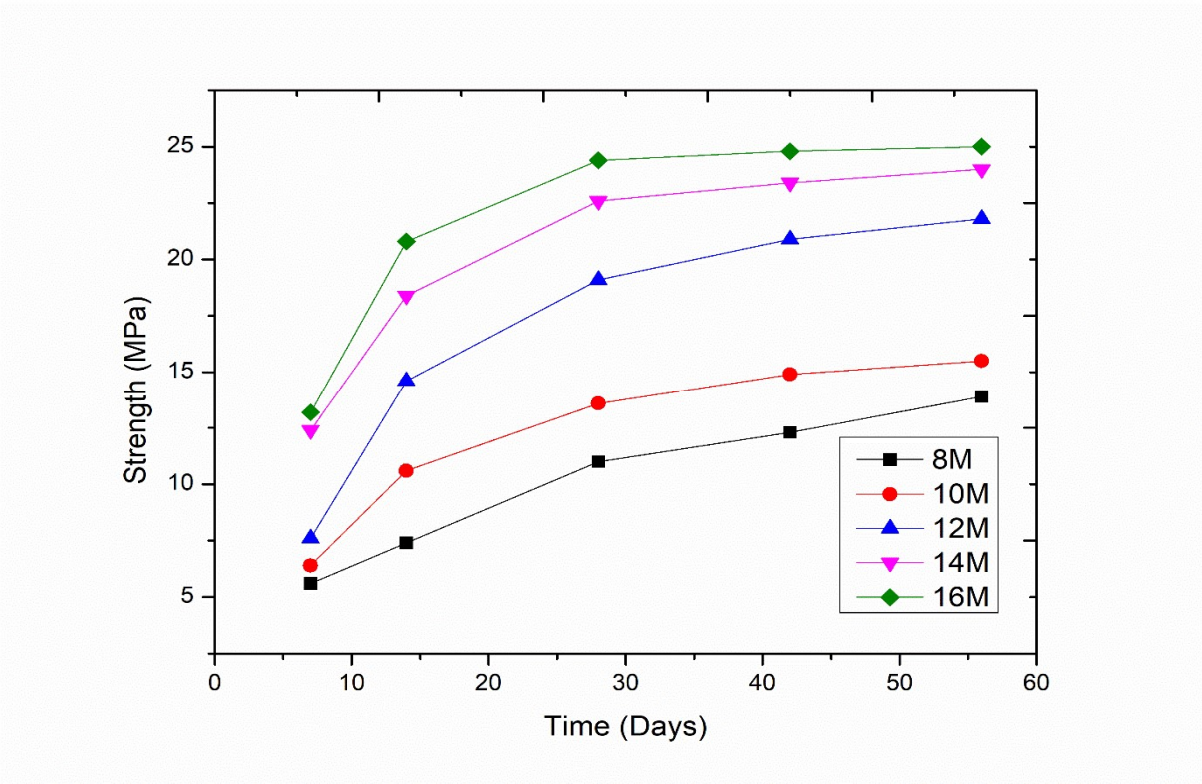

Fig. 4.42 Compressive strength variations with the molarity of sodium hydroxide of ambient-cured GPC

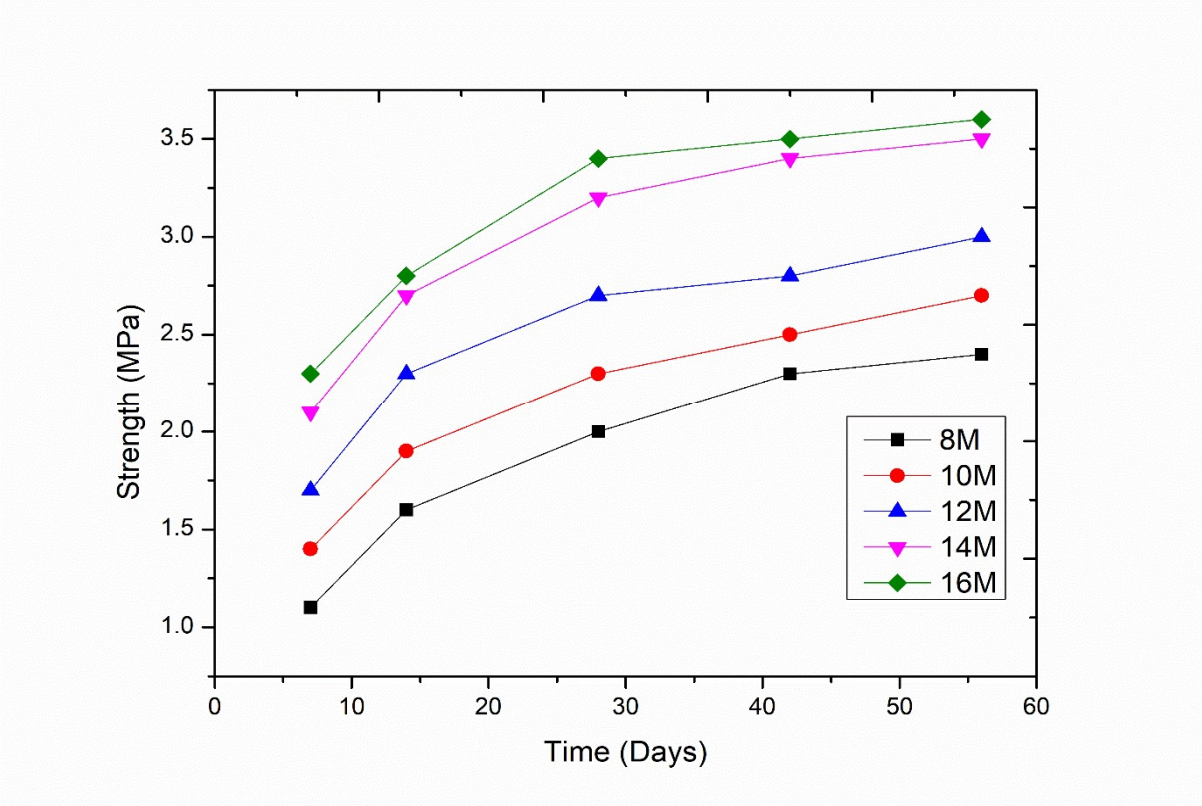

Fig. 4.43 Compressive strength variations with the molarity of sodium hydroxide of oven-cured GPC

Table 4.35 Compressive strength of oven-cured

Molar Concentration	7 days	14 days	28 days	42 days	56 days
8M	18.2	20.8	22.4	22.9	23.2
10M	20.6	22.9	24.5	24.8	25.0
12M	23.2	25.7	27.2	27.6	27.9
14M	26.4	29.6	33.2	33.8	34.2
16M	27.5	28.9	30.2	30.8	31.0

4.4.3 Splitting strength

The splitting tensile strength test is used to find the indirect tensile strength of the design mix of the GPC. Fig. 4.44 shows the splitting strength of ambient-cured specimens of mix designs, and Fig. 4.45 shows the splitting strength of the mix designs' oven-cured samples, which varies the molarity of NaOH in the mix design of GPC from 8M-16M. In the ambient cured specimens, 16M got the highest splitting tensile strength of 3.6 N/mm2 at 56 days, but in oven-cured samples, 14M got the most upper splitting tensile strength of 5.2 N/mm^2 at 56 days. The highest splitting tensile strength of 8M, 10M, 12M, 14M and 16M are 2.4N/mm^2, 2.7N/mm^2, 3.0N/mm^2, 3.5N/mm^2 and 3.6N/mm^2 respectively at 56 days after ambient-curing but after oven-curing splitting tensile strength of 8M, 10M, 12M, 14M and 16M are 3.4N/mm^2, 3.8N/mm^2, 4.4N/mm^2, 5.2N/mm^2 and 5.0N/mm^2 respectively at 56 days.

Table 4.36 Splitting tensile of ambient-cured

Molar Concentration	7 days	14 days	28 days	42 days	56 days
8M	1.1	1.6	2.0	2.3	2.4
10M	1.4	1.9	2.3	2.5	2.7
12M	1.7	2.3	2.7	2.8	3.0
14M	2.1	2.7	3.2	3.4	3.5
16M	2.3	2.8	3.4	3.5	3.6

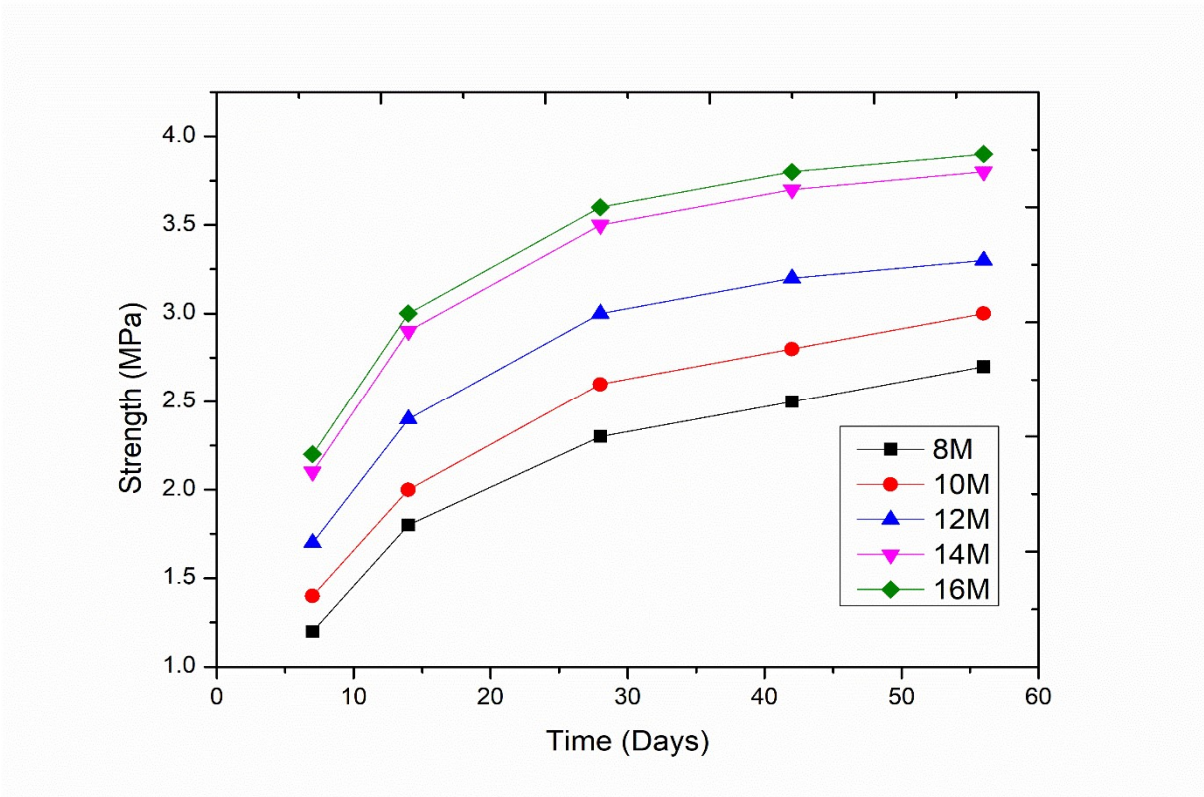

Fig. 4.44 Splitting tensile variations with the molarity of sodium hydroxide of ambient-cured GPC

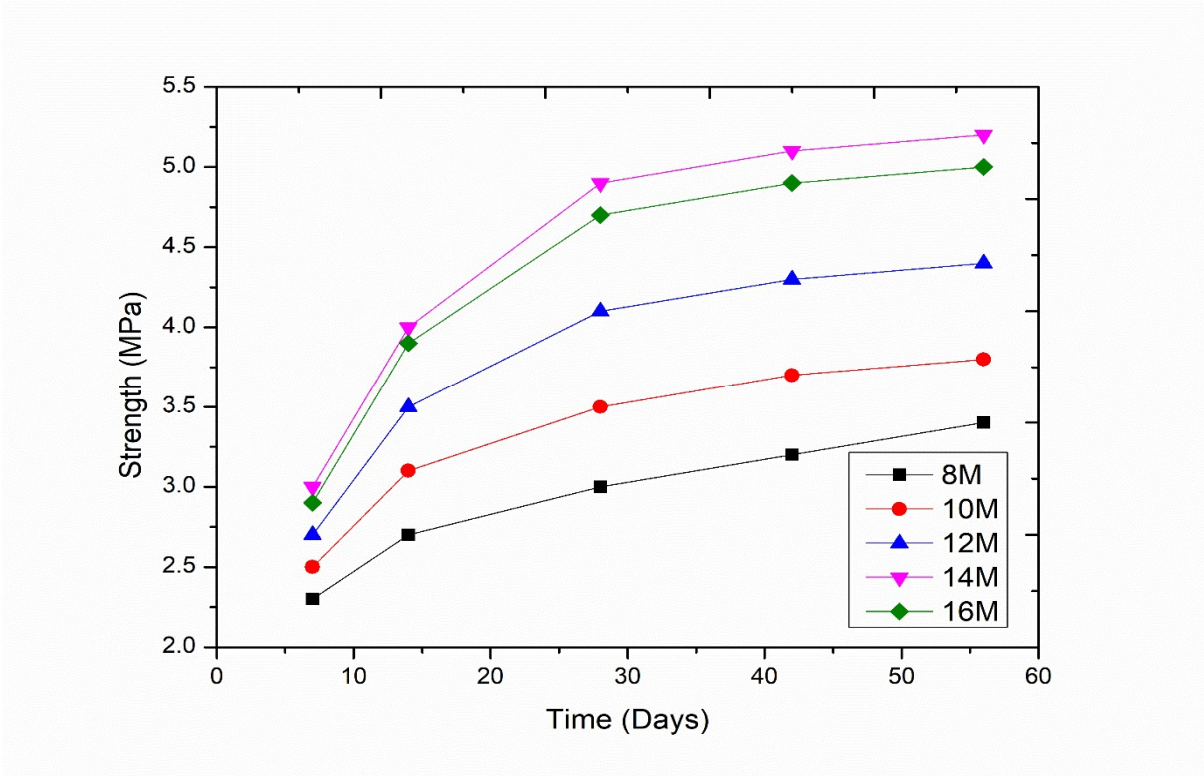

Fig. 4.45 Splitting tensile variations with the molarity of sodium hydroxide of oven-cured GPC

Table 4.37 Splitting tensile of oven-cured

Molar Concentration	7 days	14 days	28 days	42 days	56 days
8M	2.3	2.7	3.0	3.2	3.4
10M	2.5	3.1	3.5	3.7	3.8
12M	2.7	3.5	4.1	4.3	4.4
14M	3.0	4.0	4.9	5.1	5.2
16M	2.9	3.9	4.7	4.9	5.0

4.4.4 Flexural Strength

Flexural tensile strength is used to find the bending tension of the beam specimen. Fig. 4.46 and Fig. 4.47 shows the flexural tensile strength of mixed ambient cured samples and oven cured samples, respectively. Similarly, the oven-cured samples got more flexural tensile strength as compared to the ambient-cured specimens, the highest strength of oven-cured specimens of 14M mix is 5.4N/mm^2 at 56 days, but in ambient-cured specimens, the most upper strength of 16M mix is 3.9N/mm^2. In both curing conditions, the flexural tensile strength increases with the increment of the molarity of NaOH in mix design but in the oven-cured, strength decreases beyond the 14M NaOH in mixes. The highest flexural tensile strength of 8M, 10M, 12M, 14M and 16M are 2.7N/mm^2, 3.0N/mm^2, 3.3N/mm^2, 3.8N/mm^2 and 3.9N/mm^2 respectively at 56 days after ambient-curing but after oven-curing flexural tensile strength of 8M, 10M, 12M, 14M and 16M are 3.7 N/mm^2, 4.0 N/mm^2, 4.6 N/mm^2, 5.4 N/mm^2 and 5.3 N/mm^2 respectively at 56 days.

Table 4.38 Flexural strength of ambient-cured

Molar Concentration	7 days	14 days	28 days	42 days	56 days
8M	1.2	1.8	2.3	2.5	2.7
10M	1.4	2.0	2.6	2.8	3.0
12M	1.7	2.4	3.0	3.2	3.3
14M	2.1	2.9	3.5	3.7	3.8
16M	2.2	3.0	3.6	3.8	3.9

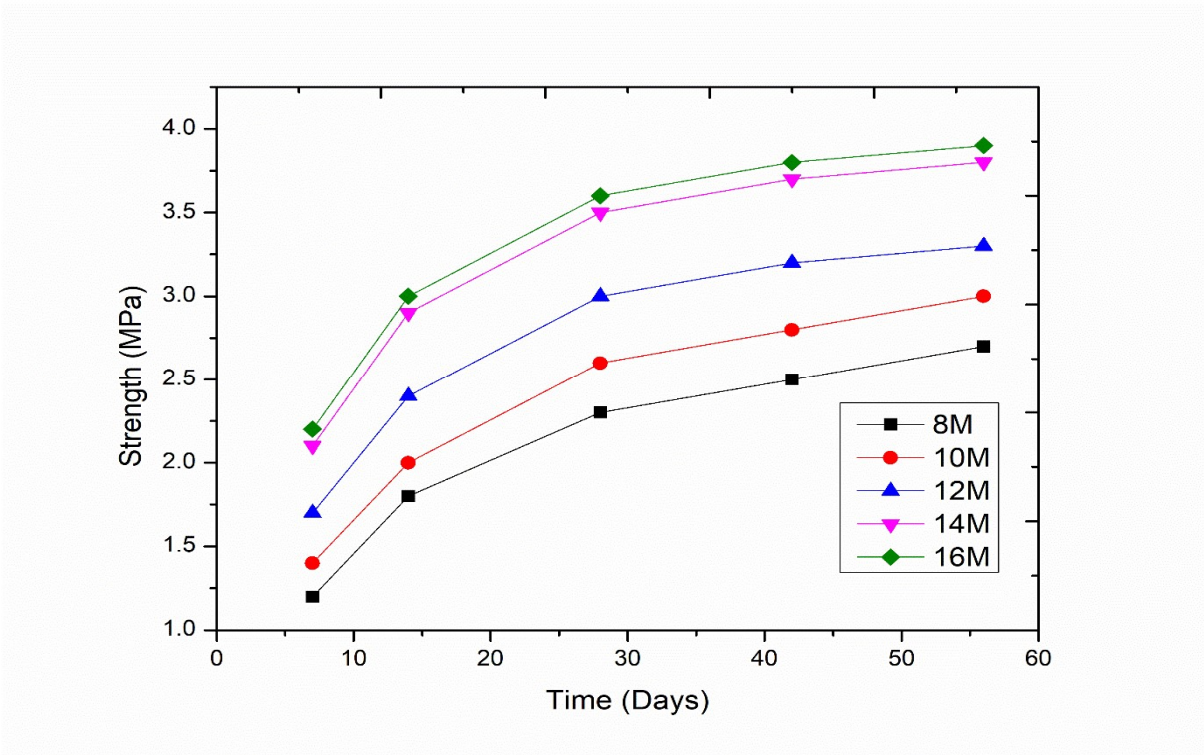

Fig. 4.46 Flexural strength variations with the molarity of sodium hydroxide of ambient-cured GPC

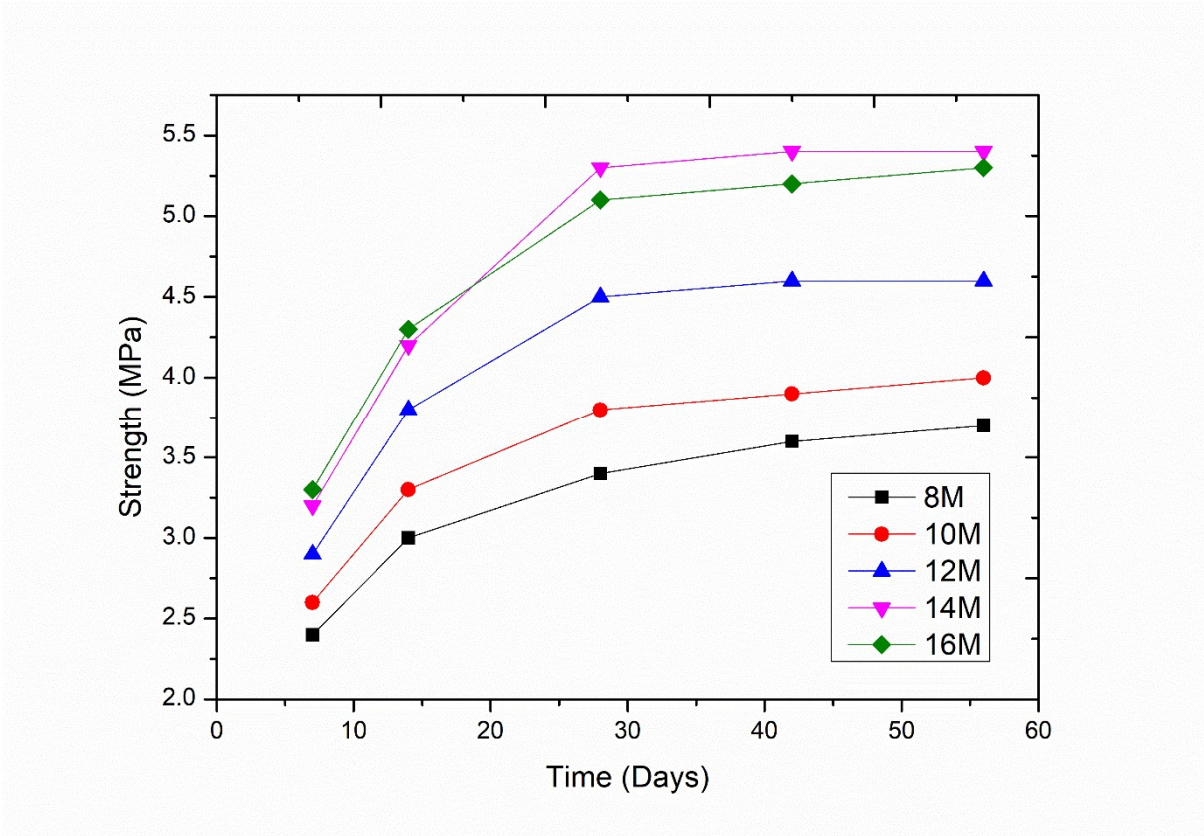

Fig. 4.47 Flexural strength variations with the molarity of sodium hydroxide of oven-cured GPC

Table 4.39 Flexural strength of oven-cured

Molar Concentration	7 days	14 days	28 days	42 days	56 days
8M	2.4	3.0	3.4	3.6	3.7
10M	2.6	3.3	3.8	3.9	4.0
12M	2.9	3.8	4.5	4.6	4.6
14M	3.2	4.2	5.3	5.4	5.4
16M	3.3	4.3	5.1	5.2	5.3

4.4.5 Rebound strength

The rebound test is a non-destructive experiment for the specimens. All mixed specimens of both cured conditions were tested for rebound strength at 7, 14, 28, 42, and 56 days after casting and before the destructive test on the samples.The oven-cured samples' rebound strength is higher than the ambient-cured samples of the same mix of GPC. In the GPC mixes, the 16M NaOH mix got a higher strength than the other mixes with various dosages in the ambient-cured specimens. Fig. 4.48 and Fig. 4.49 show the rebound strength graph with the time variation of both curing conditions. Fig. 4.48 shows the ambient-cured specimens strength, and Fig. 4.49 shows the oven-cured specimens of the GPC. The rebound strength is slightly higher than the destructive compressive strength but does not exceed the IS code's limit. The rebound strength is based on the surface hardness of the specimens.

Table 4.40 Rebound strength of ambient-cured

Molar Concentration	7 days	14 days	28 days	42 days	56 days
In ambient8M	10.2	15.2	18.0	19.0	19.4
10M	12.5	16.1	20.1	21.2	21.6
12M	14.6	18.6	22.4	23.0	23.5
14M	17.0	22.0	25.0	25.4	25.7
16M	17.2	22.1	25.2	25.6	25.9

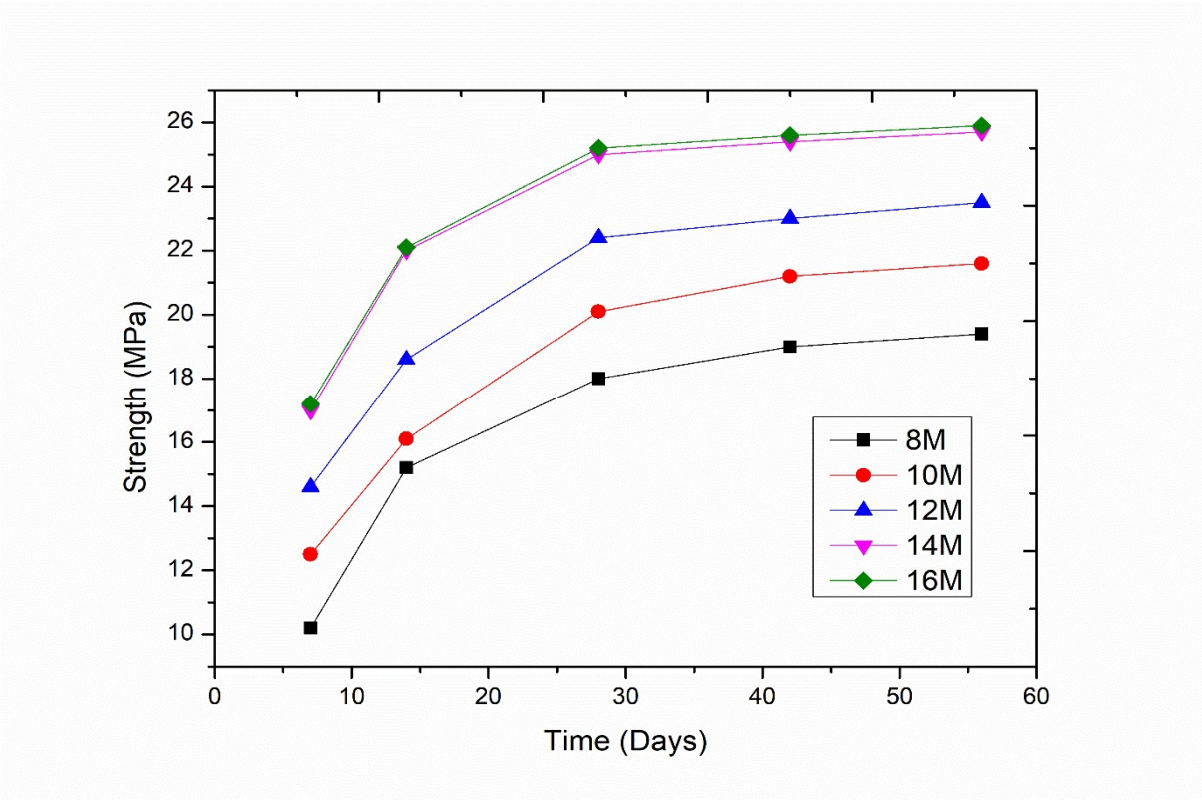

Fig. 4.48 Rebound strength variations with the molarity of sodium hydroxide of ambient-cured GPC

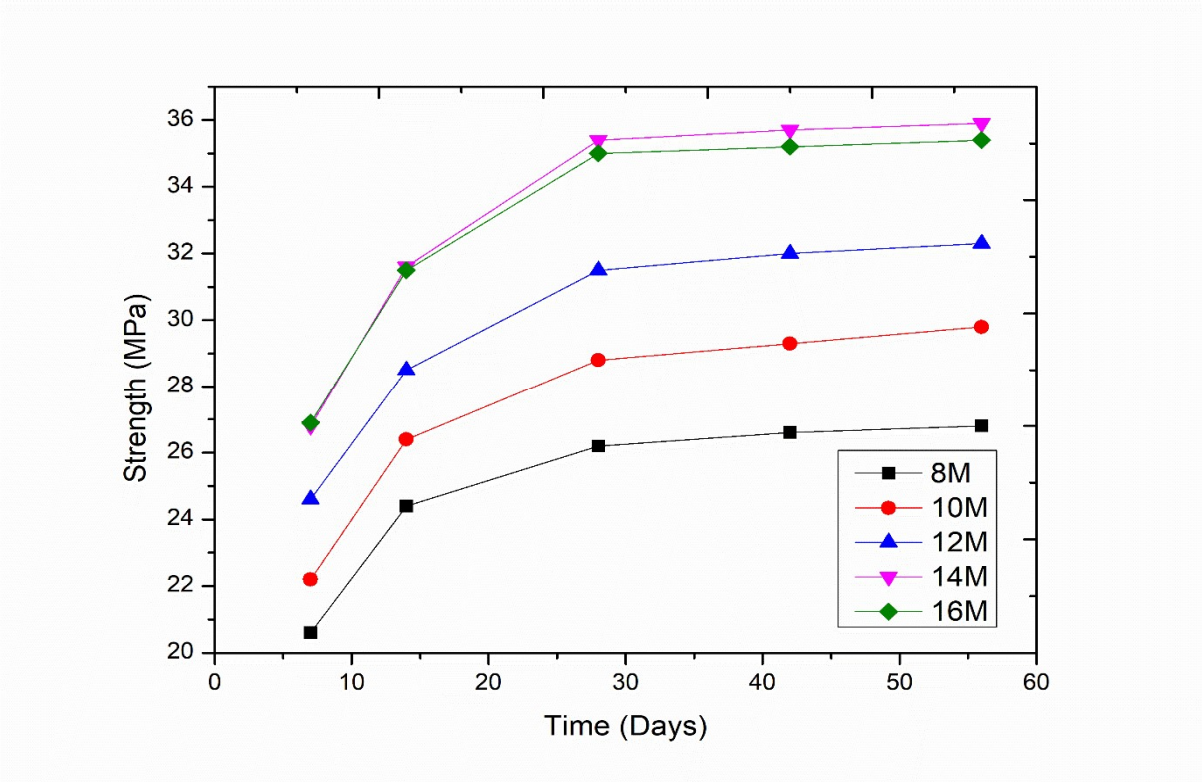

Fig. 4.49 Rebound strength variations with the molarity of sodium hydroxide of oven-cured GPC

Table 4.41 Rebound strength of oven-cured

Molar Concentration	7 days	14days	28 days	42 days	56 days
8M	20.6	24.4	26.2	26.6	26.8
10M	22.2	26.4	28.8	29.3	29.8
12M	24.6	28.5	31.5	32.0	32.3
14M	26.8	31.6	35.4	35.7	35.9
16M	26.9	31.5	35.0	35.2	35.4

4.4.6 UPVT(Ultrasonic Pulse Velocity Test)

The UPV test uses the quality of the hard material by quantifying the time passage from the specimens. It is a non-destructive test to evaluate concrete strength without destruction. The UPV tests are conducted on cube samples at 7 days, 14 days, 28 days, 42 days, and 56 days after the casting and before the destructive tests conducted on the samples. The apparatus records the time duration of the UPV wave and calculates the velocity that defines the quality of GPC samples. When the time passage of the UPV wave is high, it shows less strength and vice-versa. The 16M mix shows a higher velocity than the other mixes in the ambient curing conditions. Fig. 4.50 and Fig. 4.51 describe the graph of UPV of various mixes in the same graph in which Fig. 4.50 shows the ambient-cured results and Fig. 4.51 shows the oven-cured GPC samples. The maximum velocity of oven-cured specimens and ambient-cured specimens is 4.52km/sec and 2.93km/sec, respectively, at 56 days of testing.

Table 4.42 UPV of ambient-cured

Molar Concentration	7 days	14 days	28 days	42 days	56 days
8M	1.02	1.23	1.46	1.49	1.52
10M	1.08	1.42	1.58	1.61	1.63
12M	1.12	1.53	1.92	2.11	2.18
14M	1.53	1.86	2.04	2.23	2.32
16M	1.58	2.02	2.68	2.86	2.93

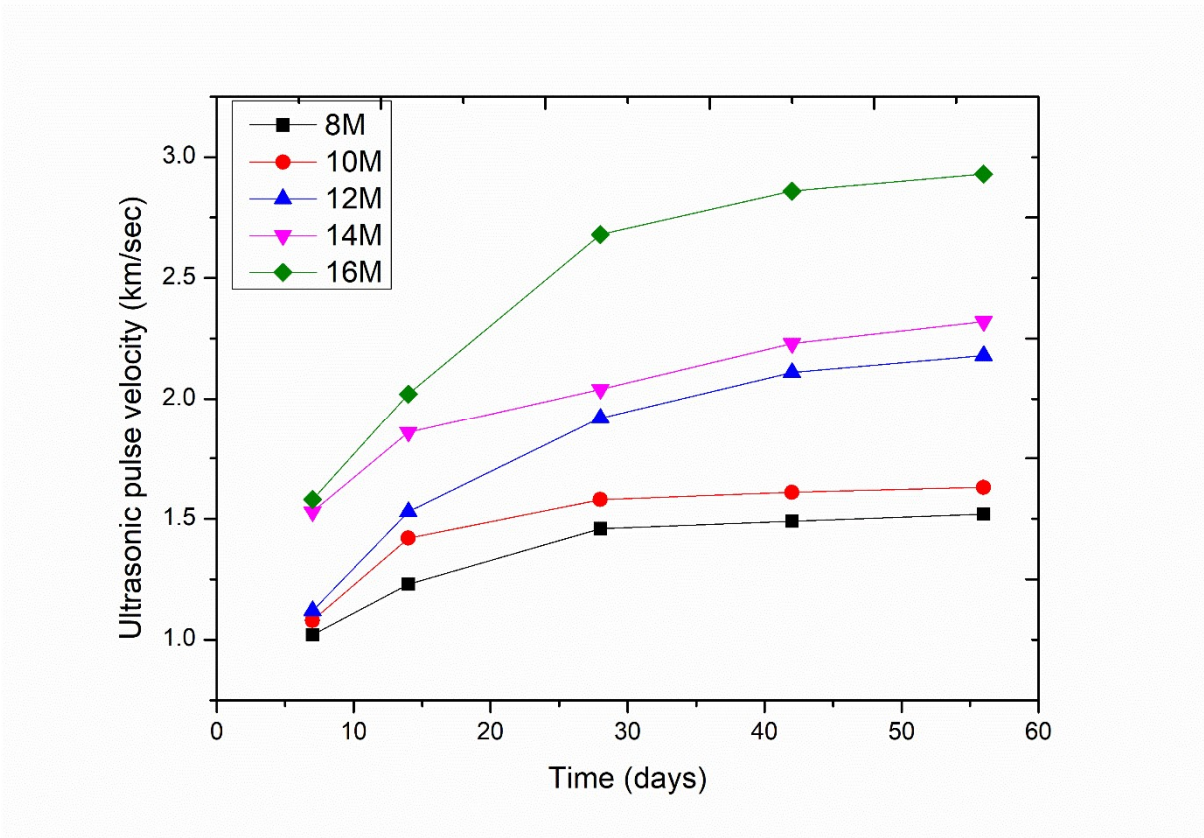

Fig. 4.50 UPV variations with the molarity of sodium hydroxide of ambient-cured GPC

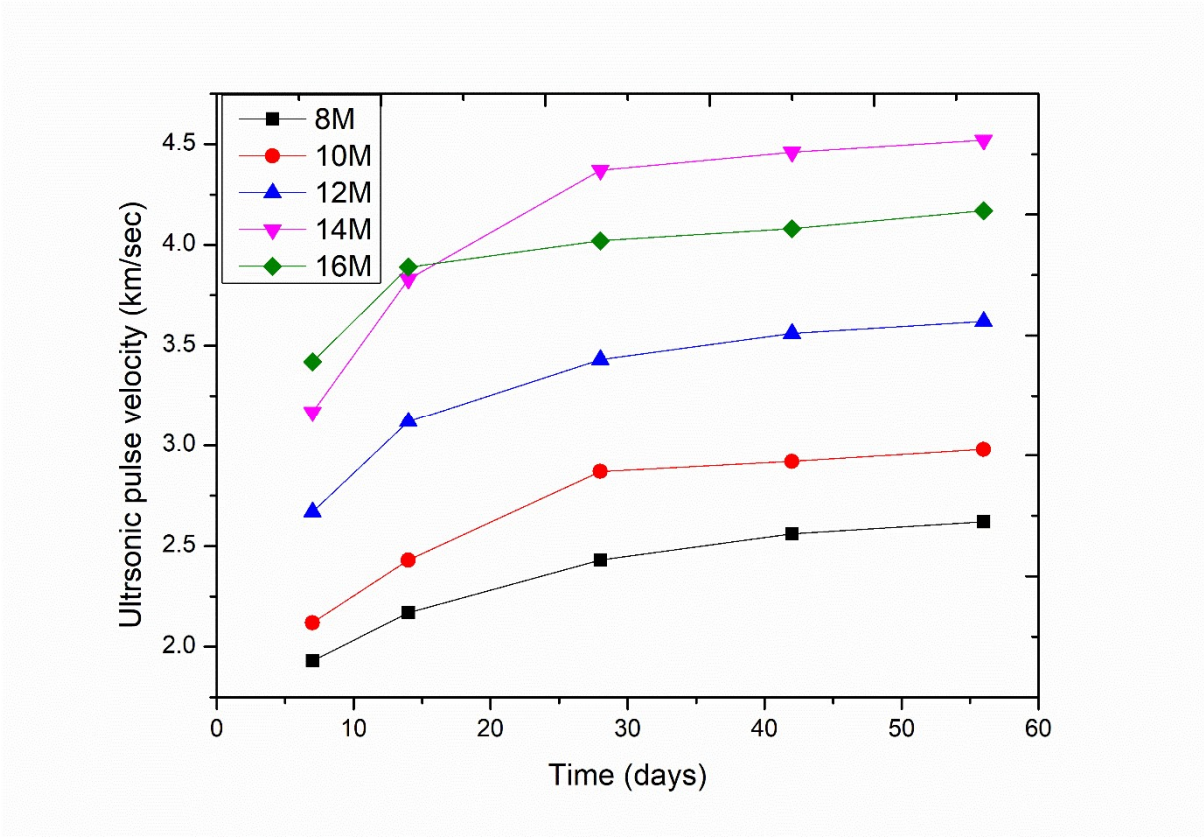

Fig. 4.51 UPV variations with the molarity of sodium hydroxide of oven-cured GPC

Table 4.43 UPV of oven-cured

Molar Concentration	7 days	14 days	28 days	42 days	56 days
8M	1.93	2.17	2.43	2.56	2.62
10M	2.12	2.43	2.87	2.92	2.98
12M	2.67	3.12	3.43	3.56	3.62
14M	3.17	3.83	4.37	4.46	4.52
16M	3.42	3.89	4.02	4.08	4.17

4.4.7 Poisson ratio and Modulus of Elasticity

Fig. 4.52 presented the density of the mix designs to analyse the effect of the molarity of NaOH in mix designs of GPC specimens. All the specimens of various mixes with a variation of molarity of 8M-16M were cured under both ambient and oven-curing conditions. Analysis of the variation in results of the Poisson ratio, modulus of elasticity, and density was drawn out from the samples tested. Density, Poisson ratio and modulus of elasticity were tested after the 28 days of the casting. Density finds out through the weight of the cube specimens of the various mixes. The Poisson ratio finds the cylindrical specimens tested in the UTM machine by applying static compression loading along the longitudinal direction and finding the vertical and horizontal strain. The elastic modulus found through the stress-strain curve made by the cyclic loading on the cylindrical specimen is about one-third of the fracture load statically. The ambient cured sample has a higher density than the oven-cured GPC specimens of different mix designs. A mix of molarity of NaOH in mixes rises in the density of the design mix specimens, but after the increase beyond 14M, the density of the mixed specimens slightly decreases. The 16M mix design samples got the highest average density of 2482 kg/m^3 at 28 days of ambient cured specimens, whereas the oven-cured samples got 2474 kg/m^3. The Poisson ratio of the ambient-cured GPC specimens is slightly higher than that of the oven-cured specimens, but the modulus of elasticity of the GPC mix designs is higher for the oven-cured samples. shows the maximum modulus of elasticity of the 14M mix design of oven cured specimens is 22.3 GPa, whereas the ambient cured specimens' modulus of elasticity is 21.5 GPa of the 14M mix design of GPC.

Table 4.44 Poissons ratio, density, and MOE of GPC

Molar Concentration	Slump Value (mm)	Compaction factor	Density in Kg/m^3		Poissons Ratio		Modulus of Elasticity in GPA	
			Ambient Cured	Oven Cured	Ambient Cured	Oven Cured	Ambient Cured	Oven Cured
8M	136	0.94	2400	2386	.17	.16	20.5	20.9
10M	123	0.92	2423	2405	.16	.15	20.9	21.5
12M	110	0.9	2449	2431	.15	.15	21.2	21.8
14M	98	0.88	2474	2459	.14	.14	21.5	22.3
16M	86	0.84	2482	2452	.15	.15	21.4	22.1

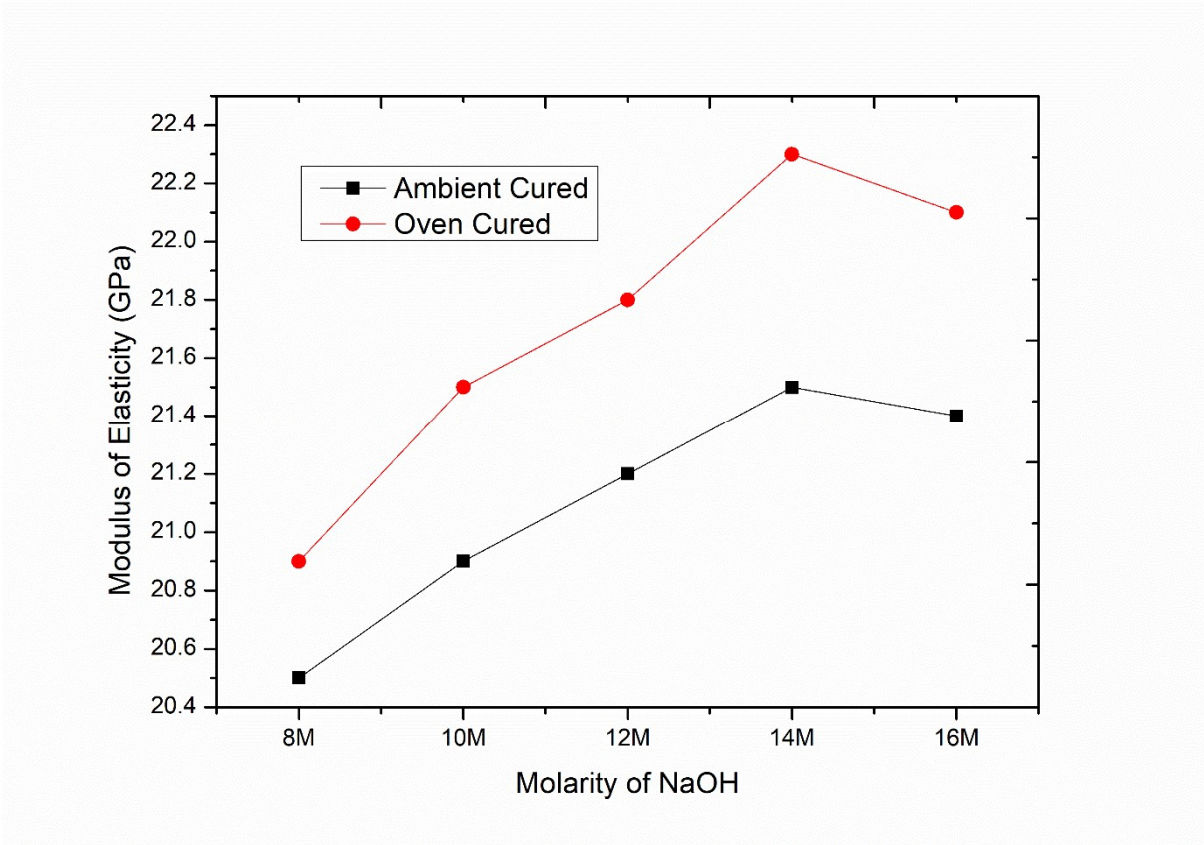

Fig. 4.52 MOE variations with the molarity of sodium hydroxide of both cured GPC

4.5 Effect of Sodium Silicate to Sodium Hydroxide Ratio

The changes in the ratio of Na_2SiO_3/NaOH directly affect the mix design of the GPC. The effect of the rate of Na_2SiO_3/NaOH in mix designs of the GPC was studied by varying the ratio of 0.5-3.0 and examining the test results of the specimens of all design mixes by the destructive strength test, non-destructive rebound strength test, and UPVT.

4.5.1 Slump and Compaction Factor

The slump value decreases with the increment of the ratio of Na_2SiO_3/NaOH in the mix design. Similarly, the compaction factor value also decreases with the increment of the ratio of Na_2SiO_3/NaOH. Fig. 4.53 describes the effect of the ratio of Na_2SiO_3/NaOH on both slump value and compaction factor on the fresh mix of GPC.

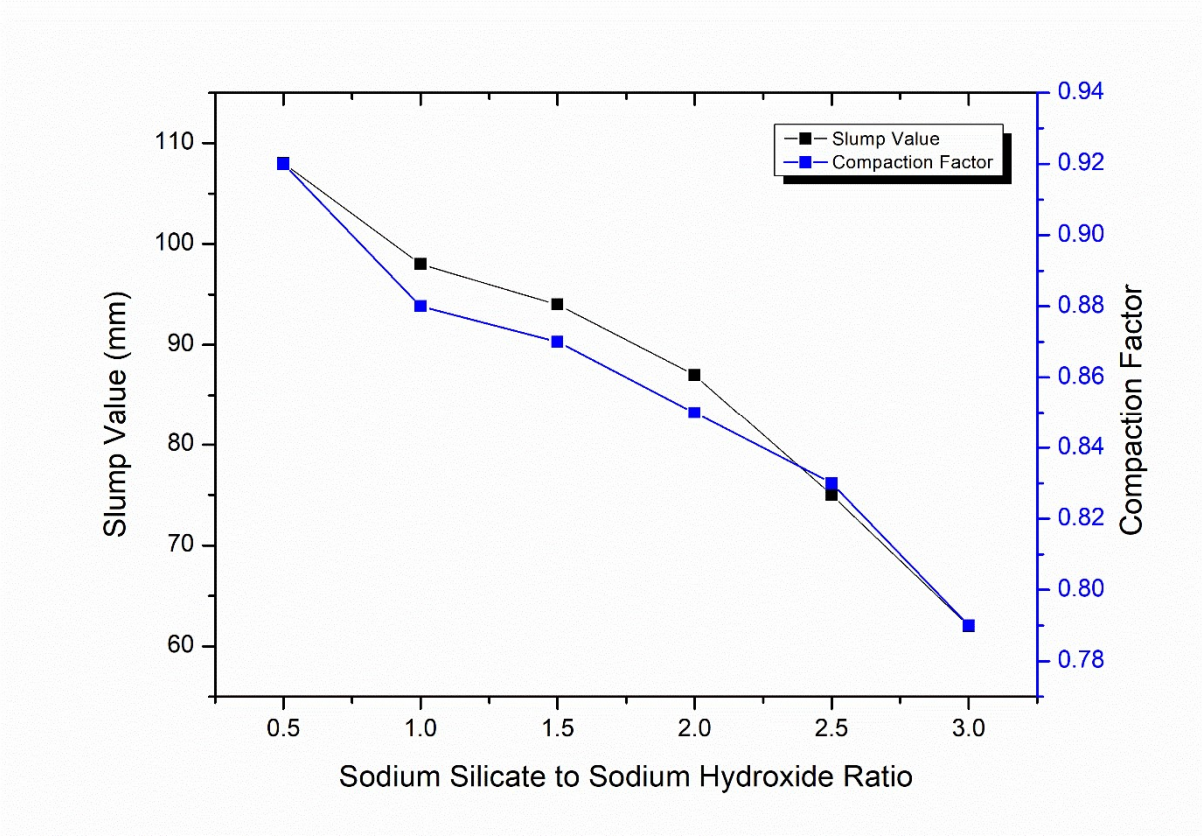

Fig. 4.53 Slump and compaction factor variations with the alkaline ratio of GPC

4.5.2 Density

The mix's density is measured through the weight of specimens before the destructive test of cube samples. The ambient-cured specimens got higher density than the oven-cured samples, and the specimens' density increases continuously from the ratio of

Na_2SiO_3/NaOH in the GPC mix design. The 2.5 ratios of Na_2SiO_3/NaOH mix design got the optimum density point in both cured specimens. The 2.5 ratios of Na_2SiO_3/NaOH mix of ambient cured got the highest of all mixes of GPC. Fig. 4.54 describes the relationship between the density of the mix and the ratio of Na_2SiO_3/NaOH in the mixes for both curing conditions.

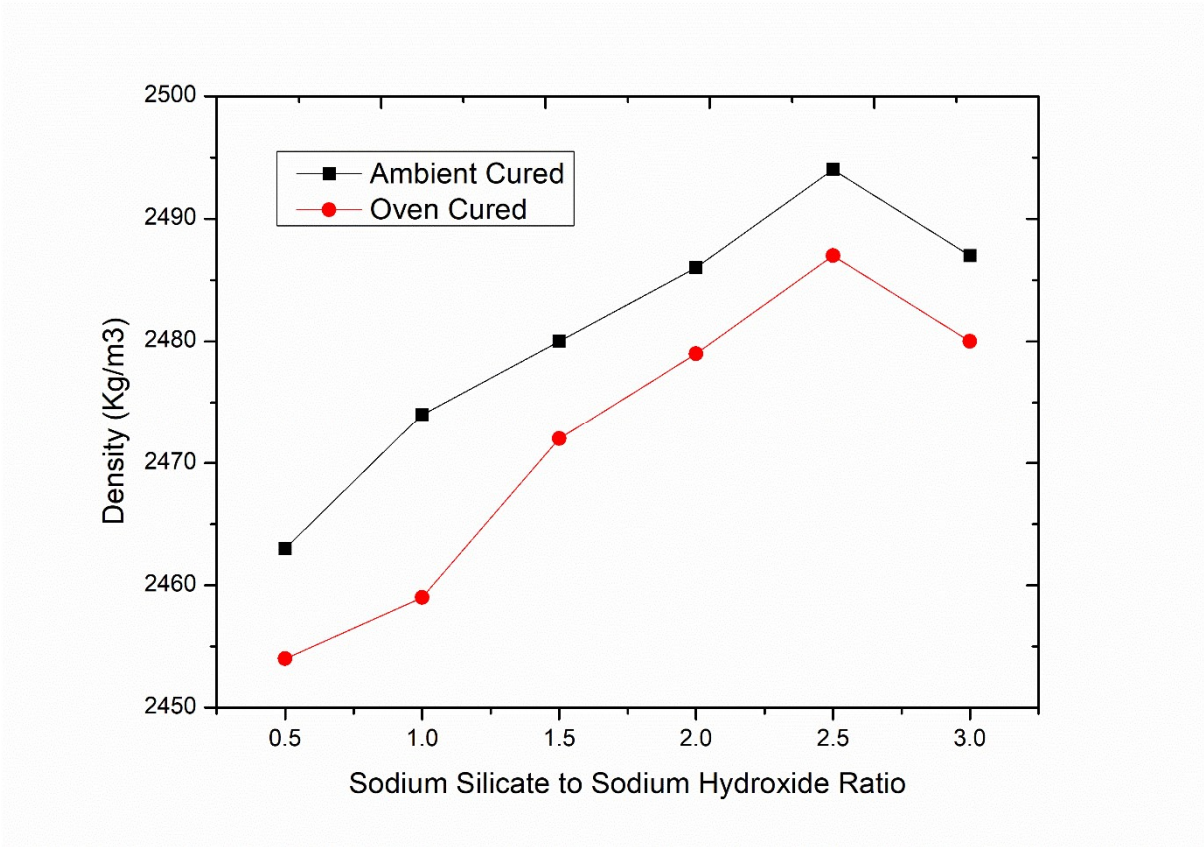

Fig. 4.54 Density variations with the alkaline ratio of both cured GPC

4.5.3 Compressive Strength

The compressive strength of the GPC varies with the ratio of Na_2SiO_3/NaOH and curing conditions. The compressive strength increases with the increment in the ratio in the mix design, but beyond a point, it decreases the compressive strength in both the curing condition samples. The highest compressive strength of the oven cured 2.5 alkaline ratio mix is 35.7N/mm^2 at 56 days, and in the ambient cured specimen it is 25.8N/mm^2 at 56 days. Fig. 4.55 shows the compressive strength of ambient cured specimens, and Fig. 4.56 shows the compressive strength of oven cured specimens with the ratio of Na_2SiO_3/NaOH in the design mix of GPC. The highest compressive strength of design mixes of ratio 0.5, 1.0, 1.5, 2.0, 2.5 and 3.0 are 20.3 MPa, 24.0 MPa, 25.0 MPa, 25.4 MPa, 25.8 MPa and 23.4 MPa respectively at 56 days after ambient-curing but after oven-

curing compressive strength of the ratio 0.5, 1.0, 1.5, 2.0, 2.5 and 3.0 are 24.6MPa, 34.2MPa, 34.7MPa, 35.1MPa, 35.7MPa and 32.5MPa respectively at 56 days.

Table 4.45 Compressive strength of ambient-cured

Na_2SiO_3/NaOH Ratio	7 days	14 days	28 days	42 days	56 days
0.5	7.9	15.0	19.3	19.8	20.3
1.0	12.4	18.4	22.6	23.4	24.0
1.5	12.8	19.2	23.5	24.4	25.0
2.0	13.0	19.6	24.0	24.9	25.4
2.5	13.5	20.2	24.8	25.3	25.8
3.0	12.3	18.4	22.0	23.0	23.4

Table 4.46 Compressive strength of oven-cured

Na_2SiO_3/NaOH Ratio	7 days	14 days	28 days	42 days	56 days
0.5	20.0	22.1	23.8	24.3	24.6
1.0	26.4	29.6	33.2	33.8	34.2
1.5	26.6	29.9	33.8	34.4	34.7
2.0	26.9	30.2	34.4	34.8	35.1
2.5	27.5	30.8	35.0	35.4	35.7
3.0	26.4	29.7	31.8	32.2	32.5

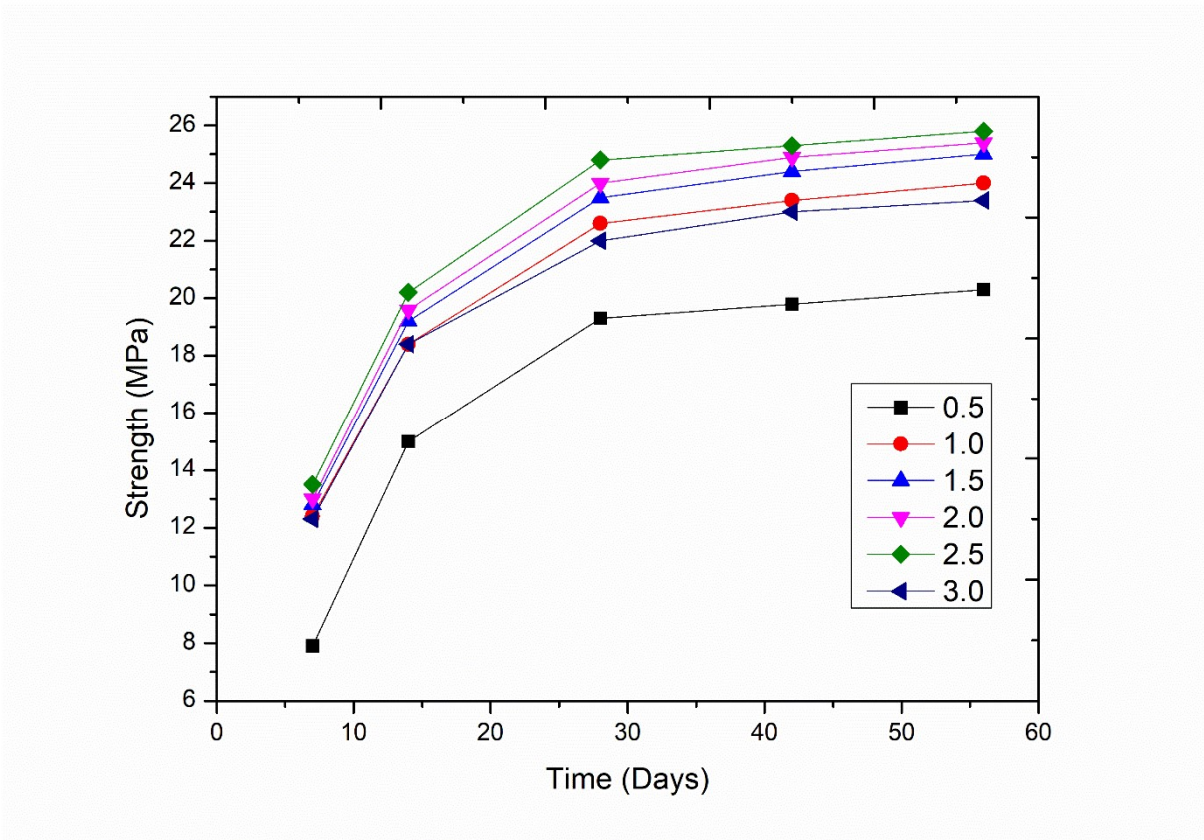

Fig. 4.55 Compressive strength variations with the alkaline ratio of ambient-cured GPC

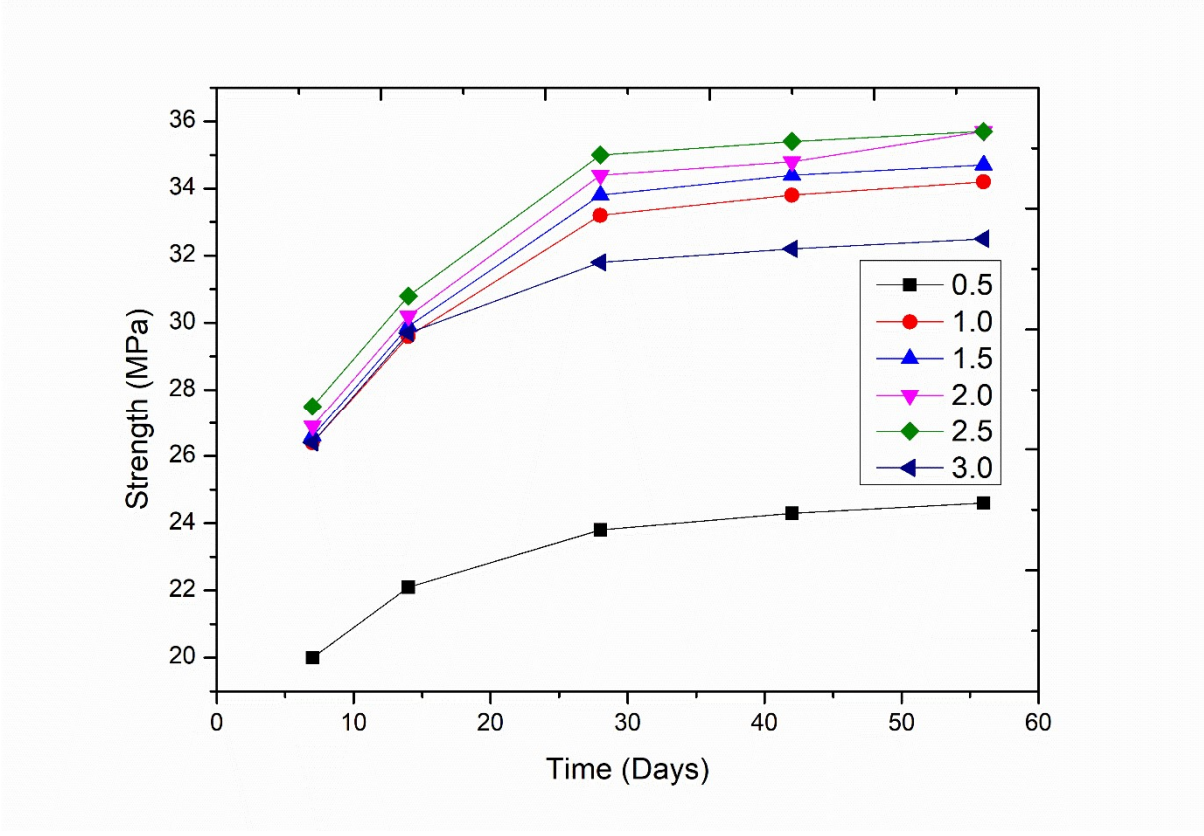

Fig. 4.56 Compressive strength variations with the alkaline ratio of oven-cured GPC

4.5.4 Splitting strength

The splitting tensile strength test is used to find the indirect tensile strength of the design mix of the GPC. Fig. 4.57 and Fig. 4.58 show the splitting tensile strength of ambient-cured specimens and oven cured samples of mix designs, which varies the ratio of Na_2SiO_3/NaOH in the mix design of GPC from 0.5 to 3.0. In both curing conditions, specimens got the highest splitting tensile strength at a ratio of 2.5, and the uppermost strength of ambient cured and oven cured specimens was 4.0 MPa and 5.2 MPa, respectively, at 56 days in the mixes of GPC. The highest Splitting Tensile strength of design mixes of ratio 0.5, 1.0, 1.5, 2.0, 2.5 and 3.0 are 2.7MPa, 3.5MPa, 3.6MPa, 3.8MPa, 4.0MPa and 3.6MPa respectively at 56 days after ambient-curing but after oven-curing compressive strength of the ratio 0.5, 1.0, 1.5, 2.0, 2.5 and 3.0 are 3.5MPa, 5.2MPa, 5.0MPa, 5.1MPa, 5.2MPa and 5.0MPa respectively at 56 days.

Table 4.47 Splitting tensile of ambient-cured

Na_2SiO_3/NaOH Ratio	7 days	14 days	28 days	42 days	56 days
0.5	1.3	1.9	2.6	2.7	2.7
1.0	2.1	2.7	3.2	3.4	3.5
1.5	2.4	2.9	3.5	3.6	3.6
2.0	2.5	3.1	3.7	3.8	3.8
2.5	2.6	3.2	3.8	3.9	4.0
3.0	2.4	2.8	3.4	3.5	3.6

Table 4.48 Splitting tensile of oven-cured

Na_2SiO_3/NaOH Ratio	7 days	14 days	28 days	42 days	56 days
0.5	2.4	2.9	3.4	3.5	3.5
1.0	3.0	4.0	4.9	5.1	5.2
1.5	3.1	4.1	4.9	5.0	5.0
2.0	3.2	4.2	5.0	5.1	5.1
2.5	3.4	4.3	5.1	5.2	5.2
3.0	3.1	4.0	4.8	5.0	5.0

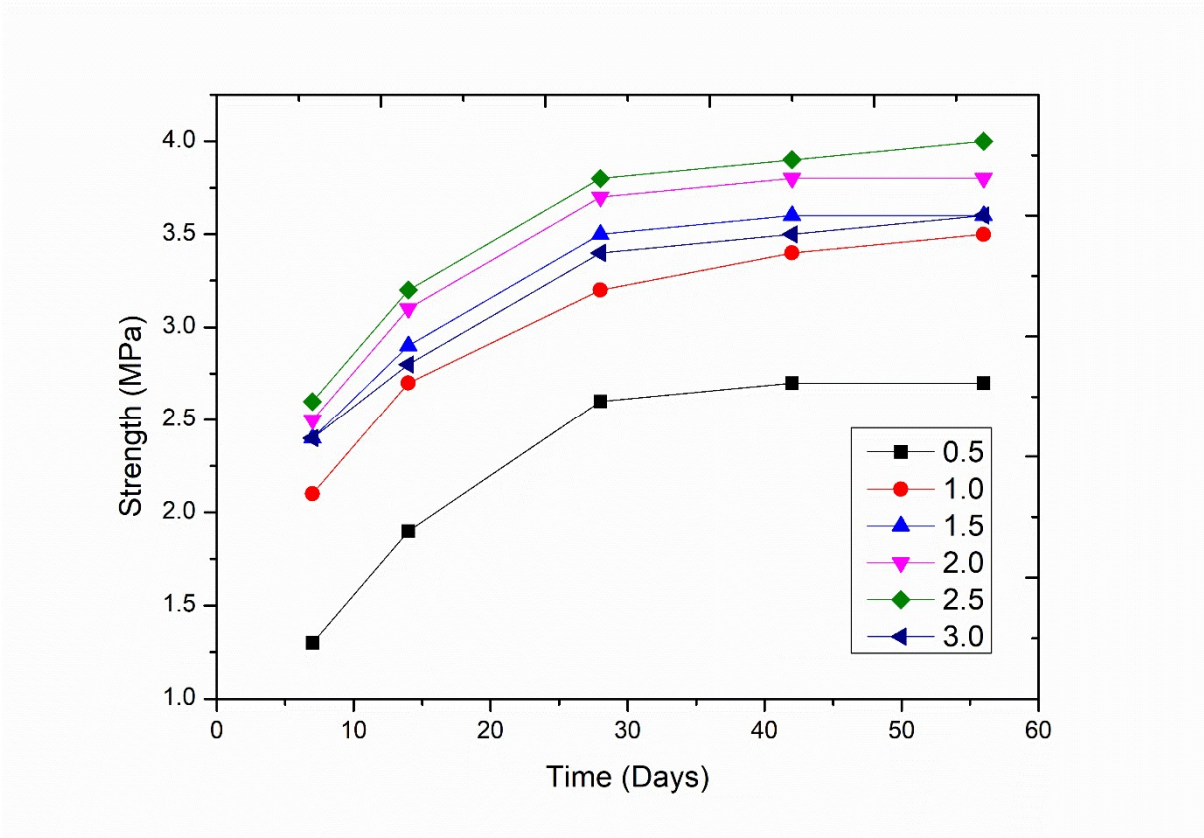

Fig. 4.57 Splitting tensile variations with the alkaline ratio of ambient-cured GPC

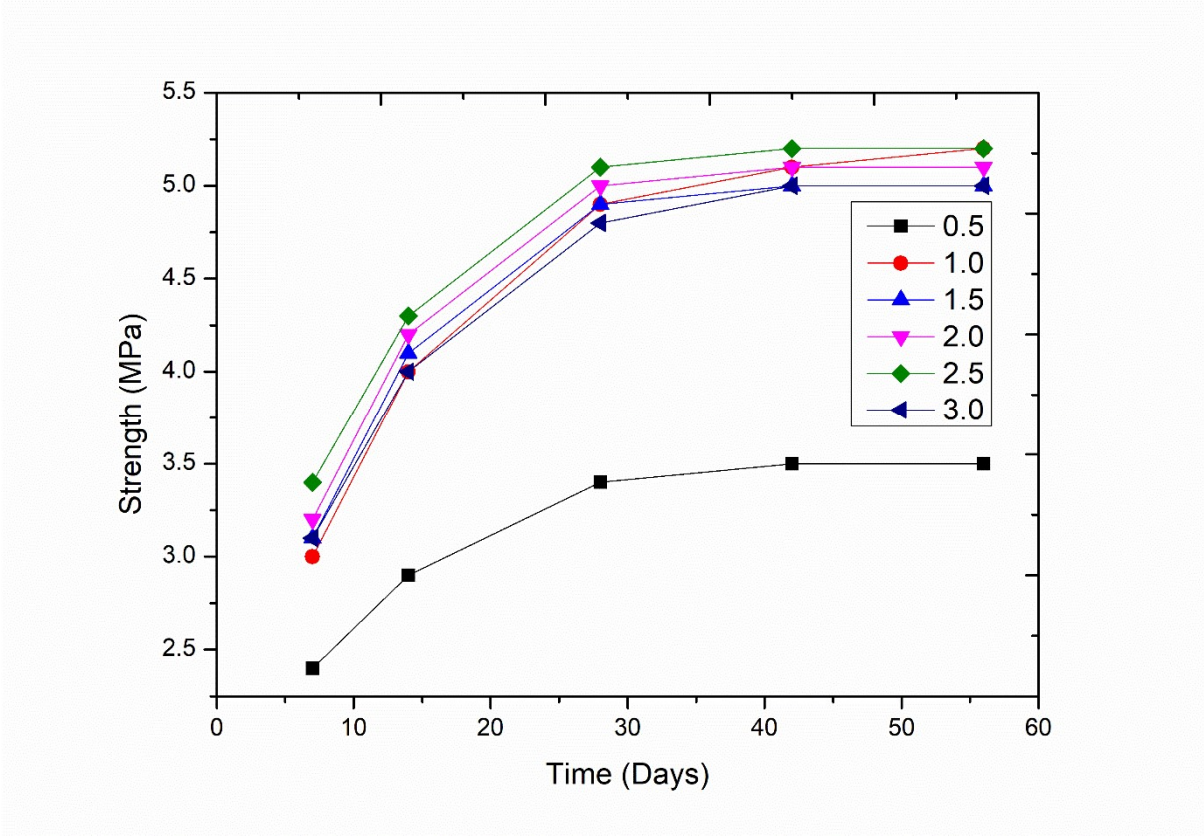

Fig. 4.58 Splitting tensile variations with the alkaline ratio of oven-cured GPC

4.5.5 Flexural Strength

Flexural tensile strength is used to find the bending tension of the beam specimen. Fig. 4.59 and Fig. 4.60 show the flexural tensile strength of mixed ambient-cured samples and oven-cured samples, respectively. Similarly, the oven-cured samples got more flexural tensile strength as compared to the ambient-cured specimens. The highest strength of oven-cured specimens at the ratio of 2.5 in the mix is 5.6MPa at 56 days, but in ambient-cured samples, the strongest part of the ratio is 4.0MPa. In both curing conditions, the flexural tensile strength rises with the increment of the rate of sodium silicate to sodium hydroxide in mix design, but in the oven-cured, strength decreases beyond the ratio of 2.5 in design mixes. The highest flexural tensile strength of design mixes of ratio 0.5, 1.0, 1.5, 2.0, 2.5 and 3.0 are 3.0MPa, 3.8MPa, 4.0MPa, 4.0MPa, 4.0MPa and 3.9MPa respectively at 56 days after ambient-curing but after oven-curing compressive strength of the ratio 0.5, 1.0, 1.5, 2.0, 2.5 and 3.0 are 5.4MPa, 5.4MPa, 5.6MPa, 5.6MPa, 5.3MPa and 5.0MPa respectively at 56 days.

Table 4.49 Flexural strength of ambient-cured

Na_2SiO_3/NaOH Ratio	7 days	14 days	28 days	42 days	56 days
0.5	1.6	2.3	2.7	2.9	3.0
1.0	2.1	2.9	3.5	3.7	3.8
1.5	2.2	3.0	3.6	3.8	4.0
2.0	2.3	3.1	3.7	3.9	4.0
2.5	2.4	3.2	3.8	3.9	4.0
3.0	2.3	3.0	3.6	3.8	3.9

Table 4.50 Flexural strength of oven-cured

Na_2SiO_3/NaOH Ratio	7 days	14 days	28 days	42 days	56 days
0.5	2.5	2.8	3.2	3.3	3.3
1.0	3.2	4.2	5.3	5.4	5.4
1.5	3.3	4.3	5.3	5.4	5.4
2.0	3.4	4.4	5.4	5.5	5.6
2.5	3.6	4.6	5.5	5.6	5.6
3.0	3.3	4.2	5.2	5.3	5.3

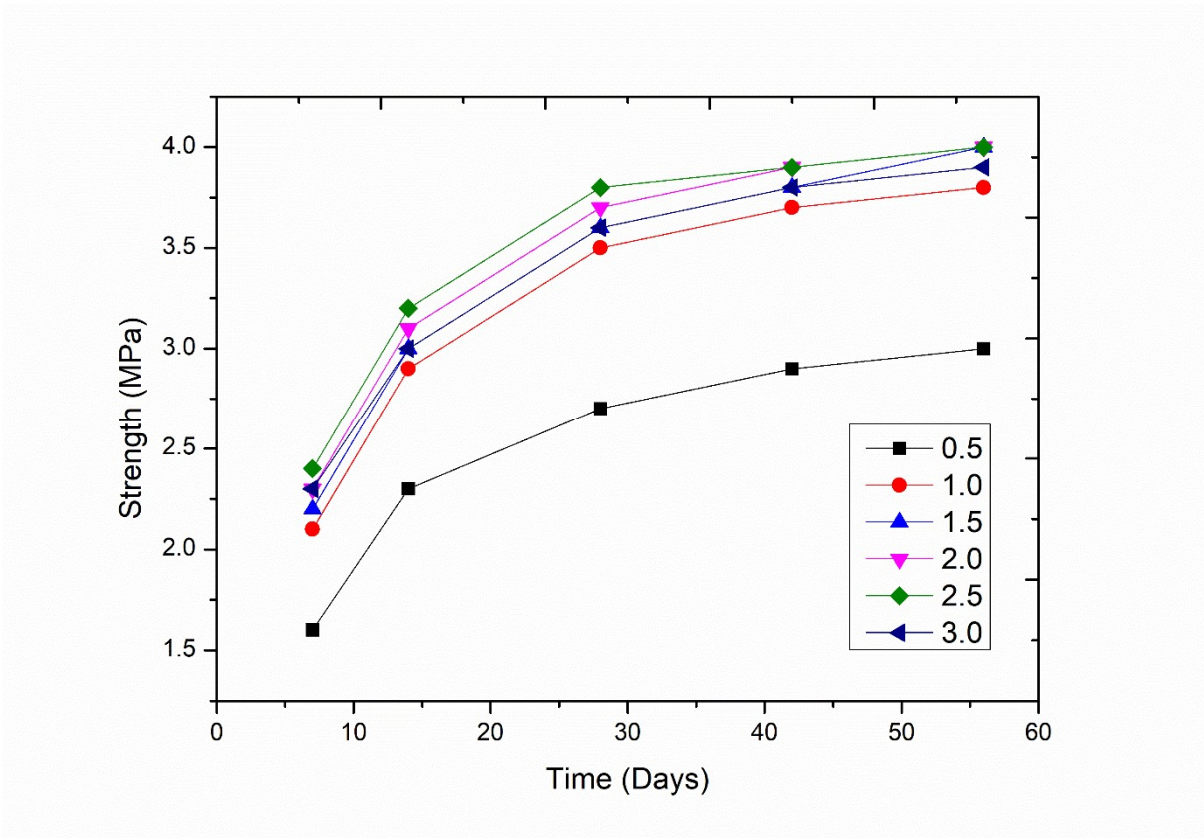

Fig. 4.59 Flexural strength variations with the alkaline ratio of ambient-cured GPC

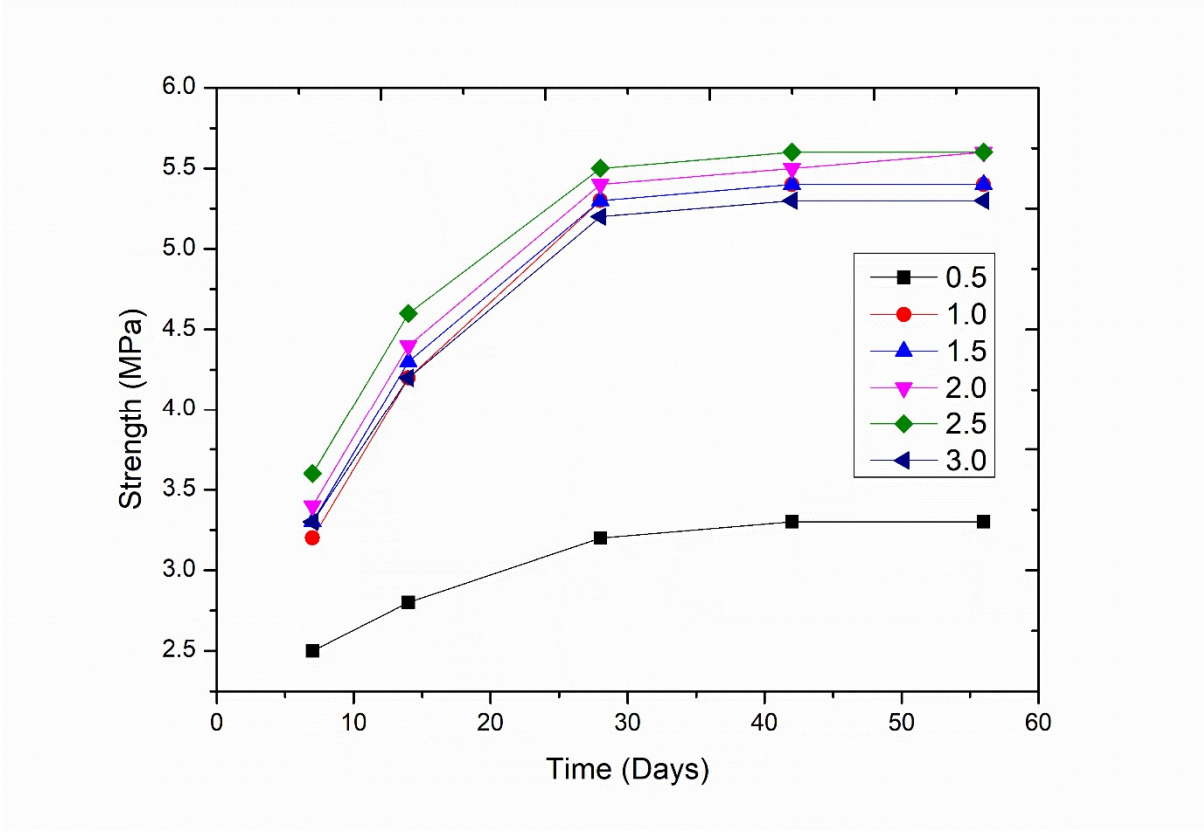

Fig. 4.60 Flexural strength variations with the alkaline ratio of oven-cured GPC

4.5.6 Rebound strength

The rebound test is a non-destructive experiment for the specimens. All mixed specimens of both cured conditions were tested for rebound strength at 7, 14, 28, 42, and 56 days after casting and before the destructive test on the samples.The oven-cured samples' rebound strength is higher than the ambient-cured samples of the same mix of GPC. In the GPC mixes, the 2.5 ratios of sodium silicate to sodium hydroxide mix got a higher strength than the other mixes with various dosages in both-cured specimens. Fig. 4.61 and Fig. 4.62 show the graph of rebound strength with the time variation of both curing conditions. Fig. 4.61 shows the ambient-cured specimens strength, and Fig. 4.62 shows the oven-cured specimens of the GPC. The rebound strength is slightly higher than the destructive compressive strength but does not exceed the IS code's limit. The rebound strength is based on the surface hardness of the specimens.

Table 4.51 Rebound strength of ambient-cured

Na_2SiO_3/NaOH Ratio	7 days	14 days	28 days	42 days	56 days
0.5	13.4	15.0	17.4	17.8	18.0
1.0	17.0	22.0	25.0	25.4	25.7
1.5	17.2	22.1	25.1	25.5	25.8
2.0	17.4	22.5	25.8	26.1	26.3
2.5	17.7	23.0	26.1	26.6	26.9
3.0	17.2	22.0	24.9	25.4	25.7

Table 4.52 Rebound strength of oven-cured

Na_2SiO_3/NaOH Ratio	7 days	14days	28 days	42 days	56 days
0.5	22.0	24.2	27.5	27.9	28.1
1.0	26.8	31.6	35.4	35.7	35.9
1.5	26.9	31.6	35.4	35.6	35.8
2.0	27.1	31.8	35.6	35.8	35.9
2.5	27.3	32.0	35.9	36.1	36.2
3.0	26.8	31.4	35.2	35.4	35.5

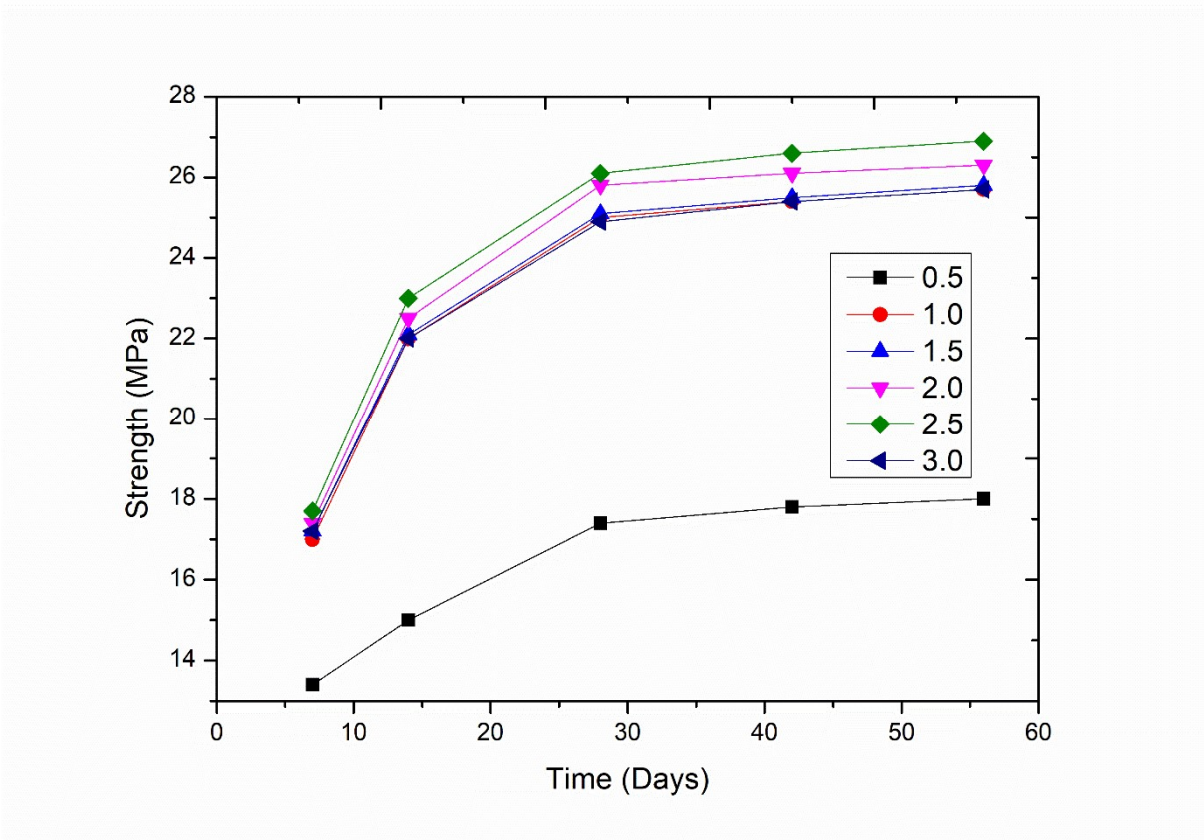

Fig. 4.61 Rebound strength with the alkaline ratio of ambient-cured GPC

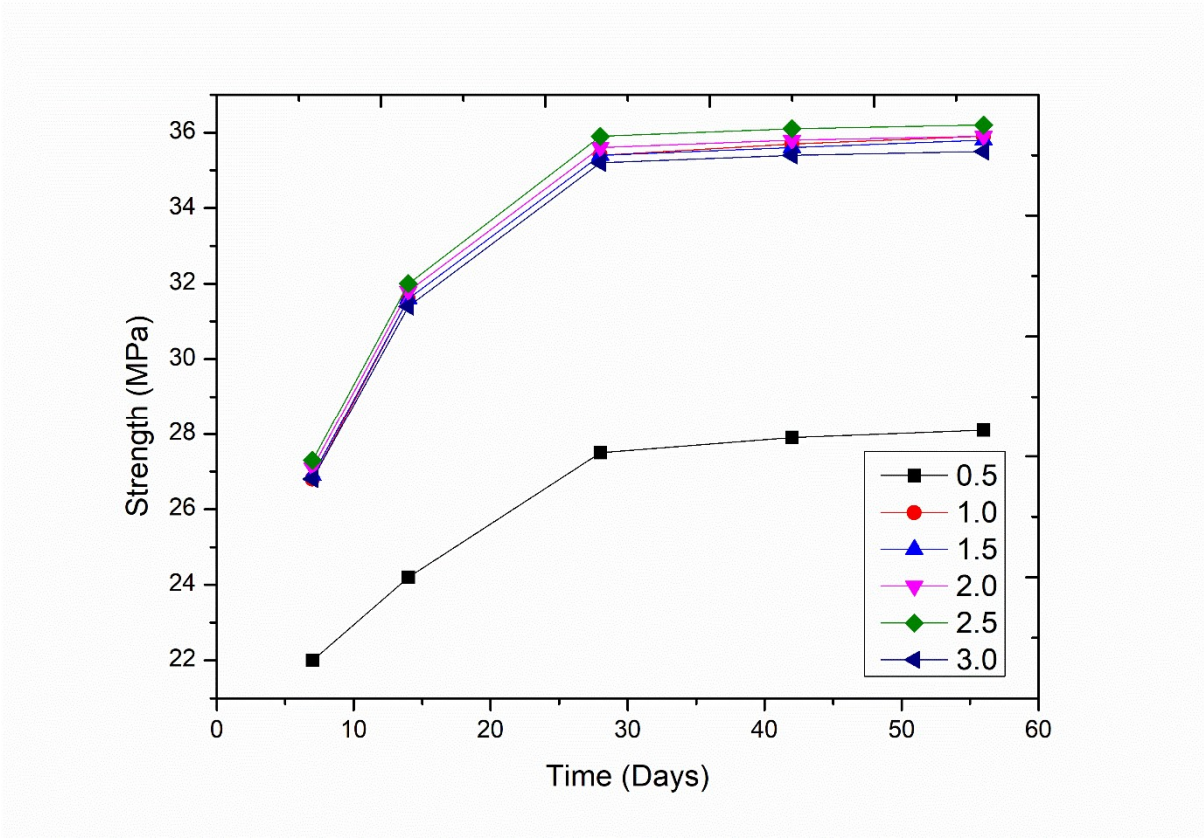

Fig. 4.62 Rebound strength variations with the alkaline ratio of oven-cured GPC

4.5.7 UPVT(Ultrasonic Pulse Velocity Test)

The UPV test uses the quality of the hard material by quantifying the time passage from the specimens. It is a non-destructive test to evaluate concrete strength without destruction. The UPV tests are conducted on cube samples at 7 days, 14 days, 28 days, 42 days, and 56 days. The apparatus records the time duration of the UPV wave and calculates the velocity that defines the quality of GPC samples. When the time passage of the UPV wave is high, it shows less strength and vice-versa. The 2.5 ratios of sodium silicate to sodium hydroxide mix shows a higher velocity than the other mixes in both curing conditions. Fig. 4.63 and Fig. 4.64 describe the graph of UPV of various mixes in the same graph in which Fig. 4.63 shows the ambient-cured results and Fig. 4.64 shows the oven-cured GPC samples. The maximum velocity of oven-cured specimens and ambient-cured specimens is 4.61km/sec and 3.12km/sec, respectively, at 56 days of testing.

Table 4.53 UPV of ambient-cured

Na_2SiO_3/NaOH Ratio	7 days	14days	28 days	42 days	56 days
0.5	1.21	1.68	1.89	1.92	1.94
1.0	1.53	1.86	1.94	2.03	2.12
1.5	1.52	1.93	2.64	2.76	2.83
2.0	1.63	1.94	2.63	2.71	2.78
2.5	1.68	2.10	2.93	3.02	3.12
3.0	1.46	1.87	2.23	2.42	2.49

Table 4.54 UPV of oven-cured

Na_2SiO_3/NaOH Ratio	7 days	14days	28 days	42 days	56 days
0.5	2.02	2.43	2.67	2.83	2.86
1.0	3.17	3.83	4.37	4.46	4.52
1.5	3.18	3.87	4.25	4.39	4.42
2.0	3.24	4.01	4.42	4.47	4.51
2.5	3.41	4.13	4.47	4.52	4.61
3.0	3.21	3.87	4.12	4.23	4.29

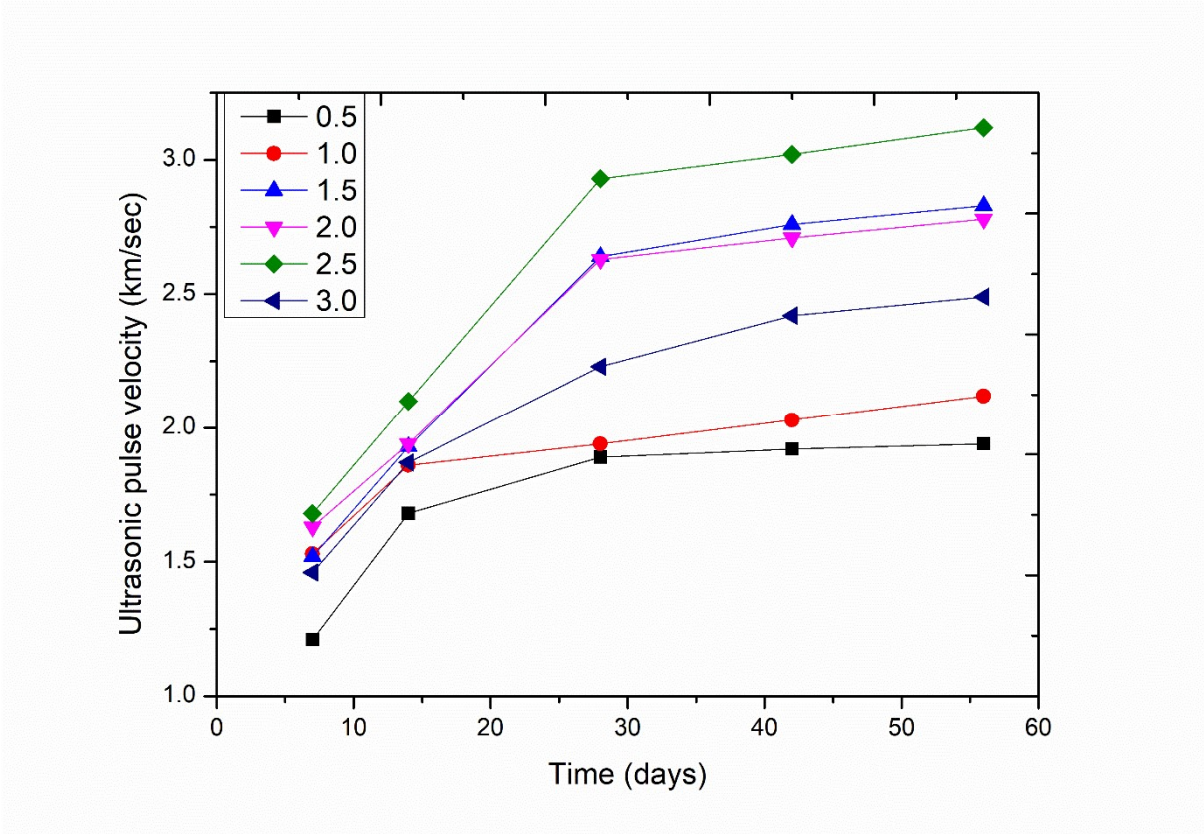

Fig. 4.63 UPV variations with the alkaline ratio of ambient-cured GPC

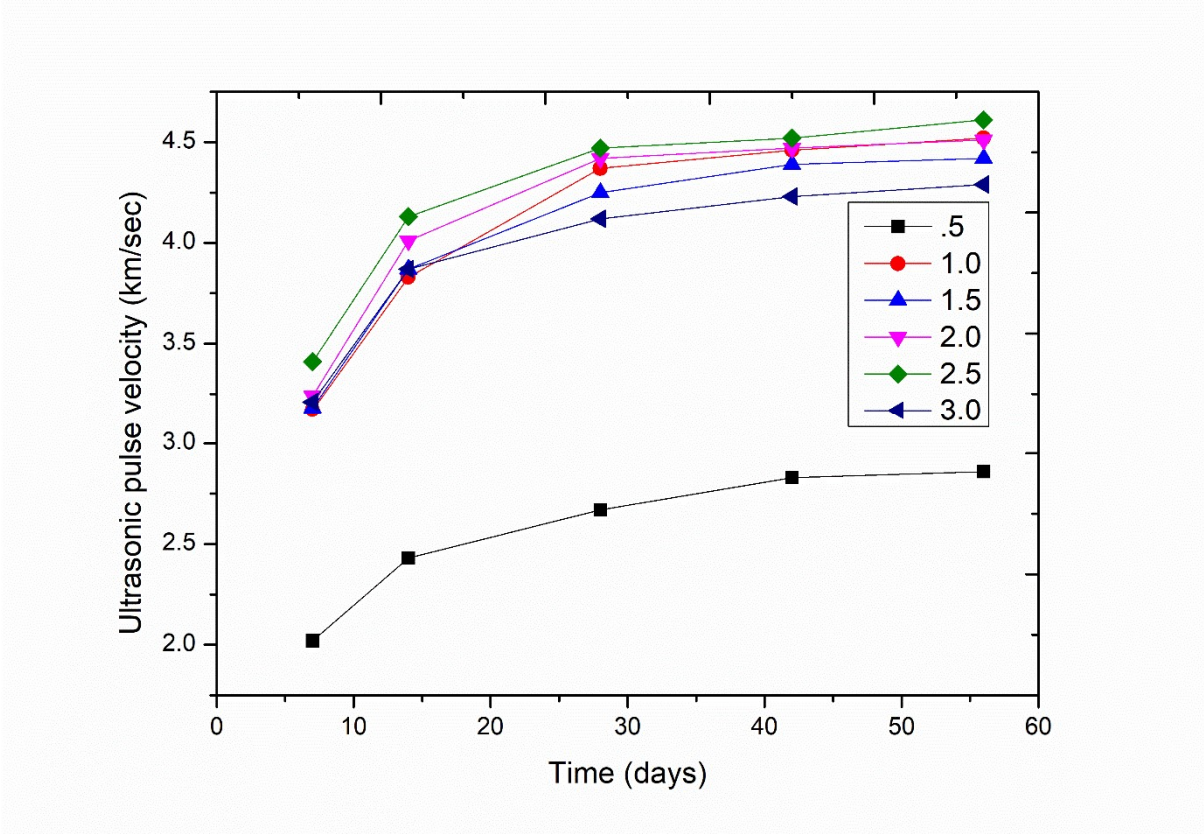

Fig. 4.64 UPV variations with the alkaline ratio of oven-cured GPC

4.5.8 Poisson ratio and Modulus of Elasticity

Fig. 4.54 represents the effect of the ratio of Na_2SiO_3/NaOH on the density of the mix design of GPC. Ambient cured specimens have higher density compared to oven-cured samples, and the ones that got the highest density are 2494 kg/m^3 at a ratio of 2.5 of ambient cured specimens. Fig. 4.65 represents the effect of the ratio of Na_2SiO_3/NaOH on the modulus of elasticity of mix design of GPC. Oven cured samples have an excessive modulus of elasticity compared to the ambient cured samples and got the highest Modulus of Elasticity at the ratio of 2.5 are 24 GPa of oven cured samples.

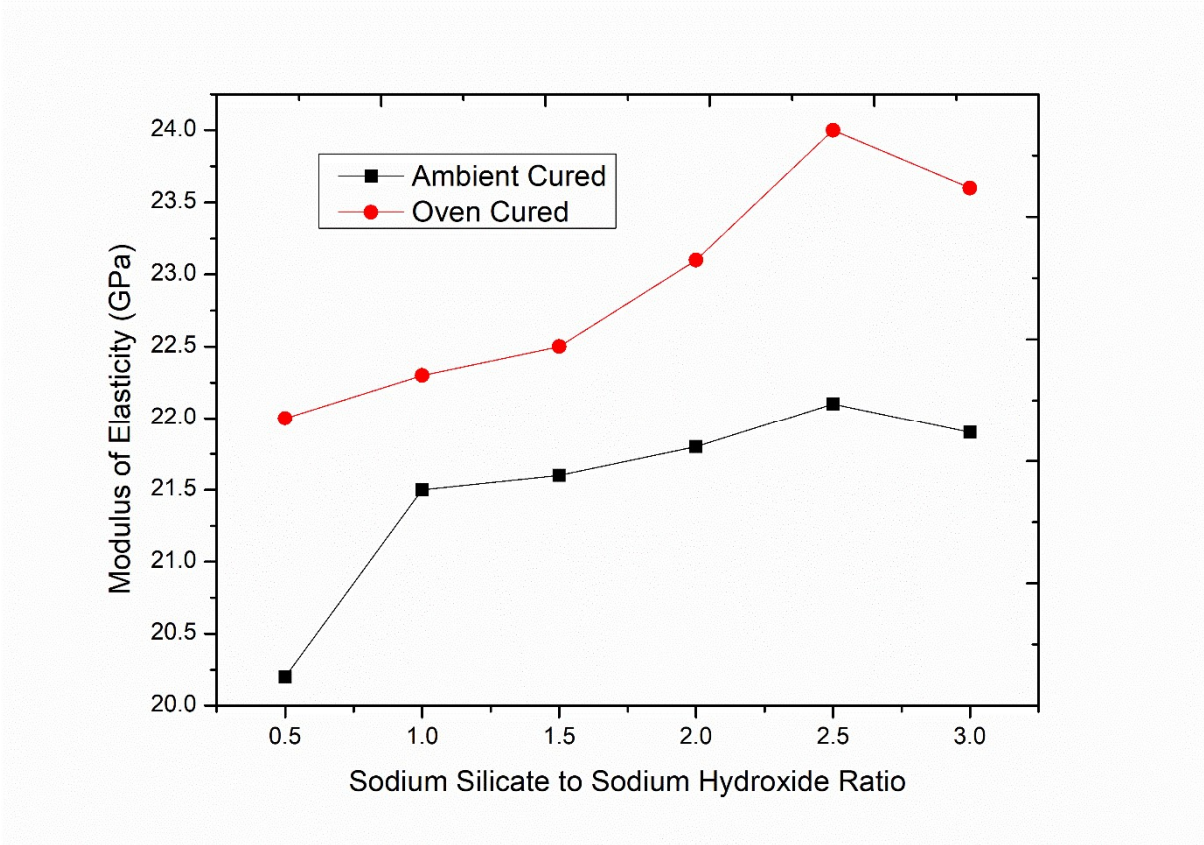

Fig. 4.65 Graph between MOE and sodium silicate to sodium hydroxide ratio of both cured conditions

Table 4.55 Poissons ratio, density, and MOE of GPC

Na_2SiO_3/ NaOH Ratio	Slump Value (mm)	Comp action factor	Density in Kg/m^3	Poissons Ratio	Modulus of Elasticity in GPa

			Ambient Cured	Oven Cured	Ambient Cured	Oven Cured	Ambient Cured	Oven Cured
0.5	108	0.92	2463	2454	.16	.16	20.2	22.0
1.0	98	0.88	2474	2459	.14	.14	21.5	22.3
1.5	94	0.87	2480	2472	.15	.14	21.6	22.5
2.0	87	0.85	2486	2479	.15	.15	21.8	23.1
2.5	75	0.83	2494	2487	.14	.14	22.1	24.0
3.0	62	0.79	2487	2480	.15	.15	21.9	23.6

4.6 Effect of curing temperature

The curing temperature varies from 60^0C to 120^0C in the optimum GPC mix design. The chemical and mechanical properties of the GPC specimens would change with the variation of the curing temperature. In the experimental analysis, to check the effect of curing temperature on the GPC mix design specimens.

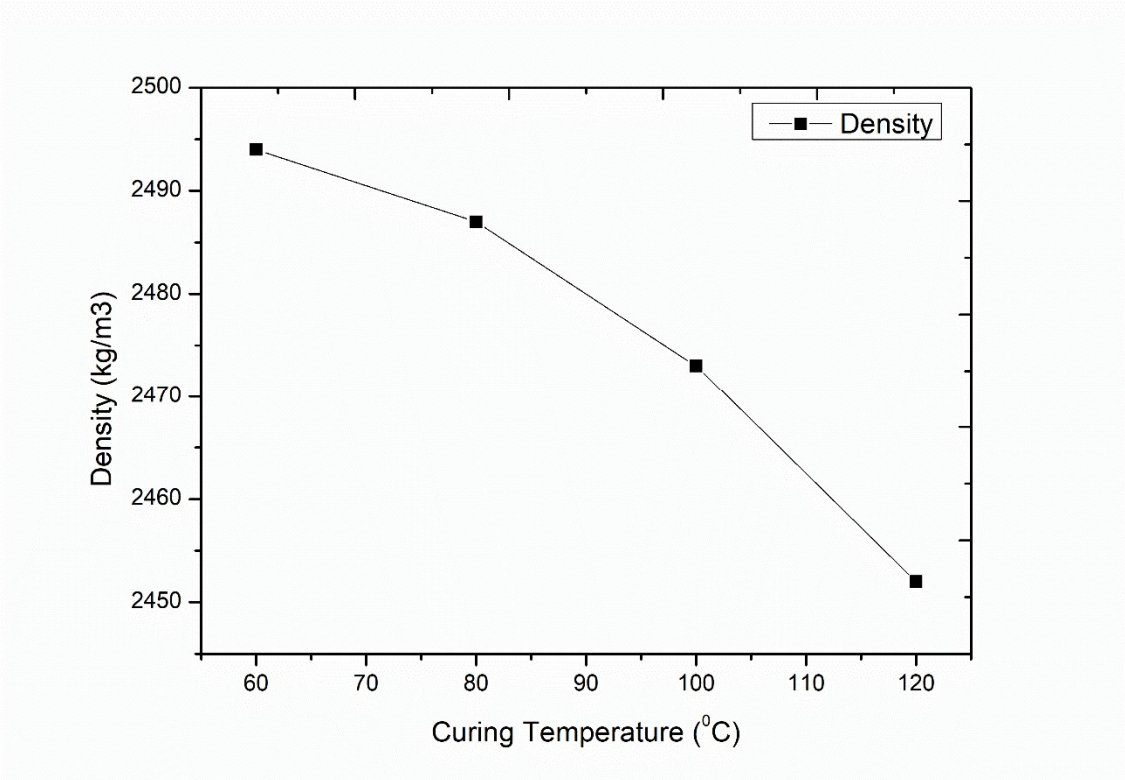

Fig. 4.66 Density variation with curing temperature

4.6.1 Density

The concrete mix specimens' density was measured by the weight of specimens on a digital weighing machine. The density of the GPC mix specimens decreases with the increment of curing temperature because of the evaporation of water present inside the matrix or concrete specimens. Fig. 4.66 shows the graph of density variation with the curing temperature. The maximum density found at the initial curing temperature was 2494 kg/m^3.

4.6.2 Compressive Strength

The compressive strength of the GPC mix design increases with the increment in curing temperature, but it reduces beyond the 100^{0}C curing temperature. The compressive strength increases due to increases in the geopolymerisation rate of the matrix with the increment of curing temperature. Fig. 4.67 describes the variation of compressive strength with the different curing temperatures. It shows that the GPC specimens cured at 100^{0}C got the maximum strength among all other curing temperatures. The maximum strength is 38.2MPa at 28 days, which is cured at 100^{0}C.

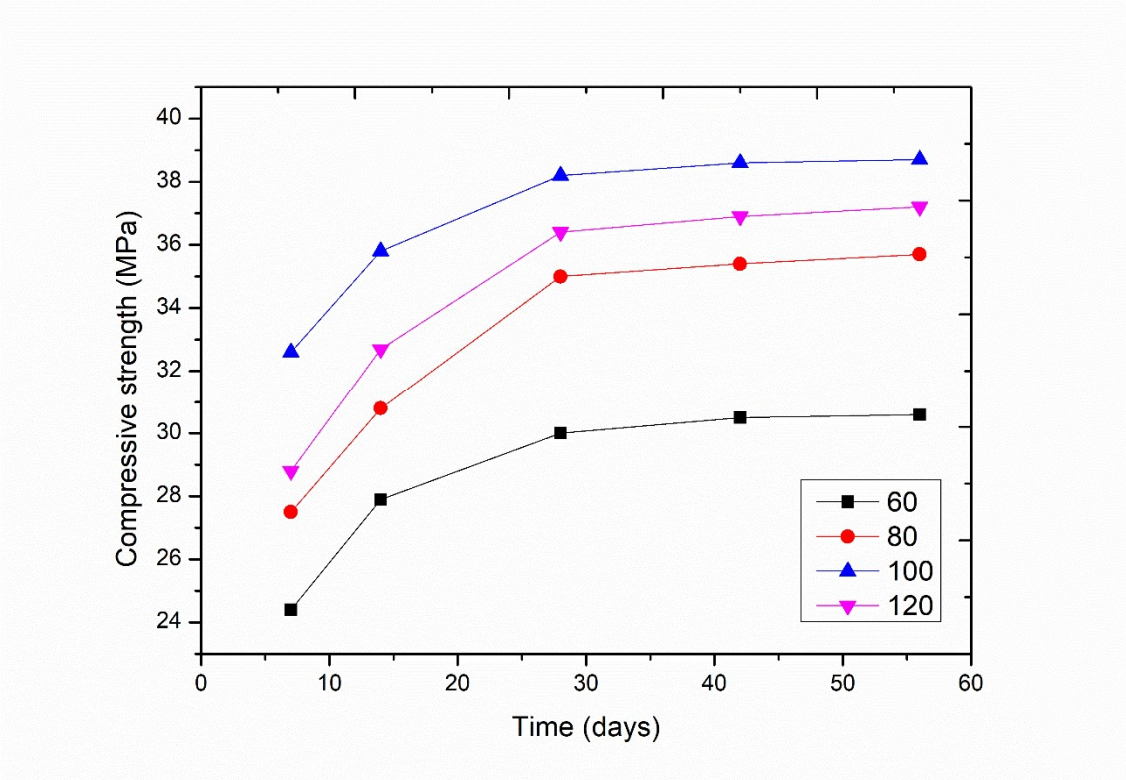

Fig. 4.67 Compressive strength variation with curing temperature

Table 4.56 Compressive strength

Curing Temperature (^{0}C)	7 days	14 days	28 days	42 days	56 days
60	24.4	27.9	30	30.5	30.6
80	27.5	30.8	35.0	35.4	35.7
100	32.6	35.8	38.2	38.6	38.7
120	28.8	32.7	36.4	36.9	40

Table 4.57 Splitting tensile

Curing Temperature (^{0}C)	7 days	14 days	28 days	42 days	56 days
60	3.0	3.7	4.3	4.4	4.5
80	3.4	4.3	5.1	5.2	5.2
100	3.6	4.6	5.3	5.4	5.4
120	3.5	4.4	5.2	5.3	5.3

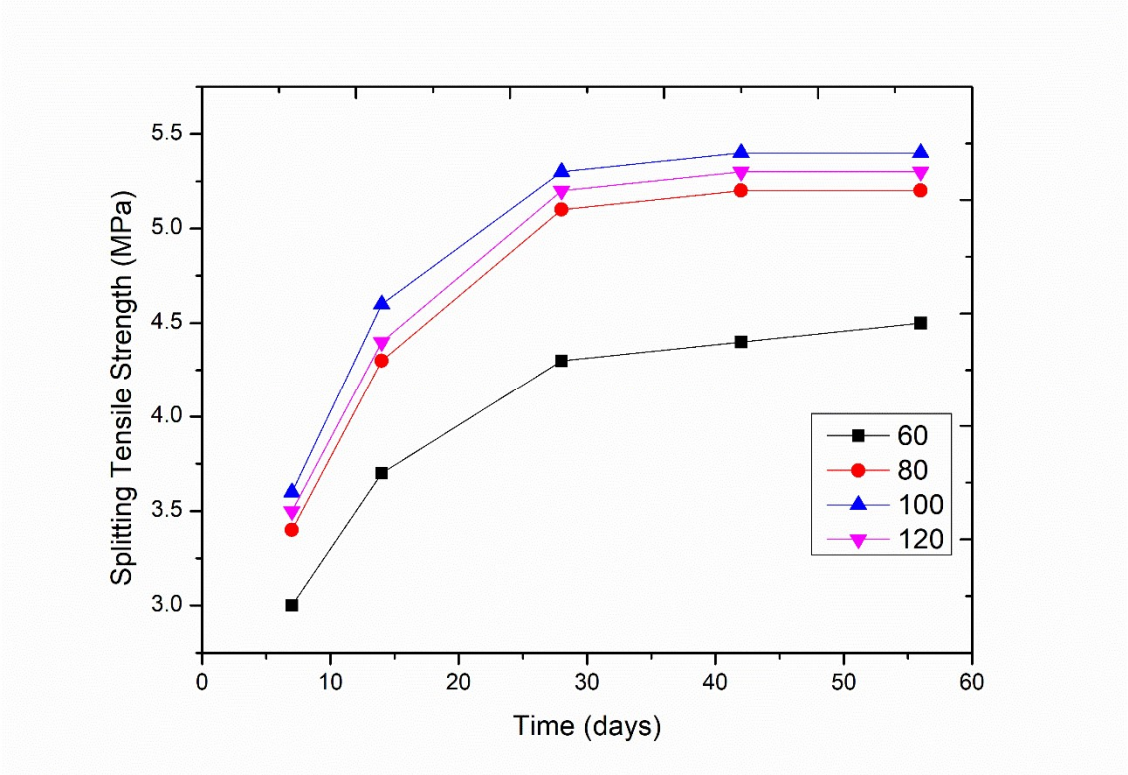

Fig. 4.68 Splitting tensile variation with curing temperature

4.6.1 Splitting Tensile

The splitting tensile strength shows the concrete's indirect tensile, which is tested on the cylindrical specimens. The splitting tensile shows a similar pattern of strength compared to the compressive strength. The GPC specimens cured at 100^0C got the maximum strength among all other curing temperatures. The GPC specimens achieved the optimum point at 100^0C curing temperature, and the maximum splitting tensile at 28 days is 5.3MPa.Fig. 4.68 shows the graph of the splitting tensile of different temperature-cured GPC specimens. The splitting tensile increases with the increment in temperature, but it reduces beyond the 100^0C curing temperature.

4.6.2 Flexural Strength

The flexural strength of the concrete shows the bending tensile strength of the specimens. The flexural strength shows a similar pattern to the compressive strength, and it got 15%-20% of the compressive of the GPC mix design. The GPC specimens reached their optimum point of strength at a 100^0C curing temperature. Fig. 4.69 shows the graph of the flexural strength of the GPC mix at the different curing temperatures. The maximum flexural strength is 5.8MPa at 28 days, which is cured at a 100^0C temperature.

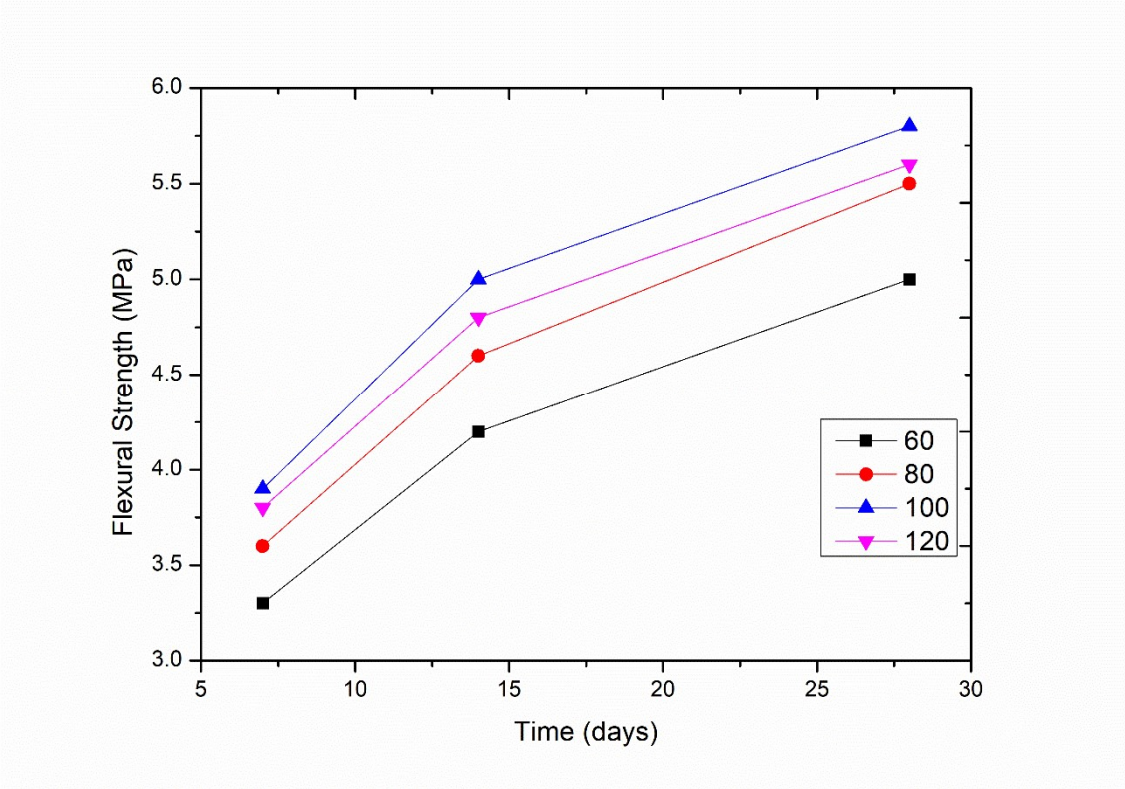

Fig. 4.69 Flexural strength variation with curing temperature

Table 4.58 Flexural strength

Curing Temperature (^{0}C)	7 days	14 days	28 days	42 days	56 days
60	3.3	4.2	5.0	5.2	5.3
80	3.6	4.6	5.5	5.6	5.6
100	3.9	5	5.8	5.9	5.9
120	3.8	4.8	5.6	5.7	5.7

4.6.3 Rebound Strength

The rebound hammer test is one of the non-destructive tests used for the strength check of the hard material's objectives. The rebound strength is based on the surface hardness of the objectives. It strikes on the surface of the specimens and gives the strength value without destruction of the specimens. Fig. 4.70 shows the graph of the rebound strength of the GPC mix designs at various curing temperatures. It increases with the increment of the curing temperature, but it reduces beyond the 100^{0}C curing temperature. It has a 5-10% greater compressive strength than the mixed specimens.The maximum rebound strength is 40MPa at 28 days of testing, which is cured at a 100^{0}C temperature. Table 4.59 illustrates the rebound hammer strength at various curing temperatures with the different test days.

Table 4.59 Rebound strength

Curing Temperature (^{0}C)	7 days	14 days	28 days	42 days	56 days
60	25.4	30.6	32.8	33.3	33.5
80	27.3	32.0	35.9	36.1	36.2
100	33.6	38.4	40	40.4	40.5
120	31.4	36.8	38.6	38.9	39

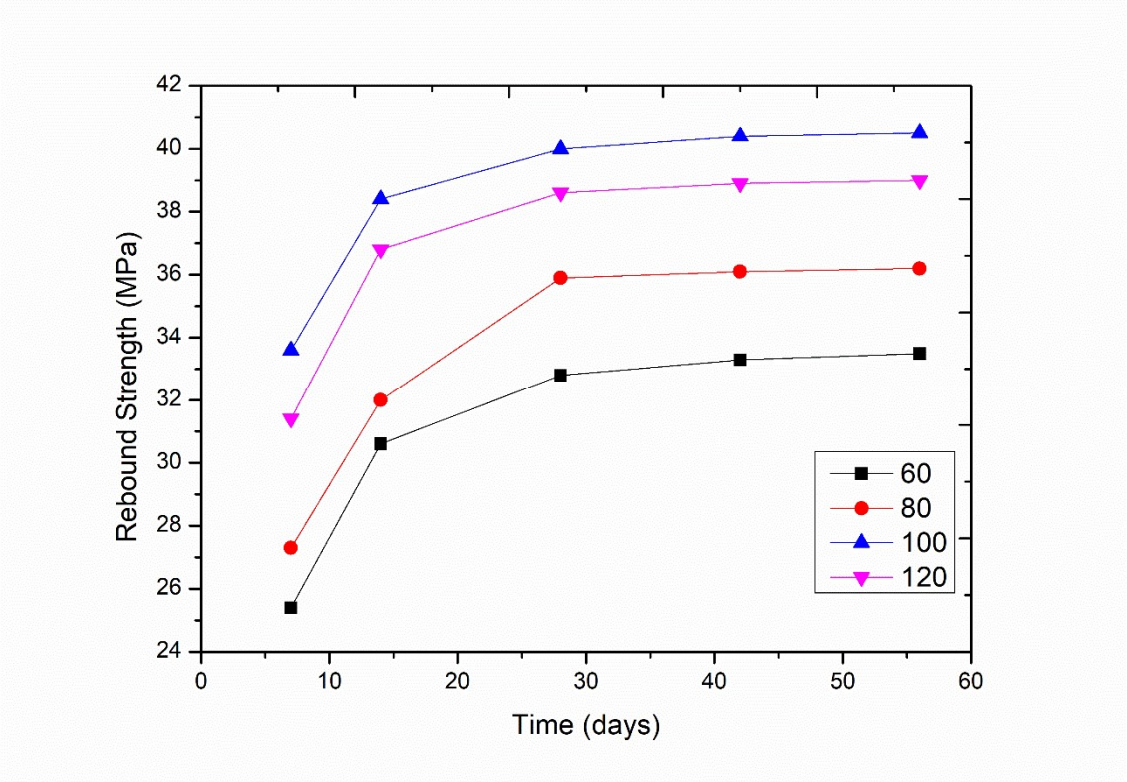

Fig. 4.70 Rebound strength variation with curing temperature

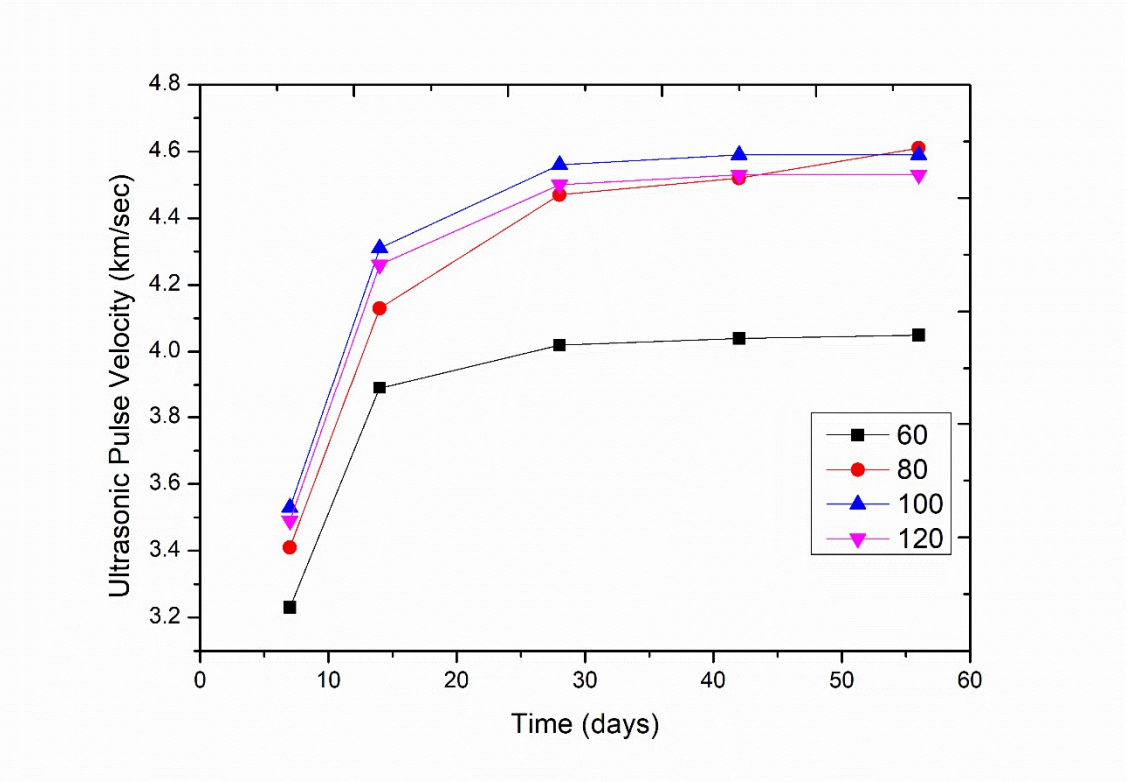

Fig. 4.71 UPV variation with curing temperature

4.6.4 UPV Test

The UPV test is also one of the non-destructive tests for concrete specimens, and it is based on the time passage reading of ultrasonic pulse waves through the objectives. The time passage of the ultrasonic pulse wave increases with the reduction of the objective strength or hardness. The UPV test easily checks the insides of the crack of the objective, and the test was conducted on any size of the specimens. It is very useful in the real field of life for quality assessment of the structure. Fig. 4.71 shows the graph of UPV variations with the curing temperatures. The UPV increases with the increment in curing temperature, but it reduces beyond the 100^0C curing temperature. The maximum UPV is 4.56km/sec at 28 days, which is cured at a 100^0C temperature. Table 4. 60 illustrates the UPV at various curing temperatures with the different test days.

Table 4.60 UPV of GPC specimens

Curing Temperature (^{0}C)	7 days	14 days	28 days	42 days	56 days
60	3.23	3.89	4.02	4.04	4.05
80	3.41	4.13	4.47	4.52	4.61
100	3.53	4.31	4.56	4.59	4.59
120	3.49	4.26	4.50	4.53	4.53

4.6.5 Modulus of Elasticity

The modulus of elasticity of the concrete is an essential mechanical property of the mix design. It is calculated and tested on the cylindrical specimens as per the IS code. The modulus of elasticity directly depends on the compressive strength of the concrete. Fig. 4.72 shows the variation of modulus of elasticity with the curing temperature of the specimens. It increases with the increment of the curing temperature, but it reduces beyond the 100^0C curing temperature. The maximum modulus of elasticity is 24.5GPa at 28 days after the casting, which is cured at a 100^0C temperature. Table 4.61 illustrates the density, poison ratio, and modulus of elasticity of various cures.

Table 4.61 Poissons ratio, density, and MOE of GPC

Mix Design	Density in Kg/m^3	Poisson Ratio	Modulus of Elasticity in GPA
60	2494	.15	23.6
80	2487	.14	24
100	2473	.14	24.5
120	2452	.13	24.2

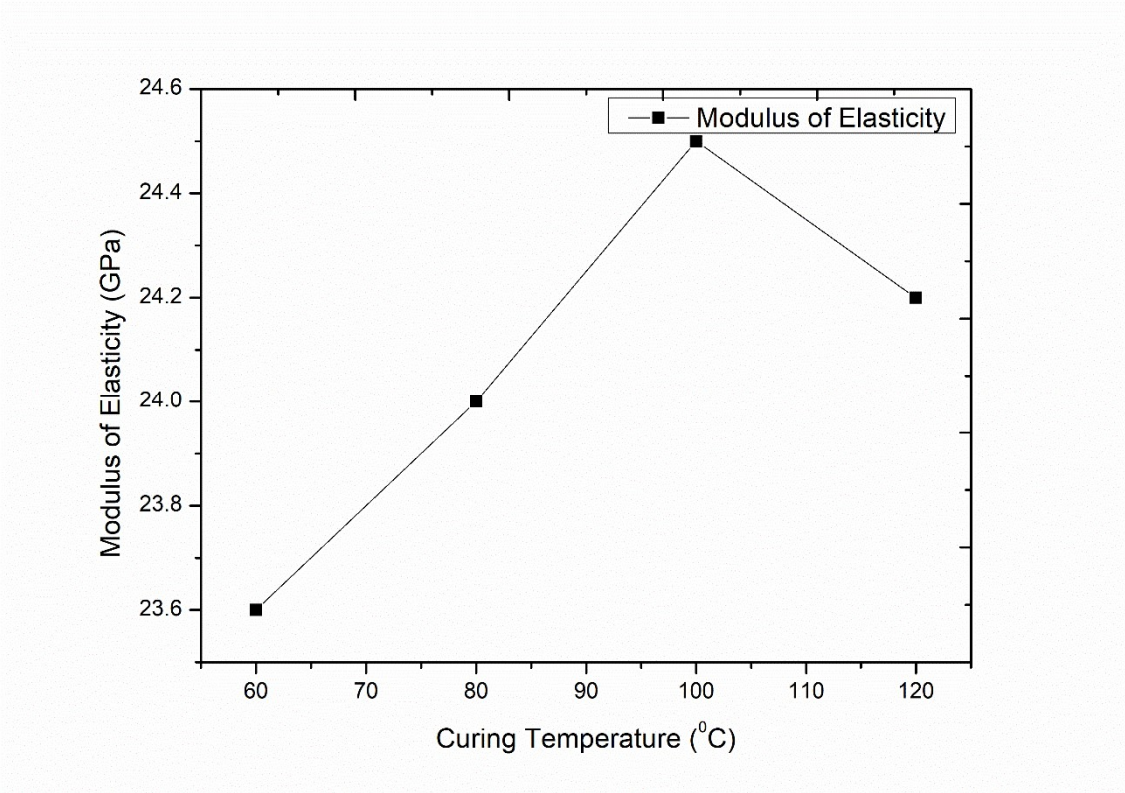

Fig. 4.72 MOE variation with curing temperature

4.7 Effect of elevated temperature

The elevation of the temperature was conducted in the muffle furnace with full control of temperature stability and rate of increment of temperature with time. The OPC concrete and GPC specimens are put in the muffle furnace for 2 hours at a specific controlled elevated temperature ranging from 100^{0}C to 800^{0}C, in which the rate of increment of temperature is 10^{0}C/minute. After the exposure to elevated temperature, the specimens were tested for mass loss, UPV, and compressive strength.

4.7.1 Mass loss

Fig. 4.73 shows the graph of the density variation of both types of concrete specimens after 100^0C, 200^0C, 300^0C, 400^0C, 500^0C, 600^0C, 700^0C, and 800^0C exposure to elevated temperatures, which shows that the density of both concrete specimens gets lower after the increment of exposure temperature, whereas the OPC concrete specimens spall after 500^0C temperature exposure [156]. Furthermore, Fig. 4.74 shows the mass loss of both concrete specimens after exposure to various elevated temperatures from 100^0C to 800^0C, which shows that both concrete specimens' mass losses increase with the increment of exposure to elevated temperatures, whereas the OPC concrete specimens fail after 500^0C. The mass loss of GPC specimens after 800^0C exposure temperature is around 12% of the original, whereas the OPC concrete specimens fail at 600^0C and show around 7% mass loss after 500^0C exposure. It concludes that the GPC specimens are more stable at elevated temperatures.

The high-temperature effect severely damages the solid matrix of the geopolymer, and rising temperatures accelerate the growth of fractures and the loss of compressive strength leading to matrix void formation. When the temperature rises, a dehydration reaction occurs, in which moisture travels towards the sample surface and exits, causing internal damage to the microstructure and, as a result, weight loss in the geopolymer composite [20]. Due to free water and structured water, weight loss in the geopolymer sample happens fast during the early stages of heating [157].

Table 4.62 Mass loss of both concrete

Exposure Temperature (^{0}C)	Mass loss (%)	
	Geopolymer concrete	OPC concrete
100	0.8	0.26
200	2.4	2.05
300	4.3	5.11
400	8.7	5.78
500	9.2	7.2
600	10.3	Fail
700	11.1	-
800	12.1	-

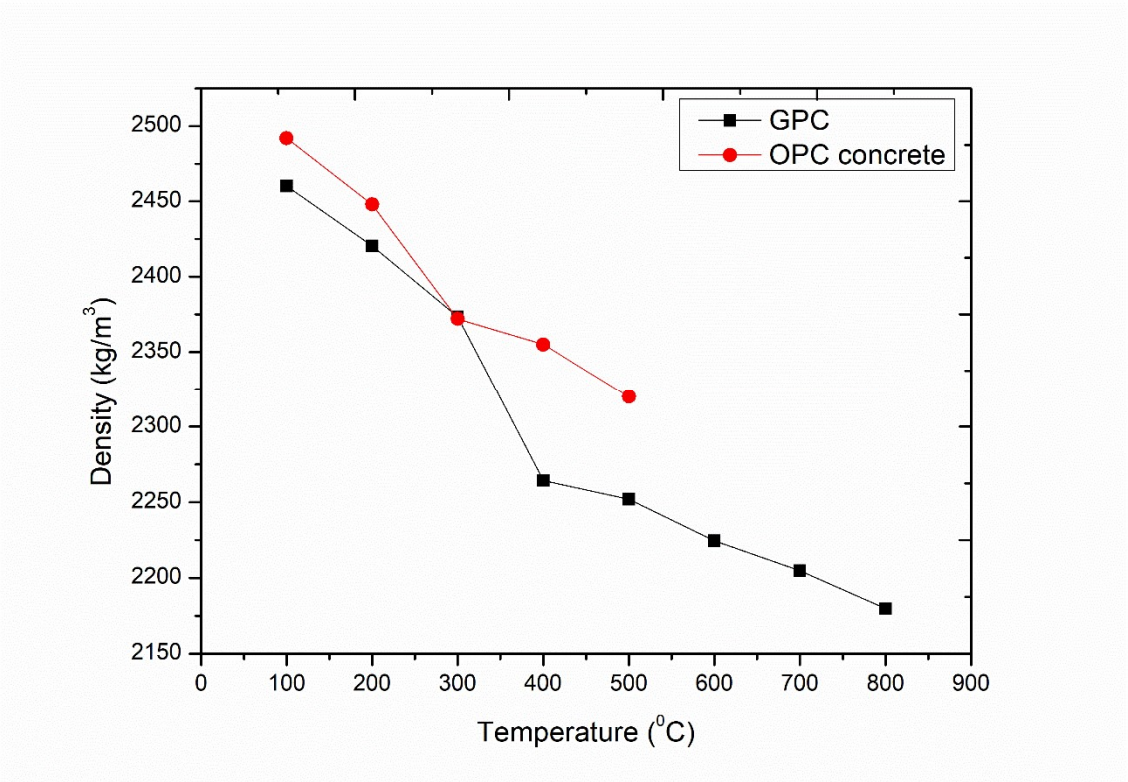

Fig. 4.73 Density variation with the temperature

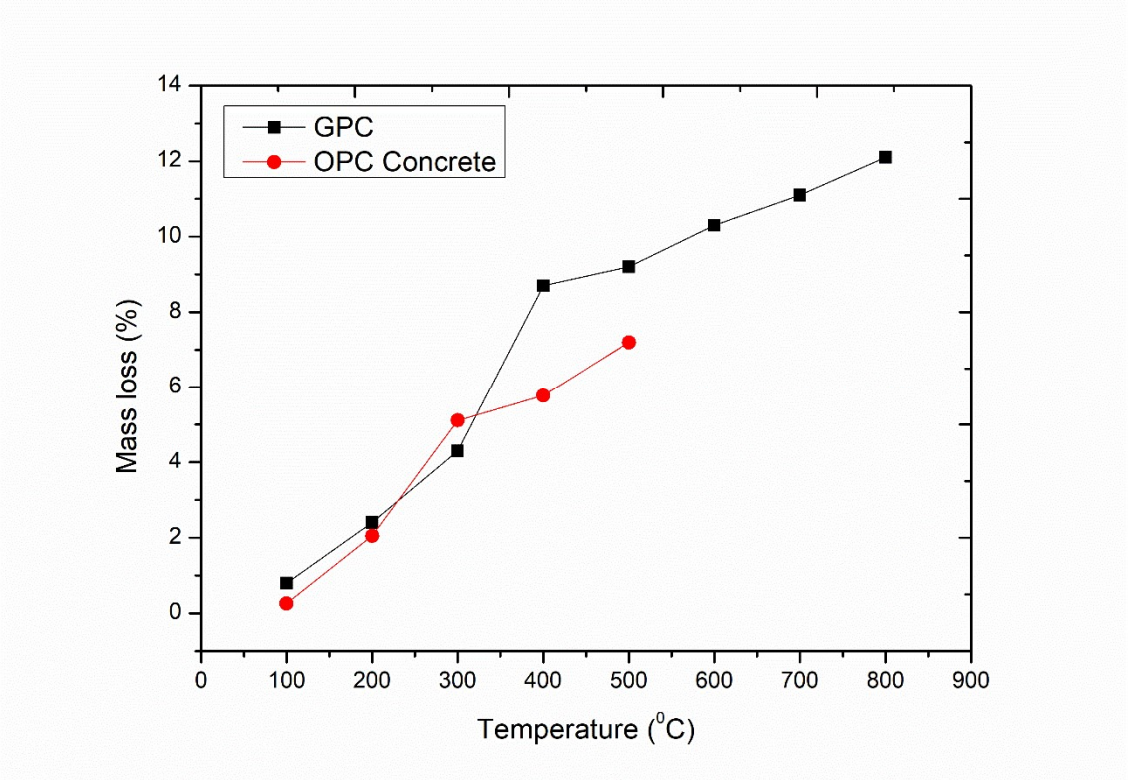

Fig. 4.74 Mass loss variation with the temperature

4.7.2 Ultrasonic pulse velocity test (UPVT)

The UPVT is a non-destructive test used to identify the quality of materials via passing ultrasonic pulse velocity [155]. Fig. 4.75 shows the graph between the UPV and exposure of elevated temperature of both concrete specimens, which shows that the UPV of GPC specimens initially increases up to 200^0C exposure temperature, whereas the OPC concrete specimens UPV increases up to 100^0C exposure temperature, and after these exposure temperatures the degradation of the specimens continuously. The GPC specimen UPVs are slightly lower than the conventional concrete specimens in the initial up to 100^0C exposure, but they go higher after that. The OPC concrete specimens failed at the 600^0C exposure temperature, whereas the GPC specimens failed at the 800^0C exposed temperature. Table 4.62 illustrates the mass loss of both concretes after various temperature exposures.

The sample pore structure and water evaporation in the matrix both increase as the temperature rises. As a result of the mass loss, more voids emerge. As a result of the additional voids, the ultrasonic pulse velocity is reduced [158]. Furthermore, the production of microfractures was expedited by greater temperature effects, the density of the composites was lowered, the propagation duration of ultrasonic velocity waves was extended, and lower UPV values were generated. Due to the melting of fibres in matrix composites and the formation of tiny channels over 300^0C, lower UPV values were also generated [159].

4.7.1 Compressive strength

The compressive strength of the GPC and conventional concrete specimens were tested after 100^0C, 200^0C, 300^0C, 400^0C, 500^0C, 600^0C, 700^0C, and 800^0C exposure to elevated temperature. Fig. 4.76 shows the compressive strength variation of both concrete specimens after exposure to elevated temperatures. The compressive strength of the conventional concrete specimens is higher than the GPC specimens at 100^0C, but it gets lower beyond the 100^0C exposure temperature. The GPC specimens are strengthened up to a 200^0C exposure temperature, but they degrade continuously beyond this. Fig. 4.77 shows the graph between the residual compressive strength variation of concrete specimens with elevated temperature exposure. The GPC and conventional specimens

failed after 600^0C and 800^0C exposure temperatures, respectively. The GPC specimens retained the 60% compressive strength of the original after 700^0C temperature exposure, whereas the OPC concrete specimens retained their 52% compressive strength of the original after 500^0C temperature exposure. Thus, the GPC specimens show higher resistance to elevated temperatures than conventional concrete specimens. Table 4.63 illustrates the residual compressive strength of both concrete after various elevated temperature exposures.

Due to evaporation of water and dehydration of the geopolymer matrix, melting of the fibres due to high temperature, and the thermal response mechanism of free water evaporation, the geopolymer composites' strengths were considerably lowered by a temperature range 600^0C to 900^0C [160]. The compressive strength of the geopolymer paste and mortar is substantially higher than that of the LWAGC. Because of the low strength and porous morphology of the LWA, which weakens the LWAGC structure, the strength of LWAGC was predicted to be significantly lower than that of geopolymer paste and mortar [161]. Flexural strength decreased more than compressive strength in the geopolymer mortar sample due to the high-temperature effect. Flexural strength was more susceptible to developing internal microstructure flaws, such as crack propagation and the formation of porous structures, at high temperatures [162]. Compressive strength losses in fiberless geopolymer samples varied from 31.07% to 86%, whereas in polypropylene fibrous geopolymer samples, this rate increased slightly and ranged from 32.07% to 86.54%. Flexural strength losses in fiberless geopolymer samples varied from 49.19% to 84.95%, while in polypropylene fibrous samples, this rate was reduced and ranged between 43.91–84.60%. The purpose of incorporating fibre into cement or geopolymer mortar is to improve flexural strength and toughness [57,163]. Polymer fibres are a common type of material used to reinforce geopolymer composites, and it has been proven that fibres may significantly increase the geopolymer's flexural strength and toughness [164–168].

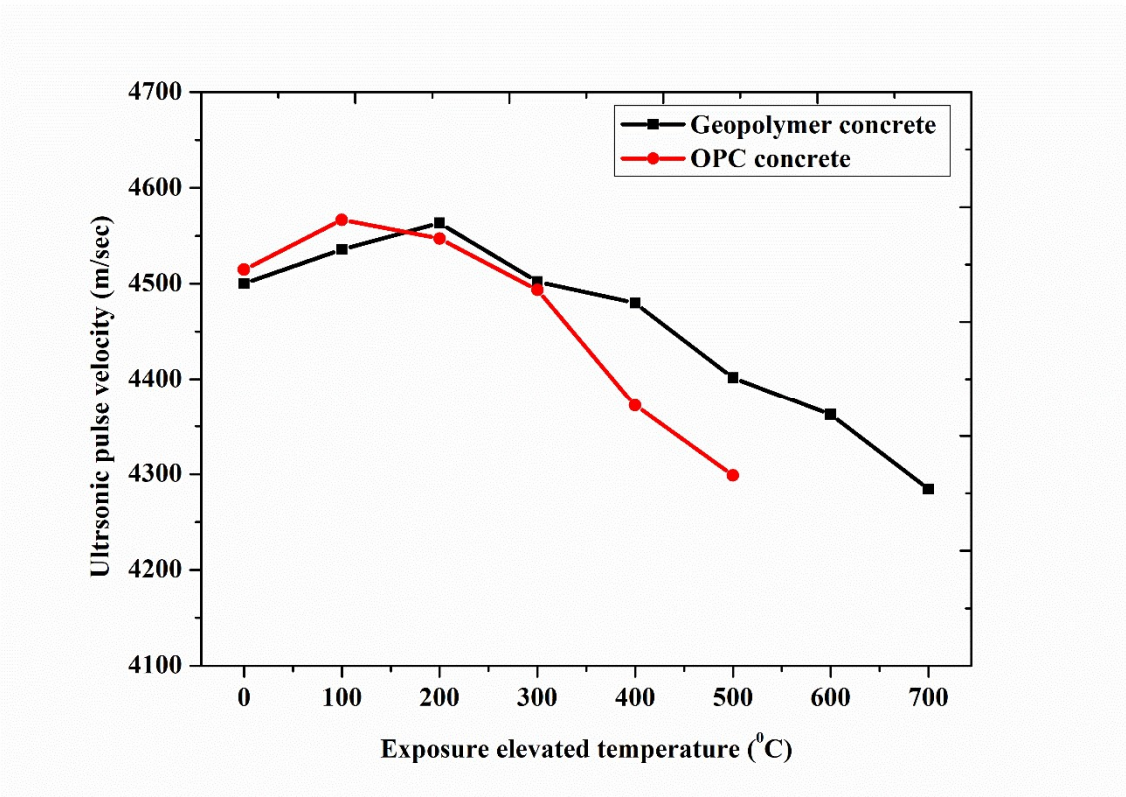

Fig. 4.75 UPV variation with exposure temperature

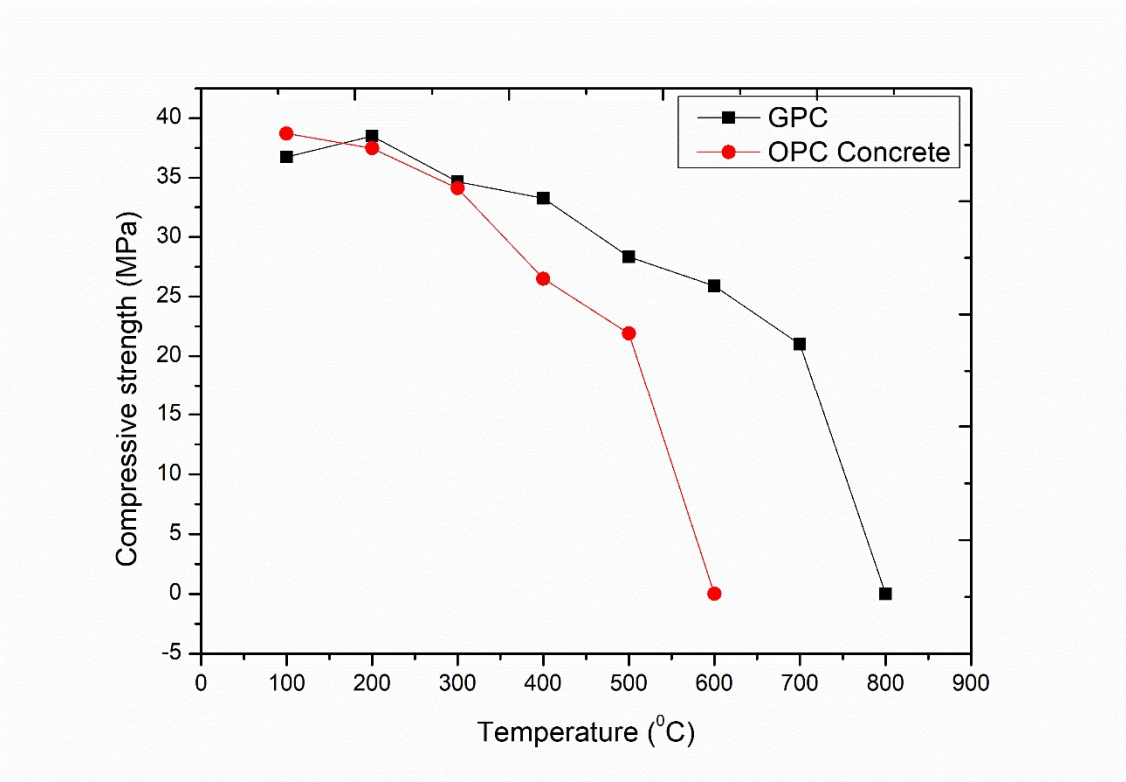

Fig. 4.76 Compressive strength variation with the temperature

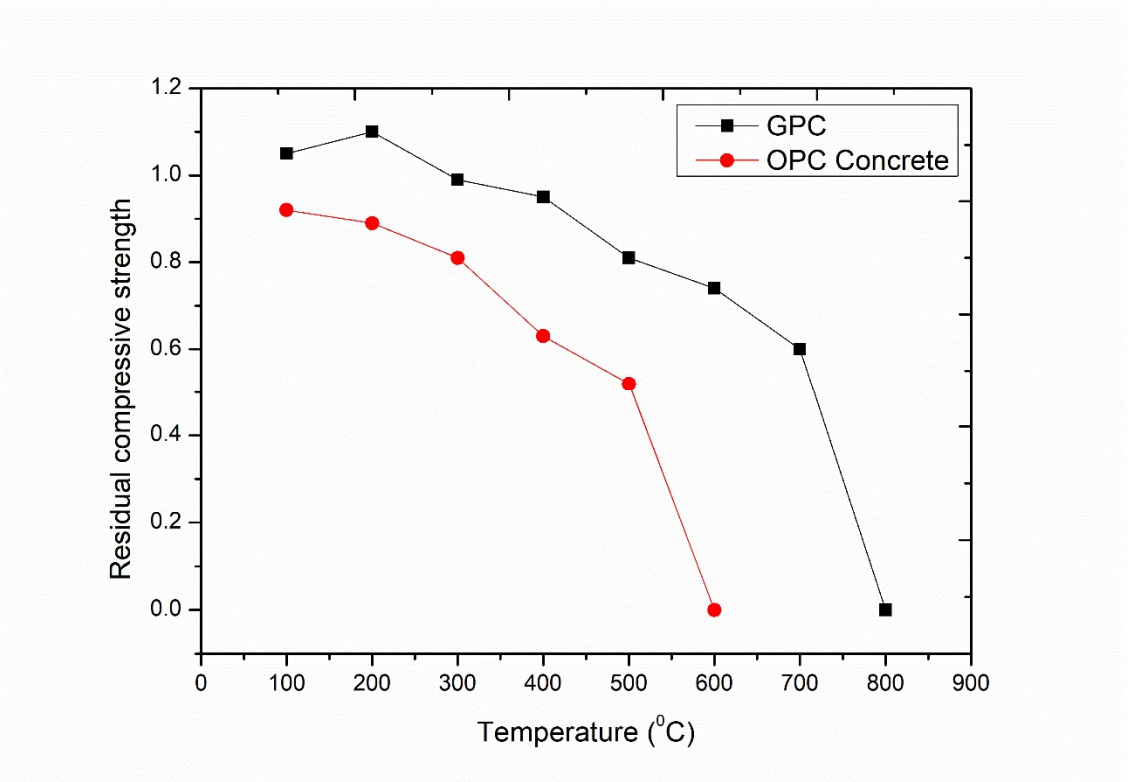

Fig. 4.77 Residual compressive strength variation with the temperature

Table 4.63 Residual compressive strength

Exposure Temperature (°C)	Residual compressive strength (%)	
	Geopolymer concrete	OPC concrete
100	105	92
200	110	89
300	99	81
400	95	633
500	81	52
600	74	Fail
700	60	-
800	Fail	-

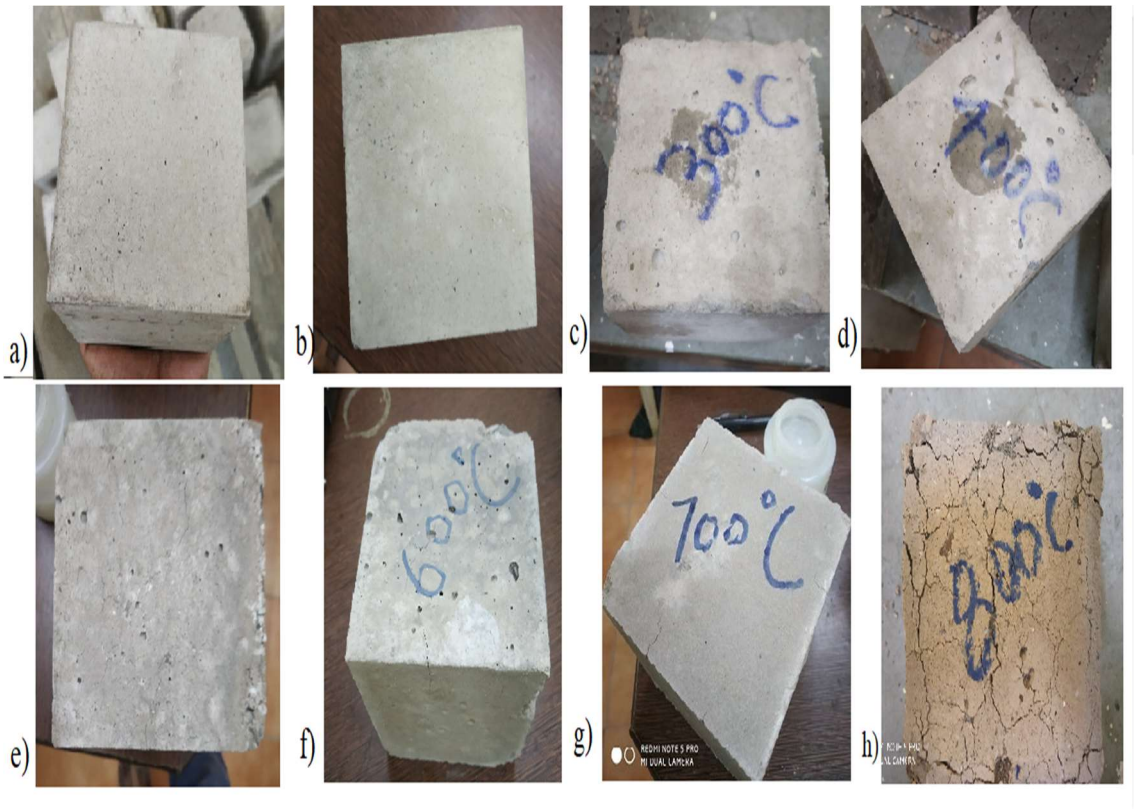

Fig. 4.78 Picture of cubes after exposure to elevated temperature

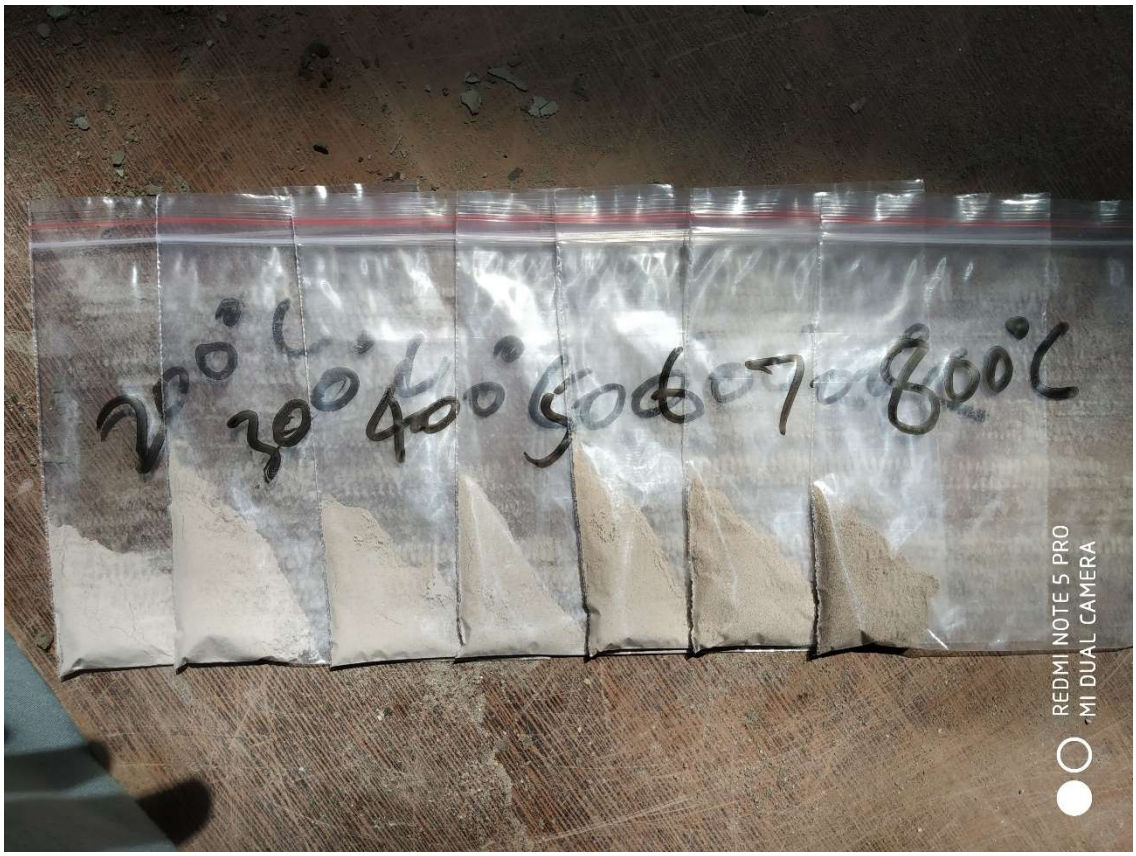

Fig. 4.79 Picture of various temperature exposure Geopolymer matrix

4.7.2 Visual inspection

The visual inspection clears the effect of elevated temperature exposure to concrete cubes for 2 hours in a muffle furnace. Fig 4.78 depicts the cube GPC specimens' pictures after exposure to elevated temperatures from 100^0C to 800^0C, which shows that the GPC specimens fail at 800^0C temperature exposure. Fig. 4.79 depicts the geopolymer matrix powder after exposure to an elevated temperature, which shows that the geopolymer matrix darkens with the increment of exposure temperature. The cracks develop with the increment of exposure temperature due to evaporation of the hygroscopic water inside the GPC matrix.

4.8 Effect of seawater condition

The seawater condition means making a saline solution like seawater as per the ASTM code in the laboratory. GPC and conventional concrete specimens were put in the solution for a long duration. The specimens for both GPC and conventional concrete tests for a weight check, UPVT, and compressive strength analysis after 6 weeks, 12 weeks, 18 weeks, and 24 weeks were put into the solution.

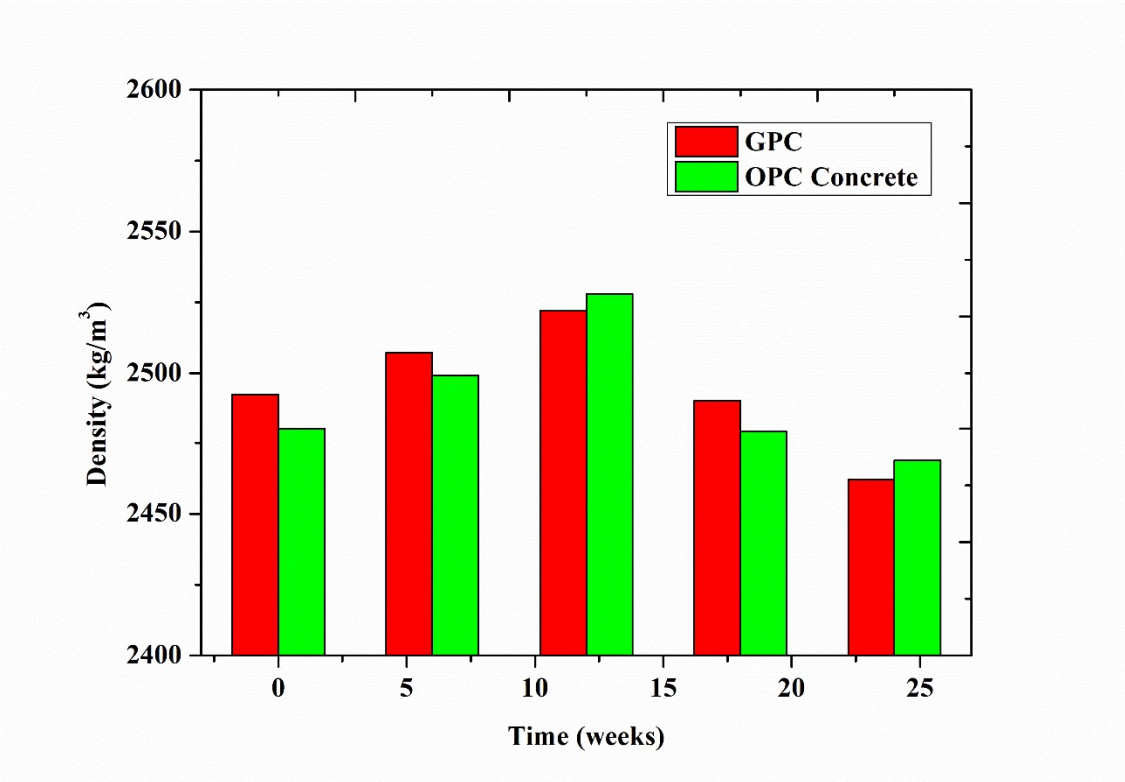

Fig. 4.80 Graph between the density vs seawater immersion time

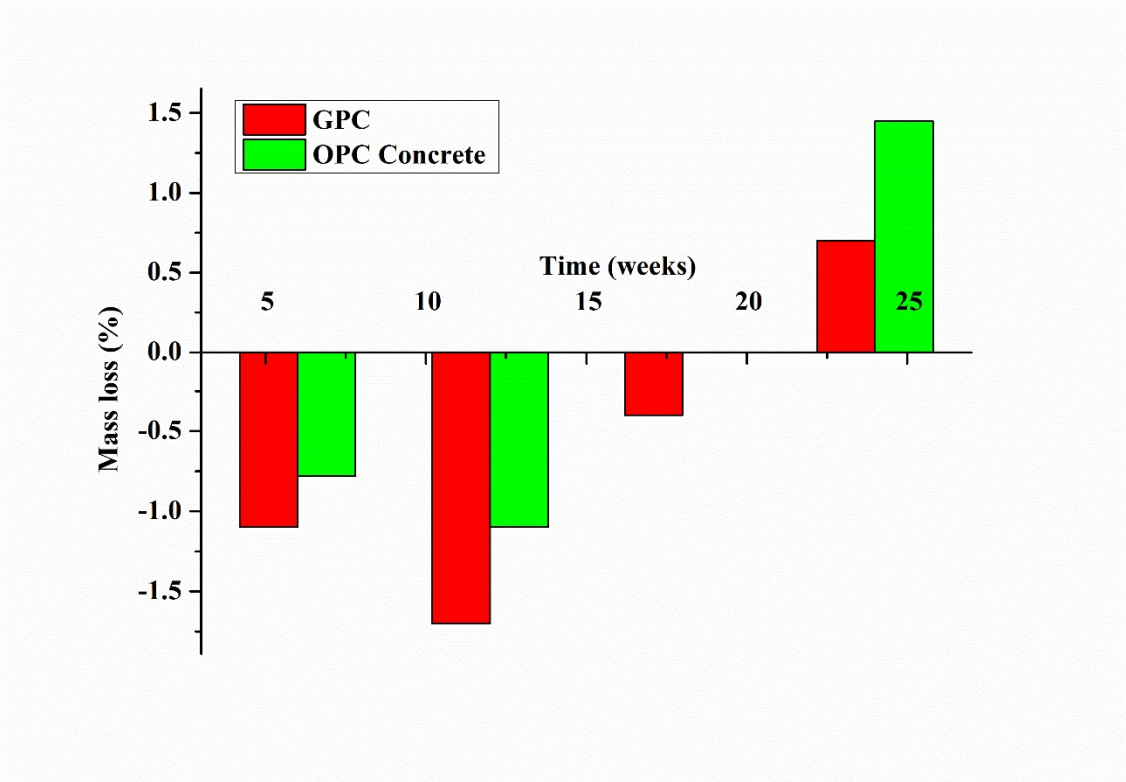

Fig. 4.81 Graph between mass loss vs seawater immersion time

4.8.1 Mass loss

Fig. 4.80 shows the graph of the density variation of both types of concrete specimens after 6 weeks, 12 weeks, 18 weeks, and 24 weeks in seawater. It shows that the density of GPC specimens is higher than conventional concrete after 6 weeks and decreases after 24 weeks. Furthermore, Fig. 4.81 shows the mass loss of both concrete specimens after putting in the seawater condition solution after 6 weeks, 12 weeks, 18 weeks, and 24 weeks, which shows that both concrete specimens initially increase their mass or weight up to 12 weeks. Then, in both concrete specimens, mass loss starts continuously. As a result, the mass loss of the OPC concrete specimens is greater than that of the GPC specimens, and the GPC specimens are more stable in seawater conditions.

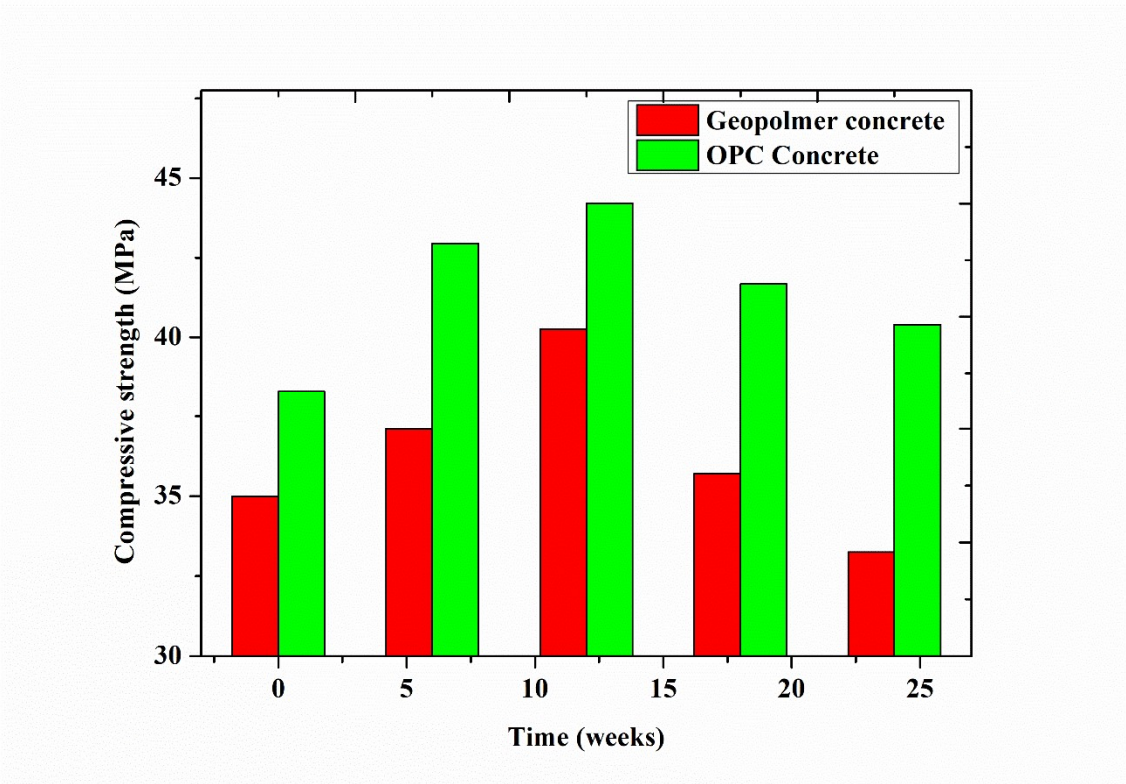

Fig. 4.82 Graph between compressive strength vs seawater immersion time

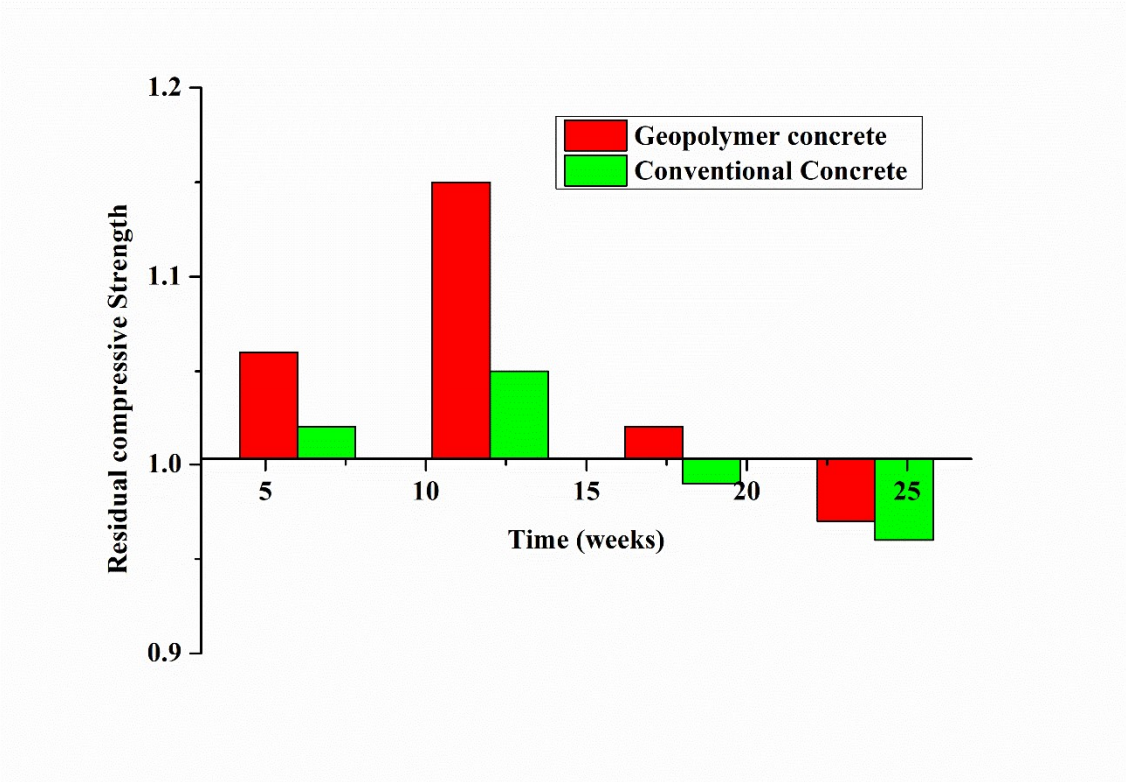

Fig. 4.83 Graph between residual compressive strength vs seawater immersion time

4.8.2 Compressive strength

The compressive strength of the GPC and conventional concrete specimens were tested after 6weeks, 12weeks, 18weeks, and 24weeks after putting in the seawater solution. Fig. 4.82 shows the compressive strength variation of both concrete specimens after merging into a seawater solution for a long duration. The compressive strength of the conventional concrete specimens is higher than GPC specimens after merging into the seawater solution for 24 weeks. Initially, both concrete specimens strengthened up to 12 weeks of immersion in the seawater solution, then strengthened afterward. Fig. 4.83 shows the graph of the residual strength variation of both concrete specimens with the immersion time. The GPC and conventional specimens were strengthened after immersion in the seawater solution for up to 12 weeks, with the GPC specimens being stronger than the conventional concrete specimens. However, both concrete specimens degraded continuously after 12 weeks. Thus, the GPC specimens show higher resistance than conventional concrete specimens against seawater conditions. Adam (2009) stated that the fly ash-based geopolymer concrete's durability characteristics. The investigation revealed the strength and durability of GPC in terms of carbonation, chloride resistance and the impact of the Na_2O dose on GPC sample compression.

wo important criteria for the synthesis of GPC are the Na_2O dose and the activators module. It has been proven to have a strength similar to OPC concrete, based on fly ash geopolymer concrete. However, in terms of carbonation and chloride resistance, it is superior to OPC concrete, the fly ash-based geopolymer concrete [169]. In 2% H_2SO_4, 5% NaCl and 5% Na_2SO_4 solutions, geopolymer concretes were shown to be more durable. There is still a considerable knowledge gap in relation to geopolymerisation, strength and durability problems [170].

4.8.3 Ultrasonic pulse velocity test (UPVT)

The UPVT is a non-destructive test used to identify the quality of materials via passing ultrasonic pulse velocity. Fig. 4.84 shows the graph between the UPV and exposure time of both concrete specimens in seawater conditions. The GPC specimen UPVs are a little bit lower than the conventional concrete specimens. However, it shows a similar pattern to the compressive strength graph, which shows it initially increases up to 12 weeks of exposure and continuously degrades.

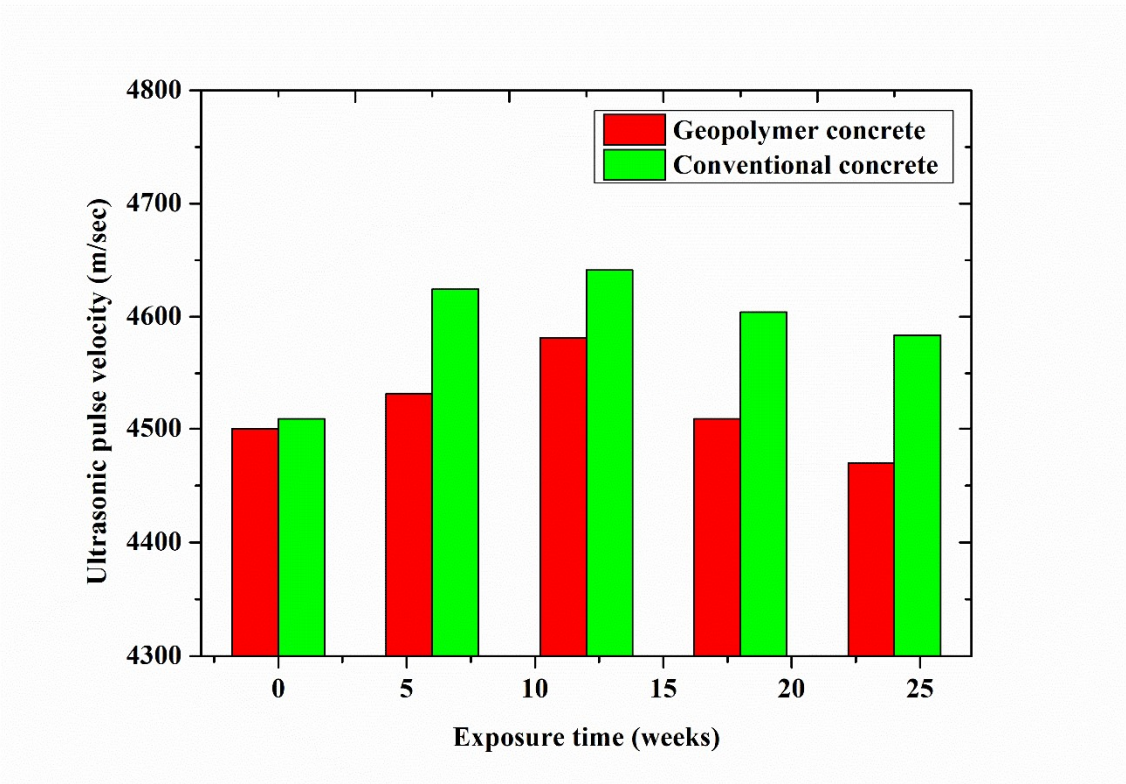

Fig. 4.84 Graph between UPV vs seawater immersion time

4.9 Effect of sulphate attack

The sulphate attack entails creating a sulphate solution in the laboratory by combining sodium sulphate or magnesium sulphate with tap water according to the ASTM code. Two types of sulphate solution were made in the laboratory using sodium sulphate and magnesium sulphate separately. The GPC and conventional concrete specimens were put in the solution for a long duration. The specimens for both GPC and conventional concrete tests for a weight check, UPVT, and compressive strength analysis after 6 weeks, 12 weeks, 18 weeks, and 24 weeks were put into the sulphate solution.

4.9.1 Mass loss

The density and mass are found through the weight of the specimens after their immersion in the sulphate solution. Fig. 4.85 shows the graph between the density variation of both concrete specimens with the exposure time in the sodium sulphate solution, showing that the OPC concrete specimen density is higher than GPC specimens up to 12 week immersion lowers after it. Fig. 4.86 shows the graph between the mass loss of both concrete specimens with the exposure time in the sodium sulphate solution, which shows that both concrete specimens gain in mass up to 12 weeks and then degrade

continuously. The GPC specimens show higher stability against the sulphate solution water and show less mass loss in sulphate attack than conventional concrete specimens.

Fig. 4.87 shows the graph of density variation with the exposure time in the magnesium sulphate solution, which shows that the GPC specimens have higher resistance than conventional concrete against the magnesium sulphate attack for a long duration. In the initial test, both concrete specimens strengthened up to 12 weeks of exposure to magnesium sulphate solution, but beyond that 12 week exposure, the density continuously degraded. Fig. 4.88 shows the graph between mass loss with the exposure time in the magnesium sulphate solution, which shows that the GPC specimens have higher resistance than conventional concrete against the magnesium sulphate attack for a long duration. Both concrete specimen mass and weight increase up to 12 weeks of exposure to magnesium sulphate, and after that it reduces continuously and shows the mass loss of GPC and conventional concrete specimens are 1.7% and 2.4%, respectively, after exposure of 24 weeks.

Magnesium causes the decalcification of the phases of Ca-rich gel present in the mixed slag/flyash system, leading the binder system to degrade and gypsum to precipitate. Magnesium sulphate attack products are weakly cohesive and expansive, resulting in dimensional instability and mechanical performance loss. On the other hand, immersion of Na_2SO_4 geopolymer pastes does not lead to any apparent binder breakdown, and there is no conversion into sulphate-containing precipitates of the Binder phase components [171]. Karthik et al. (2017) reported that the minimal sulphate and chloride attack loss of weight and strength is in relation to conventional concrete. After 90 days, the highest weight loss was 0.68% in 5% sodium sulphate and 5% chloride solutions, 0.51% in weight, and strength dropped 2.95% in 1,33% of all bio-additives in geopolymer specimens [172].

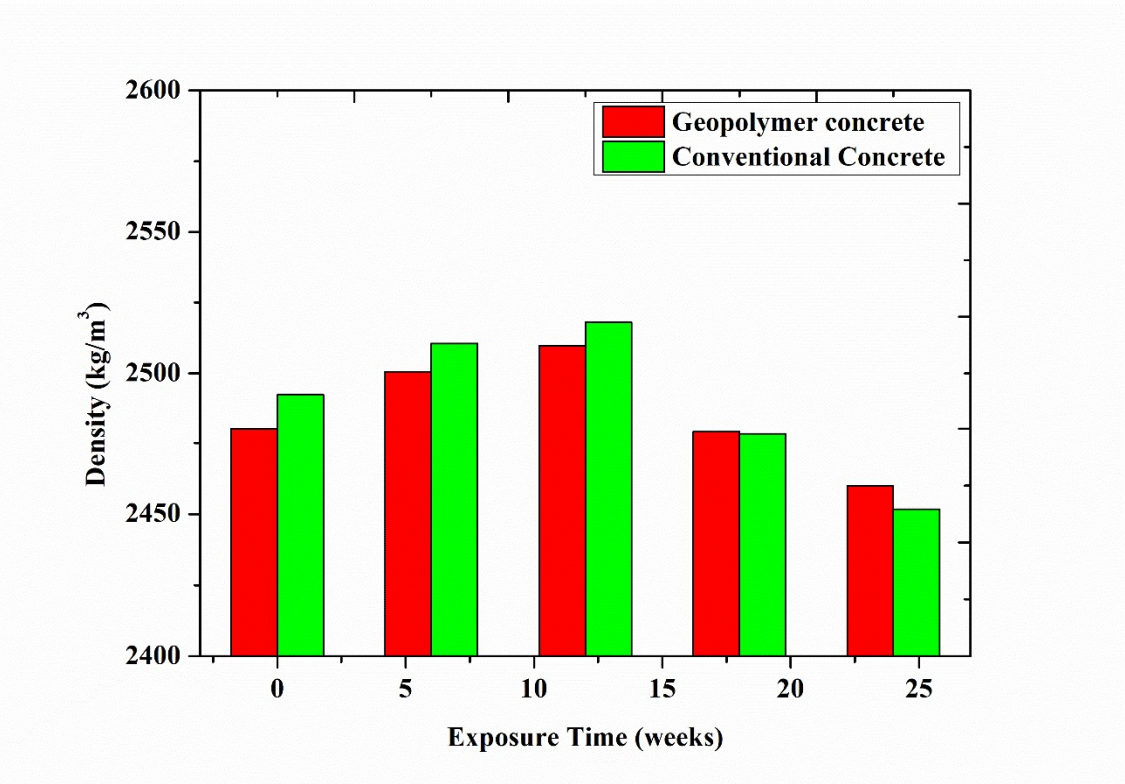

Fig. 4.85 Graph between density vs exposure time

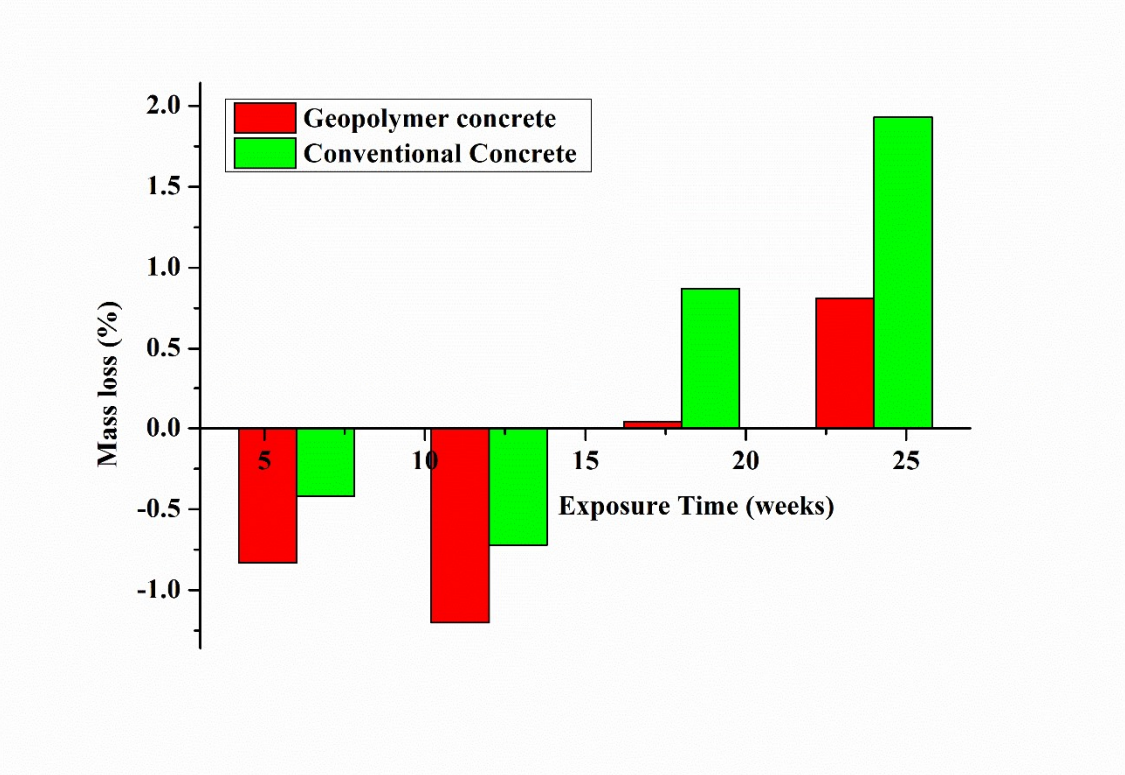

Fig. 4.86 Graph between mass loss vs exposure time

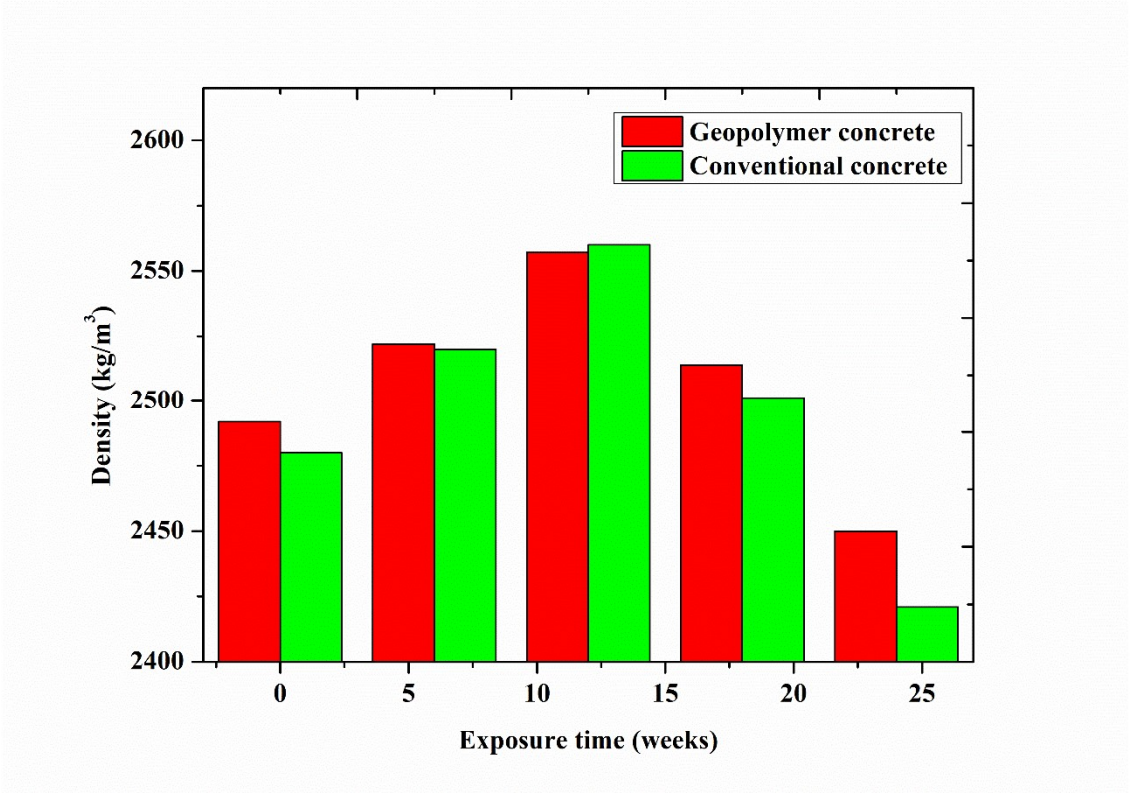

Fig. 4.87 Graph between density vs exposure time

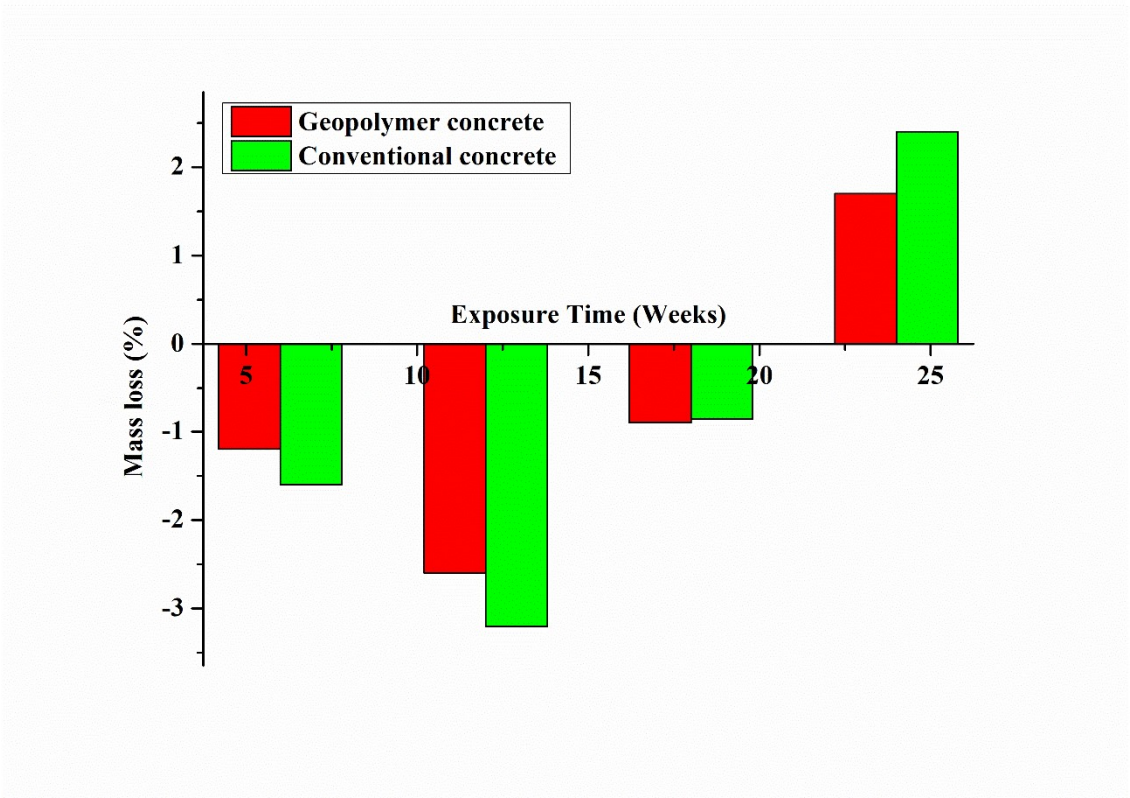

Fig. 4.88 Graph between mass loss vs exposure time

4.9.2 Compressive strength

The compressive strength of the GPC and conventional concrete specimens were tested after 6 weeks, 12 weeks, 18 weeks, and 24 weeks after putting them in the sodium sulphate solution. Fig. 4.89 shows the compressive strength variation of both concrete specimens after merging into a sodium sulphate solution for a long duration. The compressive strength of the conventional concrete specimens is higher than GPC specimens after merging into the sodium sulphate solution for 24 weeks. Initially, both concrete specimens strengthened up to 12 weeks of immersion in the solution after the compressive strength was degraded. Fig. 4.90 shows the graph of residual strength variation of both concrete specimens with the immersion time. The GPC and conventional specimens got more strength after immersion in the sodium sulphate solution for up to 12 weeks, whereas the GPC specimens were stronger than conventional concrete specimens; then, after 12 weeks, both concrete specimens got degraded continuously. Thus, the GPC specimens show higher resistance than conventional concrete specimens against seawater conditions. Fig. 4.91 shows the graph between the compressive strength variation of both concrete specimens with the exposure time in the magnesium sulphate solution, which shows that the compressive strength of the GPC specimens is higher than conventional concrete specimens after merging into the magnesium sulphate solution for 24 weeks. Fig. 4.92 describes the graph between residual compressive strength vs exposure time in magnesium sulphate solution of concrete specimens, which shows that the GPC specimens are more resistant to conventional concrete specimens. The GPC specimens retained 94% compressive strength, whereas the conventional concrete specimens retained 86% compressive strength after 24 weeks of exposure to the magnesium sulphate solution.

There are some variations in GPC and OPC concrete's compressive strength and exposure to 5% from Na_2SO_4 and $MgSO_4$, which might be associated with the alkaline transition from geopolymers to solutions. Compared to those produced with a sodium silicate activator, the test findings of GPC with sodium hydroxide are more crystalline. Only better than OPC concrete was the geopolymer concrete activated with the NaOH solution. GPC strength and durability have risen throughout time, irrespective of the type of chemical solution in which samples were taken into consideration [173–175].

With an increase in the amount and exposure period of $MgSO_4$, both geopolymer and OPC-based concrete samples lost their compression strength [176].

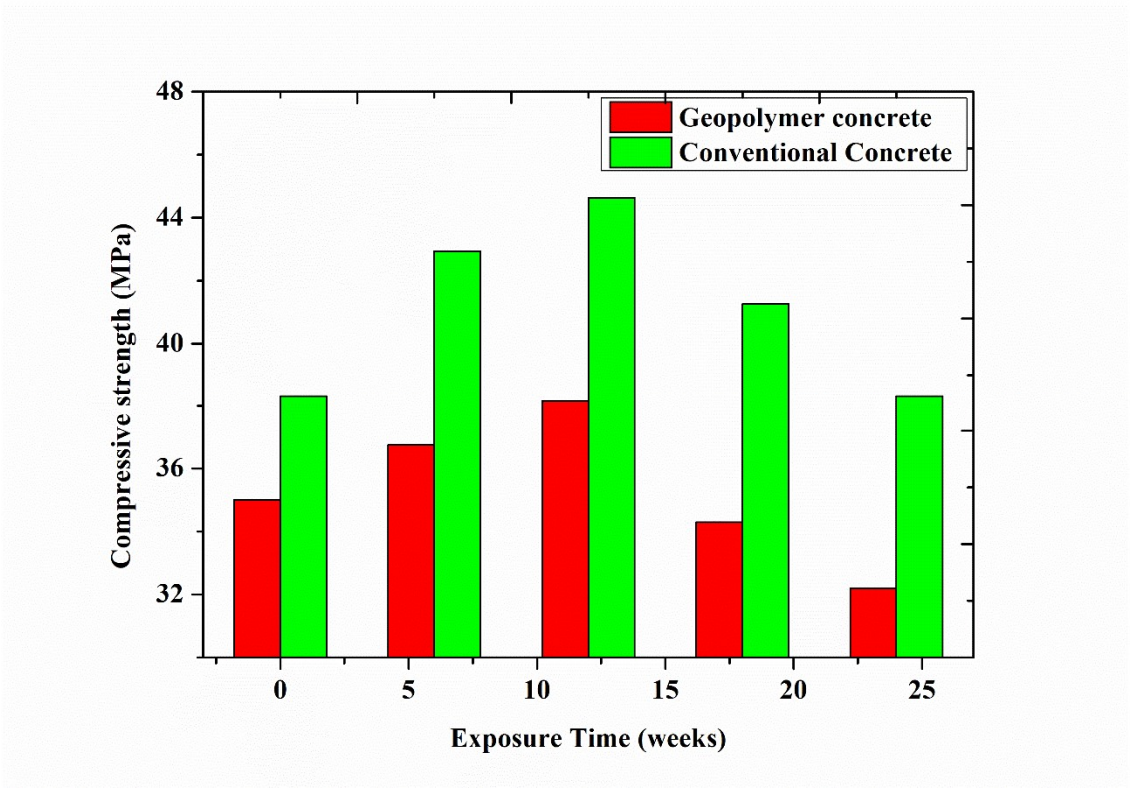

Fig. 4.89 Graph between the compressive strength vs exposure time

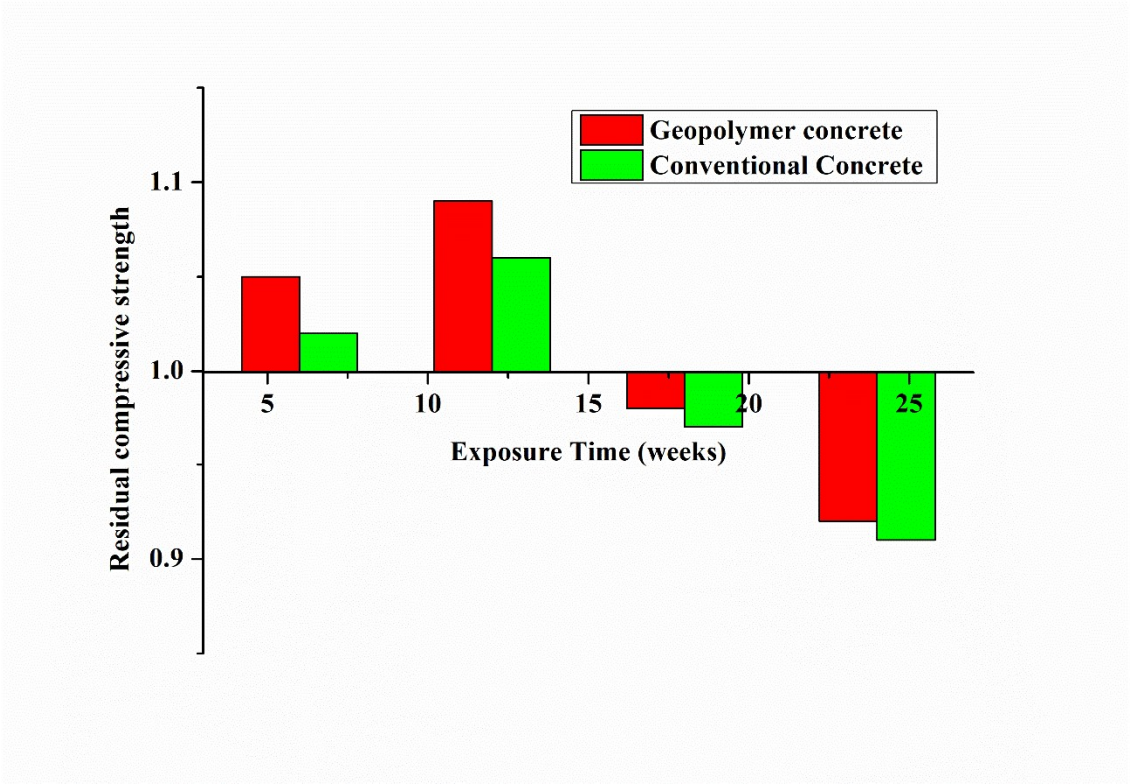

Fig. 4.90 Graph between the residual compressive strength vs exposure time

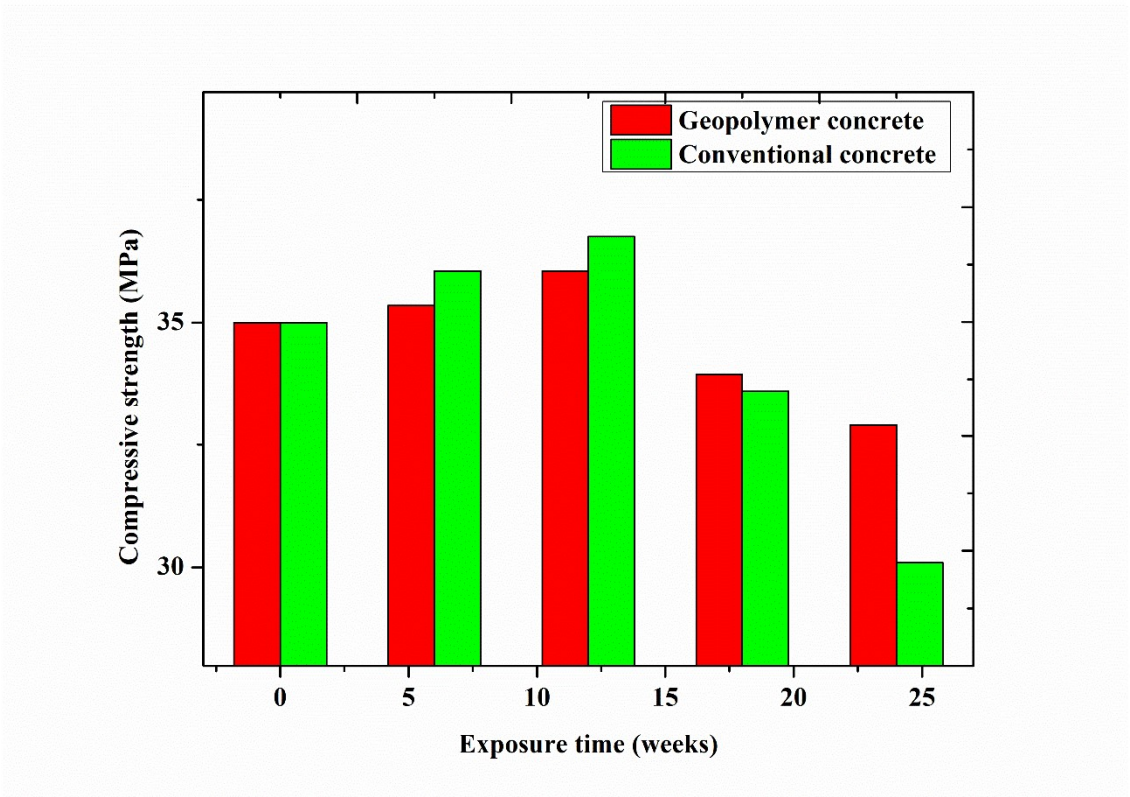

Fig. 4.91 Graph between the compressive strength vs exposure time

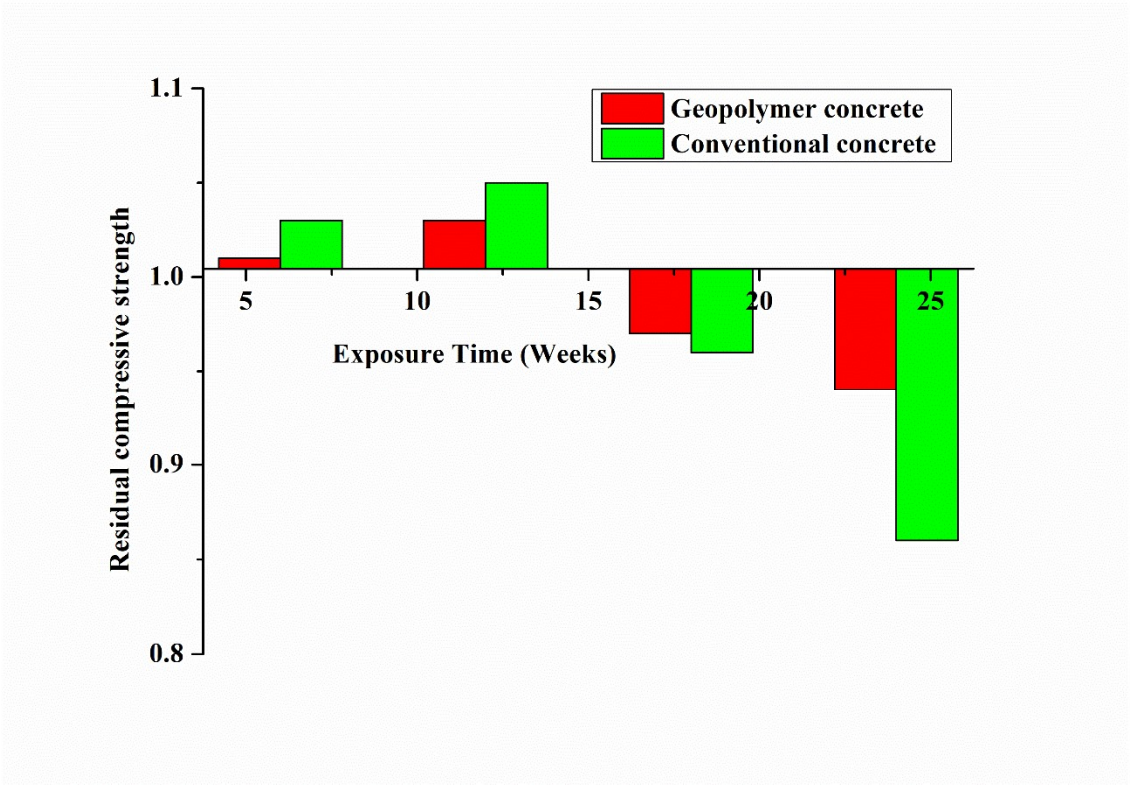

Fig. 4.92 Graph between the residual compressive strength vs exposure time

4.9.3 Ultrasonic pulse velocity test (UPVT)

The UPVT is a non-destructive test used to identify the quality of materials via passing ultrasonic pulse velocity. Fig. 4.93 depicts the graph between the UPV and exposure time of both concrete specimens in the sodium sulphate solution, showing that exposure to sulphate solution doesn't affect both types of concrete specimens. The UPV of both types of concrete specimens is of good quality with a little bit of change. Fig. 4.94 depicts the graph between the UPV variation of both concrete specimens with the exposure time in the magnesium sulphate solution, which shows that the UPV of the GPC specimens is higher than conventional concrete specimens after merging into the magnesium sulphate solution for 24 weeks. The GPC specimens show 4464.11m/sec UPV, whereas the conventional concrete specimens show 4419.43m/sec UPV after 24 weeks of exposure to magnesium sulphate solution.

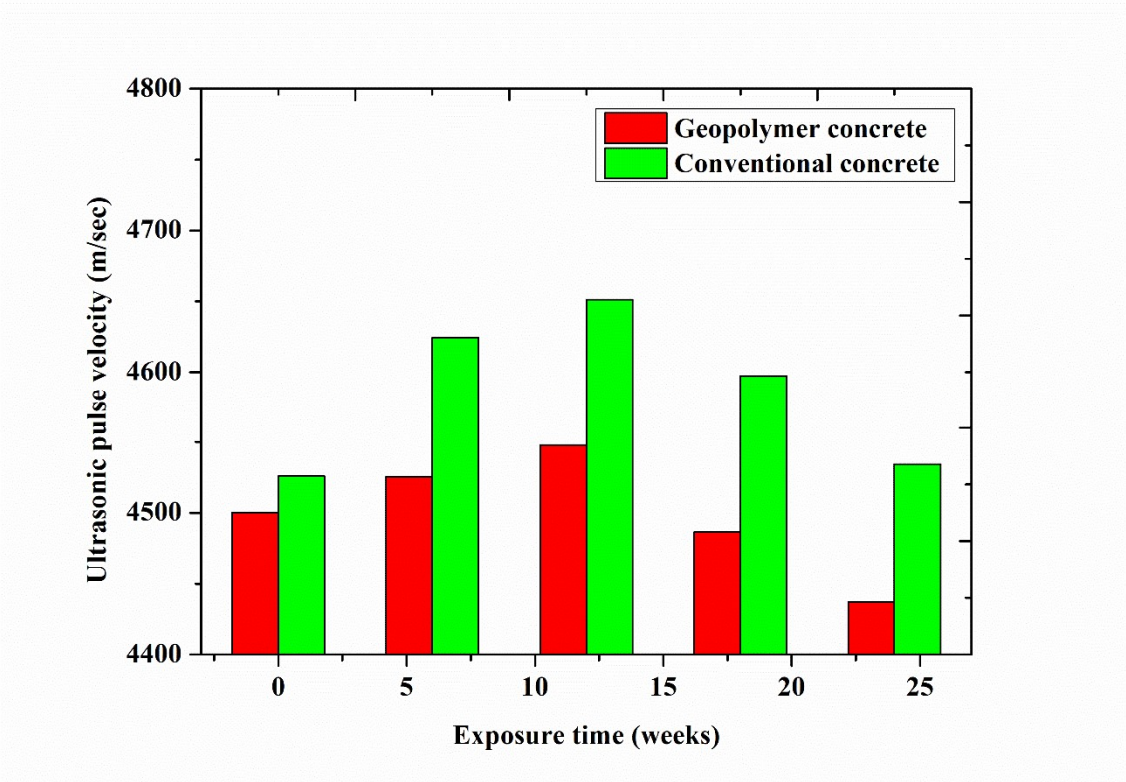

Fig. 4.93 Graph between the UPV vs exposure time

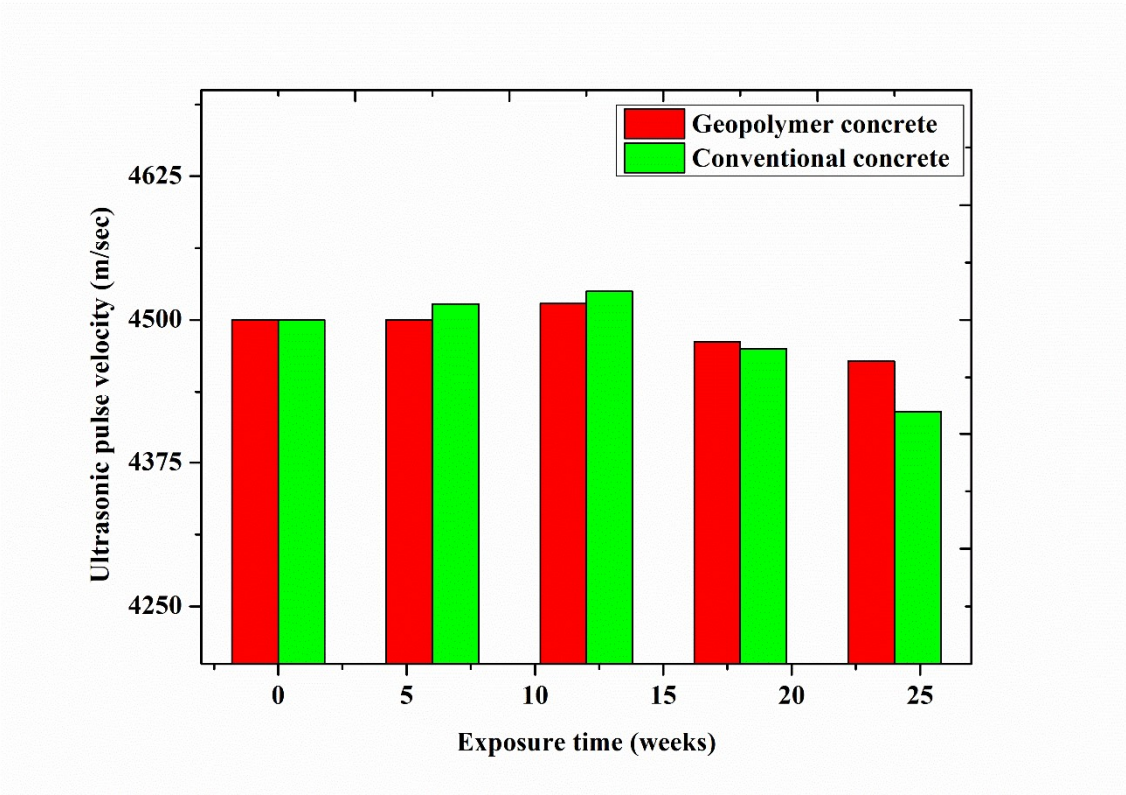

Fig. 4.94 Graph between the UPV vs exposure time

4.10 Effect of acid attack

The acid attack means making an acidic water solution with a 5% concentration of sulphuric acid as per the ASTM code in the laboratory. GPC and conventional concrete specimens were put in the solution for a long duration. The specimens of both GPC and conventional concrete tests for a weight check, UPVT, and compressive strength analysis after 6 weeks, 12 weeks, 18 weeks, and 24 weeks were put in the solution.

4.10.1 Mass Loss

Fig. 4.95 shows the graph of the density variation of both types of concrete specimens after 6 weeks, 12 weeks, 18 weeks, and 24 weeks with the exposure time in acidic water, which shows the GPC specimens' density is higher than conventional concrete after exposure to acidic water at all testing ages. Fig. 4.96 depicts the mass loss of both concrete specimens after putting them in the acidic water solution after 6weeks, 12weeks, 18weeks, and 24weeks, which shows that both concrete specimens degrade continuously with exposure time. The mass loss of the OPC concrete specimens is higher than the GPC

specimens, and GPC specimens show better stability against acidic attack conditions. The GPC specimens show an 8.1% mass loss after 24 weeks of exposure time, whereas the conventional concrete specimens show a 14.2% mass loss in acidic conditions. Okeyo et al. (2017) reported that the process for an acid attack on geopolymer concrete is quite similar and depends on the acid strength, activator content, the mineralogic and physicochemical composition of the products as exposure duration. It may be determined that sodium hydroxide solution is more resistant to acid in fly ash-based geopolymer concrete. In addition, GPC's durability is better than that of OPC [177].

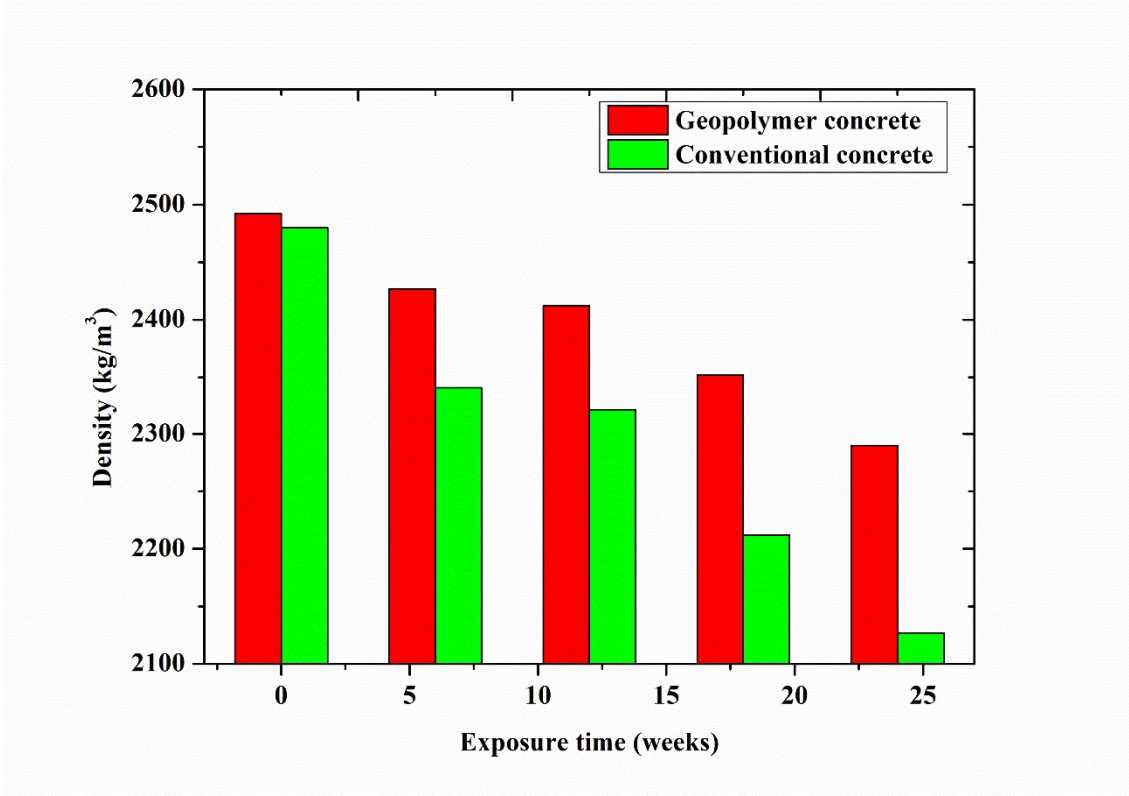

Fig. 4.95 Graph between density vs exposure time

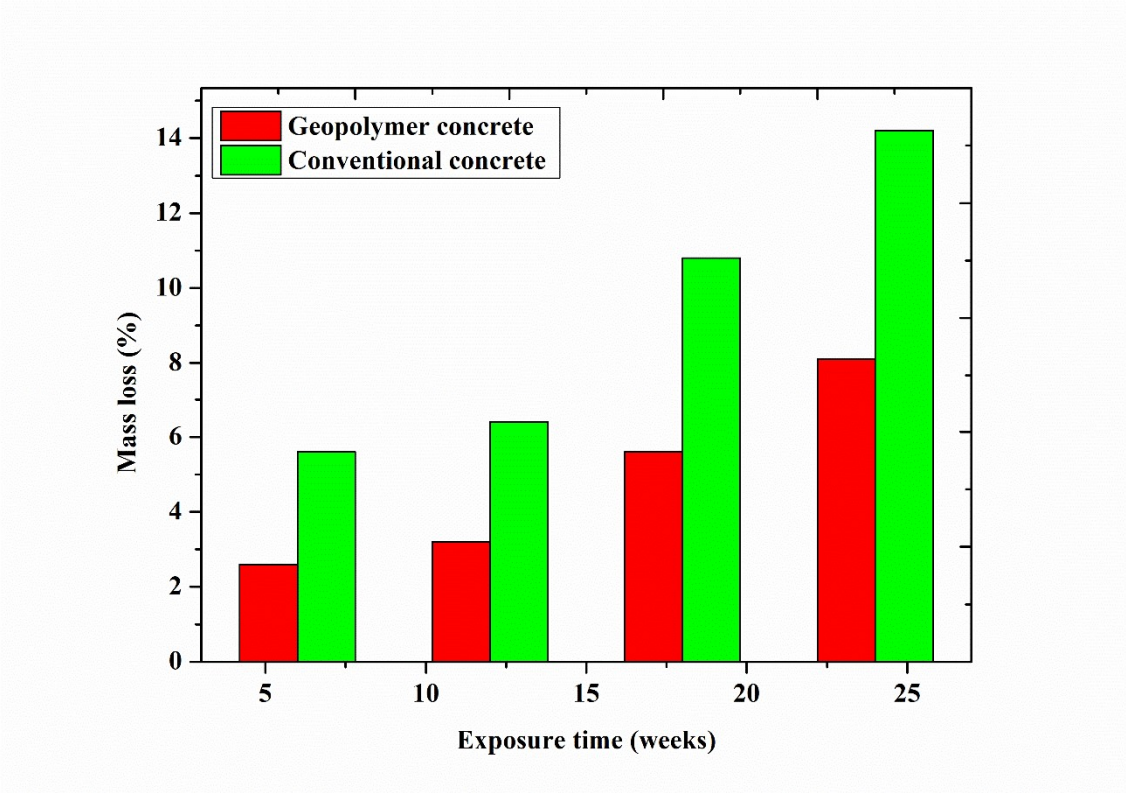

Fig. 4.96 Graph between the mass loss vs exposure time

4.10.2 Compressive strength

The compressive strength of the GPC and conventional concrete specimens were tested after 6weeks, 12weeks, 18weeks, and 24weeks after putting in the acidic water solution. Fig. 4.97 shows the compressive strength variation of both concrete specimens after merging into an acidic water solution for a long duration. The compressive strength of the conventional concrete specimens is lower than GPC specimens after merging into the acidic water solution for 24 weeks. Both concrete specimens will degrade indefinitely after being immersed in the acidic water solution. Fig. 4.98 shows the graph of residual compressive strength variation of both concrete specimens with the exposure time in acidic conditions. The GPC depicts higher resistance than conventional concrete specimens against acid attack. The GPC and conventional concrete specimens degrade compressive strength with exposure time, in which the GPC specimens retain 56% of their compressive strength and conventional concrete specimens retain only 32% of their compressive strength after 24 weeks of exposure to an acidic water solution. GPC's performance with the silicate activator to resist sulfuric acid or carbon dioxide is high, and Na's inclination to make hydrated salts with these acids is attributable to this [178].

At the same water to cement or alkaline solution to binder ratio, OPC specimens performed somewhat better than fly ash based GPC specimens in terms of mechanical strength (compressive, splitting, flexural strength). However, because of the high CaO concentration, mechanical strength degradation was greatest for OPC specimens when subjected to chemical attacks [179].

4.10.3 Ultrasonic pulse velocity test (UPVT)

The UPVT is a non-destructive test used to identify the quality of materials via passing ultrasonic pulse velocity. Fig. 4.99 depicts the graph between the UPV and exposure time of both concrete specimens in the acidic water solution, which shows that exposure to acidic solution affects both types of concrete specimens seriously. The GPC specimens show 3661.88 m/sec UPV, whereas the conventional concrete specimens show 3368.42 m/sec UPV after 24 weeks of exposure to an acidic water solution. Thus, the UPV of both types of concrete specimens shows good quality, with a large change occurring after acidic exposure.

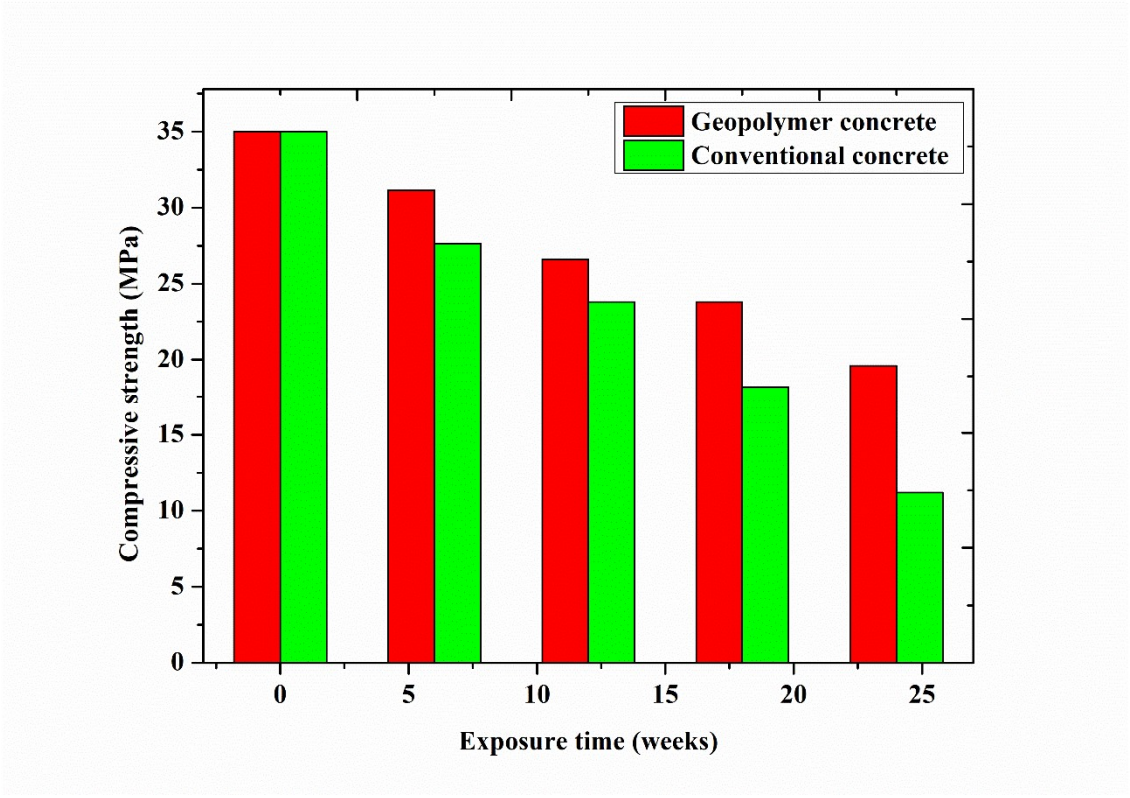

Fig. 4.97 Graph between the compressive strength vs exposure time

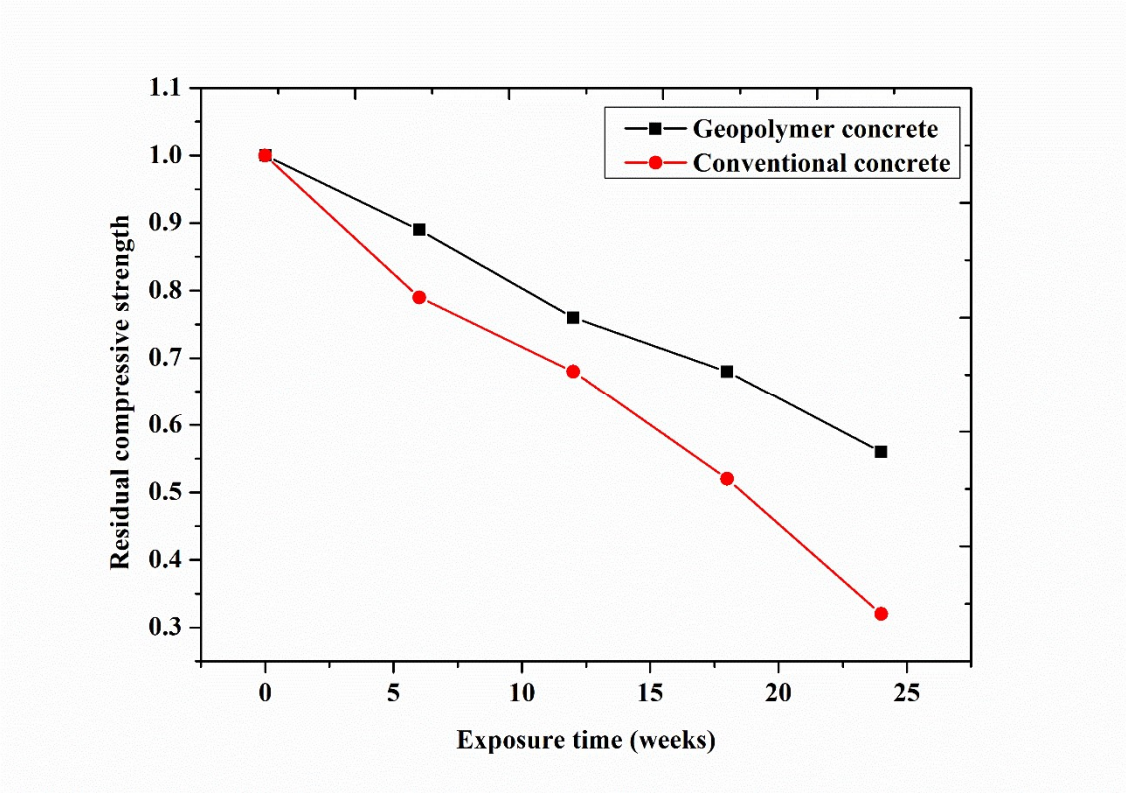

Fig. 4.98 Graph between the residual compressive strength vs exposure time

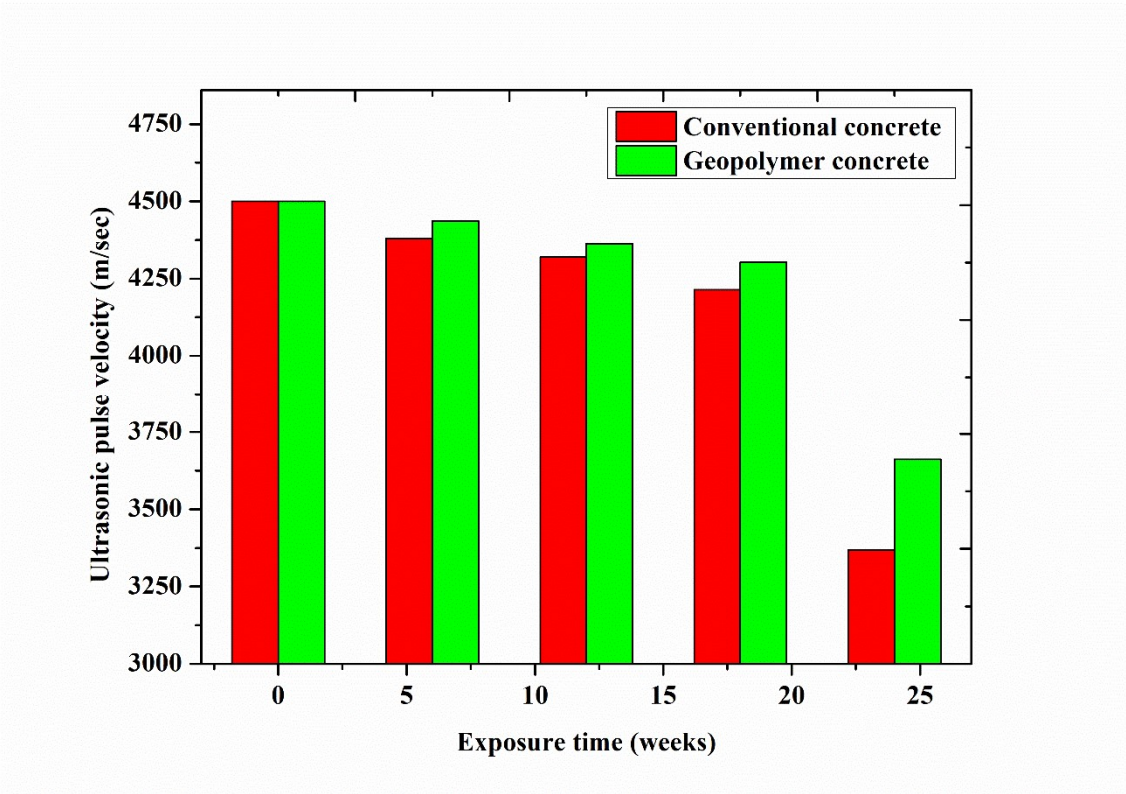

Fig. 4.99 Graph between the UPV vs exposure time

4.11 Freeze-thaw condition

The freeze-thaw condition is created through the following cycle of work, in which you first put the specimens in the water and, after putting them in the deep freezer for a stipulated time and after continuing the cycle for a longer period, up to the completion of 90 cycles. This procedure was performed on both concrete specimens and was tested for mass loss, compressive strength, and ultrasonic pulse velocity at 30, 45, 60, 75, and 90 cycles.

4.11.1 Mass loss

Fig. 4.100 depicts the graph between the density variation of both types of concrete specimens after 30 cycles, 45 cycles, 60 cycles, 75 cycles, and 90 cycles with freeze-thaw cycles, which shows the conventional concrete specimens' density is higher than GPC after freezing-thawing condition. Furthermore, Fig. 4.101 shows the mass loss of both concrete specimens after freezing-thawing conditions after 30 cycles, 45 cycles, 60 cycles, 75 cycles, and 90 cycles, demonstrating that both concrete specimens degrade their mass continuously as the number of freeze-thaw cycles increases, but conventional concrete specimens show better stability against freezing-thawing conditions. Therefore, the mass loss of the GPC specimens is higher than the conventional concrete specimens. For example, the mass loss of GPC specimens is 7.2% after 90 cycles of freeze-thaw, whereas the conventional concrete specimens show only 2.1% mass loss after freeze-thaw 90 cycles. The use of air-training admixtures has decreased compressive and bending properties and results in ultrasonic pulses. It is a result of a reduction in the volume of the pore. The functioning is linked to this. The application of air induction additives enhances the working capacity and therefore lowers the number of pores. Because air content has a negative impact on strength outcomes, strength has reduced [180].

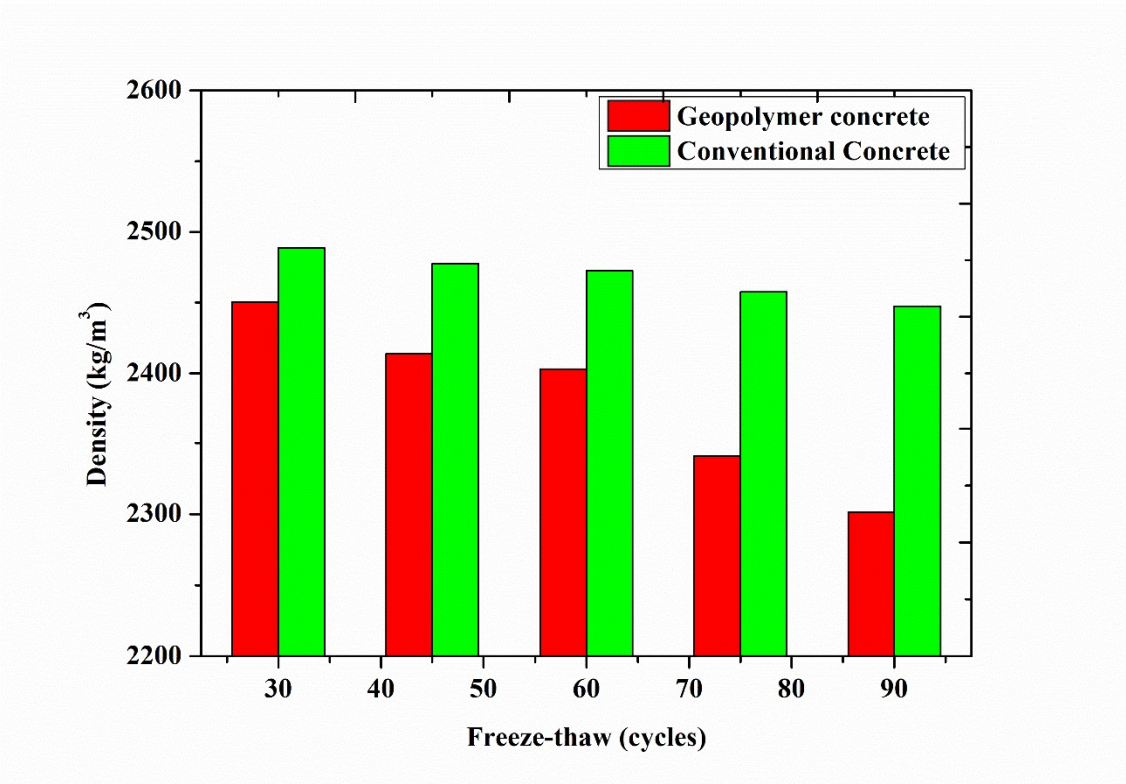

Fig. 4.100 Graph between the density vs freeze-thaw cycles

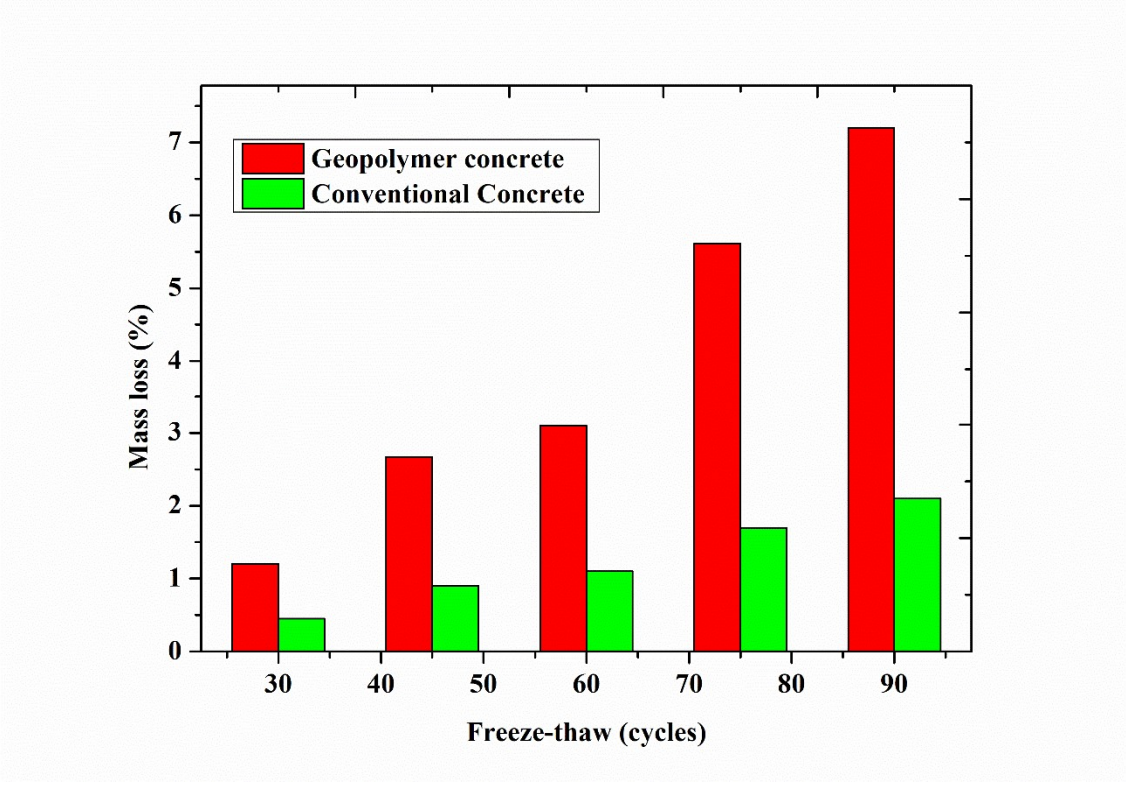

Fig. 4.101 Graph between the mass loss vs freeze-thaw cycles

4.11.2 Compressive strength

After freezing-thawing conditions, the compressive strength of GPC and conventional concrete specimens was tested after 30 cycles, 45 cycles, 60 cycles, 75 cycles, and 90 cycles. Fig. 4.102 shows the compressive strength variation of both concrete specimens after freezing-thawing conditions. The compressive strength of the conventional concrete specimens is higher than GPC specimens after the freeze-thaw cycles. Both concrete specimens degrade continuously after being put in a freezing-thawing condition. Fig. 4.103 shows the graph of residual compressive strength variation of both concrete specimens with the freeze-thaw cycles. Conventional concrete is more resistant to freezing-thawing conditions than GPC specimens. The GPC and conventional concrete specimens degrade compressive strength with the freeze-thaw cycles, in which the GPC specimens retained 55% compressive strength and conventional concrete specimens retained 87% compressive strength of the original after the 90 freeze-thaw cycles.

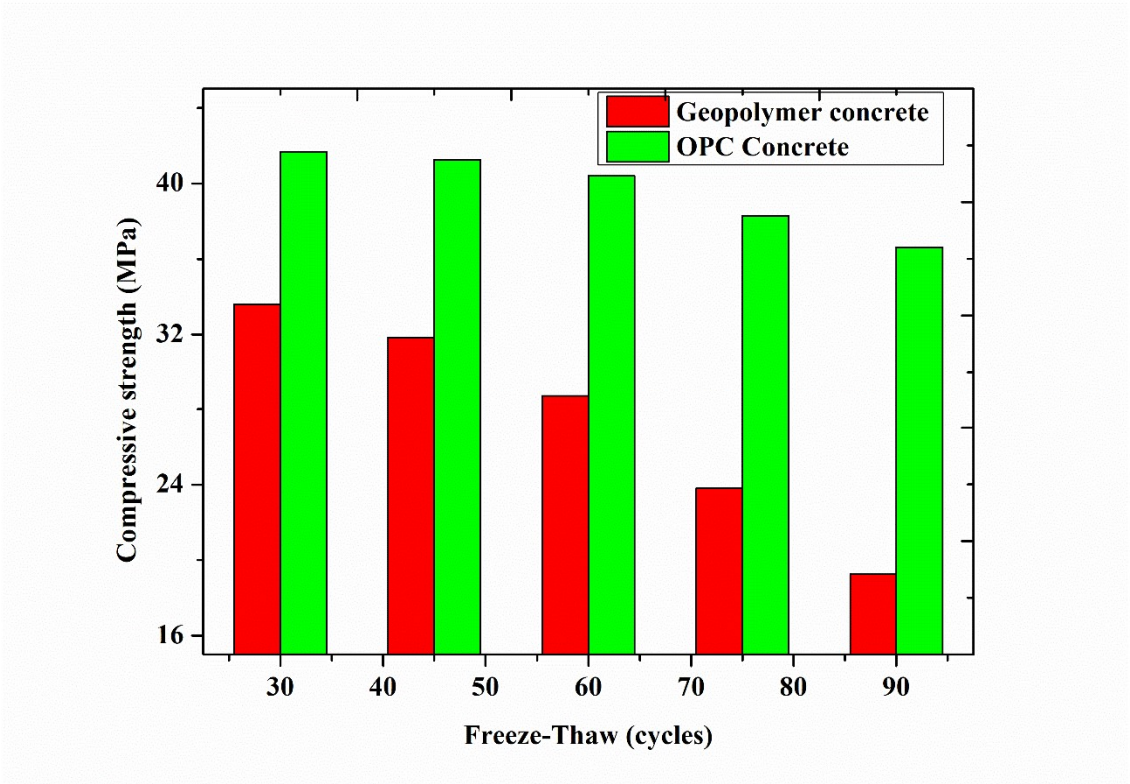

Fig. 4.102 Graph between the compressive strength vs freeze-thaw cycles

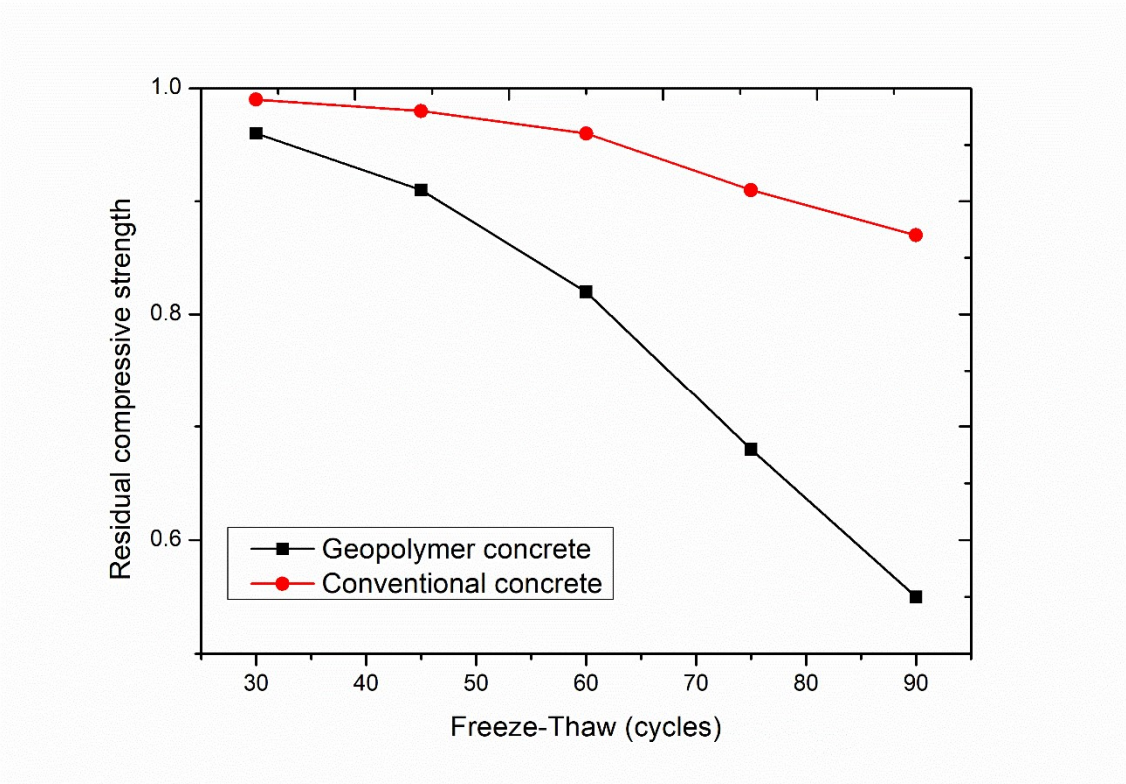

Fig. 4.103 Graph between the residual compressive strength vs freeze-thaw cycles

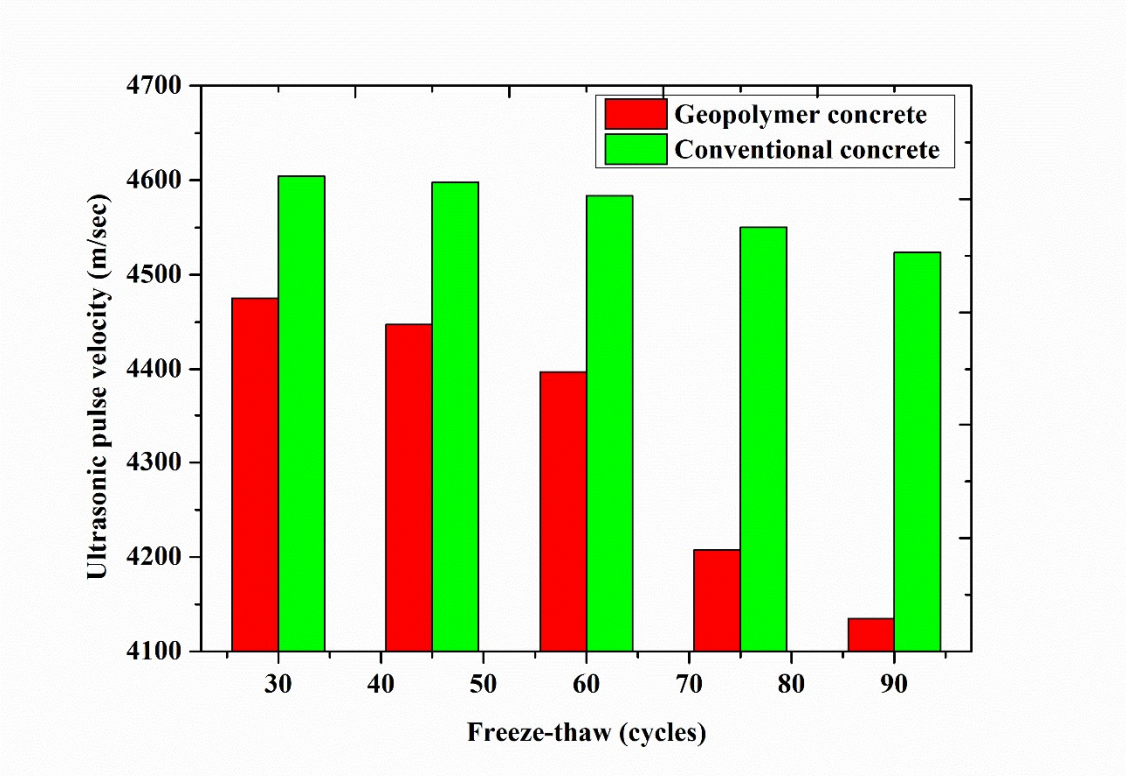

Fig. 4.104 Graph between the UPV vs freeze-thaw cycles

4.11.3 Ultrasonic pulse velocity test (UPVT)

The UPVT is a non-destructive test used to identify the quality of materials via passing ultrasonic pulse velocity. Fig. 4.104 depicts the graph between the UPV and freeze-thaw cycles of both concrete specimens, which shows that the freezing-thawing condition affects both types of concrete specimens. The UPV of both types of concrete specimens shows good quality, with a large change occurring after the freeze-thaw cycles. For example, the GPC specimens show 4134.77 m/sec UPV, whereas the conventional concrete specimens show 4523.60 m/sec UPV after 90 cycles of freeze-thaw.

4.12 Wetting-drying condition

The wetting-drying condition is created through the following cycle of work, in which we first put the specimens in the water for 24 hours, and after putting them in an ambient condition for 24 hours and after continuing the cycle for a longer period, up to the completion of 90 cycles. This procedure was performed on both concrete specimens and was tested for mass loss, compressive strength, and ultrasonic pulse velocity at 30, 45, 60, 75, and 90 cycles.

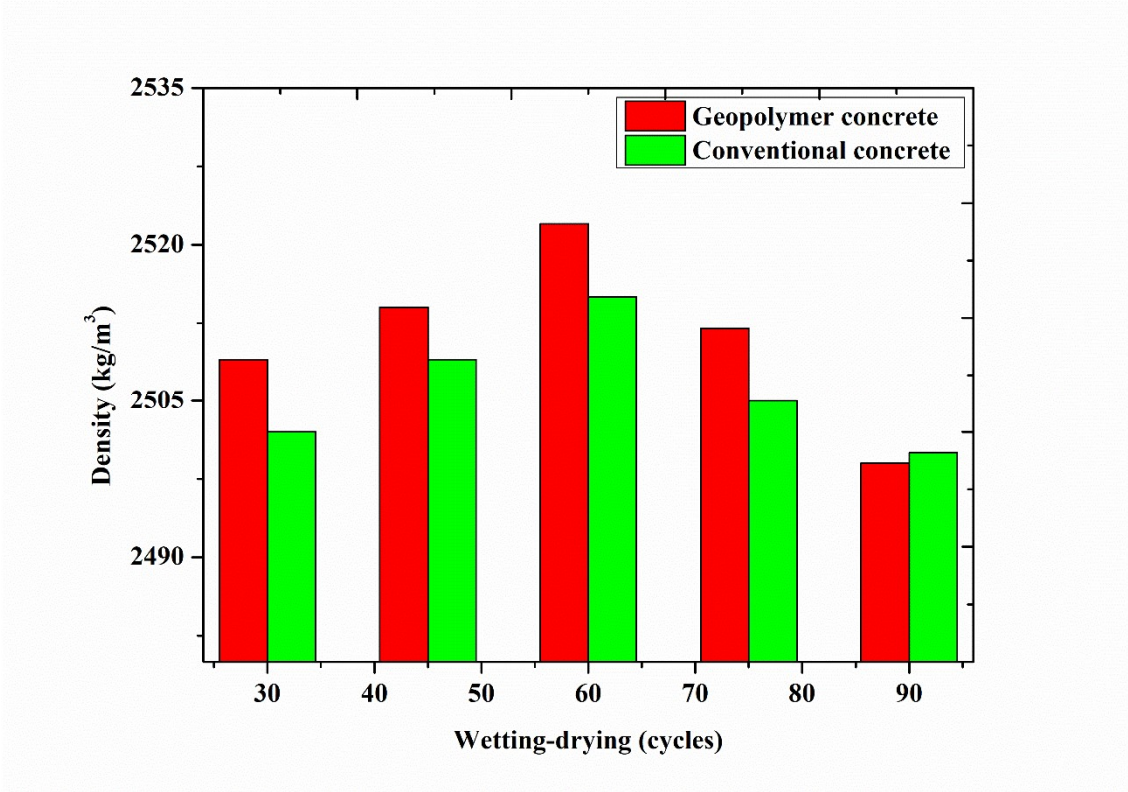

Fig. 4.105 Graph between the density vs wetting-drying cycles

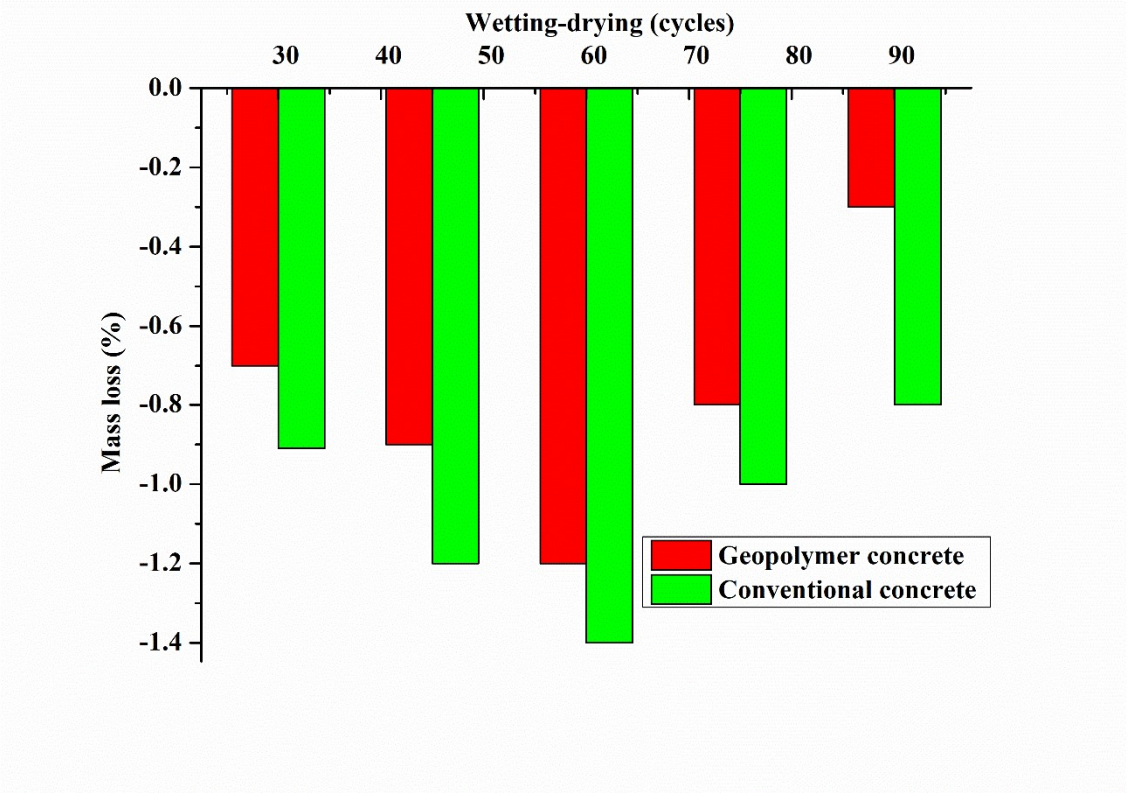

Fig. 4.106 Graph between the mass loss vs wetting-drying cycles

4.12.1 Mass loss

4.12.2 Compressive strength

The compressive strength of GPC and conventional concrete specimens was determined after 30 cycles, 45 cycles, 60 cycles, 75 cycles, and 90 cycles of wetting-drying. Fig. 4.107 shows the graph between the compressive strength variation of both concrete specimens with the wetting-drying cycles. The compressive strength of the conventional concrete specimens is higher than GPC specimens after the wetting-drying cycles. After being placed in a wet-drying condition, both concrete specimens continue to strengthen indefinitely. Fig. 4.108 shows the graph of residual compressive strength variation of both concrete specimens with the wetting-drying cycles. Conveniently, conventional concrete exhibits higher strength than GPC specimens in the wetting-drying condition. The wetting-drying cycles strengthened the compressive strength of the GPC and conventional concrete specimens, with the GPC specimens retaining 107% compressive

strength and the conventional concrete specimens retaining 109% compressive strength of the originals after 90 wetting-drying cycles.

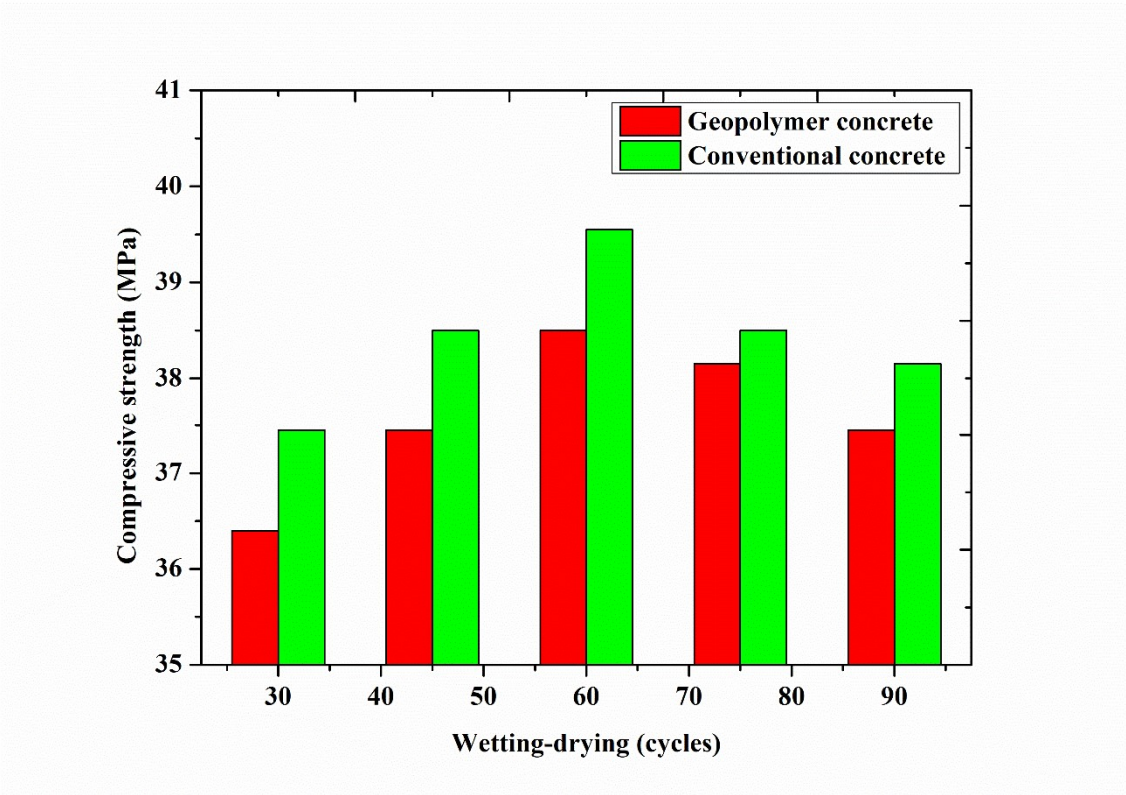

Fig. 4.107 Graph between the compressive strength vs wetting-drying cycles

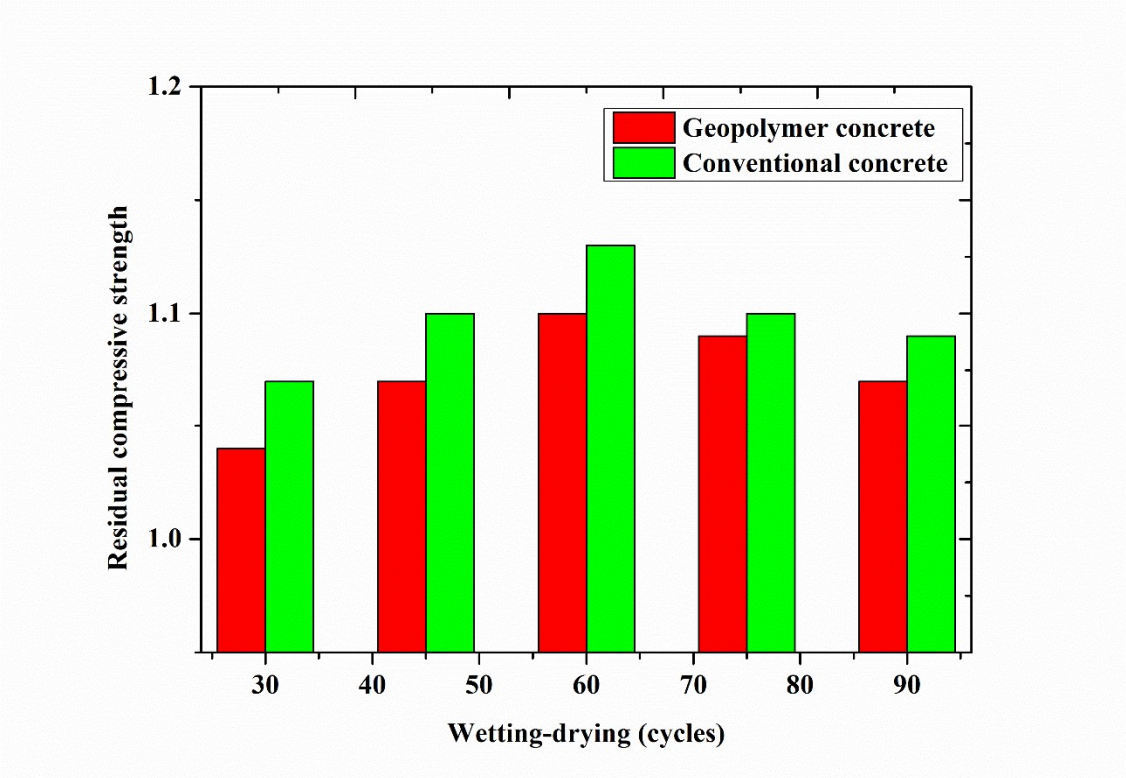

Fig. 4.108 Graph between the residual compressive strength vs wetting-drying cycles

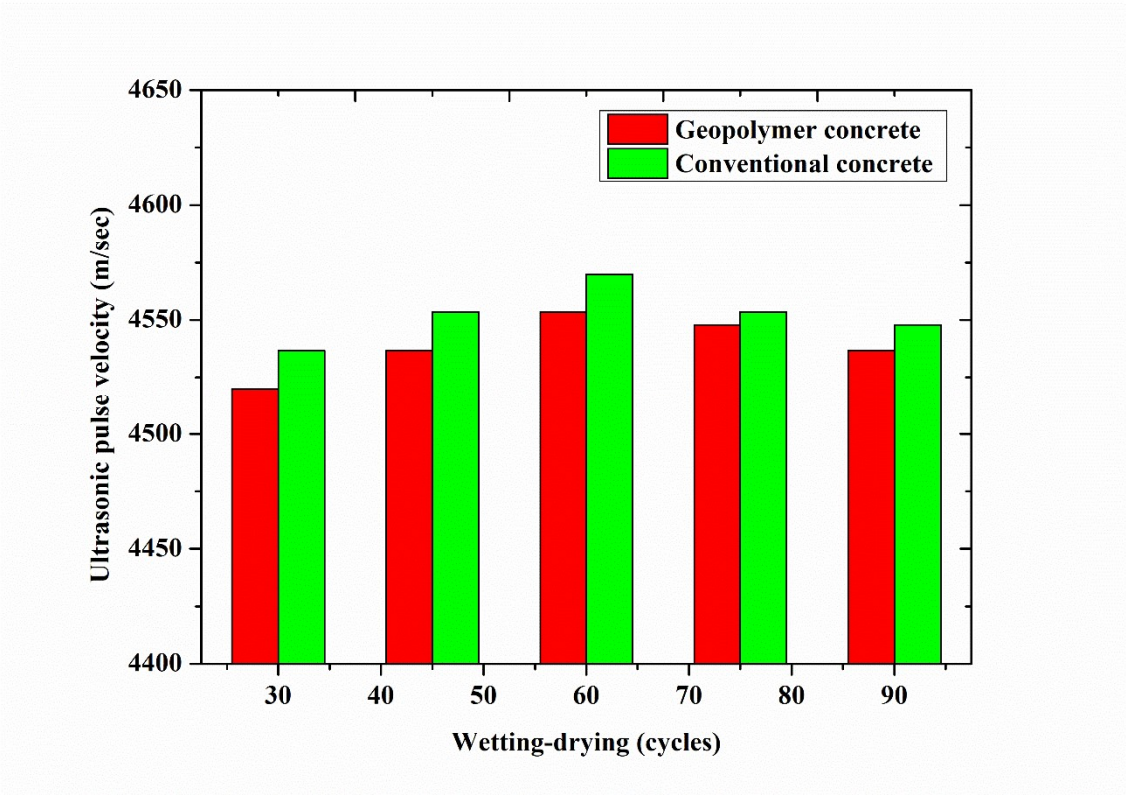

Fig. 4.109 Graph between the UPV vs wetting-drying cycles

4.12.3 Ultrasonic pulse velocity test (UPVT)

The UPVT is a non-destructive test used to identify the quality of materials via passing ultrasonic pulse velocity. Fig. 4.109 depicts the graph between the UPV and wetting-drying cycles of both concrete specimens, which shows that the wetting-drying condition affects both types of concrete specimens. The UPV of both types of concrete specimens shows good quality, with a little bit of change occurring after the wetting-drying cycles. For example, the GPC specimens show a 4536.68m/sec UPV, whereas the conventional concrete specimens show a 4547.84m/sec UPV after 90 cycles of wetting-drying.

CHAPTER 5 REGRESSION ANALYSIS

5.1 Correlation among the Mechanical Properties

After the experimental investigation, the results of the compressive strength and flexural strength of the various mixes of GPC varied by curing condition: ambient curing, oven curing, or both. The oven-cured samples of GPC generate the eqs. of correlation among the compressive strength, flexural strength, modulus of elasticity, and splitting tensile strength.

5.1.1 Correlation between the flexural strength to compressive strength

GPC specimens of various mixes get the compressive strength and flexural strength in the oven curing condition, which generates the Eq. (1) of the correlation between the compressive strength and flexural strength, and the other Eq. given by the various authors or codes. The Eq. (2) given by the ACI Committee in the state of the art report on high-strength concrete [181] and Eq. (3) elaborated in the building code requirements for structural concrete by the ACI committee [182]. AS 3600-2009 provides the RCC design procedure and provides Eq. (4) between flexural strength and compressive strength [183]. Eq. (5) given by the Indian Code of practise for plain and reinforced concrete and Eq. (6) provided by M. Ahmed in the international journal of structural engineering, vol. 5 in 2014 [184,185]. Bellum et al. proposed the relationship in Eq. (7) between compressive and flexural strength [186]. Fig. 5.1 and Fig. 5.2 shows the proposed Eq. with the other relative equations.

$$f_{fs} = 0.25 f_c^{0.85} \quad (5.1)$$

$$ACI363R-92: f_{fs} = 0.94\sqrt{f_c} \quad (5.2)$$

$$ACI\ 318-99: f_{fs} = 0.62\sqrt{f_c} \quad (5.3)$$

$$AS\ 3600: f_{fs} = 0.6\sqrt{f_c} \quad (5.4)$$

$$IS\ 456-2000: f_{fs} = 0.7\sqrt{f_c} \quad (5.5)$$

$$M.Ahmed: f_{fs} = 1.055\sqrt{f_c} \quad (5.6)$$

$$Bellum\ et\ al.: f_{fs} = 0.57 f_c^{0.74} \quad (5.7)$$

Where; f_c are characteristic strength in MPa, f_{fs} are flexural strength in MPa

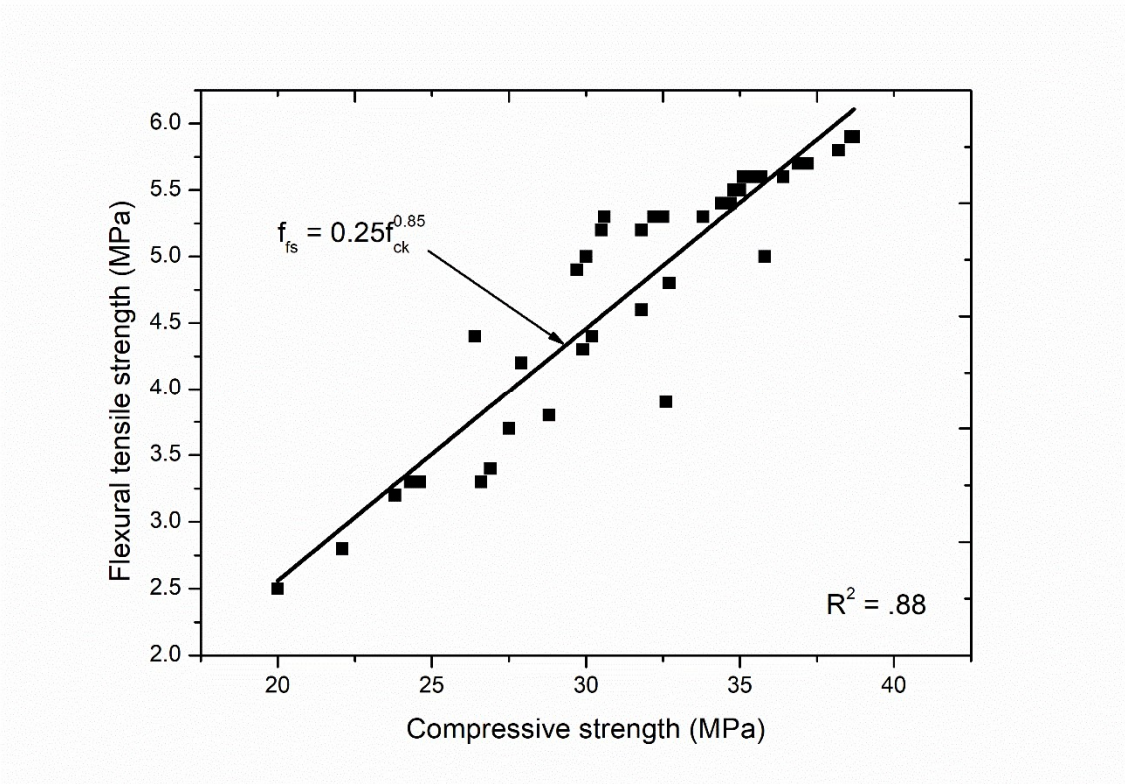

Fig. 5.1 Correlation Eq. generation between flexural strength and compressive strength

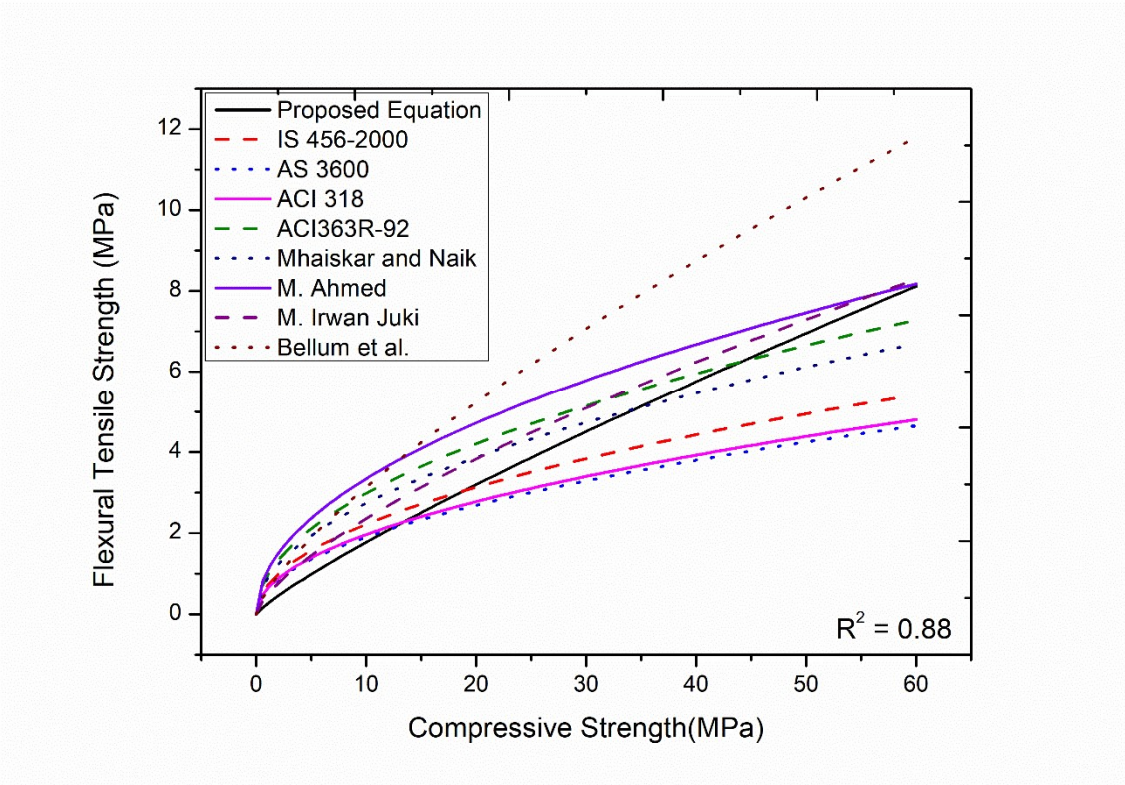

Fig. 5.2 Comparison of correlation Eq.s between flexural strength and compressive strength

Table 5.1 Correlation between flexural strength and compressive strength

	Proposed Eq.	**ACI 363R-92**	**ACI 318-99**	**AS 3600**	**IS 456: 2000**	**M. Ahmed et al.**	**Bellum et al.**	**Mhaiskar & Naik**	**M. Irwan Juki et al.**
fc	**fs = .25(fc)^0.85**	**fs = 0.94(fc)^.5**	**fs = 0.62(fc)^.5**	**fs = 0.6(fc)^.5**	**fs = .7(fc)^.5**	**fs = 1.055(fc)^.5**	**fs = 0.57(fc)^.74**	**fs = .864(fc)^.5**	**fs = .466(fc)^.703**
15	2.50	3.64	2.40	2.32	2.71	4.09	4.23	3.35	3.13
17.5	2.85	3.93	2.59	2.51	2.93	4.41	4.74	3.61	3.49
20	3.19	4.20	2.77	2.68	3.13	4.72	5.23	3.86	3.83
22.5	3.53	4.46	2.94	2.85	3.32	5.00	5.71	4.10	4.16
25	3.86	4.70	3.10	3.00	3.50	5.28	6.17	4.32	4.48
27.5	4.18	4.93	3.25	3.15	3.67	5.53	6.62	4.53	4.79
30	4.50	5.15	3.40	3.29	3.83	5.78	7.06	4.73	5.09
32.5	4.82	5.36	3.53	3.42	3.99	6.01	7.49	4.93	5.39
35	5.13	5.56	3.67	3.55	4.14	6.24	7.92	5.11	5.67
37.5	5.44	5.76	3.80	3.67	4.29	6.46	8.33	5.29	5.96
40	5.75	5.95	3.92	3.79	4.43	6.67	8.74	5.46	6.23

5.1.2 Splitting tensile strength to compressive strength

After the experimental investigation of various parameters used in the mix designs, they proposed the Eq. (9) between the compressive strength and splitting tensile relationship in fly ash-slag-based GPC. Eq. (10) given by the ACI committee in the report of high strength concrete, and Eq. (11) proposed by the Euro-International committee for concrete in CEB/FIP in 1990 [181,187]. Eq. (12) for the relationship between splitting and compressive strength is provided by an ACI standard and report (ACI 318-14) [182]. Ahmed et al. proposed the relationship Eq. (13), and Ryu et al. proposed Eq. (14) to predict the splitting strength based on the compressive strength of the GPC [40,185]. Fig. 5.3 anf Fig. 5.4 shows the proposed Eq. with the other relative Eqs.

$$\boldsymbol{Proposed\ Eq.:\ f_{st} = 0.25 f_c^{0.73}} \quad (\mathbf{5.8})$$

$$\boldsymbol{ACI363R-92: f_{st} = 0.59\sqrt{f_c}} \quad (\mathbf{5.9})$$

$$\boldsymbol{CEB-FIP:\ f_{st} = 0.301 f_c^{0.67}} \quad (\mathbf{5.10})$$

$$\boldsymbol{ACI\ 318-14: f_{st} = 0.56 f_c^{0.5}} \quad (\mathbf{5.11})$$

$$\boldsymbol{Ahmed\ et\ al.:\ f_{st} = 0.462 f_c^{0.55}} \quad (\mathbf{5.12})$$

$$\boldsymbol{Ryu\ et\ al.:\ f_{st} = 0.17 f_c^{0.75}} \quad (\mathbf{5.13})$$

$$\boldsymbol{Gardener\ et\ al.:\ f_{st} = 0.6 f_c^{\left(\frac{2}{3}\right)}} \quad (5.14)$$

$$\boldsymbol{Raphael\ et\ al.:\ f_{st} = 0.2 f_c^{0.7}} \quad (5.15)$$

$$\boldsymbol{De-larrard\ et\ al.:\ f_{st} = 0.6 + 0.06 f_c} \quad (5.16)$$

Where $\boldsymbol{f_{st}}$ are Splitting Strength in MPa, f_c= Characteristics Strength of Concrete in MPa.

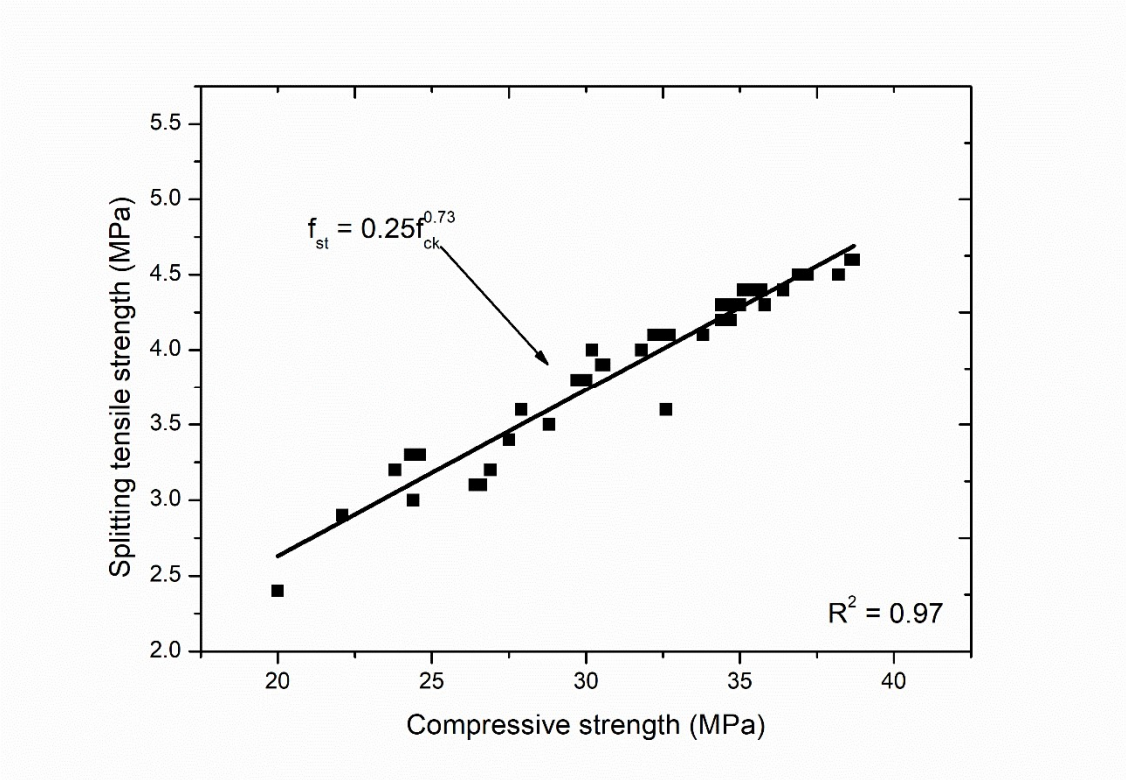

Fig. 5.3 Correlation Eq. generation between splitting tensile and compressive strength

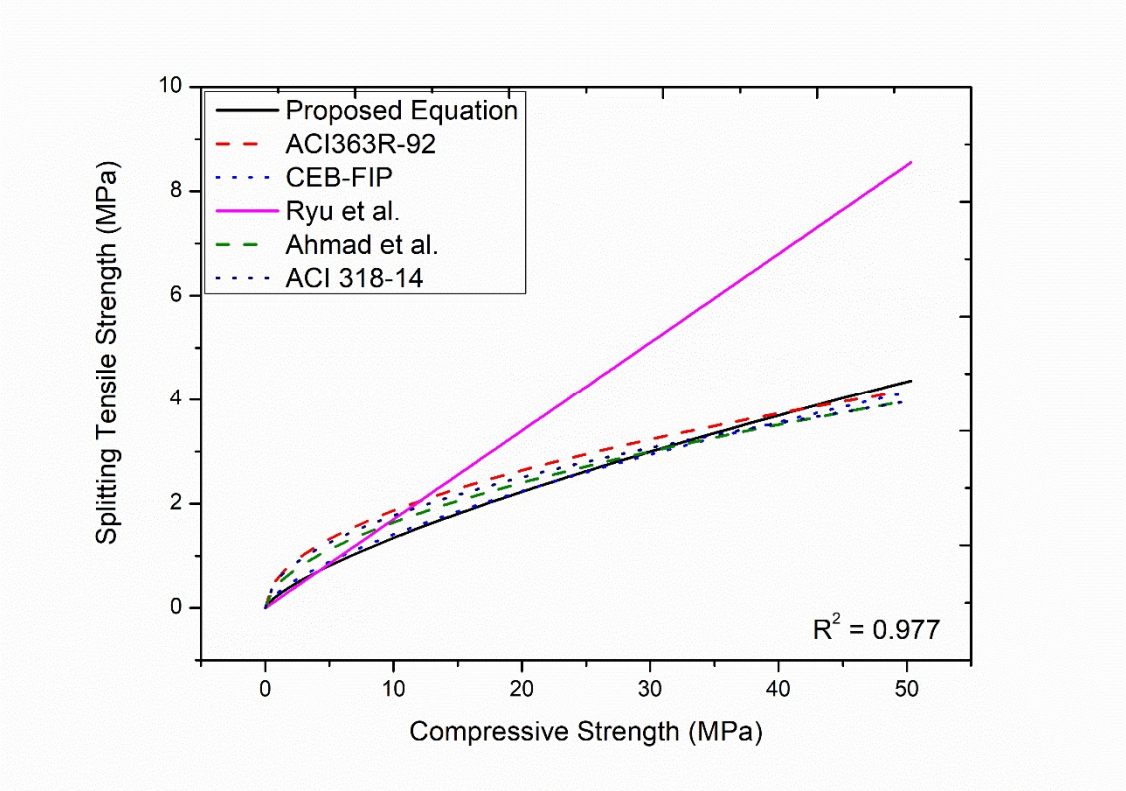

Fig. 5.4 Comparision among correlation Eq.s between splitting tensile and compressive strength

Table 5.2 Correlation between compressive strength and splitting tensile

	Proposed Eqs.	ACI 363R-92	CEB-FIP	ACI 318-99	Ahmad et al.	Ryu et al.	Gardener et al.	Raphael et al.	De-larrard et al.
fc	**fs = 0.25(fc)^0.73**	**fs= .59(fc)^.5**	**fs= .301(fc)^.67**	**fs= .56(fc)^.5**	**fs= .462(fc)^.55**	**fs= .17(fc)^(3/4)**	**fs= .6(fc)^(2/3)**	**fs= .2(fc)^.7**	**fs= .6+.06fc**
15.00	1.81	2.29	1.85	2.17	2.05	1.30	3.65	1.33	1.50
17.50	2.02	2.47	2.05	2.34	2.23	1.45	4.04	1.48	1.65
20.00	2.23	2.64	2.24	2.50	2.40	1.61	4.42	1.63	1.80
22.50	2.43	2.80	2.42	2.66	2.56	1.76	4.78	1.77	1.95
25.00	2.62	2.95	2.60	2.80	2.71	1.90	5.13	1.90	2.10
27.50	2.81	3.09	2.77	2.94	2.86	2.04	5.47	2.03	2.25
30.00	2.99	3.23	2.94	3.07	3.00	2.18	5.79	2.16	2.40
32.50	3.17	3.36	3.10	3.19	3.13	2.31	6.11	2.29	2.55
35.00	3.35	3.49	3.26	3.31	3.26	2.45	6.42	2.41	2.70
37.50	3.52	3.61	3.41	3.43	3.39	2.58	6.72	2.53	2.85
40.00	3.69	3.73	3.56	3.54	3.51	2.70	7.02	2.65	3.00

5.1.3 Modulus of elasticity to compressive strength

MOE measures the defiance capacity against the elastic deformation under the load applied. The MOE of GPC was tested according to ASTM C469/469M-14 [188]. After the experimental investigation, they proposed the relationship Eq. (15) between the MOE and compressive strength for MOE prediction based on compressive strength. According to ACI 318-14 (ACI Building Code), the MOE of conventional concrete is predicted based on Eq. (16) for the density ranges between 1442 to 2483 kg/m^3 [182]. The CEB-FIP gives Eq. (17) for conventional concrete for MOE prediction based on compressive strength [187]. According to the Indian Standard Code IS 456-2000, this represents the Eq. (18) for predicting MOE for average weight conventional concrete Lee and Lee proposed the Eq. (19) for the prediction of MOE of GPC [32], and Nath and Sarker proposed the Eq. (20) for the prediction of MOE of ambient-cured low-calcium fly ash blended GPC. Bellum et al. proposed Eq. (21) to predict MOE based on fly ash-GGBFS-based GPC [186]. Fig. 5.5 and Fig. 5.6 shows the proposed Eq. with the other relative Eqs.

$$\boldsymbol{Proposed\ Eq.:\ E_c = 3622 f_c^{0.537}} \quad (\mathbf{5.17})$$

$$\boldsymbol{ACI318-14: E_c = 0.043 \times \rho^{1.5} \times \sqrt{f_c}} \quad (\mathbf{5.18})$$

$$\boldsymbol{CEB-FIP: E_c = 0.85 \times 2.15 \times 10^4 (f_c/10)^{1/3}} \quad (5.19)$$

$$\boldsymbol{IS\ 456-2000: E_c = 5000\sqrt{f_c}} \quad (5.20)$$

$$\boldsymbol{Lee\ and\ Lee: E_c = 5300 f_c^{1/3}} \quad (\mathbf{5.21})$$

$$\boldsymbol{Nath\ and\ Sarker\ E_c = 3510\sqrt{f_c}} \quad (\mathbf{5.22})$$

$$\boldsymbol{Bellum\ et\ al.:\ E_c = 3282\sqrt{f_c}} \quad (\mathbf{5.23})$$

Where $\boldsymbol{E_c}$ are modulus of elasticity in MPa, $\boldsymbol{\rho}$ are the density of the concrete in kg/m^3 and $\boldsymbol{f_c}$ are characteristic strength in MPa.

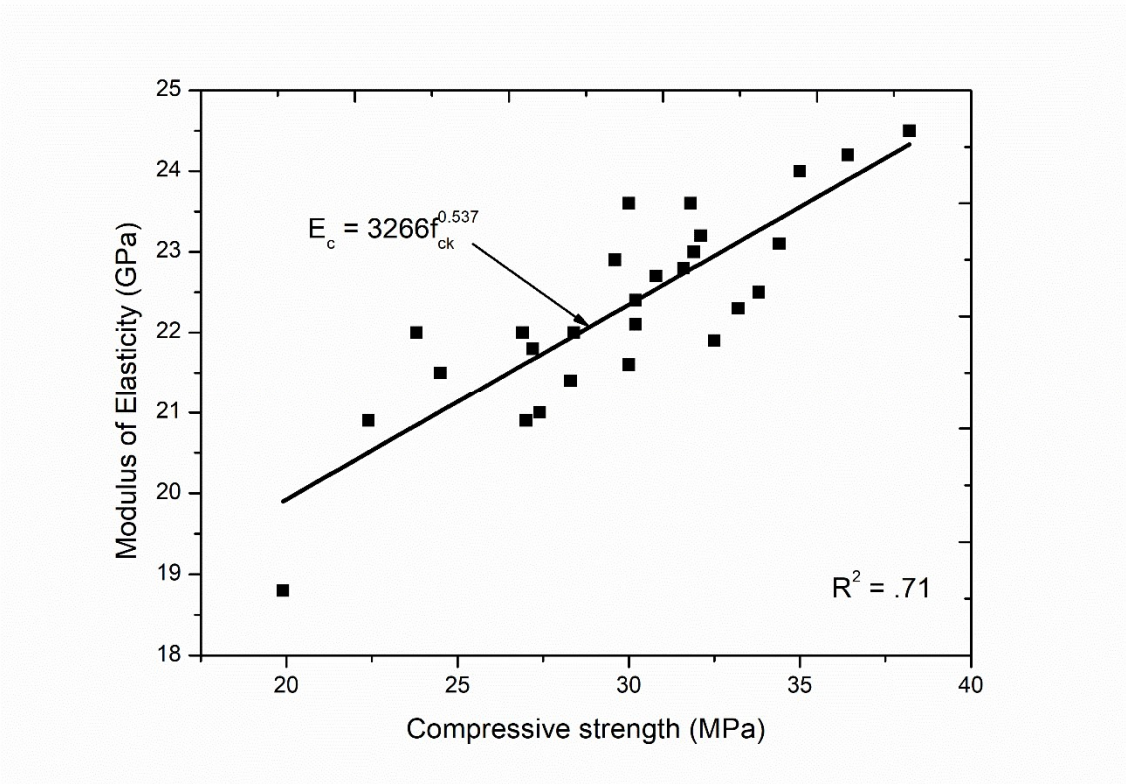

Fig. 5.5 Correlation Eq. generation between MOE and compressive strength

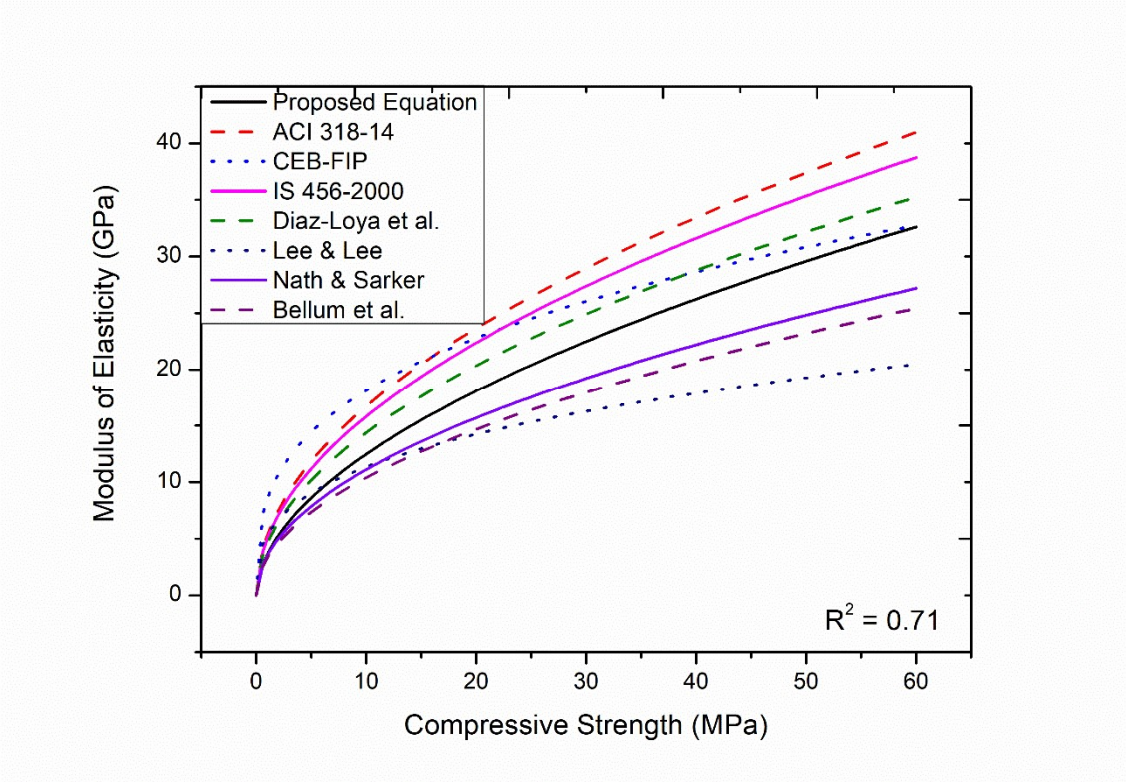

Fig. 5.6 Correlation between MOE and compressive strength comparison graph

Table 5.3 Correlation between the elastic modulus and compressive strength equations

	Proposed Eq	**ACI 318-14**	**CEB-FIP**	**IS 456-2000**	**Lee & Lee**	**Nath & Sarker**	**Bellum et al.**	**Hardjito et al.**	**Diaj-loya et al.**
fc	**Ec=15080+ 240fc**	**Ec=.043*p$^{(1.5)}$*fc$^{.5}$**	**Ec= .85*2.15*10^{4}*(fc/10)$^{1/3}$**	**Ec= 5000(fc)$^{.5}$**	**Ec= 5300(fc)$^{1/3}$**	**Ec= 3510*(fc)$^{.5}$**	**Ec= 3282*(fc)$^{.5}$**	**Ec= 2707(fc)$^{.5}$ + 5300**	**Ec = .037*p$^{1.5}$ *fc$^{.5}$**
15.00	18680.00	20567.98	20919.65	19364.92	13070.92	13594.17	12711.13	15784.17	17698.03
17.50	19280.00	22215.96	22022.67	20916.50	13760.11	14683.38	13729.59	16624.19	19116.05
20.00	19880.00	23749.85	23025.06	22360.68	14386.41	15697.20	14677.55	17406.07	20435.92
22.50	20480.00	25190.53	23947.02	23717.08	14962.47	16649.39	15567.89	18140.43	21675.57
25.00	21080.00	26553.15	24802.99	25000.00	15497.29	17550.00	16410.00	18835.00	22848.06
27.50	21680.00	27849.17	25603.63	26220.22	15997.55	18406.60	17210.95	19495.63	23963.24
30.00	22280.00	29087.51	26357.11	27386.13	16468.33	19225.06	17976.25	20126.85	25028.79
32.50	22880.00	30275.24	27069.81	28504.39	16913.64	20010.08	18710.28	20732.27	26050.79
35.00	23480.00	31418.10	27746.83	29580.40	17336.65	20765.44	19416.57	21314.83	27034.18
37.50	24080.00	32520.83	28392.34	30618.62	17739.97	21494.27	20098.06	21876.92	27983.04
40.00	24680.00	33587.37	29009.75	31622.78	18125.75	22199.19	20757.19	22420.57	28900.76

CHAPTER 6 SUSTAINABILITY AND COST ANALYSIS

6.1 Sustainability Analysis

Sustainable development is essential in the present scenario. A vast volume of industrial solid waste is now created, necessitating this trash in development activities. The use of industrial solid waste decreases carbon footprints and, as a result, indirectly lowers the use of high embodied energy items. For example, the embodied energy in the dry process of OPC cement is approximately 4.6MJ/kg, whereas flyash and slag have no embodied energy. By replacing the OPC, industrial solid waste flyash and slag are used as a binder in concrete, and those wastes are activated by a chemical solution of sodium hydroxide and sodium silicate. As a result, the GPC has less embodied energy than the OPC concrete [189–191]. Table 6.1 shows the embodied energy calculation for both concrete and concrete. The embodied energy of all constituents of concrete is calculated based on the reference papers.

Table 6.1 Embodied energy calculation of GPC and OPC

Constituents	Embodied Energy (MJ/kg)	OPC Concrete		Geopolymer Concrete	
		Mix Content (kg/m^3)	Embodied Energy Content (MJ/kg)	Mix Content (kg/m^3)	Embodied Energy Content (MJ/kg)
OPC	4.6	370	1702	-	-
Flyash	0.0	-	-	303.75	00
GGBFS	0.2	-	-	101.25	31.38
NaOH	20.5	-	-	40.5	830.25
Na_2SiO_3	5.37	-	-	101.25	543.71
Fine Aggregate	0.02	683	13.66	683	13.66
Coarse Aggregate	0.22	1289	283.58	1269	279.18
Water	0.0	148	00	40.5	00
Superplasticiser	12.6	3.7	46.62	4.05	51.03
	Total	2493.7	2045.86 MJ/m^3	2543.7	1749.21 MJ/m^3

6.2 Cost Analysis

The concrete cost was calculated by the number of the constituents present in the concrete mix design, and then, after calculating the rate of all individual constituent prices, the concrete mix design cost was found. The cost of the GPC at a bulk level reduced the cost of up to 40% of the OPC concrete. The cost of the OPC of $1m^3$ is Rs. 3758, whereas the cost of the GPC of $1m^3$ is Rs. 2230. The cost estimated only includes the materials and excludes the human resources. Table 6.1 describes all calculations of the cost of the materials and concrete. Materials and concrete costs are critical in the construction industry because construction projects are always more expensive. The project's economy always matters and goes to the optimum point, which is essential for the project's lower cost. When compared to OPC concrete, GPC concrete is less expensive and emits less carbon dioxide is a new trend in the construction industry due to sustainable development properties. Thaarrini and Dhivya (2016) compared the cost of GPC to cement concrete. Cement concrete is 11% more expensive than GPC for better quality concrete. For grades up to 30 MPa, GPC costs 1.7 percent more than cement concrete [192]. Through his experimental analysis, McLellan (2011) discovered that using fly ash-based GPC decreases building costs and greenhouse gas emissions by 7% and 64%, respectively. The cost of producing GGBS GPC was discovered to be 7% more than the cost of producing OPC-based concrete [193,194]. Assi et al. (2018) developed a novel mix design approach for fly ash-based GPC, cutting construction costs by 50% [195].

Table 6.2 Cost description of both concrete constituents

Constituents	Cost rate (Rs./kg)	OPC Concrete		Geopolymer Concrete	
		Mix Content (kg/m^3)	Cost of the Constituent ($Rs./m^3$)	Mix Content (kg/m^3)	Cost of the Constituent ($Rs./m^3$)
OPC	7.6	370	2812	-	-
Flyash	0.7	-	-	303.75	212.62

GGBFS	2.5	-	-	101.25	253.13
NaOH	10.05	-	-	40.5	407.03
Na_2SiO_3	10	-	-	101.25	1012.5
Fine Aggregate	0.25	683	170.75	683	170.75
Coarse Aggregate	0.525	1289	676.72	1269	666.23
Water	0.0	148	00	40.5	00
Superplasticiser	26.67	3.7	98.68	4.05	108.01
	Total	2493.7	Rs. 3758.15/m^3	2543.7	Rs. 2230.27/m^3

CHAPTER 7 CONCLUSIONS

This experimental study was conducted in the concrete laboratory of the civil engineering department at Delhi Technological University, India. After the experimental investigation, they checked the GPC and conventional concrete specimens against various severe conditions of durability. The following conclusions found through this study are as follows:

- The ambient-cured sample has less strength than the oven-cured samples, but in both cured samples, the 75/25 fly ash/GGBFS ratio gets the maximum engineering strength. The dosage of GGBFS by the replacement of fly ash of about 25% by weight instantaneously increases the strength, but beyond that, the strength slightly decreases in the mix designs.
- The compressive strength, splitting tensile and flexural strength got the optimum point at the 0.60 liquid-to-binder ratios in the GPC mix design. The strength increases with the increment of the liquid-to-binder ratio, but it reduces randomly beyond the 0.60 ratios. The workability of the GPC fresh mixes increases with the increment of the liquid-to-binder ratio, whereas the density decreases consecutively with the ratio increment.
- In the GPC mixes, superplasticizer is 1% in the mix, and the mix gets a higher strength than the other mixes with different percentages of superplasticiser. Similarly, the oven-cured samples' splitting tensile and flexural strength is higher than the ambient-cured samples of the same mix of GPC. In the GPC mixes, the superplasticizer is 1% in the mix, and the mix gets a higher strength than the other mixes with different percentages of superplasticiser.
- The compressive strength rises with the enlargement in molarity of NaOH in the mix design but beyond a point decreases the compressive strength in the oven-cured specimens. The highest compressive strength of the oven-cured 14M mix is 34.2N/mm2 at 56 days, but in the ambient-cured specimen at 16M mix, it is 25N/mm2 at 56 days.
- The engineering strength enlarges with the increment in the ratio in the mix design, but beyond a point, it decreases the compressive strength in both the

curing condition samples. The highest compressive strength of the oven cured 2.5 alkaline ratio mix is 35.7N/mm^2 at 56 days, and in the ambient cured specimen it is 25.8N/mm^2 at 56 days.

- The GPC design mix's mechanical strength increases with the increment of the curing temperature, but it reduces beyond the 100^{0}C curing temperature. The higher curing temperature increases the gain rate of the GPC samples.
- The GPC specimens have better stability against the elevated temperature compared to the OPC concrete specimens. The GPC specimens failed at a temperature of 800^{0}C, whereas the OPC specimens failed at 600^{0}C.
- In seawater conditions, this initially increases the strength and density, but beyond 12 weeks, degradation occurs in both types of specimens. Both types of samples show a similar pattern in strength and mass loss.
- Both types of specimens show a similar pattern of strength and mass loss in the sulphate conditions, whereas the GPC specimens show better stability than OPC concrete specimens.
- In the freeze-thaw conditions, the OPC concrete specimens show better stability than the GPC specimens. The residual strength of GPC specimens was retained at 54% after 90 cycles, whereas the OPC concrete specimens retained 87% of the original.
- Both concrete specimens strengthen the mass continuously with an increment of wetting-drying cycles up to 60 cycles, and it decreases slightly after that. Mass loss occurs beyond 60 cycles, but conventional concrete specimens show no mass loss.

Future Scope

- The present work identified many salient parameters that influence the properties of fresh and hardened fly ash GGBFS-based geopolymer concrete. A large database should be built on the engineering properties of various mixtures using fly ash and GGBFS. Such a database may identify additional parameters and lead to familiarising the utilisation of this material in many applications.

- Further research should identify possible applications of geopolymer technology. This would lead to research areas that are specifically oriented towards applications. The geopolymer technology has the potential to go beyond making concrete; there could be possibilities in other areas of infrastructure needed by the community. So the following work is needed in the future before application in the construction industry.

- To analyse the structural behaviour of the geopolymer concrete with the steel reinforcement and bond properties.

- To analyse the flexural behaviour of reinforced GPC under various point loadings.

- To analyse the eccentric load behaviour on the reinforced GPC columns and crack patterns.

- Numerical analysis of reinforced GPC structural members using a variety of software

References

[1] M. Albitar, P. Visintin, M.S.M. Ali, M. Drechsler, Assessing Behaviour of Fresh and Hardened Geopolymer Concrete Mixed with Class-F Fly Ash, KSCE J. Civ. Eng. 19 (2015) 1445–1455. https://doi.org/10.1007/s12205-014-1254-z.

[2] A. Sathonsaowaphak, P. Chindaprasirt, K. Pimraksa, Workability and strength of lignite bottom ash geopolymer mortar, J. Hazard. Mater. 168 (2009) 44–50. https://doi.org/10.1016/j.jhazmat.2009.01.120.

[3] P.S. Deb, P. Nath, P.K. Sarker, The effects of ground granulated blast-furnace slag blending with fly ash and activator content on the workability and strength properties of geopolymer concrete cured at ambient temperature, J. Mater. 62 (2014) 32–39. https://doi.org/10.1016/j.matdes.2014.05.001.

[4] J. Davidovits, S. Quentin, Geopolymers Inorganic polymeric new materials, J. OfThamalAnalysis. 37 (1991) 1633–1656.

[5] P.H.R. Borges, L.F. Fonseca, V.A. Nunes, T.H. Panzera, C.C. Martuscelli, Andreasen Particle Packing Method on the Development of Geopolymer Concrete for Civil Engineering, J. Mater. Civ. Eng. 26 (2014) 692–697. https://doi.org/10.1061/(ASCE)MT.1943-5533.0000838.

[6] D. V Reddy, J.-B. Edouard, K. Sobhan, Durability of Fly Ash-Based Geopolymer Structural Concrete in the Marine Environment, J. Mater. Civ. Eng. 6 (2013) 781–787. https://doi.org/10.1061/(ASCE)MT.1943.

[7] P.S. Deb, P.K. Sarker, Effects of Ultrafine Fly Ash on Setting, Strength, and Porosity of Geopolymers Cured at Room Temperature, J. Civ. Eng. (2016) 1–5. https://doi.org/10.1061/(ASCE)MT.1943-5533.

[8] C. Chotetanorm, P. Chindaprasirt, V. Sata, S. Rukzon, A. Sathonsaowaphak, High-Calcium Bottom Ash Geopolymer: Sorptivity, Pore Size, and Resistance to Sodium Sulfate Attack, J. Mater. Civ. Eng. 25 (2013) 105–111. https://doi.org/10.1061/(ASCE)MT.1943-5533.

[9] P. Topark-Ngarm, P. Chindaprasirt, V. Sata, P.C. and V. Sata, Pattanapong Topark-Ngarm, Setting Time, Strength, and Bond of High-Calcium Fly Ash Geopolymer Concrete, J. Mater. Civ. Eng. 27 (2015) 1–7. https://doi.org/10.1061/(ASCE)MT.1943-5533.0001157.

[10] S.T. Erdogan, Properties of Ground Perlite Geopolymer Mortars, J. Mater. Civ. Eng. 04014210 (2015) 1–10. https://doi.org/10.1061/(ASCE)MT.1943-5533.0001172.

[11] P. Chindaprasirt, P. De Silva, Effect of SiO 2 and Al 2 O 3 on the setting and hardening of high calcium fly ash-based geopolymer systems, J. Mater. Sci. 47 (2012) 4876–4883. https://doi.org/10.1007/s10853-012-6353-y.

[12] G. Nagalia, Y. Park, A. Abolmaali, P. Aswath, Compressive Strength and Microstructural Properties of Fly Ash – Based Geopolymer Concrete, J. Mater. Civ. Eng. 28 (2016) 1–11. https://doi.org/10.1061/(ASCE)MT.1943-5533.0001656.

[13] K. Kupwade-Patil, E.N. Allouche, Impact of Alkali Silica Reaction on Fly Ash-Based Geopolymer Concrete, J. Mater. Civ. Eng. 25 (2013) 131–139. https://doi.org/10.1061/(ASCE)MT.1943-5533.0000579.

[14] K. Kupwade-Patil, E.N. Allouche, Examination of Chloride-Induced Corrosion in Reinforced Geopolymer Concretes, J. Mater. Civ. Eng. 25 (2013) 1465–1476. https://doi.org/10.1061/(ASCE)MT.1943-5533.0000672.

[15] Z. Liu, C.S. Cai, H. Peng, F. Fan, Experimental Study of the Geopolymeric Recycled Aggregate Concrete, J. Mater. Civ. Eng. 28 (2016) 1–9. https://doi.org/10.1061/(ASCE)MT.1943-5533.0001584.

[16] C.C. Ban, P.W. Ken, M. Ramli, Effect of Sodium Silicate and Curing Regime on Properties of Load Bearing Geopolymer Mortar Block, J. Mater. Civ. Eng. (2015) 1–9. https://doi.org/10.1061/(ASCE)MT.1943-5533.

[17] R. Zhao, J.G. Sanjayan, Geopolymer and Portland cement concretes in simulated fire, Mag. Concr. Res. 63 (2011) 163–173. https://doi.org/10.1680/macr.9.00110.

[18] I. Ismail, S.A. Bernal, J.L. Provis, S. Hamdan, J.S.J. Van Deventer, Microstructural changes in alkali activated fly ash / slag geopolymers with sulfate exposure, Mater. Struct. Constr. 46 (2013) 361–373. https://doi.org/10.1617/s11527-012-9906-2.

[19] D.L.Y.Y. Kong, Æ.J.G. Sanjayan, K. Sagoe-Crentsil, J.G. Sanjayan, K. Sagoe-Crentsil, Factors affecting the performance of metakaolin geopolymers exposed to elevated temperatures, J. Mater. Sci. 43 (2008) 824–831. https://doi.org/10.1007/s10853-007-2205-6.

[20] D.L.Y. Kong, J.G. Sanjayan, K. Sagoe-Crentsil, Comparative performance of geopolymers made with metakaolin and fly ash after exposure to elevated temperatures, Cem. Concr. Res. 37 (2007) 1583–1589. https://doi.org/10.1016/j.cemconres.2007.08.021.

[21] Z. Pan, J.G. Sanjayan, A.B. V Rangan, An investigation of the mechanisms for strength gain or loss of geopolymer mortar after exposure to elevated temperature, J. Mater. Sci. 44 (2009) 1873–1880. https://doi.org/10.1007/s10853-009-3243-z.

[22] G.J.G. Gluth, W.D.A. Rickard, S. Werner, S. Pirskawetz, Acoustic emission and microstructural changes in fly ash geopolymer concretes exposed to simulated fire, Mater. Struct. 49 (2016) 5243–5254. https://doi.org/10.1617/s11527-016-0857-x.

[23] Z. Pan, J.G. Sanjayan, F. Collins, Cement and Concrete Research Effect of transient creep on compressive strength of geopolymer concrete for elevated temperature exposure, Cem. Concr. Res. 56 (2014) 182–189. https://doi.org/10.1016/j.cemconres.2013.11.014.

[24] Z. Pan, J.G. Sanjayan, Stress-strain behaviour and abrupt loss of stiffness of geopolymer at elevated temperatures, Cem. Concr. Compos. 32 (2010) 657–664. https://doi.org/10.1016/j.cemconcomp.2010.07.010.

[25] W.D.A.A. Rickard, J. Temuujin, A. Van Riessen, A. Van Riessen, Thermal analysis of geopolymer pastes synthesised from fi ve fl y ashes of variable composition, J. Non. Cryst. Solids. 358 (2012) 1830–1839. https://doi.org/10.1016/j.jnoncrysol.2012.05.032.

[26] U.R. Kawade, M. Hussain, P.P.A. Shirule, Enhancement of compressive strength of geopolymer concrete by varying ratio of Na 2 Si0 3 / NaoH and by varying molarity of NaoH, Int. J. Latest Res. Eng. Technol. Www.Ijlret.Com ||. 02 (2016) 47–50. www.ijlret.com.

[27] S. Luhar, U. Khandelwal, A Study on Water Absorption and Sorptivity of Geopolymer Concrete, SSRG Int. J. Civ. Eng. 2 (2015) 1–10.

[28] S. V. Patankar, Y.M. Ghugal, S.S. Jamkar, Mix design of fly ash based geopolymer concrete, in: Adv. Struct. Eng. Mater. Vol. Three, Springer India, 2015: pp. 1619–1633. https://doi.org/10.1007/978-81-322-2187-6_123.

[29] K. Suganya, L. Krishnan, S. Karthikeyan, S. Nathiya, K. Suganya, GEOPOLYMER CONCRETE AN ECO-FRIENDLY CONSTRUCTION MATERIAL, IJRET Int. J. Res. Eng. Technol. (2014) 2319–2322. http://www.ijret.org.

[30] X. Gao, Q.L. Yu, H.J.H.H. Brouwers, Reaction kinetics , gel character and strength of ambient temperature cured alkali activated slag – fly ash blends, Constr. Build. Mater. 80 (2015) 105–115. https://doi.org/10.1016/j.conbuildmat.2015.01.065.

[31] P. Chindaprasirt, T. Chareerat, V. Sirivivatnanon, Workability and strength of coarse high calcium fly ash geopolymer, Cem. Concr. Compos. 29 (2007) 224–229. https://doi.org/10.1016/j.cemconcomp.2006.11.002.

[32] N.K. Lee, J.G. Jang, H.K. Lee, Cement & Concrete Composites Shrinkage characteristics of alkali-activated fly ash/slag paste and mortar at early ages, Cem. Concr. Compos. 53 (2014) 239–248. https://doi.org/10.1016/j.cemconcomp.2014.07.007.

[33] M. Chi, R. Huang, Binding mechanism and properties of alkali-activated fly ash/slag mortars, Constr. Build. Mater. 40 (2013) 291–298. https://doi.org/10.1016/j.conbuildmat.2012.11.003.

[34] K.-H. Yang, J.-K. Song, K.-S. Lee, A.F. Ashour, Flow and Compressive Strength of Alkali-Activated Mortars, 2009.

[35] J. Temuujin, A. Van Riessen, K.J.D. MacKenzie, A. Van Riessen, K.J.D. MacKenzie, Preparation

and characterisation of fly ash based geopolymer mortars, Constr. Build. Mater. 24 (2010) 1906–1910. https://doi.org/10.1016/j.conbuildmat.2010.04.012.

[36] H.U. Shu-guang, W.U. Jing, Y. Wen, H.E. Yong-jia, Preparation and properties of geopolymer-lightweight aggregate refractory concrete, J. Cenral South Univ. Technol. 16 (2009) 914–918. https://doi.org/10.1007/s11771.

[37] P. Chindaprasirt, T. Chareerat, S. Hatanaka, T. Cao, P. Chindaprasirt; T. Chareerat; S. Hatanaka; and T. Cao, High-Strength Geopolymer Using Fine High-Calcium Fly Ash, J. Mater. Civ. Eng. 23 (2011) 264–270. https://doi.org/10.1061/(asce)mt.1943-5533.0000161.

[38] A.R. Brough, A. Atkinson, Sodium silicate-based, alkali-activated slag mortars Part I . Strength, hydration and microstructure, Cem. Concr. Res. 32 (2002) 865–879. https://doi.org/10.1016/S0008-8846(02)00717-2.

[39] G. Nagalia, Y. Park, A. Abolmaali, P. Aswath, Compressive Strength and Microstructural Properties of Fly Ash–Based Geopolymer Concrete, J. Mater. Civ. Eng. 18 (2016) 040161441–11. https://doi.org/10.1061/(ASCE)MT.1943-5533.0001656.

[40] G.S. Ryu, Y.B. Lee, K.T. Koh, Y.S. Chung, The mechanical properties of fly ash-based geopolymer concrete with alkaline activators, Constr. Build. Mater. 47 (2013) 409–418. https://doi.org/10.1016/j.conbuildmat.2013.05.069.

[41] S. V Patankar, Y.M. Ghugal, S.S. Jamkar, Effect of Concentration of Sodium Hydroxide and Degree of Heat Curing on Fly Ash-Based Geopolymer Mortar Effect of Concentration of Sodium Hydroxide and Degree of Heat Curing on Fly Ash-Based Geopolymer Mortar, Indian J. Mater. Sci. 2014 (2015) 1–6. https://doi.org/10.1155/2014/938789.

[42] S.S. Bidwe, A.A. Hamane, Effect of different molarities of Sodium Hydroxide solution on the Strength of Geopolymer concrete, Am. J. Eng. Res. 4 (2015) 139–145. www.ajer.org.

[43] S.M.A.A. Kabir, U.J. Alengaram, M.Z. Jumaat, A. Sharmin, A. Islam, Influence of Molarity and Chemical Composition on the Development of Compressive Strength in POFA Based Geopolymer Mortar, Adv. Mater. Sci. Eng. 2015 (2020). https://doi.org/10.1155/2015/647071.

[44] D. Hardjito, S.E. Wallah, On The Development of Fly Ash-based Geopolymer Concrete, ACI Mater. J. 101 (2004) 467–72. https://www.researchgate.net/publication/43649854.

[45] N.K. Lee, H.K. Lee, Setting and mechanical properties of alkali-activated fly ash/slag concrete manufactured at room temperature, Constr. Build. Mater. 47 (2013) 1201–1209. https://doi.org/10.1016/j.conbuildmat.2013.05.107.

[46] K. Somna, C. Jaturapitakkul, P. Kajitvichyanukul, P. Chindaprasirt, NaOH-activated ground fly ash geopolymer cured at ambient temperature, Fuel. 90 (2011) 2118–2124. https://doi.org/10.1016/j.fuel.2011.01.018.

[47] C.K. Yip, G.C. Lukey, J.S.J. Van Deventer, J.S.J. Van Deventer, The coexistence of geopolymeric gel and calcium silicate hydrate at the early stage of alkaline activation, Cem. Concr. Res. 35 (2005) 1688–1697. https://doi.org/10.1016/j.cemconres.2004.10.042.

[48] W.K.W.W. Lee, J.S.J. Van Deventer, J.S.J. Van Deventer, The interface between natural siliceous aggregates and geopolymers, Cem. Concr. Res. 34 (2004) 195–206. https://doi.org/10.1016/S0008-8846(03)00250-3.

[49] P. Nath, P.K. Sarker, Effect of GGBFS on setting, workability and early strength properties of fly ash geopolymer concrete cured in ambient condition, Constr. Build. Mater. 66 (2014) 163–171. https://doi.org/10.1016/j.conbuildmat.2014.05.080.

[50] X. Guo, H. Shi, W.A. Dick, Cement & Concrete Composites Compressive strength and microstructural characteristics of class C fly ash geopolymer, Cem. Concr. Compos. 32 (2010) 142–147. https://doi.org/10.1016/j.cemconcomp.2009.11.003.

[51] A. Silva, D. Vargas, D.C.C. Dal, A.C.F. Vilela, F. José, B. Pavão, H. Veit, Cement & Concrete Composites The effects of Na 2 O / SiO 2 molar ratio , curing temperature and age on compressive strength , morphology and microstructure of alkali-activated fly ash-based geopolymers, Cem. Concr. Compos. 33 (2011) 653–660. https://doi.org/10.1016/j.cemconcomp.2011.03.006.

[52] Z. Pan, J.G. Sanjayan, D.L.Y. Kong, Effect of aggregate size on spalling of geopolymer and

Portland cement concretes subjected to elevated temperatures, Constr. Build. Mater. 36 (2012) 365–372. https://doi.org/10.1016/j.conbuildmat.2012.04.120.

[53] P. Engineering, Yliniemi, Paiva, Ferreira, Tiainen, Illikainen, Development and incorporation of lightweight waste-based geopolymer aggregates in mortar and concrete, Constr. Build. Mater. 131 (2017) 784–792. https://doi.org/10.1016/j.conbuildmat.2016.11.017.

[54] C. Sreenivasulu, A. Ramakrishnaiah, J. Guru Jawahar, MECHANICAL PROPERTIES OF GEOPOLYMER CONCRETE USING GRANITE SLURRY AS SAND REPLACEMENT, 2015.

[55] M. Basha, B. Reddy Ch, & Vasugi, M.B. S, B.R. Ch, K. Vasugi, Strength behaviour of geopolymer concrete replacing fine aggregates by M- sand and E-waste, Int. J. Eng. Trends Technol. (2016) 401–407. http://www.ijettjournal.org.

[56] Saravanan S, Strength properties of geopolymer concrete using msand by assessing their mechanical characteristics Investigation of Structural Members with Basalt Rebar Reinforcement as an Effective Alternative of Standard Steel Rebar View project NON-LINEAR TIME HISTORY ANALYSIS OF BUILDING RESTING ON SLOPING GROUND SUBJECTED TO BLAST LOAD View project, 2018. https://www.researchgate.net/publication/326723487.

[57] F.U.A. Shaikh, F. Uddin, A. Shaikh, Mechanical and durability properties of fly ash geopolymer concrete containing recycled coarse aggregates, Int. J. Sustain. Built Environ. 5 (2016) 277–287. https://doi.org/10.1016/j.ijsbe.2016.05.009.

[58] J.G.S. Van Jaarsveld, J.S.J. Van Deventer, J.G.S. Van Jaarsveld, J.S.J. Van Deventer, Effect of the Alkali Metal Activator on the Properties of Fly Ash-Based Geopolymers, Ind. Eng. Chem. Res. (1999) 3932–3941. https://doi.org/10.1021/ie980804b.

[59] T.W. Cheng, J.P. Chiu, Fire-resistant geopolymer produce by granulated blast furnace slag, Miner. Eng. (2003). https://doi.org/10.1016/S0892-6875(03)00008-6.

[60] T. Bakharev, Thermal behaviour of geopolymers prepared using class F fly ash and elevated temperature curing, Cem. Concr. Res. 36 (2006) 1134–1147. https://doi.org/10.1016/j.cemconres.2006.03.022.

[61] H.M. Khater, Studying the effect of thermal and acid exposure on alkali-activated slag geopolymer, Adv. Cem. Res. 29 (2014) 1–9. https://doi.org/10.1680/adcr.11.00052.

[62] P. Duxson, G.C. Lukey, J.S.J. Van Deventer, J.S.J. van Deventer, Thermal evolution of metakaolin geopolymers : Part 1 – Physical evolution, J. Non. Cryst. Solids. 352 (2006) 5541–5555. https://doi.org/10.1016/j.jnoncrysol.2006.09.019.

[63] Y. Ma, G. Ye, The shrinkage of alkali activated fly ash, Cem. Concr. Res. (2015). https://doi.org/10.1016/j.cemconres.2014.10.024.

[64] I. Ismail, S.A. Bernal, J.L. Provis, R. San Nicolas, S. Hamdan, J.S.J. Van Deventer, R. San, S. Hamdan, J.S.J. Van Deventer, Cement & Concrete Composites Modification of phase evolution in alkali-activated blast furnace slag by the incorporation of fly ash, Cem. Concr. Compos. 45 (2014) 125–135. https://doi.org/10.1016/j.cemconcomp.2013.09.006.

[65] H.M. Khater, Studying the effect of thermal and acid exposure on alkali- activated slag geopolymer, Adv. Cem. Res. 26 (2014) 1–9. https://doi.org/http://dx.doi.org/10.1680/adcr.11.00052.

[66] J.G. Jang, N.K. Lee, H.K. Lee, Fresh and hardened properties of alkali-activated fly ash/slag pastes with superplasticizers, Constr. Build. Mater. 50 (2014) 169–176. https://doi.org/10.1016/j.conbuildmat.2013.09.048.

[67] P. Nath, P.K. Sarker, Flexural strength and elastic modulus of ambient-cured blended low-calcium fly ash geopolymer concrete, Constr. Build. Mater. 130 (2017) 22–31. https://doi.org/10.1016/j.conbuildmat.2016.11.034.

[68] S. Kumar, R. Kumar, Influence of granulated blast furnace slag on the reaction , structure and properties of fly ash based geopolymer, (2010) 607–615. https://doi.org/10.1007/s10853-009-3934-5.

[69] D.L.Y. Kong, J.G. Sanjayan, Damage behavior of geopolymer composites exposed to elevated temperatures, Cem. Concr. Compos. 30 (2008) 986–991.

https://doi.org/10.1016/j.cemconcomp.2008.08.001.

[70] K.S. Finnie, D.S. Perera, O. Uchida, E.R. Vance, K.S. Finnie, Influence of curing schedule on the integrity of geopolymers, J. Mater. Sci. 42 (2007) 3099–3106. https://doi.org/10.1007/s10853-006-0533-6.

[71] D. Bondar, C.J. Lynsdale, N.B. Milestone, N. Hassani, Sulfate Resistance of Alkali Activated Pozzolans, Int. J. Concr. Struct. Mater. 9 (2015) 145–158. https://doi.org/10.1007/s40069-014-0093-0.

[72] Y.S. Zhang, W. Sun, J.Z. Li, Hydration process of interfacial transition in potassium polysialate (K-PSDS) geopolymer concrete, Mag. Concr. Res. (2005) 33–38. https://doi.org/10.1680/macr.2005.57.1.33.

[73] W.K.W. Lee, J.S.J. Van Deventer, J.S.J. van Deventer, Chemical interactions between siliceous aggregates and low-Ca alkali-activated cements, Cem. Concr. Res. 37 (2007) 844–855. https://doi.org/10.1016/j.cemconres.2007.03.012.

[74] S. Demie, M.F. Nuruddin, N. Shafiq, M. Fadhil, N. Shafiq, Effects of micro-structure characteristics of interfacial transition zone on the compressive strength of self-compacting geopolymer concrete, Constr. Build. Mater. 41 (2020) 91–98. https://doi.org/10.1016/j.conbuildmat.2012.11.067.

[75] O.A. Abdulkareem, A.M.M. Al, H. Kamarudin, I.K. Nizar, A.A. Saif, A.M. Mustafa Al Bakri, H. Kamarudin, I. Khairul Nizar, A.A. Saif, Effects of elevated temperatures on the thermal behavior and mechanical performance of fly ash geopolymer paste , mortar and lightweight concrete, Constr. Build. Mater. 50 (2014) 377–387. https://doi.org/10.1016/j.conbuildmat.2013.09.047.

[76] P. Rovnaník, S.O. Al, Effect of curing temperature on the development of hard structure of metakaolin-based geopolymer, Constr. Build. Mater. 24 (2010) 1176–1183. https://doi.org/10.1016/j.conbuildmat.2009.12.023.

[77] C.Y. Heah, H. Kamarudin, A.M.M. Al, M. Binhussain, A.M. Mustafa Al Bakri, M. Binhussain, M. Luqman, I. Khairul Nizar, C.M. Ruzaidi, Y.M. Liew, Effect of Curing Profile on Kaolin-based Geopolymers, Phys. Procedia. 22 (2011) 305–311. https://doi.org/10.1016/j.phpro.2011.11.048.

[78] E.N. Kani, A. Allahverdi, Effects of curing time and temperature on strength development of inorganic polymeric binder based on natural pozzolan, J. Mater. Sci. 44 (2009) 3088–3097. https://doi.org/10.1007/s10853-009-3411-1.

[79] N.A. Lloyd, B. V Rangan, Geopolymer Concrete with Fly Ash, Second Int. Conf. Sustain. Constr. Mater. Technol. (2010) 1–7. https://www.researchgate.net/publication/228825101.

[80] A. Islam, U.J. Alengaram, M.Z. Jumaat, I.I. Bashar, S.M.A.A. Kabir, Engineering properties and carbon footprint of ground granulated blast- furnace slag-palm oil fuel ash-based structural geopolymer concrete, Constr. Build. Mater. 101 (2015) 503–521. https://doi.org/10.1016/j.conbuildmat.2015.10.026.

[81] D. Bondar, C.J. Lynsdale, N.B. Milestone, N. Hassani, A.A. Ramezanianpour, Engineering Properties of Alkali Activated Natural Pozzolan Concrete, Second Int. Conf. Sustain. Constr. Mater. Technol. (2010) 1–10. http://www.claisse.info/Proceedings.htm.

[82] C.K. Yip, G.C. Lukey, J.L. Provis, J.S.J. van Deventer, J.S.J. Van Deventer, Effect of calcium silicate sources on geopolymerisation, Cem. Concr. Res. 38 (2008) 554–564. https://doi.org/10.1016/j.cemconres.2007.11.001.

[83] S. Puligilla, P. Mondal, Role of slag in microstructural development and hardening of fly ash-slag geopolymer, Cem. Concr. Res. (2013). https://doi.org/10.1016/j.cemconres.2012.10.004.

[84] D.L.Y. Kong, J.G. Sanjayan, Cement and Concrete Research Effect of elevated temperatures on geopolymer paste, mortar and concrete, Cem. Concr. Res. 40 (2010) 334–339. https://doi.org/10.1016/j.cemconres.2009.10.017.

[85] B. Nematollahi, J. Sanjayan, Effect of different superplasticizers and activator combinations on workability and strength of fly ash based geopolymer, Mater. Des. (2014). https://doi.org/10.1016/j.matdes.2014.01.064.

[86] A. Kusbiantoro, M.S. Ibrahim, K. Muthusamy, A. Alias, The 3 rd International Conference on

Sustainable Future for Human Security Development of sucrose and citric acid as the natural based admixture for fly ash based geopolymer, Procedia Environ. Sci. 17 (2013) 596–602. https://doi.org/10.1016/j.proenv.2013.02.075.

[87] M. Palacios, M. Palacios, P.F.G. Banfill, F. Puertas, Rheology and setting of alkali-activated slag pastes and mortars : Effect of organ admixture Rheology and Setting of Alkali-Activated Slag Pastes and Mortars : Effect of Organic Admixture, ACI Mater. J. 105 (2008) 140–148.

[88] M. Palacios, P.F.G. Banfill, F. Puertas, Rheology and setting of alkali-activated slag pastes and mortars: Effect if organic admixture, ACI Mater. J. 105 (2008) 140–148. https://doi.org/10.14359/19754.

[89] P. Duxson, J.L. Provis, G.C. Lukey, S.W. Mallicoat, W.M. Kriven, J.S.J. Van Deventer, J.S.J. Van Deventer, Understanding the relationship between geopolymer composition, microstructure and mechanical properties, Colloids Surfaces A Physicochem. Eng. Asp. 269 (2005) 47–58. https://doi.org/10.1016/j.colsurfa.2005.06.060.

[90] A. Hajimohammadi, J.S.J. van Deventer, J.S.J. Deventer, Characterisation of One-Part Geopolymer Binders Made from Fly, Waste and Biomass Valorization. 8 (2017) 225–233. https://doi.org/10.1007/s12649-016-9582-5.

[91] R. Priyanka, R. Selvaraj, B. Rajesh, CHARACTERISATION STUDY ON CLAY BASED GEOPOLYMER CONCRETE, 2015. http://www.euroasiapub.org.

[92] P. De Silva, K. Sagoe-Crenstil, V. Sirivivatnanon, Kinetics of geopolymerization: Role of Al2O3and SiO2, Cem. Concr. Res. (2007). https://doi.org/10.1016/j.cemconres.2007.01.003.

[93] I. Ismail, S.A. Bernal, J.L. Provis, S. Hamdan, J.S.J. Van Deventer, Microstructural changes in alkali activated fly ash/slag geopolymers with sulfate exposure, Mater. Struct. Constr. (2013). https://doi.org/10.1617/s11527-012-9906-2.

[94] W. Gustavo, V. Saavedra, D.E. Angulo, R.M. De Gutiérrez, D. Ph, ; Daniela, E. Angulo, R. Mejía De Gutiérrez, Fly Ash Slag Geopolymer Concrete : Resistance to Sodium and Magnesium Sulfate Attack, J. Mater. Civ. Eng. 28 (2016) 1–9. https://doi.org/10.1061/(ASCE)MT.1943-5533.0001618.

[95] P. Sukmak, P. De Silva, S. Horpibulsuk, P. Chindaprasirt, Sulfate Resistance of Clay-Portland Cement and Clay High-Calcium Fly Ash Geopolymer, J. Mater. Civ. Eng. (2015). https://doi.org/10.1061/(ASCE)MT.1943-5533.0001112.

[96] M.A.R. Bhutta, W.M. Hussin, M. Azreen, M.M. Tahir, M. Aamer, R. Bhutta, D. Ph, W.M. Hussin, D. Ph, M. Azreen, D. Ph, M.M. Tahir, D. Ph, Sulphate Resistance of Geopolymer Concrete Prepared from Blended Waste Fuel Ash, J. Mater. Civ. Eng. 26 (2014) 1–6. https://doi.org/10.1061/(ASCE)MT.1943-5533.0001030.

[97] K.V. Manjeeth, J.S.K. Rama, An Experimental Investigation on the behaviour of Portland Cement Concrete and Geopolymer Concrete in acidic environment ., SSRG Int. J. Civ. Eng. 2 (2015) 64–68.

[98] A.R. Brough, M. Holloway, J. Sykes, A. Atkinson, Sodium silicate-based alkali-activated slag mortars, Cem. Concr. Res. 20 (2000) 1375–1379. https://doi.org/10.1016/S0008-8846(00)00356-2.

[99] D. Wiyono, D. Hardjito, P. Antoni, D. Hardjito, Improving the durability of pozzolan concrete using alkaline solution and geopolymer coating, Procedia Eng. 125 (2015) 747–753. https://doi.org/10.1016/j.proeng.2015.11.121.

[100] M. Olivia, H. Nikraz, Properties of fly ash geopolymer concrete designed by Taguchi method, Mater. Des. 36 (2012) 191–198. https://doi.org/10.1016/j.matdes.2011.10.036.

[101] K. Pasupathy, M. Berndt, A. Castel, J. Sanjayan, R. Pathmanathan, Carbonation of a blended slag-fly ash geopolymer concrete in field conditions after 8 years, Constr. Build. Mater. 125 (2016) 661–669. https://doi.org/10.1016/j.conbuildmat.2016.08.078.

[102] O. Sanusi, B. Tempest, V.O. Ogunro, J. Gergely, Leaching Characteristics of Geopolymer Cement Concrete Containing Recycled Concrete Aggregates, J. Hazardous, Toxic, Radioact. Waste. 20 (2016) 1–8. https://doi.org/10.1061/(ASCE)HZ.2153-5515.0000312.

[103] F. Matalkah, P. Soroushian, A. Balchandra, A. Peyvandi, Characterization of Alkali-Activated Nonwood Biomass Ash – Based Geopolymer Concrete, J. Mater. Civ. Eng. 29 (2017) 1–9. https://doi.org/10.1061/(ASCE)MT.1943-5533.

[104] W. Ren, J. Xu, E. Bai, D. Ph, Strength and Ultrasonic Characteristics of Alkali-Activated Fly Ash-Slag Geopolymer Concrete after Exposure to Elevated Temperatures, J. Mater. Civ. Eng. 28 (2016) 1–8. https://doi.org/10.1061/(ASCE)MT.1943-5533.0001406.

[105] Z. Pan, J.G. Sanjayan, Cement & Concrete Composites Stress – strain behaviour and abrupt loss of stiffness of geopolymer at elevated temperatures, Cem. Concr. Compos. 32 (2010) 657–664. https://doi.org/10.1016/j.cemconcomp.2010.07.010.

[106] V.F.F. Barbosa, K.J.D. Mackenzie, Synthesis and thermal behaviour of potassium sialate geopolymers, Mater. Lett. 57 (2003) 1477–1482. https://doi.org/10.1016/S0167-577X(02)01009-1.

[107] V.D. Cao, S. Pilehvar, C. Salas-bringas, A.M. Szczotok, J.F. Rodriguez, M. Carmona, N. Al-Manasir, A.L. Kjøniksen, V. Duy, S. Pilehvar, C. Salas-bringas, A.M. Szczotok, J.F. Rodriguez, M. Carmona, N. Al-Manasir, A.L. Kjøniksen, Microencapsulated phase change materials for enhancing the thermal performance of Portland cement concrete and geopolymer concrete for passive building applications, Energy Convers. Manag. 133 (2017) 56–66. https://doi.org/10.1016/j.enconman.2016.11.061.

[108] C. Snell, B. Tempest, T. Gentry, Comparison of the Thermal Characteristics of Portland Cement and Geopolymer Cement Concrete Mixes, J. Archit. Eng. 23 (2017) 1–10. https://doi.org/10.1061/(ASCE)AE.1943-5568.0000240.

[109] O.G. Rivera, W.R. Long, C.A. Weiss, R.D. Moser, B.A. Williams, K. Torres-cancel, E.R. Gore, P.G. Allison, C.A.W. Jr, R.D. Moser, B.A. Williams, K. Torres-cancel, E.R. Gore, P.G. Allison, Cement and Concrete Research Effect of elevated temperature on alkali-activated geopolymeric binders compared to portland cement-based binders, Cem. Concr. Res. 90 (2016) 43–51. https://doi.org/10.1016/j.cemconres.2016.09.013.

[110] P.K. Sarker, Bond strength of reinforcing steel embedded in fly ash-based geopolymer concrete, Mater. Struct. Constr. (2011) 1021–1030. https://doi.org/10.1617/s11527-010-9683-8.

[111] M. Albitar, P. Visintin, M.S.M. Ali, O. Lavigne, E. Gamboa, Bond Slip Models for Uncorroded and Corroded Steel Reinforcement in Class-F Fly Ash Geopolymer Concrete, J. Mater. Civ. Eng. (1992) 1–10. https://doi.org/10.1061/(ASCE)MT.1943-5533.0001713.

[112] M. Sofi, J.S.J. van Deventer, P.A. Mendis, G.C. Lukey, Engineering properties of inorganic polymer concretes (IPCs), Cem. Concr. Res. (2007). https://doi.org/10.1016/j.cemconres.2006.10.008.

[113] B.H. Tekle, A. Khennane, O. Kayali, Bond Properties of Sand-Coated GFRP Bars with Fly Ash – Based Geopolymer Concrete, 20 (2016) 1–13. https://doi.org/10.1061/(ASCE)CC.

[114] T. Sing Ng, S. Wales, A. Ali Amin, A.J. Stephen Foster, The behaviour of steel-fibre-reinforced geopolymer concrete beams in shear, Mag. Concr. Res. 65 (2013) 308–318. https://doi.org/10.1680/macr.12.00081.

[115] G. Maranan, A. Manalo, K. Karunasena, B. Benmokrane, Bond Stress-Slip Behavior : Case of GFRP Bars in Geopolymer Concrete, J. Mater. Civ. Eng. 27 (2015) 1–9. https://doi.org/10.1061/(ASCE)MT.1943-5533.0001046.

[116] J.R. Yost, A. Radlińska, S. Ernst, M. Salera, Structural behavior of alkali activated fly ash concrete . Part 1 : mixture design , material properties and sample fabrication, Mater. Struct. Constr. (2013) 435–447. https://doi.org/10.1617/s11527-012-9919-x.

[117] A. Suriya prakash, G. Senthil kumar, A. Suriya, G. Senthil, A. Fly, Experimental Study on Geopolymer Concrete using Steel Fibres, Int. J. Eng. Trends Technol. 21 (2015) 396–399. http://www.ijettjournal.org.

[118] D.M.J. Sumajouw, D. Hardjito, S.E. Wallah, B. V. Rangan, Fly ash-based geopolymer concrete : study of slender reinforced columns, J. Mater. Sci. (2007) 3124–3130. https://doi.org/10.1007/s10853-006-0523-8.

[119] T.S. Lin, D.C. Jia, P.G. He, M.R. Wang, L.I.N. Tie-song, J.I.A. De-chang, H.E. Pei-gang, W. Mei-

rong, Thermal-mechanical properties of short carbon fiber reinforced geopolymer matrix composites subjected to thermal load, J. Cent. South Univ. Technol. (English Ed. 16 (2009) 881–886. https://doi.org/10.1007/s11771.

[120] F. Pacheco-Torgal, Z. Abdollahnejad, S. Miraldo, S. Baklouti, Y. Ding, An overview on the potential of geopolymers for concrete infrastructure rehabilitation, Constr. Build. Mater. 36 (2012) 1053–1058. https://doi.org/10.1016/j.conbuildmat.2012.07.003.

[121] S.M. Rao, I.P. Acharya, Synthesis and Characterization of Fly Ash Geopolymer Sand, J. Mater. Civ. Eng. 1 (2014) 912–917. https://doi.org/10.1061/(ASCE)MT.1943-5533.0000880.

[122] Bureau of Indian Standard, Determination of Initial and Final Setting Time, IS 4031 (Part 5). 4031 (2002) 3–6.

[123] Bureau of Indian Standard, METHODS OF PHYSICAL TESTS FOR HYDRAULIC CEMENT PART II Determination of Density, IS 4031(Part 11). 4031 (1995) 1–2.

[124] Bureau of Indian Standard, Fineness by dry sieving, IS 4031 (Part I). 4031 (1996).

[125] Bureau of Indian Standard, Determination of Soundness, IS 4031 (Part 3). 4031 (2002) 2–7.

[126] Bureau of Indian Standard, Determination of Consistency of Standard Cement Paste, IS 4031 (Part 4). 4031 (1997).

[127] Bureau of Indian Standard, Determination of False Set, IS 4031 (Part 14). 4931 (1999).

[128] Bureau of Indian Standards, 43 GRADE ORDINARY PORTLAND CEMENT - SPECIFICATION, IS 81121989. (1990).

[129] ASTM International, Standard Specification for Chemical Admixtures for Concrete, C494/C494M − 17. (2019) 1–10. https://doi.org/10.1520/C0494.

[130] ASTM C 618 − 19, Standard Specification for Coal Fly Ash and Raw or Calcined Natural Pozzolan for Use in concrete, 2019. https://doi.org/10.1520/C0618-19.2.

[131] Bureau of Indian Standard, Mechanical Properties, IS 2386(Part IV). 2386 (1997).

[132] Bureau of Indian Standard, Estimation of Deleterious Materials and Organic Impurities, IS 2386 (Part II). 2386 (1998).

[133] Bureau of Indian Standard, Coarse and Fine Aggregate from Natural Sources for Concrete, IS 383-1970. (1997) 1–20.

[134] Bureau of Indian Standard, Particle Size and Shape, Is 2386(Part I). 2386 (1997).

[135] Bureau of Indian Standard, Specific Gravity, Density, Voids, Absorption and Bulking, IS 2386 (Part III). 2386 (1997).

[136] Bureau of Indian Standard, MEASURING MORTAR MAKING PROPERTIES OF FINE AGGREGATE, IS 2386 (Part VI). 2386 (1997).

[137] Bureau of Indian Standard, Soundness, IS 2386. (1997).

[138] ASTM C117 − 17, Standard Test Method for Materials Finer than 75-µm (No . 200) Sieve in Mineral Aggregates by Washing, ASTM Int. (2019) 7–10. https://doi.org/10.1520/C0117-17.

[139] ASTM C70 − 13, Standard Test Method for Surface Moisture in Fine Aggregate, ASTM Int. (2019) 1–3. https://doi.org/10.1520/C0070-13.2.

[140] ASTM C29/C29M − 17a, Standard Test Method for Bulk Density (“ Unit Weight ”) and Voids in Aggregate, ASTM Int. (2019) 1–5. https://doi.org/10.1520/C0029.

[141] ASTM C136/C136M − 14, Standard Test Method for Sieve Analysis of Fine and Coarse Aggregates, ASTM Int. (2019) 1–5. https://doi.org/10.1520/C0136.

[142] ASTM International, Standard Test Method for Relative Density (Specific Gravity) and Absorption of Coarse, C127 − 15. (2019) 1–5. https://doi.org/10.1520/C0127-15.2.

[143] Bureau of Indian Standards, CONCRETE ADMIXTURES-Specification, IS 91031999. April (1999).

[144] Bureau of Indian Standard, GENERAL REQUIREMENT FOR PAN MIXTURES FOR

CONCRETE, IS 12119-1987. (1999).

[145] M. Verma, N. Dev, Geopolymer concrete : A way of sustainable construction, Int. J. Recent Res. Asp. 5 (2018) 201–205. https://www.academia.edu/39203400/Geopolymer_concrete_A_way_of_sustainable_constructio n.

[146] Bureau of Indian Standards, Method of non-destructive testing of concrete-methods of test Part 2: Rebound hammer, Is 13311-2. (1992). https://law.resource.org/pub/in/bis/S03/is.13311.2.1992.pdf.

[147] ASTM International, Rebound Number of Hardened Concrete, C805/C805M − 18. (2002) 2–4. https://doi.org/10.1520/C0805.

[148] Bureau of Indian Standard, Non-destructive testing of concrete methods of test Part 1: Ultrasonic pulse velocity, IS 13311 (Part1) 1992. (1992).

[149] ASTM International, Standard Practice for the Preparation of Substitute Ocean Water, ASTM D1141 − 98. 98 (2008) 98–100. https://doi.org/10.1520/D1141-98R08.2.

[150] ASTM International, Standard test method for length change of hydraulic-cement mortars exposed to a sulfate solution, ASTM IC1012/C1012M − 18b. 11 (2015) 5–9. https://doi.org/10.1520/C1012.

[151] ASTM International, Standard Test Methods for Determining the Chemical Resistance of Concrete Products to Acid Attack, ASTM C1898 − 20. (2020) 9–10. https://doi.org/10.1520/D1898-20.1.

[152] ASTM International, Standard Test Method for Resistance of Concrete to Rapid Freezing and Thawing, ASTM IC666/C666M − 15. 03 (2003) 1–6.

[153] ASTM International, Standard Test Method for Evaluation of Durability of Rock for Erosion Control Under Wetting and Drying Conditions, ASTM D5313/D5313M − 21. 92 (1997) 5–7. https://doi.org/10.1520/D5313.

[154] M.S. and S.T. C. Antony Jeyasehar, G. Saravanan, DEVELOPMENT OF FLY ASH BASED GEOPOLYMER PRECAST CONCRETE ELEMENTS, ASIAN J. Civ. Eng. 14 (2013) 605–615.

[155] ASTM C597 − 16, Standard Test Method for Pulse Velocity Through Concrete ASTM C 597, ASTM Int. (2016) 4. https://doi.org/10.1520/C0597-16.2.

[156] ASTM C138/C138M − 17a, Standard Test Method for Density (Unit Weight), Yield, and Air Content (Gravimetric) of Concrete, ASTM Int. (2019) 1–6. https://doi.org/10.1520/C0138.

[157] K. tuo Wang, Y. He, X. ling Song, X. min Cui, Effects of the metakaolin-based geopolymer on high-temperature performances of geopolymer/PVC composite materials, Appl. Clay Sci. 114 (2015) 586–592. https://doi.org/10.1016/j.clay.2015.07.008.

[158] I.B. Topçu, C. Karakurt, Properties of reinforced concrete steel rebars exposed to high temperatures, Adv. Mater. Sci. Eng. 2008 (2008). https://doi.org/10.1155/2008/814137.

[159] J. Eidan, I. Rasoolan, A. Rezaeian, D. Poorveis, Residual mechanical properties of polypropylene fiber-reinforced concrete after heating, Constr. Build. Mater. 198 (2019) 195–206. https://doi.org/10.1016/j.conbuildmat.2018.11.209.

[160] Y.J. Zhang, S. Li, Y.C. Wang, D.L. Xu, Microstructural and strength evolutions of geopolymer composite reinforced by resin exposed to elevated temperature, J. Non. Cryst. Solids. 358 (2012) 620–624. https://doi.org/10.1016/j.jnoncrysol.2011.11.006.

[161] K.H. Yang, J.K. Song, J.S. Lee, Properties of alkali-activated mortar and concrete using lightweight aggregates, Mater. Struct. 43 (2010) 403–416. https://doi.org/10.1617/s11527-009-9499-6.

[162] H.Y. Zhang, V. Kodur, B. Wu, L. Cao, F. Wang, Thermal behavior and mechanical properties of geopolymer mortar after exposure to elevated temperatures, Constr. Build. Mater. 109 (2016) 17–24. https://doi.org/10.1016/j.conbuildmat.2016.01.043.

[163] F.U.A. Shaikh, Review of mechanical properties of short fibre reinforced geopolymer composites, Constr. Build. Mater. 43 (2013) 37–49. https://doi.org/10.1016/j.conbuildmat.2013.01.026.

[164] Z.J. Zhang, G.Z. Dai, S.N. Wu, L.X. Dong, L.L. Liu, Simulation of 42CrMo steel billet upsetting

and its defects analyses during forming process based on the software DEFORM-3D, Mater. Sci. Eng. A. 499 (2009) 49–52. https://doi.org/10.1016/j.msea.2007.11.135.

[165] A. Natali, S. Manzi, M.C. Bignozzi, Novel fiber-reinforced composite materials based on sustainable geopolymer matrix, Procedia Eng. 21 (2011) 1124–1131. https://doi.org/10.1016/j.proeng.2011.11.2120.

[166] F. Xu, X. Deng, C. Peng, J. Zhu, J. Chen, Mix design and flexural toughness of PVA fiber reinforced fly ash-geopolymer composites, Constr. Build. Mater. 150 (2017) 179–189. https://doi.org/10.1016/j.conbuildmat.2017.05.172.

[167] M.Z.N. Khan, Y. Hao, H. Hao, F.U.A. Shaikh, Mechanical properties of ambient cured high strength hybrid steel and synthetic fibers reinforced geopolymer composites, Cem. Concr. Compos. 85 (2018) 133–152. https://doi.org/10.1016/j.cemconcomp.2017.10.011.

[168] M.M. Al-mashhadani, O. Canpolat, Y. Aygörmez, M. Uysal, S. Erdem, Mechanical and microstructural characterization of fiber reinforced fly ash based geopolymer composites, Constr. Build. Mater. 167 (2018) 505–513. https://doi.org/10.1016/j.conbuildmat.2018.02.061.

[169] A.A. Adam, Strength and Durability Properties of Alkali Activated Slag and Fly Ash-Based Geopolymer Concrete, 2009.

[170] F.N. Okoye, J. Durgaprasad, N.B. Singh, Effect of silica fume on the mechanical properties of fl y ash based-geopolymer concrete, Ceram. Int. 42 (2016) 3000–3006. https://doi.org/10.1016/j.ceramint.2015.10.084.

[171] I. Ismail, S.A. Bernal, J.L. Provis, S. Hamdan, J.S.J. Van Deventer, Microstructural changes in alkali-activated fly ash/slag geopolymers with sulfate exposure, Mater. Struct. Constr. 46 (2013) 361–373. https://doi.org/10.1617/s11527-012-9906-2.

[172] A. Karthik, K. Sudalaimani, C.T. Vijayakumar, Durability study on coal fl y ash-blast furnace slag geopolymer concretes with bio-additives, Ceram. Int. 43 (2017) 11935–11943. https://doi.org/10.1016/j.ceramint.2017.06.042.

[173] M. Criado, A. Ferna, A. Palomo, I. Sobrados, J. Sanz, Effect of the SiO 2 / Na 2 O ratio on the alkali activation of fly ash . Part II : Si MAS-NMR Survey, Microporous Mesoporous Mater. 109 (2008) 525–534. https://doi.org/10.1016/j.micromeso.2007.05.062.

[174] M. Criado, A. Fernández-jiménez, A.G. De Torre, M.A.G. Aranda, A. Palomo, An XRD study of the effect of the SiO 2 / Na 2 O ratio on the alkali activation of fly ash, 37 (2007) 671–679. https://doi.org/10.1016/j.cemconres.2007.01.013.

[175] M. Criado, A. Ferna, A. Palomo, Alkali activation of fly ash : Effect of the SiO2 /Na2O ratio Part I : FTIR study, Microporous Mesoporous Mater. 106 (2007) 180–191. https://doi.org/10.1016/j.micromeso.2007.02.055.

[176] M. Burhan, İ. Türkmen, M. Murat, F. Kantarci, R. Demirbo, Sulfate resistance of ferrochrome slag based geopolymer concrete, Ceram. Int. 42 (2016) 1254–1260. https://doi.org/10.1016/j.ceramint.2015.09.058.

[177] F.N. Okoye, S. Prakash, N.B. Singh, Durability of fly ash based geopolymer concrete in the presence of silica fume, J. Clean. Prod. (2017). https://doi.org/10.1016/j.jclepro.2017.02.176.

[178] R. Shadnia, L. Zhang, P. Li, Experimental study of geopolymer mortar with incorporated PCM, Constr. Build. Mater. 84 (2015) 95–102. https://doi.org/10.1016/j.conbuildmat.2015.03.066.

[179] A. Çevik, R. Alzeebaree, G. Humur, M. Eren, Effect of nano-silica on the chemical durability and mechanical performance of fl y ash based geopolymer concrete, Ceram. Int. 44 (2018) 12253–12264. https://doi.org/10.1016/j.ceramint.2018.04.009.

[180] H. Su, J. Xu, W. Ren, Mechanical properties of geopolymer concrete exposed to dynamic compression under elevated temperatures, Ceram. Int. 42 (2016) 3888–3898. https://doi.org/10.1016/j.ceramint.2015.11.055.

[181] H.G. Russell, A.R. Anderson, J.O. Banning, J.E. Cook, G.C. Frantz, W.T. Hester, J. Moreno, B.R. Mastin, W.C. Moore, A.H. Nilson, W.F. Perenchio, P.C. Aitcin, F.D. Anderson, R.W. Black, I.G. Cantor, K.D. Drake, G.C. Frantz, T.G. Guennewig, M.D. Luther, W.C. Moore, A.H. Nilson, C.R. Ohwiler, M.T. Russell, State-of-the-Art Report on High-Strength Concrete Reported by ACI

Committee 363, 1997.

[182] A.C.I. Committee, Building Code Requirements for Structural Concrete (ACI 318-14), 2014.

[183] C. Concrete, Reinforced Concrete Design in accordance with AS 3600—2009, 2009.

[184] Bureau of Indian Standard, PLAIN AND REINFORCED CONCRETE - CODE OF PRACTICE, IS 4562000. (2000).

[185] J.M. Mohd Ahmed, Khalid Mohammad El Hadi, Mohammad Abul Hasan, Evaluating the co-relationship between concrete flexural tensile strength and compressive strength, Int. J. Struct. Eng. 5 (2014) 115–131.

[186] R.R. Bellum, K. Muniraj, S. Rama, C. Madduru, Annales de Chimie - Science des Matériaux Empirical Relationships on Mechanical Properties of Class-F Fly Ash and GGBS Based Geopolymer Concrete, Ann. Chim. - Sci. Des Matériaux. 43 (2019) 189–197.

[187] C. of E. International, ceb-fip-model-code-1990-design-code.pdf, 1990.

[188] ASTM International, Standard Test Method for Static Modulus of Elasticity and Poisson's Ratio of Concrete, C469/C469M − 14. (2019) 1–5. https://doi.org/10.1520/C0469.

[189] J.K.R. VARSHA BN, SARANYA S, EMBODIED ENERGY OF AGGREGATES AND MASONRY UNITS PRODUCED AROUND BENGALURU, INDIA, Int. J. Adv. Sci. Eng. Technol. 6 (2018) 42–45.

[190] L.G. Breitenbach, U. Ppgem, F. Kirch, A case study about embodied energy in concrete and structural masonry buildings, J. Constr. 13 (2014) 9–14.

[191] S.R. Anvekar, L.R. Manjunatha, S.R. Anvekar, S. Sagari, K. Archana, An Economic and Embodied Energy Comparison of Geo-polymer, Blended Cement and Traditional Concretes, J. Civ. Eng. Technol. Res. 1 (2014) 33–40.

[192] T. Janardhanan, J. Thaarrini, & S. Dhivya, S. Dhivya, Comparative Study on the Production Cost of Geopolymer and Conventional Concretes, Int. J. Civ. Eng. Res. 7 (2016) 117–124. http://www.ripublication.com.

[193] B.C. McLellan, R.P. Williams, J. Lay, A. Van Riessen, G.D. Corder, Costs and carbon emissions for geopolymer pastes in comparison to ordinary portland cement, J. Clean. Prod. 19 (2011) 1080–1090. https://doi.org/10.1016/j.jclepro.2011.02.010.

[194] B.J. Mathew, M. Sudhakar, C. Natarajan, Strength , Economic and Sustainability Characteristics of Coal Ash – GGBS Based Geopolymer Concrete ., Int. J. Comput. Eng. Res. 3 (2013) 207–212.

[195] L. Assi, K. Carter, E. (Eddie) Deaver, R. Anay, P. Ziehl, Sustainable concrete: Building a greener future, J. Clean. Prod. 198 (2018) 1641–1651. https://doi.org/10.1016/j.jclepro.2018.07.123.